Investigating Glial Roles of Alzheimer's Disease Risk Genes, Using *Drosophila* Models

By

Eilish Mackinnon

Thesis submission for the degree of

Doctor of Philosophy (PhD)

December 2022

Acknowledgements

I would like to firstly express a dept of gratitude to my primary supervisor Owen Peters, his continuous guidance, support and encouragement has been invaluable to my PhD. I especially valued his approachable nature, willingness to listen and ideas contributed to this thesis. I would like to extend my thanks to Prof. Yves Barde, who offered a fresh perspective and insight into my research during progress monitoring meetings. A special thanks goes to Freya Storer for her collaboration with me on the sl/PLCG2 work and providing a soundboard for ideas and discussion. I am very grateful to everyone who has worked in the DRI fly lab, past and present, I could not have asked for a better lab group to share my PhD experience with - filled with lots of cake, pub trips and everlasting memories.

Particular thanks goes to our lab technician Leo Amadio for his exceptional managing of the lab and always keeping up with my constant demand of fly food. Expertise, advice and technical assistance from Daniel Maddison, Bilal Malik and Dina Fathalla has also been greatly appreciated. I would also like to acknowledge the assistance from undergraduate and master students in help analysing my RING assay data, you shared my pain! A special thanks goes to the day one's, Andrew Lloyd and Louise Townsend, for getting me through the high and lows of PhD life. In particular, Andrew for your wit and banter and Louise for listening to my many rants and all the advice given. Thanks to both for providing me with endless entertainment, in and out of the lab and making lockdown shift work that much more bearable. Next, I would like to thank the wider DRI community for being such a welcoming, friendly work environment and particularly my new lab group, who have supported me in starting my new post doc role whilst having to write this thesis. Just want to say, Elena you are the queen of formatting!

Last but by no means least I would like to thank my family, particularly Mum and Dad for their undivided support and motivation given throughout my PhD and life in general. Thanks for always believing in me, having patience and listening to me talk endlessly about flies - you both have gotten me through my PhD journey in more ways than one!

Summary

Genetics plays a significant role in Alzheimer's disease (AD) risk, with multiple genetic risk variants uncovered by Genome Wide Association Studies (GWAS), many of which are enriched in microglia, the brains resident immune cells. Microglia are responsible for central nervous system (CNS) maintenance, injury response and fighting infection. There is clear evidence microglial dysfunction plays an critical role in AD pathogenesis, suggesting therapeutically targeting these cells may be of benefit. Our understanding of how these risk genes influence glial responses throughout age is limited, and how their activity in glia contributes to disease onset and development is largely unknown. This present study sets out to investigate potential glial roles of conserved AD risk genes, using *Drosophila melanogaster* as a model, with the aim to elucidate novel mechanisms contributing to disease risk.

A reverse candidate knockdown screen of multiple conserved AD risk genes was conducted to assess AD risk genes roles in glial mediated neurological dysfunction and longevity. Results from this screen identified novel candidate genes, including orthologs of *MEF2C*, *NME8* and *ACE* that expression in glia likely contributes to a healthy ageing nervous system and survival.

PLCG2 is an important candidate gene to study AD relevant functions in flies, with a coding variant (P522R) linked to reduced late onset AD (LOAD) risk. This thesis aimed to characterise the glial role of the *Drosophila PLCG2* ortholog, *small wing* and it substrates (PI(4,5)P2 and PI(3,4,5)P3) in ageing and $A\beta_{42}$ related pathology. This study characterised the utility of genetically encoded, cell type specific fluorescent reporters for measuring the PI(4,5)P2 and PI(3,4,5)P3 dynamics in the fly brain, as well as a quantifiable model of glial driven $A\beta_{42}$ toxicity. Finally, transgenic *Drosophila* expressing human *PLCG2* wildtype (P522) and AD protective (R522) variants were created to explore functional changes associated with the hypermorphic R522 variant and its contribution to reduced LOAD risk. Results highlighted a conserved role for glial *sl/PLCG2* in modifying $A\beta_{42}$ toxicity and confirmed a protective role of the R522 reduced risk variant compared to the common P522 variant in $A\beta_{42}$ associated pathology. Taken together these results indicate modulating PLCG2 activity may be a promising therapeutic target for treatment of AD.

Contents

Table of Figures

Table of Tables

List of Abbreviations

aa – amino acid
Aβ – amyloid beta
ABCA7 – ATP-binding cassette sub-family A member 7
ABI3 – Abi gene family member 3
ACE – angiotensin-converting enzyme
AD – Alzheimer's Disease
ADAM10 – ADAM Metallopeptidase Domain 10
ADAM17 – ADAM Metallopeptidase Domain 17
ADAMTS1 – a disintegrin and metalloproteinase with thrombospondin motifs 1
AICD – APP intracellular domain
AKT – PKB Protein Kinase B
ALS - Amyotrophic Lateral Sclerosis
AMP – Adenosine monophosphate
amp - ampicillin
Amph – Amphiphysin
ANK1 – ankyrin 1
ANK2 – ankyrin 2
ANOVA - Analysis of Variance
aos - Argos
AP3 – Adapter protein complex 3
APLAID - autoinflammatory-PLAID
APOE – apolipoprotein
APP – Amyloid precursor protein
Arc – Arctic
BACE1 – beta-site APP-cleaving enzyme 1
Bad – Bcl2-associated agonist of cell death
Bax – Bcl2-associated X protein
BCA – Bicinchoninic Acid
BDNF – Brain-Derived Neurotrophic Factor
BDSC – Bloomington *Drosophila* stock center
BIN1 – Bridging integrator-1
BMDM – Bone marrow-derived macrophages
bp – base pair
Bru1 – Bruno 1
BTK – Bruton's tyrosine kinase
C1q – complement component 1q
C1QB – Complement C1q B chain
C2 domain – protein kinase C conserved region 2
Cas9 - CRISPR-associated protein 9
CASS4 – Cas scaffolding protein family member 4
CD2AP – CD2-associated protein
CD33 – Cluster of differentiation 33, also known as SIGLEC3
CD36 – Cluster of differentiation 36
CD68 – Cluster of differentiation 68
CDK5 - cyclin dependent kinase 5
cDNA – complementary DNA
C.elegans – Caenorhabditis elegans

CELF1 – CUGBP ELav-like family member 1
cindr – CIN85 and CD2AP related
CLU – Clusterin precursor 14
CNS – central nervous system
CNTNAP2 – contactin-associated protein 2
CPD - carboxypeptidase D
CR1 – Complement receptor 1
CREB – cAMP response element binding protein
CRISPR – Clustered regularly interspaced short palindromic repeats
CRIMIC - CRISPR Mediated Integration Cassette
CSF – Cerebrospinal fluid
CSFR1 – Colony stimulating factor 1 receptor
CTRL - Control
DAG – Diacylglycerol
dBace – *Drosophila* beta-site APP cleaving enzyme
DIOPT – DRSC Integrative Orthologue Prediction Tool
DGRC – *Drosophila* Genomics Resource Center
DMSO – Dimethyl sulfoxide
DNA – Deoxyribonucleic acid
dNTPs – Deoxynucleotide triphosphates
DOR – Diabetes and obesity regulated
DRI – Dementia Research Institute
d.p.e – days post eclosion
dPsn – Drosophila presenilin
DRSC – *Drosophila* RNAi screening database
E.coli – Escherichia coli
EDTA – Ethylenediaminetetraacetic acid
EGF – Epidermal Growth Factor
ELISA - Enzyme-Linked Immunosorbent Assay
Elav – embryonic lethal abnormal visual system
EPHA1 – Eph receptor A1
Eph – Eph receptor tyrosine kinase
EOAD – Early-onset Alzheimer's disease
eQTL - expression Quantitative Trait Loci 15
ERK – Extracellular signal-Regulated Kinases
Ets98B – Ets at 98B
EWAS – Epigenome Wide Associated Studies
FAD – Familial Alzheimer's disease
Fak – Focal adhesion kinase
FDA - Food and Drug Administration
FERMT2 – Fermitin family member 2
Fit1 – Fermitin 1
FRT – Flippase recognition target
FTDP - Frontotemporal Dementia with Parkinsonism
GABA - Gamma-aminobutyric acid
GAL4 – Galactokinase 4
GAL80 – Galactokinase 80
GD – VDRC P-element RNAi stocks
GDNF - glial-derived neurotrophic factor

GFAP – Glial fibrillary acidic protein
GFP – Green fluorescent protein
GPCR – G-protein-coupled receptors
GRP1 – general receptor for phosphoinositides, isoform 1
GSK-3β – glycogen synthase kinase 3β
GTP – Guanosine triphosphate
GWAS – Genome Wide Association Studies
Hasp - High-anchoring scaffold protein
HEPES – 4-(2-hydroxyethyl)-1 piperazineethanesulfonic acid
HF – High fidelity
HMC3 - Human microglia clone 3
HS - Heparan sulphate
HS3ST1 – Heparan sulfate glucosamine 3-O-sulfotransferase 1
Hs3st-A – Heparan sulfate 3-O sulfotransferase-A
Hs3st-B – Heparan sulfate 3-O sulfotransferase-B
IL-1β – Interleukin - 1β
IL-6 – Interleukin - 6
Imd - Immunodeficiency
INPP5D – Phosphatidylinositol 3,4,5-trisphosphate 5-phosphatase 1
IP3 – Inositol trisphosphate
iPSC - Induced pluripotent stem cells
ITAM – Immunoreceptor tyrosine-based activation motif
ITIM - Immunoreceptor tyrosine-based inhibitory motif
JAK-STAT - Janus Kinase protein and the Signal Transducer and Activator of Transcription
Kb – Kilobase
kDa – Kilodalton
KD – knockdown
KI – knockin
KK – VDRC phiC31 RNAi Stocks
KO – knockout
LB - Luria-Bertani
lap – like-AP180
LpR2 – lipophorin receptor 2
LOAD – Late-onset Alzheimer's disease
MAPT – microtubule-associated phosphoprotein tau
mCD8 – mouse cluster of differentiation 8
MCI – mild cognitive impairment
MEGF10 – Multiple epidermal growth factor-like domains protein 10
MADD – MAP kinase- activating death domain
MAF – Minor allele frequency
MAPK – Mitogen-activated protein kinase
MARK – Microtubule affinity regulating kinase
Mef2 - Myocyte enhancing factor 2
MMSE - mini-mental state examination
mTOR – mammalian target of rapamycin
mTORC1 – mammalian target of rapamycin complex 1
mRNA – messenger RNA
MS4A6A – Membrane spanning 4-domains A6A
MS4A4 – Membrane spanning 4-domains A4A

MSD - Meso Scale Discovery
NaCl – Sodium chloride
NF-kB – Nuclear factor kappa B
NFTs - neurofibrillary tangles
NFAT – Nuclear factor of activated T cells
NME8 – NME family member 8
NorpA – no receptor potential A
Notch – Neurogenic locus notch homolog protein
Nrx-IV – Neurexin-IV
Ocrl – Oculocerebrorenal syndrome of Lowe (inositol polyphosphate-5-phosphatase)
PBS – phosphate Buffered Saline
PCR – polymerae chain reaction
PCV – posterior crossvein
PDK1 – phosphoinositide-dependent kinase 1
PFA – paraformaldehyde
PH – pleckstrin homology
PI – Phosphatidylinositol
PIPs - Phosphoinositides
PI3K - Phosphoinositide 3-kinase
PICALM – Phosphatidylinositol binding clathrin assembly protein
PIP2 - Phosphatidylinositol 4,5-bisphosphate
PIP3 - Phosphatidylinositol 3,4,5-trisphosphate
PKA - protein kinase A
PKC – Protein kinase C
PLAID - PLCG2 associated antibody deficiency and immune dysregulation
PLC - Phospholipase C
PLC-21C – Phospholipase C at 21C
PLCδ1 – Phospholipase C Delta-1
PLCG1 – Phospholipase C Gamma-1
PLCG2 – Phospholipase C Gamma-2
PLD3 – Phospholipase D 3
PNS – peripheral nervous system
PP2A – Protein phosphatase A
PSP – Progressive supranuclear palsy
PRS – polygenic risk scores
PSEN 1 – Presenilin 1
PSEN 2 – Presenilin 2
PTEN – Phosphatase and tensin homolog
PTK2B - Protein Tyrosine Kinase 2 Beta
PTMs – post-translational modifications
PTx – phosphate-buffered saline-triton Xion 10x
qPCR – real-time polymerase chain reaction
R7 – Rabdomere 7
raf – rapidly accelerated fibrosarcoma
ras – rat sarcoma virus

repo – reversed polarity
RFP – Red fluorescent protein
RIN3 – Ras and Rab Interactor 3

RING – Rapid Iterative Negative Geotaxis
RIPA – Radioimmunoprecipitation assay buffer
RNA – ribonucleic acid
RNAi – ribonucleic acid interference
RNAseq – RNA sequencing
ROS – reactive oxygen species
RPM – revolution per minute
RT – room temperature
RTK – receptor tyrosine kinase
sAPP-α – Soluble APP fragment cleaved by α-secretase
sAPP-β - Soluble APP fragment cleaved by β-secretase
scRNAseq – Single cell RNA sequencing
SEM – Standard error of mean
SH2 – Src Homology 2
SH3 – Src Homology 3
SHIP1 – Src homology 2 (SH2) domain-containing inositol polyphosphate 5-phosphatase 1
shark – SH2 ankyrin repeat kinase (syk family)
sl – small wing
SLC24A4 - Solute Carrier Family 24 Member 4
SNPs – single nucleotide polymorphisms
SORL1 – Sortilin Related Receptor 1
SPI1 – Spi-1 proto-oncogene
Src – protein kinase
Syk - Spleen tyrosine kinase
TBS – TRIS-buffered saline
TBST – TBS with TWEEN
TIM - triose phosphate isomerase
TLR – toll-like receptor
mTOR – mammalian Target of Rapamycin
TORC1 – Tor complex 1
TNF-α – tumour necrosis factor-α
TREM2 – Triggering receptor expressed on myeloid cells 2
TRiP – Transgenic RNAi Project 21
ts – temperature sensitive
TYROBP – tyrosine kinase binding protein
UAS – upstream activation sequence
UV – Ultra violet
VDRC – Vienna *Drosophila* Resource Center
WES - whole exome sequencing
WGS - whole genome sequencing
WWOX – WW domain-containing oxidoreductase
ZCWPW1 – Zinc finger CW-type PWWP domain protein 1
zyd – zydeco
2D – 2 Dimensional
3D – 3 Dimensional

Chapter 1 – Introduction

1.1. Overview

Dementia describes a set of symptoms such as loss of memory, language and problem solving, common to a number of neurodegenerative diseases such as Alzheimer's, Parkinson's and Huntington's disease, vascular dementia, frontotemporal dementia and many more. Currently, dementia is estimated to affect 55 million people worldwide, with potential for this to increase to 139 million by 2050 (Gauthier et al. 2022). Alzheimer's disease (AD) is the most common form of dementia, accounting for more than 80% of dementia cases in people over the age of 65 (Kumar et al. 2015). With a growing ageing population, AD has become a major health concern worldwide, with an estimated global annual cost of US$ 1 trillion (Breijyeh et al., 2020). This is further exacerbated by limited disease modifying therapeutics and is therefore a drive to elucidate underlying causes of AD. It is understood, there is a substantial genetic basis to AD, that has recently implicated several genes in microglial function and immune signalling (Efthymiou and Goate 2017; Hansen et al. 2018). This thesis will use the power of *Drosophila* models to explore glial functions of conserved AD risk genes, in effort to uncover new pathways contributing to pathology.

1.2. Alzheimer's Disease: Where it Began

In 1906, Dr Alois Alzheimer documented the first clinical presentation of what is now universally known as AD. Upon admission of 51-year-old, Auguste Deter to an asylum in Frankfurt, Alois described a number of behavioural symptoms classic to dementia including short term memory loss, language deficit, hallucinations, delusions, paranoia, and aggression. Post-mortem examination of Augustes' brain led to characterisation of two unique lesions: extracellular amyloid plaques and intracellular neurofibrillary tangles (NFTs) (Figure 1.1). Today, these lesions are the classic neuropathological hallmarks of AD used to distinguish from other dementias, such as Parkinson's, Huntington's, and frontotemporal dementia, which present similar cognitive impairments.

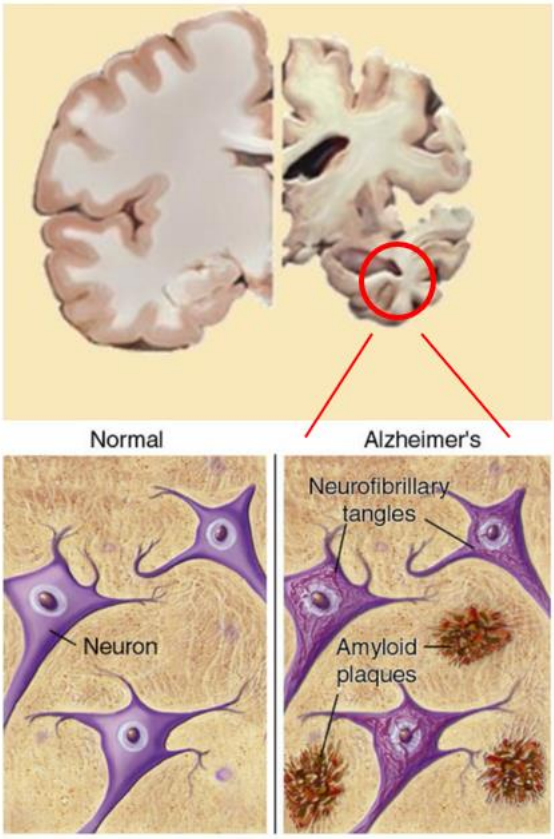

Figure 1.1: Major neuropathological hallmarks of AD.

Neuropathological differences between a healthy brain compared to one with AD pathology. An AD brain exhibits significant brain atrophy, as well as the accumulation of amyloid plaques and NFTs (Adapted from de Loof and Schoofs 2019*).*

1.3. Alzheimer's Disease Pathology

1.3.1. Clinical Presentation and Diagnoses

AD is a progressive neurodegenerative disorder associated with slow deterioration of memory and other higher order cognitive functions such as judgement, attention and language (Desai & Grossberg 2005). Other clinical presentations of AD may include personality and behavioural changes such as psychosis, depression, and agitation. AD is a complex heterogeneous disease varying in age of onset, progression rates and clinical presentations (Tarawneh & Holtzman 2012). Such heterogeneity makes diagnosis and treatment of AD difficult, whereby identifying biomarkers of pre-symptomatic stages has been a major challenge clinically (Desai & Grossberg 2005). Only 60% of patients with AD are correctly diagnosed, primarily from inclusion of symptoms outlined by standard clinical criteria (Small et al. 1997). Tests for cognitive impairment such as the mini-mental state examination (MMSE) are routinely used by clinicians, alongside medical history, physical

examination, and brain scans to best guide diagnosis of dementia and its progression. From these mental tests, it is possible to detect mild cognitive impairment (MCI) from declines in higher order cognitive functions. However, predicting the transition of MCI into full onset AD underlies the clinical challenge of accurate AD diagnosis as some individuals remain stable, whilst others revert back to normal. Until recently, post-mortem histopathological examination of characteristic lesions unique to AD has been the most definitive way of diagnosing AD. Brain scans such as computerised tomography and magnetic resonance imaging are now able to detect changes in the brain and have been widely used to support an AD diagnosis. Positron emission tomography scans with compounds such as fluoro-deoxy-d-glucose or Pittsburgh Compound B can be used to image cerebral metabolism or amyloid fibrils respectively in the human brain, representing a significant advancement to the diagnostic field of AD (Cohen and Klunk 2014; Yamin and Teplow 2017). However, such techniques are currently too expensive for routine diagnostic use (Johnson et al. 2012).

1.3.2. Macroscopic Brain Changes

AD brains exhibit gross cortical atrophy, primarily affecting frontal and parietal regions and the temporal lobes, that are important for higher executive functions such as learning and memory, language, problem solving. Lateral ventricles, particularly the temporal horns, appear dilated upon cross-sectional analysis and in early stages of pathology, the hippocampus and entorhinal cortex are severely affected (Braak and Braak 1991). Remarkably, the optical, sensory, and primary motor regions remain relatively preserved in AD pathology compared to cortical regions (Desai & Grossberg 2005). Synaptic loss and neuron degeneration are principal correlates of AD related cognitive impairment (Perl, 2010). Up to 80% of neurons in the hippocampus die and the severe loss of cholinergic neurons located in the basal forebrain contributes greatly to deficits in memory and attention (Ferreira-Vieira et al. 2016). Degeneration of glutaminergic neurons disrupts excitatory glutamate neurotransmission throughout the central nervous system (CNS), mediated largely by ionotropic glutamate receptors. These glutamate receptors play fundamental roles in synaptic plasticity which underlie the molecular mechanisms of learning and memory formation (Riedel et al. 2003)

1.3.3. Neuropathological Hallmarks

Post-mortem studies have enabled dissection of neuropathological changes to AD brains. AD pathology is defined by two neuropathological hallmarks, extracellular amyloid rich plaques, and intracellular NFTs of hyperphosphorylated tau protein (Perl 2010). Reactive changes in astrocytes and microglia (gliosis), and the accumulation of lipids were also originally described by Dr Alois Alzheimer and are often observed in the disease (Stelzmann et al. 1995; Hansen et al. 2018). These classic brain lesions manifest early in disease development, preceding clinical onset of cognitive impairment (Perl, 2010).

1.3.3.1. Amyloid Beta

The amyloid beta (Aβ) peptide is the major component of amyloid plaques, the primary histological hallmark of AD brains and has been extensively researched since its sequence was first published back in 1984 by Glenner and Wong (Glenner & Wong, 1984). The Aβ peptide is a 4kDa fragment produced from cleavage of the transmembrane amyloid precursor protein (APP) (Chen et al. 2017). APP is highly expressed in neurons, playing roles in neuronal growth, activity, and post-injury repair (Turner et al. 2003). Three secretases α, β, and γ are involved in the proteolytic cleavage of APP via two very distinct pathways: the amyloidogenic (neurodegenerative) and the non-amyloidogenic (neuroprotective) pathway (Figure 1.2).

In the amyloidogenic pathway, APP is first cleaved by β secretase (encoded by beta-site APP-cleaving enzyme 1 (*BACE1*), releasing a large N-terminal secreted APP (sAPPβ) extracellularly and leaving behind a 99 amino acid (aa) C-terminal fragment (C99) at the plasma membrane (Chen et al. 2017). C99 is internalised and cleaved by γ-secretase (encoded by presenilin-1/2 (*PSEN-1/2*) in endocytic compartments, releasing cleavage fragments ranging from 30 to 51 aa in length (Olsson et al. 2014). These are further cleaved in to the two predominant forms of Aβ: the 40 aa ($Aβ_{40}$) and 42 aa ($Aβ_{42}$). $Aβ_{40}$ is the most common form, however the less abundant $Aβ_{42}$ fragment is far more neurotoxic, due to its propensity to oligomerise and form fibrils (Chow et al. 2010). Whilst the more aggregation prone $Aβ_{42}$ peptide constitutes a small portion of total Aβ generated, it is the main oligomeric species associated in senile plaque formation (Zhang et al. 2011).

Alternatively, in the non-amyloidogenic pathway, α-secretase, encoded by *ADAM10*, cleaves within the Aβ domain of APP, precluding Aβ formation and releasing soluble APP fragment (sAPPα). The remaining 83 aa C-terminal fragment (C83) is then cleaved by γ secretase,

either at the plasma membrane or in endosomes, which in turn releases the P3 peptide (24aa) and APP intracellular domain (AICD) into the extracellular space (Chow et al. 2010). AICD gets rapidly degraded by the insulin degrading enzyme or transported to the nucleus where it plays a role in transcriptional regulation (Edbauer et al. 2002).

Under normal physiological conditions, the processing of APP by β secretase accounts for around 10% of the total cellular APP, whereas 90% or more of APP is cleaved by α secretase in the non-amyloidogenic pathway (Nalivaeva & Turner, 2013). While both pathways are constitutively active in the brain throughout life, physiological imbalances in either the production or clearance of pathway metabolites contributes to the progression of AD. Under a physiological state Aβ is typically secreted extracellularly where it is rapidly removed and degraded. However, with age or in a pathological state, protein turnover is impaired, resulting in the accumulation of Aβ.

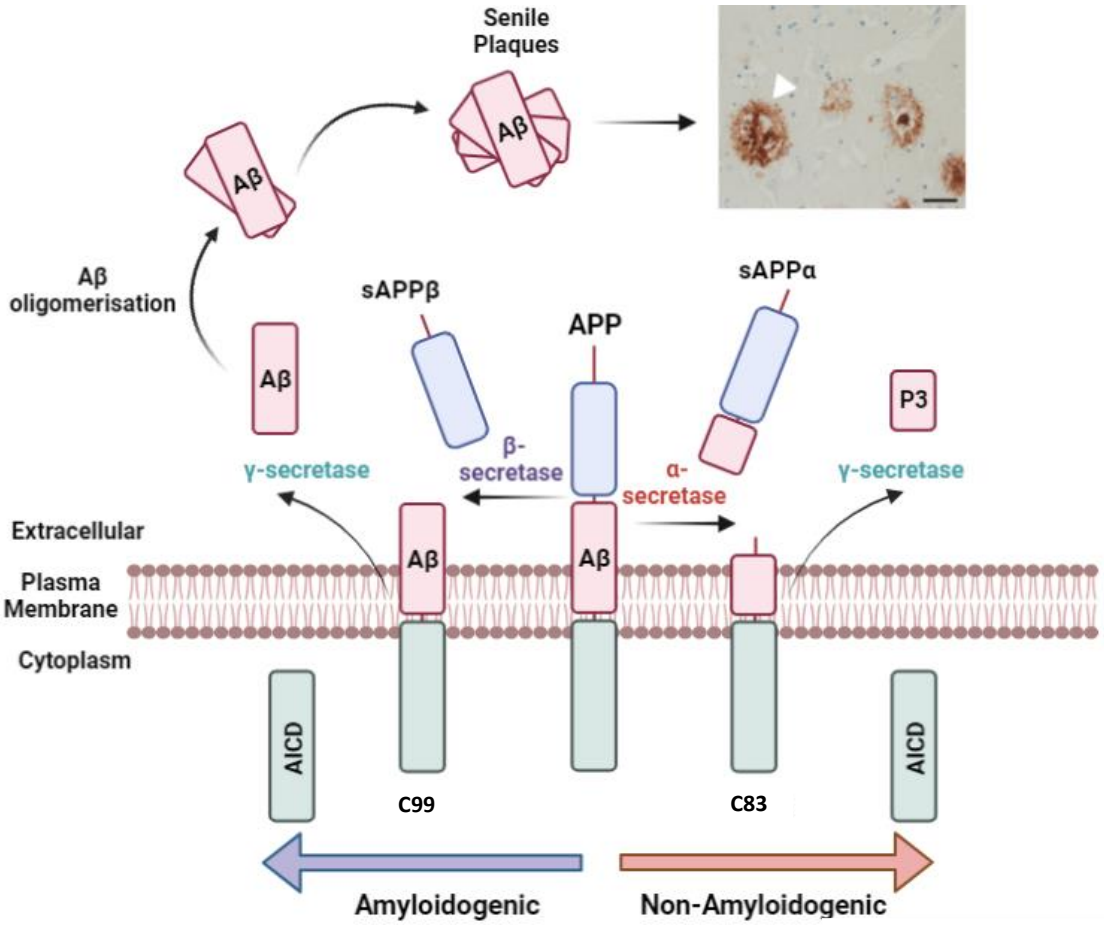

Figure 1.2: Amyloidogenic and non-amyloidogenic pathways of APP processing.

APP is processed in two distinct pathways dependent on the secretases involved in the reaction. In the amyloidogenic pathway, sequential cleavage by β then γ secretase liberates Aβ peptides of 40 and 42 aa ($Aβ_{40}$ & $Aβ_{42}$). Aβ monomers aggregate into oligomers and further into senile plaques, resulting in Aβ deposition in the brain. Representative image of senile plaque in AD affected brain tissue, taken from: (Deture & Dickson, 2019). In the non-amyloidogenic pathway, a secretase cleaves within the Aβ domain of APP, thus precluding formation of Aβ and instead releases sAPP-α.

Aβ monomers produced in the amyloidogenic pathway can aggregate into oligomers, protofibrils and amyloid fibrils. Amyloid fibrils are large and insoluble which can further assemble into amyloid plaques, whereas Aβ oligomers are soluble and able to spread about the brain (G. F. Chen et al. 2017). The Aβ monomer typically forms an alpha helix and has no known direct toxicity, however amyloid plaques formed upon Aβ fibrillisation are largely

composed of β sheet fibrillar structures which are extremely stable and resistant to degradation (G. F. Chen et al. 2017). These amyloid plaques are believed to exert some neurotoxic effects given the substantial synaptic loss and neuronal dystrophy observed in close proximity to the plaques (Kuchibhotla et al. 2008). However, recent studies have indicated that soluble Aβ oligomers, rather than their fibrillar aggregates drive AD pathogenesis (Yang et al. 2017; Tolar et al. 2021). Several studies have highlighted the presence of soluble Aβ species correlates stronger with AD pathology than insoluble amyloid plaques (McLean et al. 1999;McDonald et al. 2010). Furthermore, the formation of insoluble fibrils and plaques appear to reduce oligomeric toxicity, whereby toxic oligomers are sequestered into the plaques (Gaspar et al. 2010; Brody et al. 2017).

1.3.3.2. Tau

The second classic histopathological hallmark of AD are NFTs, which arise from abnormal accumulation of hyperphosphorylated tau protein located intra-neuronally (Naseri et al. 2019). Brains exhibiting tau pathology, termed tauopathies, are characterised in a wide range of neurodegenerative diseases, including Alzheimer's, Parkinson's, and Picks disease, frontotemporal dementia and progressive supranuclear palsy (PSP). NFT pathology assumes a stereotypical pattern of spread throughout brain regions as the disease progresses. This can be split in to six 'Braak' stages, based on the location of NFTs and the severity of changes: transentorhinal stages I-II: clinically silent cases; limbic stages III-IV: incipient AD; neocortical stages V-VI: fully developed AD (Braak & Braak, 1995). Braak staging is now commonly used as a clinical diagnostic tool for assessing disease progression.

Tau is a microtubule associated protein encoded by the *MAPT* gene and is required in regulating microtubule assembly and their structural stability (Weingarten et al. 1975). Tau expression is predominantly neuronal, localising mainly to axons where it serves as an important regulator of axonal transport (Dixit et al. 2008). Six tau isoforms exist in the human brain, generated by alternative splicing of exon 2, 3 and 10 in the MAPT gene transcript (Figure 1.3). These isoforms are differentially expressed throughout neurodegeneration (Boyarko & Hook, 2021). Splicing of exon 2 and 3 produce variants containing zero (0N), one (1N) or two (2N) of the 29 aa N-terminal inserts, which through further splicing of exon 10 can either contain three (3R) or four (4R) microtubule binding repeats. 3R tau isoforms bind to microtubules with greater affinity than 4R tau isoforms (Panda et al. 2003). In a healthy human brain, 3R and 4R isoforms are found in a 1:1 ratio, whereas several studies

have shown a general increase in 4R isoform expression in AD brains (Ginsberg et al. 2006).

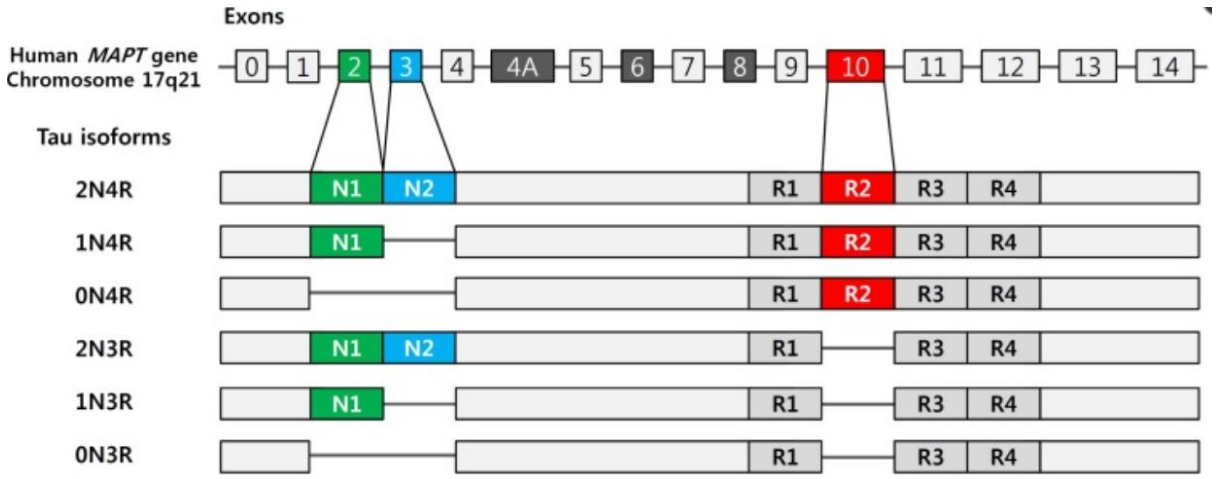

Figure 1.3: Tau protein isoforms in the human brain.

Alternative splicing of exon 2, 3 and 10 of the MAPT gene gives rise to six tau isoforms (Figure taken from: Park et al. 2016).

Post-translational modifications (PMTs) of tau such as phosphorylation, acetylation, glycosylation, proteolysis, and ubiquitination can regulate tau's function and have been implicated in AD pathogenesis (Ramesh et al. 2020). Out of all the tau PTMs, phosphorylation is one of the most well studied. Hyperphosphorylation of tau is common to AD pathology, promoting tau's fibrillisation and aggregation into NFTs. Changes in expression of various tau kinases and phosphatases have been documented in AD and are thought to contribute to the imbalance in tau's phosphorylation state (Liu et al. 2008; Pei et al. 2006; Zhou et al. 2008). Hyperphosphorylation of tau is generally considered secondary to Aβ accumulation, however, studies have demonstrated that in the absence of Aβ, tau dysfunction is still sufficient to trigger neurodegeneration (Hutton et al. 1998; Poorkaj et al. 1998; Spillantini et al. 2006). Phosphorylated tau has even been proposed as a biomarker given its positive correlation with cognitive impairment and its early detection in the cerebral spinal fluid (CSF) of AD patients (Buerger et al. 2006). It is evident the amyloid hypothesis only represents part of a complete story, as new tau targeting therapies for AD come to light. Nonetheless, Aβ remains the more attractive target for preventative medicines given Aβ pathology appears to precede tau pathology.

1.3.3.3. Neuroinflammation

Neuroinflammation is an innate immunological response required in defence against harmful/foreign pathogens or substances. Neuroinflammation is characterised by the activation of astrocytes and microglia, the brains resident immune cells. Activated microglia and astrocytes have long been recognised as histological hallmarks of AD brains, where microglia and astrocytes assume 'reactive' states and are found concentrated around amyloid plaques (McGeer et al. 1987; Zotova et al. 2011; Hansen et al. 2018). A number of studies have demonstrated that in addition to Aβ plaques and NFTs, AD brains exhibit a sustained inflammatory response, involving the production of nitric oxide, reactive oxygen species (ROS) and pro-inflammatory cytokines such as TNF-α, IL-1β and IL-6 (Akiyama et al. 2000; Meraz-Ríos et al. 2013). Additionally, there is clear evidence for the early involvement of neuroinflammation, where activation of glial cells precedes Aβ deposition (Heneka et al. 2015). Finally, genetic association studies and pathway analysis implicate immune response and microglial functions in AD pathogenesis, whereby several genetic risk loci have been found in genes preferentially expressed by microglia (refer to Table 1.1) (Sims et al. 2017; Efthymiou and Goate 2017). These genes include microglial receptors *TREM2* and *CD33* along with other genes such as *CR1*, *ABCA7*, *ABI3* and *PLCG2*, which have been implicated in microglial functions, predominantly phagocytosis. The role of microglia and their contribution to AD pathology will be discussed further in section 1.5.2.

Proposed AD Risk Gene	Enriched in Microglial
ABCA1	
ABCA7	
ABI3	
ACE	
ADAM10	
ADAM17	
ADAMTS1	
ANK3	
APOE	
APH1B	
APP	
BIN1	
BLNK	
CASS4	
CD2AP	
CD33	
CLU	
COX7C	
CR1	
CTSB	
CTSH	
DGKQ	
DOC2A	
ECHDC3	
EGFR	
EPHA1	
FERMT2	
FOXF1	
GRN	
HLA	
HS3ST1	
HS3ST5	
ICA1	
INPP5D	
IQCD	
IQCK	
JAZF1	
KLF16	
LILRB2	
LIME1	
MAF	
MAPT	
MME	
MS4A	
NCK2	
NME8	
OTULIN	

PICALM	
PLCG2	
PLEKHA1	
PTK2B	
RASGEF1C	
RHOH	
RBCK1	
RIN3	
SHARPIN	
SINGLEC	
SORL1	
SORT1	
SPI1	
TMEM106B	
TNIP1	
TREM2	
TSPAN14	
TSPOAP1	
UMAD1	
WWOX	
ZCWPW1	

Table 1.1 Table of proposed AD risk genes.

List of AD risk genes identified from GWAS with microglial enriched genes indicated in orange.

1.4. Genetics of Alzheimer's Disease

Twin studies highlight a strong genetic association with AD, were heritability falls around 58-79% (Gatz et al. 2006). The first genetic link for AD was the *APP* gene, located on chromosome 21. The genetic link came about as individuals with Down's syndrome (Trisomy 21), who possess triplicate copies of chromosome 21, exhibited increased production of the Aβ peptide (Glenner & Wong, 1984) and would typically develop neuropathology comparable to AD. Since this discovery, a number of genetic loci have been associated with early or late onset AD, as introduced below.

1.4.1. Types of AD

AD is categorised into two main types, early and late onset, based on the pattern of inheritance and age in which symptoms clinically present. Early onset AD (EOAD) accounts for approximately 5% of all AD cases with symptoms developing before the age of 60 and in some cases as young as 30 (Mendez, 2017). EOAD cases are largely familial, driven by an autosomal dominant pattern of inheritance. In cases of familial EOAD, there is a clear genetic link, with at least two generations of family members having had the disease. Sporadic cases of EOAD are however much rarer but can arise from *de novo* genetic mutations.

Familial EOAD has been attributed to genetic mutations in three particular genes (*APP, PSEN1* and *PSEN2*) (Lanoiselée et al. 2017). The amyloid precursor protein is encoded by the *APP* gene on chromosome 21, whilst *Presenilin 1* and *2* (*PSEN1 & 2*) encodes protein components of the γ secretase enzyme responsible for proteolytic processing of APP (Schott et al. 2002). Highly penetrant mutations in these genes lead to altered processing of APP and favoured production of the more neurotoxic aggregation prone Aβ species – $A\beta_{42}$.

To date, 32 unique missense mutations linked to the APP gene have been found to be involved in AD pathology (Lanoiselée et al. 2017). Dependent on the mutations position within the APP gene the resulting effect varies. For instance, mutations near the N-terminal site of the Aβ peptide domain increases Aβ production as such with the Swedish mutation (Mullan et al. 1992; Citron et al. 1992). The propensity of Aβ to aggregate increases in individuals displaying the classic Artic mutation (E693G), (Nilsberth et al. 2001; Murakami et al. 2002). In the London mutation, a V717I substitution (Goate et al. 1991) favours production of the more neurotoxic aggregation prone $A\beta_{42}$ oligomer relative to $A\beta_{40}$ (Suzuki

et al. 1999). Gene duplications, as seen with Down's syndrome and mutations in the APP promoter also result in symptoms invariable from AD, due to increased APP levels, the substrate for Aβ (Tokuda et al. 1997). On the other hand, a rare protective variant (A673T), in the APP gene, associated with minimal amyloid deposition, has been described in an Icelandic population (Jonsson et al. 2012). The A673T mutation located within the β-secretase cleavage site, was found to reduce amyloidogenic processing of APP and lower Aβ aggregation, therefore protecting against amyloid pathology (Maloney et al. 2014).

Mutations linked to the *APP* gene however only account for only 1% of EOAD cases (Brouwers et al. 2008). The familial form typically results from *PSEN 1/2* gene mutations, implicating proteins of the γ-secretase catalytic core. *PSEN1* is the most commonly implicated gene with 221 reported pathogenic mutations, while *PSEN2* has 19 (Lanoiselée et al. 2017). Such mutations may decrease catalytic γ-secretase activity or alter the cleavage site position, elevating the ratio of $A\beta_{42}$:$A\beta_{40}$.

In contrast, late onset AD (LOAD) is largely sporadic, with individuals developing symptoms much later in age, ~65 and above (Harman 2006). LOAD is the most common form of AD, constituting ~95% of AD cases, with age presenting as the highest influential risk factor. Beyond the age of 65, the risk of LOAD exponentially increases (Figure 1.4). There is no definitive familial link and no specific causal genes identified. Nonetheless, Genome Wide Association Studies (GWAS) have been able to identify several common genetic risk factors (as discussed in section 1.4.3), with over 75 genetic loci being implicated in LOAD pathogenesis to date (Bellenguez et al. 2022). Besides genetic risk factors, several other modifiable risk factors can be attributed to LOAD pathology, for instance smoking, excessive alcohol use, obesity, diabetes, lack of physical activity and depression. Sex specific variations have also been documented in AD, whereby there is a higher incidence of AD in women compared to men (Anstey et al. 2021).

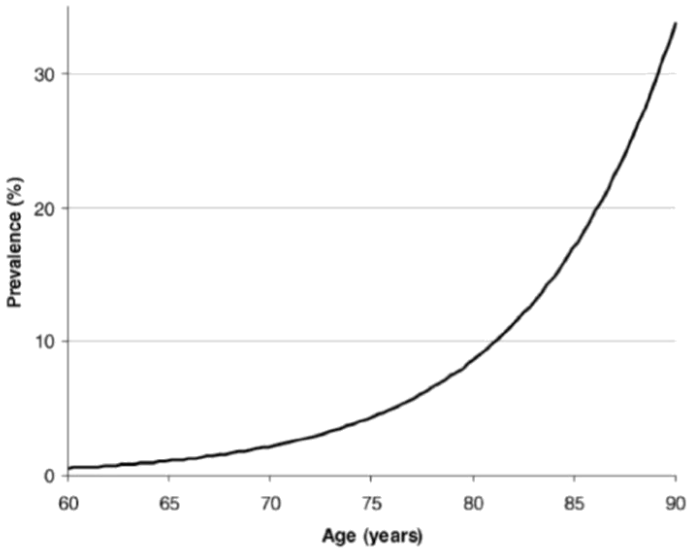

Figure 1.4: Prevalence of AD with age.

Risk of AD rises exponentially beyond the age of 65, where prevalence nearly doubles every five years (Ferri et al. 2005).

.

1.4.2. The APOE Genotype

To date, the strongest genetic risk factor identified for LOAD is the *Apolipoprotein E* (*APOE*) gene which encodes the apolipoprotein E protein (apoE) and was the first LOAD susceptibility loci identified by linkage analysis (Corder et al. 1993). In binding receptors on various lipoproteins, such as very low density (VLD) and high density lipoproteins, apoE facilitates the distribution and redistribution of lipids and cholesterol among various tissues in the body, playing a key role in regulating plasma lipids and cholesterol levels (Huang & Mahley, 2014). Three alleles (ε2, ε3, ε4) of the *APOE* gene exist, arising from aa substitutions (Arg and Cys) at positions 112 and 158 of the protein (Lambert et al. 2002). The *APOE* ε4 allele has been associated with a dose dependent increase in AD risk, whereby those carrying one copy of the ε4 allele (*APOE* ε3/ε4) have a 3-fold increased risk of developing AD than those carrying two ε3 alleles (*APOE* ε3/ε3) (Corder et al. 1993). Homozygous ε4 carriers (*APOE* ε4/ε4) in fact exhibit a 12-fold increased risk in AD onset. Contrary to the ε4 allele, bearing the ε2 allele is proposed to offer a small degree of protection (Farrer, 1997), regardless of ε4 alleles presence (Talbot et al. 1994). Whilst there is large variation in risk attributable to apoE in the population, the *APOE* genotype currently stands as the strongest genetic risk factor for AD.

The role of apoE in AD pathogenesis is thought largely to be Aβ dependent, whereby each isoform presents differential effects on Aβ clearance and accumulation, as well as Aβ neurotoxicity (Castellano et al. 2011). Firstly, apoE associates with neuritic amyloid plaques *in vivo* and Aβ peptide abundance is greater in those carrying the ε4 allele. Increased AD susceptibility conferred by the ε4 allele is thought to be due to inefficacy of catalysing Aβ peptide breakdown (Jiang et al. 2008). However, specific biological mechanisms correlating the ε4 allele and increased disease risk remain elusive. Other than the influence of apoE in the Aβ cascade, emerging evidence suggests apoE can affect also NFTs formation, neuronal survival, lipid homeostasis and intracellular signalling (Cedazo-Mínguez, 2007).

Since the discovery of the APOE genotype as a risk factor for AD, several other genetic risk loci have been identified with the advent of GWAS.

1.4.3. Genome Wide Association Studies and Common Variants

GWAS are used to identify association between a specific disease or trait with genetic loci and are used by scientists to unravel the genetic risk factors of complex polygenic disorders, such as AD. AD GWAS typically use a microarray based genotyping approach whereby genetic variants are pre-selected with common minor allele frequencies (MAF) above 0.01% (Bellenguez et al. 2022). MAF refers to the frequency of which the second most common allele occurs in a population. Genomes from several thousand disease and control cases are screened to identify common genetic variants such as single nucleotide polymorphisms (SNPs) associated with a disease. Genotype imputation prior to GWAS analysis can help increase the number of genetic variants tested for association, including low frequency and rare variants (Marchini and Howie 2010). Several lowly penetrant, common genetic variants have been identified from large meta-analysis studies, comparing SNPs across several thousand AD case and control individuals (Lambert et al. 2009; Lambert et al. 2013; Witoelar et al. 2018; Kunkle et al. 2019; Bellenguez et al. 2022). SNPs giving a signal at or above the defined threshold of genome wide significance (P=5 x10^-8) are associated with risk of developing AD. These common variants typically have a small effect size (odds ratio 1.2) and often lie in non-coding regions, therefore the most proximal gene to the SNP is typically assigned genetic association. This is a limitation of GWAS, in not being able to identify exact disease causal variants. Genetic association can however be further directed through candidate gene prioritisation strategies such as: 1) annotation and gene based testing for deleterious coding, loss of function and splicing variants; 2) expression quantitative loci analysis (eQTLs); 3) evaluation of transcriptomic expression in LOAD clinical traits such as

correlation with BRAAK stage, and differential expression in AD vs. control brains; 4) evaluation of transcriptomic expression in AD relevant tissues and finally 5) gene cluster/pathway analyses (Kunkle et al. 2019).

Over the past decade, AD GWAS, investigating large and diverse patient cohorts have identified around 75 common genetic risk loci in developing LOAD (Figure 1.5) (Lambert et al. 2009; Lambert et al. 2013; Jonsson et al. 2013; Witoelar et al. 2018; Jansen et al. 2019; Kunkle et al. 2019; Bellenguez et al. 2022). GWA studies have highlighted the complex genetic architecture of LOAD, where both protective and deleterious variants have been identified. Particularly noteworthy was the observation that several identified risk genes (including *CD33*, *MS4A6A/MS4A4*, *CLU*, *CR1*, *ABCA7*, *SPI1* and *EPHA1*) were selectively or preferentially expressed in microglia relative to other cell types in the brain. Rare coding variants in microglial genes, *TREM2*, *PLCG2* and *ABI3*, were also discovered, further adding to the evidence of microglial functions and immune response in AD pathogenesis (Sims et al. 2017). Discovery of such genes brings us away from the traditional neuro-centric perspective of AD, to one that encompasses other cell types e.g. immune cells. Pathway enrichment analysis has further identified specific sets of genes involved in common pathways such as endo-lysosomal function (*BIN1*, *CD2AP*, *SORL1* and *PICALM*), cholesterol and lipid metabolism (*TREM2*, *PLCG2*, *ABCA7*, *INPP5D* and *PLD3*) and amyloid/tau processing (*ADAM10*, *ADAMTS1*, *ACE*, *BIN1*, *FERMT2*, *PTK2B*, *CASS4* and *PICALM*) (Jones et al. 2010; Hardy et al. 2014; Kunkle et al. 2019; Sims et al. 2020). Genetic findings from the most recent 2022 GWA study further consolidated involvement of tau binding proteins and APP/Aβ peptide metabolism in LOAD processes. The study implicated for the first time the APP locus at genome wide significance and a number of other genes (*ADAM17*, *ICA1L*, *DGKQ*, *ICA1*, *DOC2A*, *WDR81* and *LIME1*) likely to modulate APP metabolism (Bellenguez et al. 2022).

The roles of these genes are clearly complex, and with still much to be learnt, however genetic evidence is beginning to fit with existing models of AD pathology e.g. Amyloid Cascade (See section: 1.5.1) and the Cellular Phase (See section: 1.5.3)

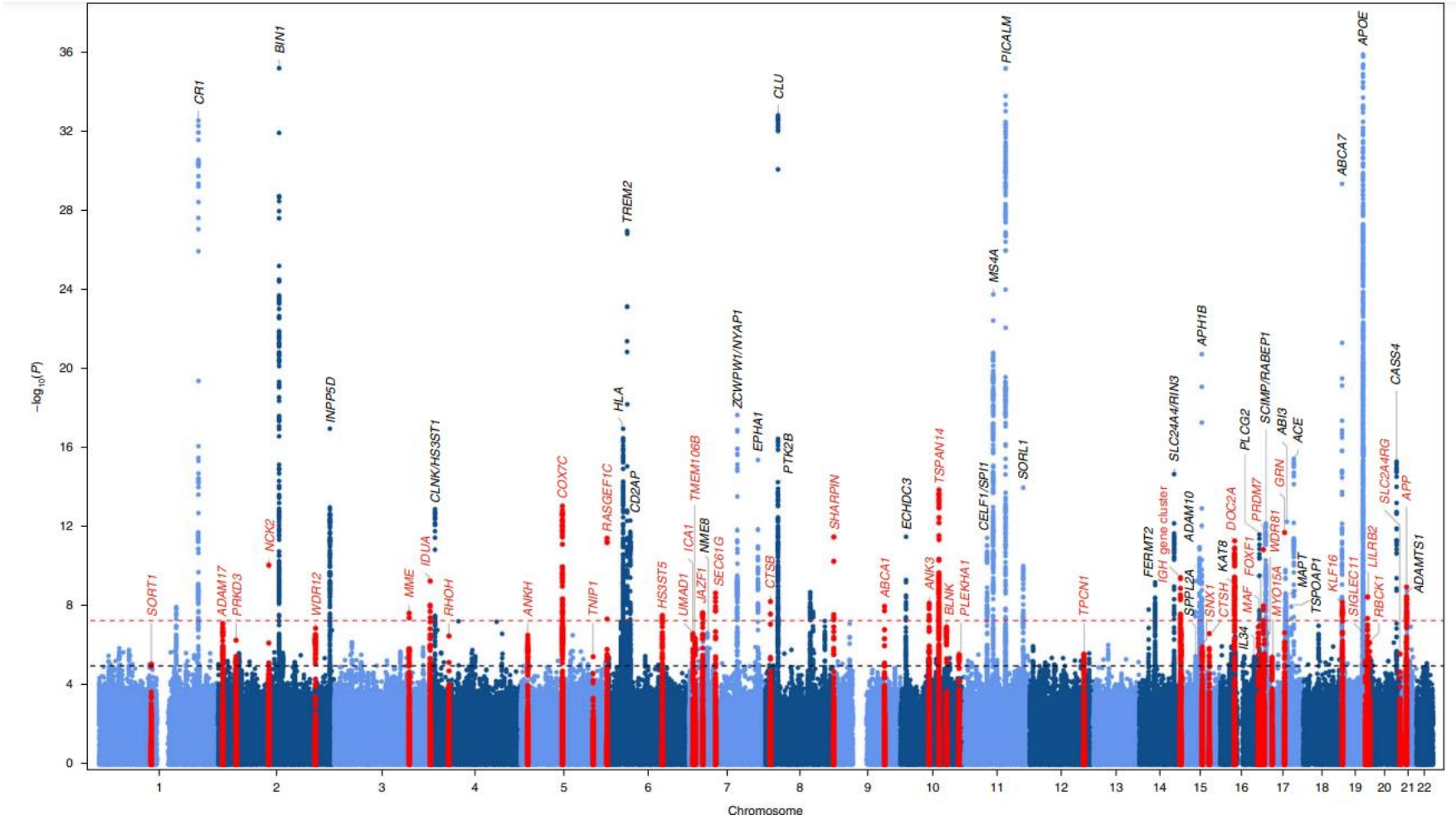

Figure 1.5: Genetic loci implicated in risk of developing LOAD.

Loci with genome wide significance (P= 5X10-8) are annotated with loci previously identified in black and newly identified in red. The red dashed line represents the level for genome wide significance whilst the black dotted line represents the suggested significance level (P=1X10-5). (Figure taken from (Bellenguez et al. 2022).

1.4.4. Rare Coding Variants

Although GWAS have made powerful strides in identifying common genetic variants underlying LOAD pathology, a large proportion (~60%) of genetic variance remains un-accounted for (Grozeva et al. 2019). GWAS uses a targeted approach, genotyping pre-selected variants in a microarray and thus is limited in being able to identify all genetic determinants of complex traits. The remaining 'missing' heritability of AD could result from non-coding, regulatory variations, rare coding variants or even epigenetic variants, that remain largely undetected by GWAS to date (Lord et al. 2014).

In the more recent years, with advancements to sequencing technologies, the focus of the field has shifted towards detecting rare variants in AD. Whole genome sequencing (WGS) is a comprehensive way of analysing entire genomes, aiming to capture all the genetic variation on an individual. This benefits detection of rare genetic variants, however, is expensive when conducted on large cohorts, and requires complex data handling. Alternatively, whole exome sequencing (WES) is used to sequence the protein coding portions of genes within the genome and has significant advantage in identifying variants that are easier to functionally characterise in cellular or animal models (Lord et al. 2014). WGS and WES have successfully identified novel rare variants such as the R47H missense variant in *TREM2* (Jonsson et al. 2013) and the V232M variant in *PLD3* (Cruchaga et al. 2014) associated with increased AD risk, but also rare variants in the *APP* (A637T) and *APOE* (L28P, R145C and V236E) loci that confer protection (Jonsson et al. 2012; Medway et al. 2014). Exome microarray based studies, such as that performed by Sims and colleagues, have also contributed to finding novel rare coding variants in *PLCG2* (P522R), *ABI3* (S209F) and *TREM2* (R62H), which despite their low frequency have strong biological effects (Sims et al. 2017; Yeh et al. 2016; Magno et al. 2019; Maguire et al. 2021; Karahan et al. 2021). Given the larger effect size and resulting protein coding changes of rare variants compared to common variation its paramount efforts are focused on identifying novel rare variants, where biological functions can be easily modelled *in silico*, *in vitro* or *in vivo*.

1.4.5. Polygenic Risk Score

Our understanding of genes underlying LOAD risk has grown such that it is possible to calculate an individual's risk of an AD diagnosis using polygenic risk scores (PRS). It is increasingly clear multiple genetic loci act in concert to cause disease, each with varying effect sizes. Most of the common variance attributed to LOAD typically have small effect sizes (odds ratio 1.0-1.2) with the exception of *APOE* and *TREM2*. PRS has shown to

accurately predict 75-84% of LOAD cases based on area under the curve (Escott-Price et al. 2015), which captures the cumulative effect of all genetic risk loci, both above and below the genome wide significance threshold (P<5x10^8). Combining these scores with other external factors affecting disease risk can provide a better idea into the risk of disease onset, progression, as well as treatment response. PRS can be a useful resource at the early stages of disease when symptoms are very general and non-specific, having the greatest potential benefit for those at high risk of AD where prognosis and intervention can be made much earlier.

1.5. Mechanisms of Alzheimer's Disease Pathology

1.5.1. The Amyloid Cascade

The amyloid cascade hypothesis is the prevailing mechanistic theory for AD which posits Aβ accumulation in the brain parenchyma is the primary driver for AD pathogenesis (Hardy and Allsop 1991). Increased production and aggregation of the more neurotoxic $A\beta_{42}$ species induces a series pathogenic events including, synaptic dysfunction, inflammation, altered neuronal ionic homeostasis, increased oxidative stress and finally tau hyperphosphorylation which leads to tau aggregation and formation of NFTs. These cytotoxic events result in widespread neuronal damage and cell death which ultimately leads to dementia (Hardy and Selkoe 2002).

The basis of the amyloid hypothesis emerged from both histopathological and human genetic findings. For instance, the Aβ peptide is the primary component of AD associated senile plaques (Masters et al. 1985), and 'familial' forms of AD are linked to mutations in *APP* and *PSEN1/2* genes that are involved in Aβ formation (Lanoiselée et al. 2017; Weggen and Beher 2012). Furthermore, the *APOE* genotype, currently the strongest genetic risk factor for LOAD, supports the idea that Aβ accumulation lies central to AD pathogenesis. For example, carriers of the APOE-ε4 isoform, that have markedly increased AD risk, display reduced clearance of Aβ (Castellano et al. 2011). There is also strong evidence implicating apoE in amyloid metabolism, where APP transgenic mice deficient in APOE, present decreased cerebral Aβ deposition (Bales et al. 1997). Human biomarker studies also confirm Aβ deposition precedes other AD related changes, such as increased tau CSF, changes in glucose metabolism, brain atrophy and cognitive decline, supporting a model whereby Aβ is the initiator of AD pathogenesis, followed by neurodegeneration and lastly clinical dementia (Jack et al. 1999; Bateman et al. 2012). The relationship between Aβ and tau pathology is

complex. *In vivo* genetic studies provide evidence that mutations in *APP*, which elevate Aβ deposition, lead to downstream alteration and aggregation of wild-type tau, however tau mutations do not lead to Aβ deposition and amyloid related dementia (Lewis et al. 2001; Selkoe & Hardy, 2016). This bolsters the theory that Aβ pathology precedes tau pathology. Nonetheless, tau is proposed to still play a crucial role in Aβ induced neurotoxicity (Rapoport et al. 2002).

Despite strong evidence supporting the amyloid hypothesis and the more recent success of Aβ targeting therapies, Aducanumab and Lecanemab (Sevigny et al. 2016; van Dyck et al. 2022), several Aβ-centric therapies have failed at preclinical trials. This has led to criticism of the amyloid hypothesis and reflection over its existing evidence. The main rebuttal being that there is poor correlation between Aβ deposition and the severity of cognitive decline. Around 30% of individuals exhibiting Aβ deposition have preserved cognitive functions (Rodrigue et al. 2009) without developing dementia in their lifetime, whilst some individuals clinically diagnosed with AD have very few amyloid deposits (Edison et al. 2007; Li et al. 2008). Such observations suggest the idea that Aβ deposition is rather a phenomenon of aging and has no direct relation with the onset of AD. There is also some evidence to suggest that tau pathology is better correlated with neuronal loss and thus cognitive impairment (Arriagada et al. 1992; Gómez-Isla et al. 1997). Nonetheless, the presence of Aβ is necessary for NFTs to spread throughout the brain (Musiek & Holtzman, 2015).

Revisiting evidence for the amyloid hypothesis has refocused attention on the soluble oligomeric forms of Aβ, that better correlate with synaptic dysfunction and neuronal loss than insoluble amyloid fibrils/plaques (McLean et al. 1999; Mc Donald et al. 2010; Koffie et al. 2009). Shankar and colleagues demonstrate soluble oligomeric Aβ, isolated from the cortex of AD patients, dose dependently decreased synaptic function and number, resulting in memory deficits of healthy adult rats. Alternatively, AD plaques isolated from the same brains did not impair long term potentiation (Shankar et al. 2008). Not only the solubility but also the propensity to aggregate affects Aβ toxicity, where the longer length, more aggregation prone $A\beta_{42}$ species is considered more neurotoxic than the shorter length Aβ species, $A\beta_{40}$ (Selkoe 2006). Moreover, individuals with high plaque abundance do not always get dementia. This controversial phenomenon can in part be explained by the oligomer to plaque ratio, whereby individuals without dementia exhibit a lower oligomer to plaque ratio than those who are mildly demented and with similar plaque densities (Esparza et al. 2013). Upon reappraisal of the amyloid hypothesis new ideas have formed, such that amyloid plaques may serve as ‘sinks’, sequestering toxic soluble oligomers until reaching a physical limit to which excess oligomers diffuse into the surrounding synaptic membranes causing neurotoxicity (Gaspar et al. 2010; Selkoe & Hardy, 2016).

A convincing argument can be made that deposition of Aβ in the central brain is a crucial step to initiating downstream neurotoxic processes, in particular tau aggregation which goes on to mediate neurodegeneration. In conclusion, Aβ appears to be necessary but not sufficient in driving AD pathology. Despite our understanding about the formation and structure of the Aβ peptide, exact mechanisms underlying Aβ induced toxicity remain largely enigmatic and require further investigation.

One hypothesis is that the slow decline of biological processes throughout ageing renders us vulnerable to neurotoxic protein aggregates Aβ and tau, that deposit and accumulate throughout age. However, it takes a specific insult whether that be environmental, genetic or lifestyle to switch the balance from a physiologic state to one resembling AD pathology. To distinguish between disease causative factors from those purely consequential of ageing, requires better understanding of biological processes normative to ageing and to establish at what point do signature symptoms of AD emerge. For instance, travelling in a car without a seatbelt only becomes problematic when there is a crash. Similar to the idea that Aβ peptide accumulation in an aged brain only triggers cytotoxic events upon a specific insult i.e. under the correct pathological setting.

1.5.2. Microglia and Neuroinflammation

Microglia are the brains resident immune cells, responsible for CNS maintenance, injury response and defence against infection (Benarroch, 2013). In healthy brains, microglia reside in an ‘resting’ homeostatic state, constantly surveying their microenvironment for detection of pathogens or cellular debris. A critical function of microglia is to phagocytose and clear pathogens or cellular debris, such as dying neurons, aggregates, or misfolded proteins, for instance Aβ (Hansen et al. 2018). Other homeostatic functions of microglia include providing neurotropic support through secretion of factors such as glial-derived neurotrophic factor (GDNF) and brain-derived neurotrophic factor (BDNF), which can modulate neuronal survival and functions (Szepesi et al. 2018). Microglia also play an important role in synaptic pruning mechanisms which regulate the number of functional synapses and thus contribute to the plasticity of neural circuits (Hong et al. 2016). In response to pathological cues for instance invasion, injury or disease, microglia however, adopt an ‘activated’ state, undergoing morphological and transcriptional changes, whilst migrating toward the site of damage and initiating an immune response.

In AD, microglia’s role in pathogenesis is considered a ‘double edged sword’. In early stages of AD, the mounted immune response of microglia is thought to be beneficial, engulfing and

degrading secreted Aβ oligomers (Fan et al. 2017). Microglia recognise and bind soluble Aβ oligomers and fibrils through pattern recognition receptors on their surface such as CD36 and Toll like receptors (TLR) 4&6 which induces microglial activation, leading to secretion of proinflammatory cytokines and chemokines (Paresce et al. 1996; Bamberger et al. 2003; Stewart et al. 2010). Genetic ablation of these receptors has shown to decrease Aβ induced cytokine production, as well as prevent intracellular amyloid accumulation and inflammasome activation (Stewart et al. 2010; El Khoury et al. 2003). Furthermore, the secretion of neurotrophic factors from microglia like BDNF can help promote neuronal repair (Szepesi et al. 2018). On the other hand, sustained activation of microglia is considered detrimental to the progression of AD, where microglia promote synaptic loss through overstimulation of synaptic pruning mechanisms (Hong et al. 2016), sustained secretion of proinflammatory cytokines such as TNF-α, IL-6 and IL1-β, as well as inducing reactive oxygen species (ROS) production which are all detrimental to neuronal survival. Furthermore, critical microglial functions such as phagocytosis become impaired upon chronic activation leading to the inefficient clearance of Aβ and ultimately Aβ accumulation, which further drives neuroinflammation (Hickman et al. 2008).

The most prominent evidence of microglial involvement in AD comes from genetic findings where several microglial genes (refer to Table 1.1) have been associated with LOAD pathogenesis (Hollingworth et al. 2011; Lambert et al. 2009; Guerreiro et al. 2013). These immune associated genes do not fit in well with the amyloid cascade hypothesis, however functional studies reveal their importance in key microglial functions, particularly phagocytosis. For instance, TREM2 is an immune receptor expressed on microglia, important in facilitating the removal of neuronal debris via phagocytosis and has been implicated as a receptor for oligomeric Aβ to bind (Zhao et al. 2018). Furthermore, AD associated TREM2 mutations (R47H and R62H), have been shown to reduce binding of Aβ oligomers, thus impacting the clearance of Aβ (Zhao et al. 2018). Another example is CD33, a sialic acid binding immunoglobulin that helps regulate innate immunity. CD33 expression in microglia is increased in brains of AD patients and has been implicated in impaired uptake and clearance of $A\beta_{42}$ in microglia cell cultures (Griciuc et al. 2013). The CD33 AD associated SNP (rs3865444) is a loss of function mutation that confers protection against AD. It is associated with reduced CD33 expression in microglia and reduced insoluble $A\beta_{42}$ levels in the brain. Insoluble levels of Aβ are also markedly reduced in brains of CD33 -/- $APP_{swe}/PS1_{\Delta E9}$ transgenic mice, which makes a compelling argument for inhibition of CD33 as a therapeutic target to help mitigate Aβ pathology (Griciuc et al. 2013).

Collectively, evidence from human genetics points to the idea that regulating microglial activity could provide therapeutic benefit to AD pathogenesis. The therapeutic benefit of

modulating microglial activity is further supported by demonstration that pharmacological inhibition of microglial proliferation using CSFR1 inhibitors attenuates neurodegeneration in models of AD (Olmos-Alonso et al. 2016; Mancuso et al. 2019) and other experimental models of neurodegenerative diseases (Gomez-Nicola et al. 2013; Martínez-Muriana et al. 2016).

In summary, neuroinflammation is thought to possess dual functions in AD, playing a neuroprotective role during acute phase response but becoming detrimental when the response is sustained. Suppressing neuroinflammatory response is thought to preserve cognition and promote survival of neurons, as individuals whose brains are resilient to AD pathology exhibit high Aβ plaque burden and NFTs but reduced neuroinflammatory signature. Studies have found AD 'resilient' brains display distinct cytokine profiles, whereby these brains exhibit decreased astrocytic and microglial activation markers Glial Fibrillary Acidic Protein (GFAP) and Cluster of differentiation 68 (CD68). These studies strongly indicate suppressed neuroinflammatory response may contribute to human brain resilience to AD pathology (Barroeta-Espar et al. 2019). These studies from AD resilient brains makes a compelling argument that neuroinflammation is a clear driver of Aβ and NFT pathology.

1.5.3. The Cellular Phase

As our understanding of the cellular changes associated with AD grows, current theories and concepts of AD have evolved. For over 20 years the amyloid cascade has been the largest theoretical concept for AD, however, has been critiqued for its neuron-centric, linear view of AD pathogenesis and failure of amyloid targeting therapeutics. The cellular phase hypothesis however encompasses other cells within the brain and a modern genetic understanding of AD, involving a complex phase of cellular interactions between, neurons, microglia, astrocytes, and the vasculature (De Strooper & Karran, 2016). Microglia are recognised as one of the key players in the cellular phase responsible for phagocytic clearance of Aβ and neuronal debris, regulation of synaptic plasticity, as well as eliciting inflammatory responses (Ji et al. 2013; Heneka et al. 2015). A number of GWA studies undisputedly support a role of microglia in AD pathogenesis having revealed many susceptibility loci enriched in microglia and attributed to pathways within innate immune system regulation (refer to Table 1.1) (Lambert et al. 2013; Karch and Goate 2015). The cellular phase connects the well-defined biochemical phase (i.e. the appearance of amyloid plaques and neuronal tangles), to the clinical phase (i.e. the manifestation of dementia) that follows long after. The theory proposes proteopathic stress of Aβ and tau accumulation induces several cellular changes, whereby defective clearance mechanisms could result in

irreversible damage (De Strooper & Karran, 2016). This fits with current genetic evidence which has identified many genetic risk factors involved in clearance mechanisms, for instance *APOE-ε4*, *PICALM*, *CLU*, and *ABCA7* (Verghese et al. 2013; Zhao et al. 2015).

Evolving gradually over two decades, the cellular phase encompasses several feedback and feedforward mechanisms between cells, involving chronic inflammation, circuitry imbalances, defective clearance mechanisms and lipid metabolism, astroglia atrophy, myelin breakdown and compromised neuro-vasculature unit. Ultimately, the cellular reaction can no longer maintain homeostasis, resulting in dementia. In this modern view, Aβ and tau accumulations are considered risk factors with cellular factors being determinative of the evolution towards dementia (De Strooper & Karran, 2016). Systematically mapping the progressive cellular alterations that occur throughout AD over the next few years will be crucial to generating a comprehensive cellular theory of the disorder.

1.6. PLCG2

The phospholipase c-γ2 (*PLCG2)* gene has received much interest in the AD field, since the discovery of a rare coding variant (P522R/rs72824905) that confers reduced risk of developing LOAD (Sims et al. 2017). Additionally, as *PLCG2* encodes an enzyme, it represents the first classically druggable target for LOAD to be identified from GWAS.

1.6.1. The PLC Family

Phospholipase c (PLC) enzymes are a diverse class of calcium dependent, membrane associated phosphodiesterases found in both prokaryotes and eukaryotes (Gresset et al. 2012). In mammals, so far 13 PLC isozymes have been identified and categorised in to 6 subtypes; δ, β, ε, γ, ζ and η, which all serve as important cell signal transducers, playing a key role in phosphoinositide metabolism (Gresset et al. 2012). Various extracellular stimuli such as, neurotransmitters, hormones and growth factors activate PLC enzymes in an isozyme dependent fashion, resulting in the hydrolysis of membrane bound phosphatidylinositol-4,5-bisphosphate (PI(4,5)P2) into secondary messengers' inositol 1,4,5 triphosphate (IP3) and diacylglycerol (DAG). In turn, IP3 induces intracellular Ca^{2+} release from the endoplasmic reticulum and DAG activates protein kinase c (PKC), which mediates cellular functions unique to PLC isozymes such as, cell proliferation, differentiation, secretion, and migration (Figure 1.6) (Suh et al. 2008; Rebecchi and Pentyala 2000). G-protein coupled receptor activation and activation through receptor and non-receptor tyrosine kinases are considered the major mechanisms involved in regulation of PLC signalling,

where the former activates PLC-β subtypes and the latter PLC-γ (Gresset et al. 2012). Specific members of these subclasses (PLC-β1 and PLC-γ2), as well as the PLC-ε subgroup can also be activated by multiple Ras superfamily GTPases (Harden & Sondek, 2006).

Whilst all PLC enzymes catalyse the same reaction (hydrolysis of PI(4,5)P2 into secondary messengers IP3 and DAG), the expression pattern, mode of activation and cellular functions differ among the six isoforms (Rebecchi and Pentyala 2000; Nakamura and Fukami 2017).

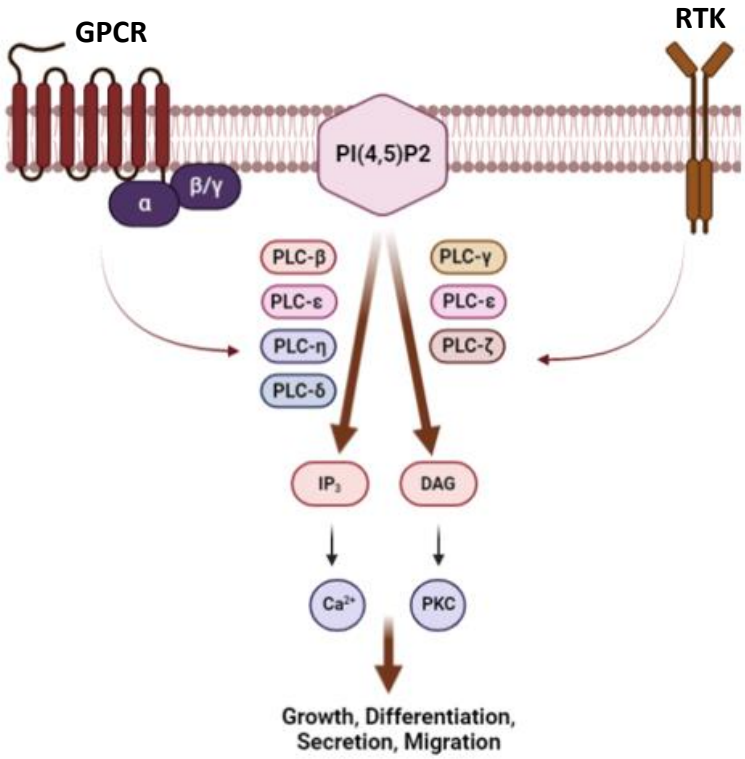

Figure 1.6: Activation and function of PLC isozymes.

Activation of PLC enzymes is isozyme dependent. PLC-β subtypes are activated by G-protein coupled receptors (GPCR), through various mechanisms (not shown), whilst PLC-γ isozymes are activated through receptor tyrosine kinases. PLC-ε subtypes can be activated by both GPCRs and RTKs via distinct mechanisms. The mechanism of activation for PLC-η, PLC-δ, PLC-ζ isozymes are yet to be distinguished. PLC enzymes play a common role in catalysing the hydrolysis of PI(4,5)P2 to produce secondary messengers IP3 and DAG. IP3 and DAG are involved in the release of intracellular Ca^{2+} and activation of PKC, respectively. PLC isozymes regulate downstream cellular functions in growth, differentiation, secretion, and migration.

1.6.2. PLCs Structure

The protein structure of PLC enzymes plays an important part in their biological functions (Figure 1.7). Structurally, eukaryotic PLC enzymes are organised into a string of modular protein domains, sharing a common core structure of a N-terminal pleckstrin homology (PH) domain, four EF hand motifs, a highly conserved catalytic core split into X and Y domains and a C-terminal C2 domain (Rebecchi & Pentyala, 2000). The catalytic domain of PLC enzymes is comprised of a conserved protein folding structure, known as a triose phosphate isomerase (TIM) barrel, formed by alternate folding of eight α helices and eight parallel β sheets. The TIM barrel is important for the catalytic activity of PLC isozymes, as it forms the active site required for substrate recognition, calcium binding and catalysis. Eukaryotic PLC enzymes hydrolyse phosophinositols in order of specificity from PI(4,5)P2>PI(4)P>PI (Rebecchi & Pentyala, 2000) .

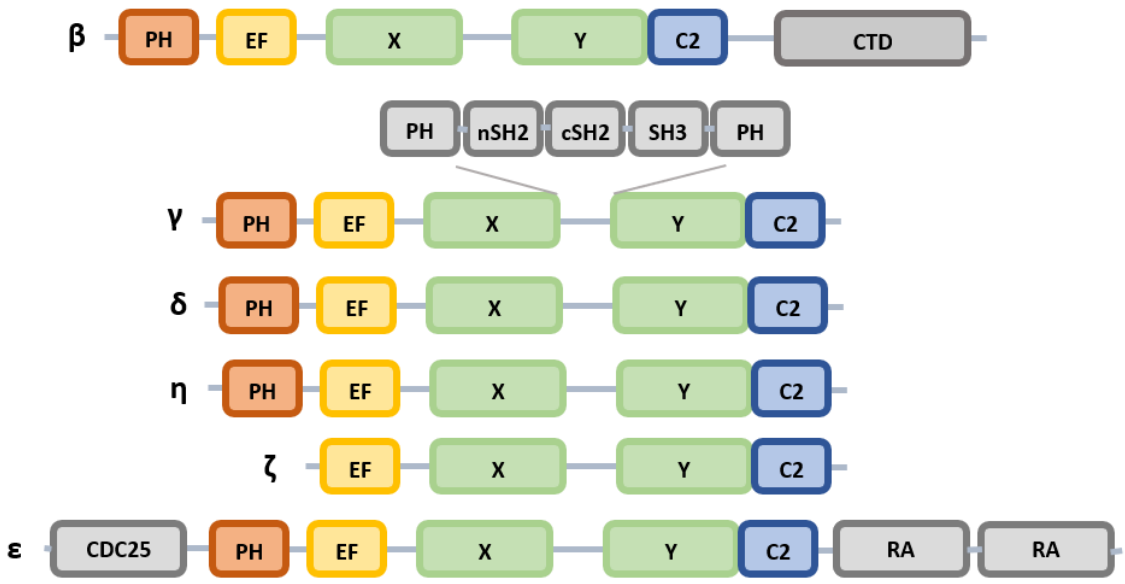

Figure 1.7: Domain organisation of PLC isozymes.

PLC isozymes are organised into a string of modular protein domains commonly comprising of a pleckstrin homology (PH) domain, EF hands, a catalytic domain (X-Y) and a protein kinase C conserved region (C2) domain. Domains unique to each PLC subtype is shown in grey. Abbreviations: CTD: c-terminal domain, C2: protein kinase C conserved region 2, nSH2: n-terminal Src homology-2 domain, cSH2: c-terminal Src homology-2 domain, SH3: Src homology-3 domain, CDC25: cell cycle division 25 (Ras GEF domain) and RA: Ras-association domain.

A single N-terminal PH domain is found in all PLC enzymes besides the PLC-ζ subgroup and is responsible for phosphoinositide binding specificity of PLC isoforms, for instance PLC-δ and PLC-γ have high affinity to PI(4,5)P2 and phosphatidylinositol (3,4,5) triphosphate (PI(3,4,5)P3) respectively (Rebecchi & Pentyala, 2000). In some cases, the PH domain mediates interaction with the heterotrimeric G protein subunit Gβγ, such as for PLC-β2 and PLC-β3 isoforms. An additional PH motif is found in PLC-γ1 and 2, split between two tandem Src homology-2 (SH2) and one Src homology 3 (SH3) domains, that lie within the X and Y catalytic region (Nakamura & Fukami, 2017; Rebecchi & Pentyala, 2000). The SH2 and SH3 domains enable specific protein-protein interactions. For instance, SH2 domains allow PLCy binding to specific phosphorylated tyrosine residues on activated RTKs, whilst the SH3 domain is required for PLC-γ dependent activation of phosphatidylinositol-3-OH kinase (PI3K) enhancer (Ye et al. 2002). Finally, the C2 domain and EF hands are thought to provide important regulatory functions and whilst the C2 domain supports enzymatic activity in an Ca^{2+} dependent manner, there is currently little evidence existing for Ca^{2+} promoted regulation of PLC enzymes through the EF hands (Rebecchi & Pentyala, 2000).

This thesis will focus on the PLC-γ (herein referred to as PLCG) subfamily and in particular the AD associated gene *PLCG2*.

1.6.3. Expression and Functions of PLCG2

Two distinct PLC enzymes are present in mammals, encoded by separate genes, *PLCG1* and *PLCG2* which share high sequence and protein domain homology, however, perform independent, non-redundant functions, owing to their distinct expression profiles (Homma et al. 1989). Being ubiquitously expressed, PLCG1 regulates multiple cellular functions in various tissues including cellular differentiation, migration, survival and mitogenic signalling. PLCG1 null mice are embryonic lethal, demonstrating the critical importance of PLCG1 functions (Ji et al. 1997). PLCG1 is also the major effector for T (immune) cell signalling, which not only is required for T cell activation but also their development and homeostasis (Fu et al. 2010).

PLCG2 expression however is restricted to cell types primarily of the hemopoietic lineage in the peripheral immune system and in the brain is predominantly expressed by microglia (Magno et al. 2019). Like other members of the PLC family, PLCG2 catalyses the hydrolysis of PI(4,5)P2 into secondary messengers IP_3 and DAG. Specifically, PLCG2 is activated upon tyrosine phosphorylation by receptor and non-receptor tyrosine kinases, which includes a variety of immune cell receptors such as the B cell and Fc receptor (Wang et al. 2000).

PLCG2 plays critical roles in B cell development, as well as survival and antibody production of mature B cells (Jackson et al. 2021) such that PLCG2 knockout (KO) mice exhibit impaired B cell maturation, downregulation to pro-survival factors such as Bcl-2 and an inability to transduce downstream signalling of the B-cell receptor (BCR), which leads to failure in inducing Ca^{2+} influx (Wang et al. 2000; Hashimoto et al. 2000). Additional to B cell functions, PLCG2 regulates development and functions of other haemopoietic cells such as platelets, mast cells, neutrophils, and natural killer cells through Fc receptor signalling (Wang et al. 2000). PLCG2 deficient mice demonstrate reduced mast cell degranulation, an inflammatory response involving the release of mediator molecules, such as antimicrobial molecules from internal secretory granules (Wang et al. 2000). PLCG2 is also thought to contribute to leukocyte recruitment to sites of inflammation, whereby deletion of PLCG2 reduces neutrophil rolling velocity compared to wildtype cells (Mueller et al. 2010). In iPSC derived macrophages, loss of PLCG2 results in changes to expression of surface markers and phenotypes such as reduced phagocytic activity and survival, although pro-inflammatory response, measured by the release of TNF-α and IL-6, was unaffected. PLCG2 KO in macrophages also compromised cell adhesion and migration (Obst et al. 2021). Gain of function mutations in PLCG2 have been implicated in immune disorders such as, PLCG2 associated antibody deficiency and immune dysregulation (PLAID) and autoinflammatory-PLAID (APLAID) which leads to immune dysregulation, antibody deficiency and autoinflammation, emphasising PLCG2's role in regulation of immune cell functions(P. Yu et al. 2005).

PLCG2 functions downstream of TREM2 in microglia and macrophages, regulating similar genetic pathways (Andreone et al. 2020; Obst et al. 2021). Downstream of TREM2, PLCG2 promotes several microglial functions such as phagocytosis, cell survival and lipid metabolism. Additionally, PLCG2 signals downstream of TLRs, independent of TREM2 signalling, to mediate inflammatory responses (Andreone et al. 2020). TREM2 is a transmembrane receptor expressed on myeloid cells which also has a strong genetic link to AD, with many TREM2 variants presenting as increased risk for LOAD (Guerreiro et al. 2013; Sims et al. 2017).

In addition to TREM2, PLCG2 also interacts with other proteins expressed by genes that have been linked to AD, such as *TYROBP (DAP12)*, *CD33* (*Singlec3*) and *INPP5D (SHIP1*) (Figure 1.7), implicating a common disease mechanism for AD. These genes are preferentially expressed in microglia and are involved in innate immune pathways.

DAP12 is an adaptor protein that associates with TREM2. Upon activation, TREM2 signals through DAP12 which contains an immunoreceptor tyrosine-based activation motif (ITAM), that becomes phosphorylated and recruits Syk, a tyrosine kinase that goes on to activate

PLCG2 by phosphorylation (Figure 1.7). Mutations in the *TYROBP* locus have been described in a cohort of EOAD patients and is also upregulated in LOAD (Pottier et al. 2016). Furthermore studies have recently implicated Syk in orchestrating neuroprotective functions of microglia, such that its deletion was found to limit microglial phagocytosis of Aβ and thus exacerbate Aβ deposition in a 5XFAD mouse model of AD. Disruption of Syk signalling has also been shown to disrupt acquisition of disease-associated microglia, alter AKT-GSK-3β signalling as well as aggravate cognitive defects in the 5XFAD mouse model (Ennerfelt et al. 2022; Schafer and Stillman, 2022).

CD33 is another transmembrane immunoreceptor expressed on myeloid cells, specifically microglia, which recognises sialic acid residues as their ligands. CD33 harbours an immunoreceptor tyrosine-based inhibitory motif (ITIM), which when phosphorylated acts as a docking site for phosphatases such as Src homology domain containing inositol polyphosphate 5-phosphatase 1 (SHIP1). SHIP1 is a critical regulator of immune cell activation, which opposes the pro-inflammatory signal from ITAM receptors by inhibiting effector molecules like Syk that are involved in downstream activation of PLCG2 (Wißfeld et al. 2021). This blocks TREM2 signalling, suppressing microglial activation and TREM2 induced phagocytosis in microglia (Peng et al. 2010). Moreover, SHIP1 poses an inhibitory effect on PI3K signalling through dephosphorylation of PIP3 back into PIP2 (Pauls & Marshall, 2017). Both *CD33* and *SHIP1* (*INPP5D*) have been reported as risk genes for LOAD (Bertram et al. 2008; Malik et al. 2015; Lambert et al. 2013).

Collectively, these data suggest PLCG2 plays a central role in a complex network of AD risk genes, that are also highly expressed in microglia and therefore presents an interesting target for modulating microglial function in AD. Further investigation into the role of PLCG2 and its AD associated variant (P522R), will thus be of benefit for understanding how the P522R variant contributes to protective mechanisms of AD.

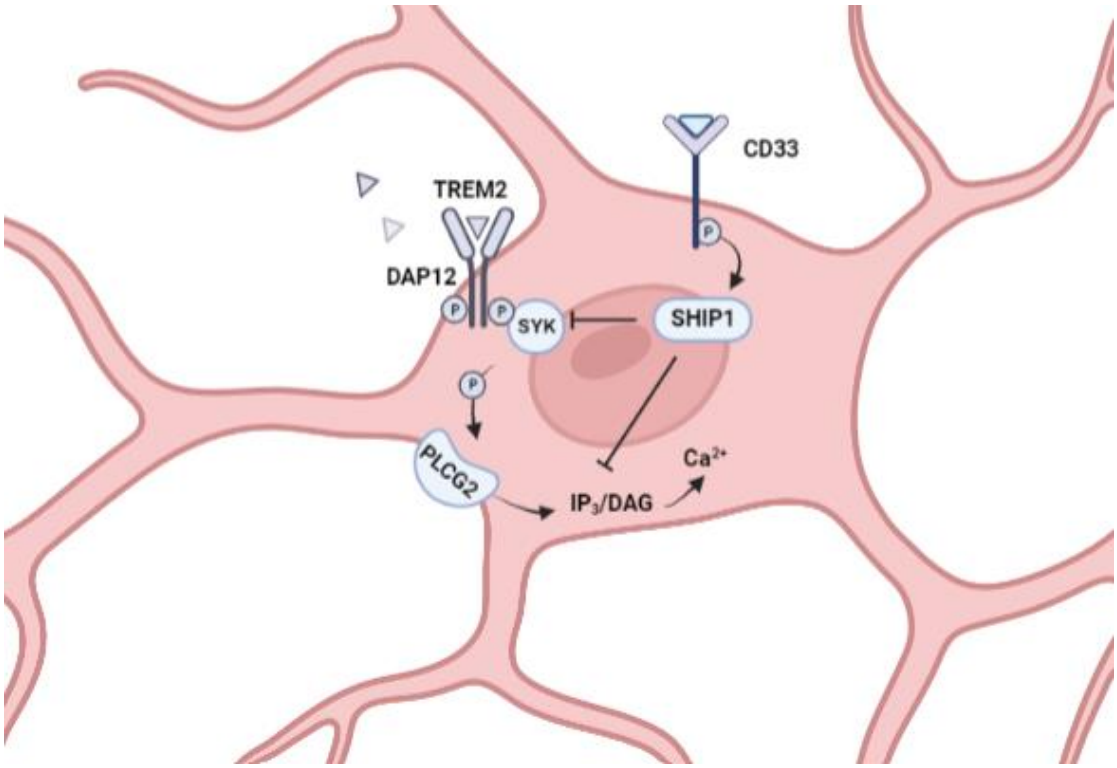

Figure 1.8: PLCG2 interacts with other AD associated genes in a complex network to regulate microglial signalling pathways.

TREM2 receptor signals through DAP12-Syk-PLCG2 to activate microglial phagocytosis and inflammatory. Contrastingly, activated CD33 recruits SHIP1 which inhibits Syk, PLCG2 signalling, to ultimately oppose microglial activation and mediated pro-inflammatory responses. Image adapted from (Hodges et al. 2021).

1.6.4. Phosphoinositides

Phosphoinositides (PIPs) are phosphorylated derivatives of the membrane phospholipid, phosphatidylinositol (PI), representing around 10-20% (mol%) of total cellular phospholipids in eukaryotes (Wenk et al. 2003). Seven PIP species exist, distributed throughout the cytoplasmic leaflet of the plasma membrane, each with unique subcellular localisation where they regulate diverse cellular processes, including signal transduction, cytoskeletal reorganisation, membrane dynamics, vesicular trafficking, and cell death (Phan et al. 2019). PIP turnover is dynamically yet tightly regulated by lipid kinases and phosphatases that add or remove phosphates on to or from hydroxy groups at positions 3,4 or 5 of the inositol ring of PI, resulting in mono (PI(3)P), PI(4)P, PI(5)P), bi (PI(3,4)P2, PI(3,5)P2, PI(4,5)P2) and tri-phosphorylated (PI(3,4,5)P3) derivatives (Figure 1.8). These small signalling lipids are enriched in the brain and have well-established roles in both homeostasis and disease,

whereby dysregulation of PIP levels and signalling have been highlighted in several forms of dementia, including AD (Volpatti et al. 2019; Stokes and Hawthorne, 1987; Landman et al. 2006; Moloney et al. 2010). Moreover, phospholipid metabolism has been implicated in AD through genetic studies whereby several AD risk genes such as *PLCG2*, *INPP5D*, *PLD3*, *CD2AP* and *PICALM* have associated roles in PIP metabolism (Tan et al. 2019; Sims et al. 2020).

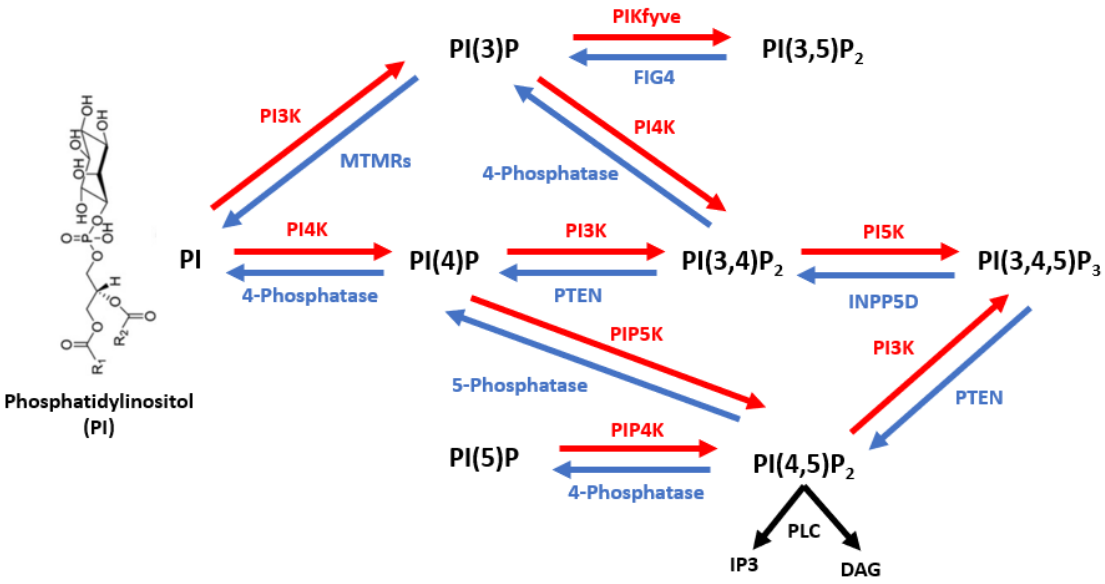

Figure 1.9: Phosphoinositide metabolism in the mammalian cell.

Metabolic pathways regulating the turnover of PIP species. Lipid kinases (red) phosphorylate positions 3, 4 or 5 of the inositol ring generating phosphorylated derivatives of PI, whilst lipid phosphatases (blue) remove the phosphate groups. Black lines indicate the PLC hydrolysis of PI(4,5)P2 to produce secondary messengers IP3 and DAG.

1.6.4.1. PI(4,5)P2 and PI(3,4,5)P3 Species

For this thesis we have focused on PI derivatives PI(4,5)P2 (herein PIP2) and PI(3,4,5)P3 (herein PIP3). PIP2 and PIP3 constitute less than 1% of the membrane phospholipids yet direct two major independent signalling cascades. PIP2 is formed primarily from sequential phosphorylation at position 4 and 5 hydroxyl residues of PI by PI4-kinase (PI4K) and PI-5 kinase (PI5K) respectively and is the primary substrate of PLC enzymes. PIP2 hydrolysis produces secondary messengers IP3 and DAG which in turn directs Ca^{2+} signalling and PKC activation. PIP3, can be subsequently generated from PIP2 via PI3K dependent phosphorylation at position 3 hydroxyl residue and is the major effector of PI3K signalling (Tariq & Luikart, 2021). The formation of PIP3 leads to the downstream activation of PKB

Protein Kinase B (AKT), which is the central regulator for cell growth, metabolism, protein translation, cytoskeletal organisation, membrane trafficking and survival (Laplante & Sabatini, 2009). PIP3 can be converted back into PIP2 upon dephosphorylation by PTEN. PI3K and PTEN work antagonistically to tightly maintain homeostatic levels of PIP2 and PIP3 in the cells, which is pivotal to maintaining various cellular signalling cascades that control cell polarisation, phagocytosis, and migration (Desale & Chinnathambi, 2021).

PIP2 and PIP3 control a variety of cellular processes in the brain, summarised in Table 1.2 (Phillips and Maguire, 2021). As such, disruption to PIP2/PIP3 metabolism has been suggested to critically influence the progression of neurodegenerative diseases such as AD. For instance, the genetic variant of PLCG2 (P522R), which confers reduced risk of AD, has been shown to increase PIP2 hydrolysis (Sims et al. 2017). Furthermore, downregulating synaptojanin, which also hydrolyses PIP2, was seen to increase clearance of amyloid plaques and improve behavioural deficits in AD mice (Zhu et al. 2013), whilst loss of function increased neuronal PIP2, resulting in defects in synaptic vesicle recycling (Cremona et al. 1999). Finally, increased activity of PI3K, an enzyme that generates PIP3, has been implicated in AD, where its downstream signalling through AKT and mammalian target of rapamycin (mTOR) activates pathways regulating oxidative stress, apoptosis, and autophagy (Chong et al. 2012).

Several pieces of evidence implicate PIP2/PIP3 dys-homeostasis in AD. One of the first indications being that levels of PIP2 are significantly reduced in the anterior temporal cortex of AD brains compared to controls (Stokes & Hawthorne, 1987). As well, presenilin mutations linked to familial AD result in aberrant PIP2 breakdown (Landman et al. 2006). Furthermore, it has been demonstrated accumulation of Aβ oligomers depletes PIP2 (Berman et al. 2008). Lowered levels of PI3K subunits (p85 and P110) are also found in AD brains, indicating reduced production of PIP3 from its precursor PIP2 (Moloney et al. 2010) . Not only does AD exhibit changes in PIP levels but differences in expression of regulatory enzymes have also been reported (Vasco et al. 2018).

PIP species	Known functions in the brain
PI(4,5)P2	• Cell signalling – transduction of signals from cell surface receptors • Regulates ~100 ion channels and transporters • Synaptic vesicle recycling and regulating synaptic plasticity • Regulates cytoskeletal function in neurons • Regulates Toll-like receptor and purinergic signalling • Actin remodelling during phagocytosis and chemotaxis • Involved in multiple steps of phagocytosis and other uptake systems
PI(3,4,5)P3	• Regulates neurotransmitter release • Increased levels of PI(3,4,5)P3 recruits protein kinases (ie AKT) to the plasma membrane • Regulates purinergic signalling • Actin remodelling during chemotaxis • Role in phagocytosis and other uptake systems

Table 1.2: Cellular functions of PIP2 and PIP3 within the brain.

1.6.4.2. PIPs Contribution to Microglia Function

An increasing body of evidence points to the involvement of PIPs in microglial function and microglial mediated neuroinflammation. These include functions such as endocytosis, toll-like receptor signalling, purinergic signalling, chemotaxis, and migration (Phillips and Maguire, 2021). Importantly, both PIP2 and PIP3 regulate remodelling of the actin cytoskeleton, which underlies cell processes such as phagocytosis and cell migration (Hilpelä et al. 2004). PIP2 and PIP3 are the main lipid derivatives involved in the process of phagosome formation and early endosome maturation during phagocytosis (Gillooly et al. 2001). Specifically, PIP2 initiates the process of phagosome formation and later on fusion with the early endosome, whilst PIP3 is involved in phagocytic cup formation and cell polarisation (Desale & Chinnathambi, 2021). Furthermore, PIP3 plays an important role in chemotactic signalling, whereby its accumulation induces actin polymerisation to promote lamellipodia mediated migration towards the chemoattractant (Desale & Chinnathambi, 2021). Imbalances in PIP2/PIP3 metabolism clearly impact microglial functions which maintain healthy brain homeostasis and therefore likely contribute to the progression of neurodegenerative phenotypes.

Co-manipulating microglial function alongside PIP metabolism could offer a new avenue for effectively targeting AD pathology. However, more research is required to firstly better understand how alterations in PIPs and their regulatory enzymes could affect microglial

functions and thereby contribute to progression of AD pathology. In this thesis, roles of PIP2 and PIP3 in glial biology are investigated and how regulating their metabolism influences neurodegenerative phenotypes associated with $A\beta_{42}$ toxicity.

1.6.4.3. Measuring PI(4,5)P2 and PI(3,4,5)P3

Common methods to detect PIPs have traditionally relied upon biochemical methods that use chemical analysis of lipid extracts from biological samples e.g. mass spec and Enzyme Linked Immunosorbent Assay (ELISA). Whilst such methods are sensitive and quantitative, they are often applied to whole tissues and do not reveal the spatiotemporal dynamics of PIPs at the single cell-level (Dickson & Hille, 2019). Furthermore, the relatively low abundance of PIPs in the cell membrane and similarities in chemical properties makes it harder to detect and distinguish between individual PIP species using such approaches.

The generation of genetically encoded fluorescent PIP probes that exploit lipid-binding properties of protein domains has been a major technical advance to the field, allowing dynamic, optical, real-time monitoring of individual PIP species at a single cell resolution. This approach involves fluorescently tagging a phosphoinositide binding domain at the N or C terminus with Green Fluorescent Protein (GFP) or one of its variants – YFP, which can then be visualised under confocal microscopy (Balla & Várnai, 2002). A variety of phosphinositide-binding modules have to date been characterised with distinct affinities and specificities to the inositide head group of specific PIPs (Halet, 2005). The pleckstrin homology (PH) domain (~120aa) is the largest family of phosphoinositide binding domains that interact with membrane phosphoinositides through establishing hydrogen bonds with specific phosphates in the PIP headgroup (Lemmon & Ferguson, 2000). Experimental studies, using biophysical techniques such as surface plasmon resonance, isothermal titration calorimetry and förster resonance energy transfer (FRET), as well as molecular dynamic simulations have provided strong evidence for the distinct membrane-binding properties of specific PH domains (Scott et al. 2012). For instance, the phospholipase C δ1 (PLCδ1) PH domain has been shown to bind specifically and with high affinity to membranes containing PI(4,5)P2 (M. Rebecchi, Peterson, and McLaughlin 1992; Cifuentes, Delaney, and Rebecchi 1994; Garcia et al. 1995) and the general receptor of phosphoinositides-1 (GRP1) PH domain to PI(3,4,5)P3 (Corbin et al. 2004; Pant and Tajkhorshid 2020).

1.7. Current Therapeutic Strategies for Alzheimer's Disease

Over the last several decades AD research has exploded in scope and scale and whilst great efforts have been made towards understanding mechanisms underlying disease pathogenesis, there has been little success in finding a therapy that delays or halts the underlying disease progression. Many of the current therapies are limited to providing symptomatic relief such as cholinesterase inhibitor medications - Donepezil, Rivastigmine and galantamine. These have shown to moderately improve cognitive function by preventing the breakdown of acetylcholine, a key neurotransmitter in the brain important for neuronal communication (Nguyen et al. 2021).

Alternatively, other therapeutics have been designed around the amyloid cascade hypothesis, targeting the production or clearance of the Aβ peptide, which is considered to be a primary driver of AD pathology. Therapies intervening with Aβ production involve inhibition or modulation of β or γ secretase activity, the key enzymes involved in cleavage of its precursor, APP (Roberson & Mucke, 2006). Stimulating α secretase activity can also reduce Aβ, as the enzyme cleaves within APP to precede Aβ formation (Ishiura et al. 2013). Targeting γ secretase activity has been slightly more problematic given its ability to cleave other substrates including Notch. Selectively interfering with APP binding by targeting the substrate docking site of γ secretase can however overcome this (Wolfe, 2006). Additionally, modulating opposed to inhibiting γ secretase activity could also provide a workaround. For instance, nonsteroidal anti-inflammatory drugs that allosterically modulate γ secretase, favour the production of $A\beta_{40}$ over $A\beta_{42}$ and are in phase III clinical trials (Eriksen et al. 2003; Lleó et al. 2004). On the other hand, β secretase has fewer substrates and less potent side effects upon gene KO in mice. β secretase thus proves to be a prime target for inhibiting Aβ production, whereby its genetic elimination has shown to prevent memory deficits in APP transgenic mice. Nonetheless current BACE1 inhibitors in clinical trials were discontinued due to lack of cognitive and functional benefit, despite showing effective reduction of Aβ in the CSF of AD patients (Vaz and Silvestre, 2020).

Another promising branch of Aβ targeting therapies that work on promoting Aβ clearance involve immunotherapy-based approaches. Aducanumab, the first Food and Drug Administration (FDA) approved disease-modifying drug for AD is a monoclonal antibody targeting Aβ aggregates including soluble oligomers and insoluble fibrils. Aducanumab has demonstrated to dose dependently reduce amyloid deposition in the brain and ultimately help reduce amyloid plaque burden (Sevigny et al. 2016). Given the success of Aducanumab and now also Lecanemab, immunotherapies in AD have gained much interest,

with strategies for targeting tau, microglia, and the gut-brain axis under development (Novak et al. 2018; Wang et al. 2020).

Various other strategies for therapeutic intervention of AD have also been proposed. For instance, targeting tau tangles through modulating kinases, such as glycogen synthase kinase - 3β (GSK-3β), involved in tau phosphorylation (Matsunaga et al. 2019), or by modulating environmental conditions such as metal ions (Wang et al. 2020). Being such a complex disorder, it is unlikely treatment of AD will fit a one drug fits all scenario. Future therapeutic strategies need to be designed around our current understanding of disease risk.

1.8. Modelling Alzheimer's Disease

To develop new AD therapeutics, it is essential we have a range of appropriate model systems to test in. Transgenic models for AD have been particularly pertinent in gaining insight into the molecular underpinnings of AD throughout various stages of disease progression, as well as providing the opportunity to test therapeutics in *in vivo* systems.

Reproducing hallmark neuropathological lesions seen in AD, such as Aβ plaques and NFTs, has been the mainstay of several transgenic AD models. Largely directed by the amyloid hypothesis, most transgenic models are engineered to overproduce $A\beta_{42}$ species, either through overexpression of human familial Alzheimer's disease (FAD) associated mutant APP (with or without FAD associated PSEN 1-2 mutations), or in some cases by direct expression of human $A\beta_{42}$. Models probing tau pathology have also been generated through overexpression of wildtype or mutant forms of human tau. Despite the increasing number of AD transgenic models for various species ranging from *Caenorhabditis elegans (C.elegans)* to mice (*Mus Musculus*), it is important to highlight that no single model currently reproduces all aspects of AD pathology together and are only able to recapitulate specific pathological features (Spires & Hyman, 2005).

1.8.1. Transgenic Mouse Models

Mice are mammals like humans and share a high degree of molecular and cellular homology, making them an excellent model organism to study aspects of AD pathology and for therapeutic treatment testing. Mice can perform complex behaviours, such as learning and memory, for which several established methods that phenotypically characterise

cognitive decline and neurodegeneration exist. Techniques permitting genetic modification in mice are also well developed, enabling the study of various gene functions. Currently, there are over a dozen mouse models attempting to replicate AD pathology using various strategies.

Most transgenic mouse models for AD are based on overexpressing transgenes containing FAD associated mutations. The PD-APP mouse model was the first successful APP-based model, which used the platelet derived growth factor-β (PDGF) promoter to drive overexpression of the human APP transgene containing the FAD associated mutation (V717F) (Games et al. 1995). Overexpression of human FAD associated mutant APP has been widely used to model amyloidosis in mice. Such models display common features of AD like neuropathology, such as age dependent Aβ deposition and accumulation, extracellular diffuse and neuritic plaques, dystrophic neurites, synaptic loss, gliosis, and cognitive impairment (Spires & Hyman, 2005). Bi-genic models, co-expressing human FAD mutant APP and PS1 transgenes have also been developed, however, lead to earlier and more extensive plaque pathology than single mutant APP transgenic models (Borchelt et al. 1997). In effort to better recapitulate the full spectrum of AD pathophysiology, triple transgenic mice (3xTg-AD) harbouring PS1 (M146V), APP (Swe), and Tau (P301L) transgenes have been made, which display marked NFT pathology following amyloid deposition, in addition to inflammation, synaptic dysfunction and cognitive decline (Oddo et al. 2003). Despite the characteristic Aβ and tau pathology, these mice do not show signs of neurodegeneration. Also, the combined overexpression of three mutant transgenes makes this model highly artificial. Such limitations of this model may attribute to its lack of translational findings.

In more recent years, APP knock-in mouse models have been created to overcome potential artefacts introduced from APP overexpression. Mice models such as the APP^{NL-G-F}, use a knock-in approach to express APP, harbouring three pathogenic FAD associated mutations (KMG670/67NL (Swedish), I716F (Iberian) and E693G (Artic) (Nilsson et al. 2014). APP is expressed at physiological levels but the combined effect of these three pathogenic mutations elevates levels of toxic Aβ. The Swedish mutation promotes total Aβ production, the Iberian mutation increases the $Aβ_{42}$:$Aβ_{40}$ ratio, whilst the Artic mutation promotes Aβ aggregation through facilitating oligomerisation and reducing proteolytic degradation (Citron et al. 1992; Guerreiro et al. 2010; Nilsberth et al. 2001). These mice models exhibit an aggressive form of amyloidosis, developing plaques as early at two months. In addition, extensive gliosis, synaptic loss, and age associated cognitive impairments are visible relatively early on. However, despite increased presence of phosphorylated tau in dystrophic

neurites, NFTs and neurodegeneration are absent in this model, which is one of the main caveats to its use (Nilsson et al. 2014).

Mouse models have provided invaluable insight in AD neuropathology, pointing to the toxic roles of soluble Aβ oligomers and tau, the differential toxic effects of various Aβ species ($A\beta_{40}$ vs $A\beta_{42}$), as well as the interaction between Aβ and tau pathology (McGowan et al. 2005; Lewis et al. 2001; Elder et al. 2010). Direct evidence that tau is essential in mechanisms leading that Aβ induced neurodegeneration have been shown in mouse models, whereby cultured hippocampal neurons from tau KO mice exhibit no signs of degeneration when treated with fibrillar Aβ. However, neurons expressing either mouse or human tau degenerate in the presence of Aβ (Rapoport et al. 2002). In addition to understanding important roles of pathogenic species Aβ and tau, mouse models have also implicated the phagocytic role of microglia in Aβ plaque clearance (Wyss-Coray & Mucke, 2002). Mice have also been used in modelling AD risk gene variants, enabling researchers to elucidate genetic risk mechanisms involved in AD pathology (Zhu et al. 2012; Xiang et al. 2018; Andrews et al. 2019; Takalo et al. 2020; Cuddy et al. 2020).

1.8.2. Invertebrate Models of Alzheimer's Disease

Although mice are used extensively to model AD, more recent years have seen the increased use of invertebrate model organisms such as *C.elegans* and *Drosophila*. Whilst invertebrate models are further removed phylo-genetically to humans, they offer a simpler, genetically tractable, *in vivo* system to uncover genetic functions and dissect underlying pathways involved in AD pathogenesis. Experimental outputs are generally much quicker and allow for a higher statistical power than what can be routinely achieved in murine models, which is conducive to large scale experiments. Furthermore, the ease of handling, lower cost and well characterised nervous system makes invertebrates an attractive model for studying of neurodegenerative diseases.

Although invertebrates express orthologs of EOAD associated genes, *APP* and *PSEN1/2*, there is no endogenous production of $A\beta_{42}$ peptides in either worms or flies (Luo et al. 1992; Periz and Fortini, 2004; Daigle and Li, 1993). To circumvent the lack of endogenous $A\beta_{42}$ production, various models have been engineered to overexpress human APP, Aβ and/or tau (Fernandez-Funez et al. 2015), which have been valuable to revealing new insights of AD pathology. *Drosophila* have been particularly pertinent in identifying genetic modifiers of tau and Aβ induced toxicity (discussed in section: 1.9.5) (Chatterjee et al. 2009; Cao et al. 2008; Rival et al. 2009; Shulman and Feany, 2003; Shulman et al. 2014; Dourlen et al.

2017). Furthermore, *C.elegans* have been used to study effects on the Aβ sequence and its propensity to aggregate, identifying Leu17Pro and Met35Cys as key aa substitutions blocking formation of *in vivo* amyloid deposits (Fay et al. 1998).

With benefits and drawbacks to each model system, their success is largely dependent on the degree of homology at the molecular, cellular and tissue level between the human and candidate organism. As multiple transgenic models exist in a variety of organisms, the challenge comes down to choosing the 'right' model for the scientific question. It is important not to make conclusions from any one model system in isolation but always with appreciation of other systems and above all the pathology seen in humans.

1.9. The *Drosophila* Model System

The common "fruit fly'', *Drosophila melanogaster* are a widely used model system for understanding molecular mechanisms of human disease. *Drosophila* are a genetically tractable system, with four chromosomes, low genetic redundancy, and a fully sequenced genome, facilitating complex genetic analyses. Moreover, approximately 75% of human disease related genes have orthologs in the *Drosophila* (Reiter et al. 2001), indicating several molecular mechanisms underlying disease in humans are evolutionary conserved in the fly. Flies provide a relatively low cost, easier to breed alternative to mammalian models, with rapid generation times (~10 days) and shorter lifespan. Furthermore, with fewer ethical constraints, such as home office licences, flies can be considered as a replacement for mammalian models in research. Furthermore, a female fly can lay up to 100 eggs per day, enabling large sample sizes to be generated in a single experiment (Roote & Prokop, 2013). Anatomically, the fly brain is much smaller and simpler in comparison to mammals, with no cortical or hippocampal regions. Nonetheless, the ellipsoid and mushroom bodies, in the fly brain are functionally analogous to these regions, respectively. The ellipsoid body has been linked to short term (working) memory and attention of the fly during task performance, whilst mushroom bodies are important for olfactory learning and memory (Akalal et al. 2006a; Grover et al. 2022; Roman & Davis, 2001). Flies can perform a wide range of complex behaviours such as learning and memory, circadian rhythms, sleep, feeding, and social behaviours including courtship and aggression, demonstrating their brains are capable of higher order cognitive functions, similar to mammals (McGuire et al. 2005; Konopka and Benzer, 1971; Shaw et al. 2000; Al-Anzi et al. 2010). Whilst many parallels can be drawn between flies and mammals, there also exits some notable differences for instance, flies do not have an adaptive immune system or immune associated microglia cells (refer to section 1.9.2). Additionally, the fly ortholog of APP, APPL, is processed differently and therefore flies

do not endogenously produce Aβ oligomers (refer to section 1.9.3). Nonetheless, flies boast an extensive range of genetic tools, including ribonucleic acid interference (RNAis), mutants, fluorescent reporters, etc, allowing the study of gene functions in any given cell type and at any life stage. For these reasons, flies have been indispensable for research, uncovering functions of conserved genes and molecular mechanisms that may contribute to disease.

1.9.1. Genetic Tools for *Drosophila* Research

A major advantage of *Drosophila* as a model organism is the range of genetic tools available to manipulate genes/pathways and thus study their roles in a simpler *in vivo* system to mammals. A commonly used tool by fly geneticists to study cell autonomous gene functions is the binary UAS/GAL4 expression system (Brand & Perrimon, 1993). It is comprised of the yeast (*Saccharomyces cerevisiae)* derived transcriptional activator, Gal4 and its target sequence, the upstream activating sequence (UAS). Gal4 is constructed downstream of a tissue specific promotor, enabling its expression in a tissue specific manner. The UAS site is a cis-acting regulatory sequence, that upon binding of Gal4 leads to expression of its adjacent transgene. Ubiquitous, somatic or germline tissue specific Gal4 drivers can be used to express any transgene downstream of a UAS, such as complementary DNA (cDNA), fluorescent reporter, or RNAi etc in any given cell type. In particular, for the benefit of this study, there exits several genome-scale *in vivo* RNAi libraries, available from public stock centres, widening the repertoire of genes that functions can be studied in a spatial and temporal manner.

The temperature sensitive Gal80 mutant ($Gal80^{ts}$), also derived from yeast, adds an additional level of gene expression regulation, being able to temporally control gene expression at permissive temperatures (McGuire et al. 2004). At 18°C, Gal80 represses Gal4 transcriptional activity, binding directly to the Gal4 activation domain. This prevents Gal4 from binding to the UAS and subsequent expression of the adjacent transgene. At temperatures 29°C or higher, a conformational change in Gal80 causes it to dissociate from Gal4, permitting expression of the gene of interest. This simple yet sophisticated mechanism enables both spatial and temporal regulation of gene expression and is of particular advantage when bypassing developmental lethal phenotypes of genes expression. This expression system has been employed throughout this thesis to study glial specific functions of conserved AD risk genes at adulthood specific stages (Figure 1.10).

Another important tool in flies, used to maintain deleterious mutations in stable stocks, are balancer chromosomes. Balancer chromosomes are a unique set of specialised

chromosomes preventing recombination through a series of Deoxyribonucleic Acid (DNA) inversions (Lindsley et al.1992).

The combination of extensive genetic tools, conservation of human AD risk genes and practicality makes the fly ideal for investigating AD risk gene association, enabling validation of gene targets and pathways prior to testing in mammals or cells. The powerful genetics of the fruit fly might help us to interpret the results of GWAS of AD patients, enabling us to triage genetics before testing them in mammals and cell lines.

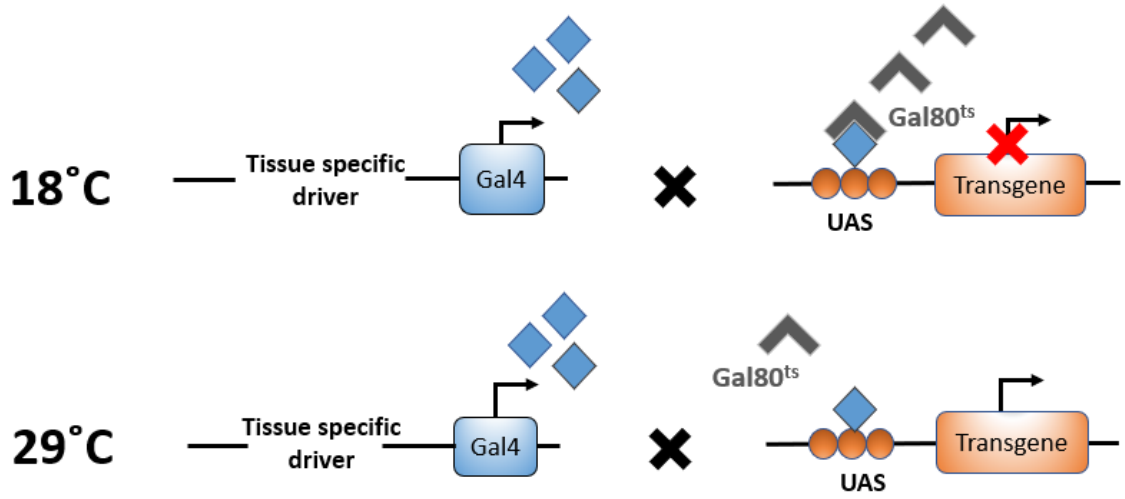

Figure 1.10: Schematic of the Gal80^{ts}/Gal4 expression system controlling spatial and temporal transcriptional activation of transgenes.

Gal4 transcriptional activity is regulated by the temperature sensitive Gal80 mutant which represses Gal4 activity at temperatures 18°C or lower, however dissociates from Gal4 at temperatures 29°C or higher, allowing Gal4 to bind upstream activating sequences, resulting in transgene expression. The tissue specific driver directs cell autonomous transgene expression whilst the temperature sensitivity of Gal80 temporally regulates transgene expression.

1.9.2. Glia in Drosophila

The *Drosophila* nervous system (central (CNS) and peripheral (PNS)) performs many analogous functions to its human and mammalian counterparts, from movement to memory. The adult fly brain, although relatively smaller to mammals, is complex and well characterised, housing over 200,000-300,000 neurons and several glial subtypes (Figure 1.11). In the fly brain, glia represents around 10% of the total brain cell population (Freeman, 2015) and are split into three main classes, characterised by their morphology and association with neurons. These include i) the surface associated glia, that form the outermost layer of the nervous system, ii) the cortex associated glia, which tightly ensheath neuronal cell bodies, and iii) the neuropil associated glia (Stork et al. 2012; Freeman 2015). Wrapping glia, ensheathing glia and astrocytic glia are all categorised under neuropil associated glia, for which the former is found only in the PNS and the latter two in the CNS. Wrapping glia ensheath individual axons or axon bundles, which serves to support fast transmission of action potentials. This glia most resemble non-myelinating vertebrate

Schwann cells that envelop bundles of axons to form Remark fibers (Stork et al.2012). Ensheathing glia extend their processes around the neuropil, ensuring compartmentalisation between the neuropil and cortex region. This subtype of glia is most analogous to mammalian microglia in that they have shown to possess phagocytic functions, clearing up neuronal debris in response to axonal injury (Doherty et al. 2009). In contrast to ensheathing glia, astrocytes extend their processes densely into the synaptic neuropil, forming a dense meshwork of fine processes surrounding the synapses. *Drosophila* astrocytes bear the strongest morphological, molecular, and functional similarities to mammalian astrocytes (Awasaki et al. 2008; Stork et al. 2014; Tasdemir-Yilmaz and Freeman 2014). Similar to mammals, astrocytes in *Drosophila* express neurotransmitter transporters required for clearance of neurotransmitter, such as glutamate or GABA from the synaptic space, which is vital for animal behaviour and survival (Rival et al. 2004; Stork et al. 2014).

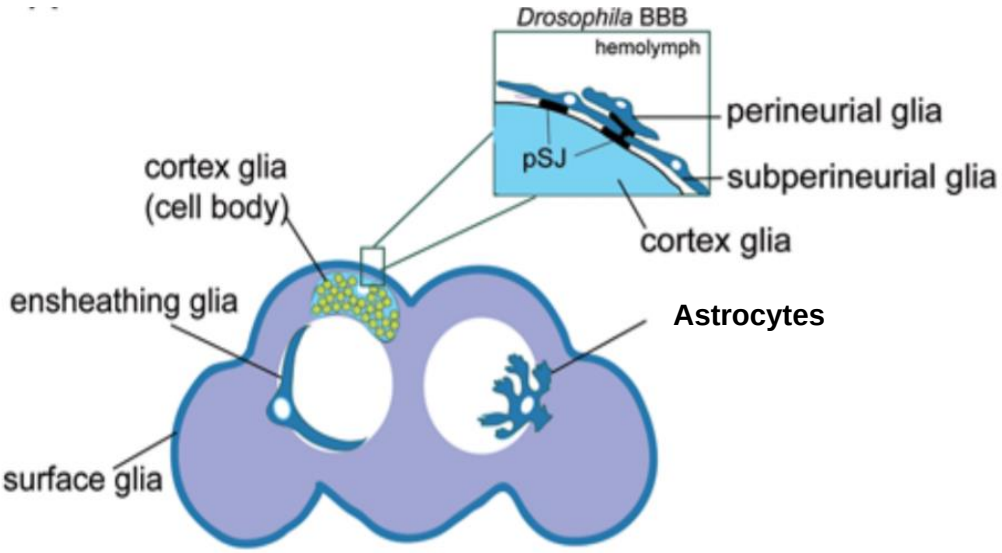

Figure 1.11: Schematic of glial subtypes located in the Drosophila brain.

Cross-sectional view of the Drosophila brain with locations of the six glial subtypes: surface glia (comprised of perineurial and subperineurial glia), cortex glia, ensheathing glia and astrocytes. Figure taken from (Ou et al. 2014).

Despite anatomical differences between the fly and mammalian brain, several specialised glial functions are well conserved. This includes 1) neurotrophic support mechanisms, 2) recycling of neurotransmitters e.g glutamate and GABA, 3) a subtype of glia capable of ensheathing nerves and axons, with similarity to mammalian Remak bundles and finally 4) the ability to perform immune-related functions, responding to pathogens and neuronal damage (Booth et al. 2000; Rival et al. 2004; Doherty et al. 2009; Stork et al. 2012). Since

flies do not have an adaptive immune system, the innate immune system constitutes important host defences against the invasion of pathogens, consisting primarily of Toll, Immunodeficiency (Imd), and Janus Kinase protein and the Signal Transducer and Activator of Transcription (JAK-STAT) pathways that are highly conserved across *Drosophila* and mammals. In particular, the Imd and Toll pathways are important in regulating the production and release of antimicrobial peptides from the fat body into the haemolymph, which serves as primary immune effectors in warding off systemic infection (de Gregorio et al. 2002; Govind, 2008). Phagocytosis is another fundamental innate immune mechanism involved in the engulfment of invading pathogens and clearance of neuronal debris. Whilst flies do not possess the immune associated microglia cells found in mammals, the ensheathing glia subtype adopt similar phagocytic functions that are capable of engulfing degenerating axons through the Draper pathway, highly conserved with the MEGF10 pathway in mammals (Doherty et al. 2009; MacDonald et al. 2006).

Drosophila have provided great insight into the contributions of glia in the development and homeostasis of the nervous system, uncovering important neuro-glial interactions. Studies have demonstrated *Drosophila* glia actively participate in the modulation of neuronal stem-cell behaviour (Chell and Brand, 2010; Ebens et al.1993), the regulation of synapse formation and function through the secretion of glial derived factors (Fuentes-Medel et al. 2012; Kerr et al. 2014), as well as sculpting of synaptic connections and axonal pruning (Keller et al. 2011; Ou et al. 2014). It is therefore clear glia in *Drosophila* are major modulators of neuronal development and function, whereby bi-directional communication between glia and neurons serves as a basis for the mechanisms underlying neurodegenerative diseases.

The conservation of specialised glial functions and the range of genetic tools developed to study them, makes *Drosophila* well positioned to gain insight into glial biology, relevant to higher order organisms. For this thesis, *Drosophila* glia were used to dissect the broad roles AD risk genes play in equivalent human glia.

1.9.3. Modelling Aβ Toxicity in *Drosophila*

Drosophila have an ortholog of the human *APP* gene, called *Appl*, exclusively expressed in neurons. Like human APP, Appl is cleaved by multiple orthologous secretases (α,β,γ) (Rooke et al. 1996; Carmine-Simmen et al. 2009; Fossgreen et al. 1998). Appl plays important roles in axonal transport, neuronal outgrowth, as well as synaptic changes. In the adult nervous system, Appl promotes neuronal survival and its cleavage has been shown to

prevent glial death (Wentzell et al. 2012; (Bolkan et al. 2012). The fly *Appl* gene shares about 30% sequence identity with the major human APP_{695} isoform, however the Aβ domain in Appl lacks significant homology (Luo et al. 1990; Rosen et al. 1989). Furthermore, whilst a β-secretase like enzyme was identified in flies *Drosophila beta-site APP-cleaving enzyme* (dBACE), it has much lower secretase activity than its human homolog (Carmine-Simmen et al. 2009; Yagi et al. 2000). As a consequence, there is no endogenous production of Aβ in the fly. Although, overexpression of the full length *Appl* was shown to be cleaved by *Drosophila* β secretase enzyme, producing a neurotoxic Aβ like peptide that leads to amyloid deposits, progressive behavioural decline, and neurodegeneration (Carmine-Simmen et al. 2009).

In addition to endogenous Aβ production, various transgenic models aiming to replicate Aβ pathology in flies have been developed. A triple transgenic fly model, expressing human APP and BACE1 along with the *Drosophila* homolog of Presenilin, dPsn have been generated and widely used to model Aβ toxicity (Greeve et al. 2004). Co-expression of human APP and BACE1, along with secondary cleavage by the endogenous fly γ-secretase leads to modest production of Aβ peptides including $Aβ_{40}$ and $Aβ_{42}$, demonstrating effective human BACE1 activity in the fly and downstream functionality of the *Drosophila* γ secretase. These flies develop Aβ deposits and experience age dependent degenerative phenotypes such as photoreceptor cell loss, severe axonal degeneration, and early lethality (Greeve et al. 2004). Expression of human presenilin FAD mutant (*L235P*) further enhanced these neurodegenerative phenotypes, whilst loss of function dPsn mutant (*psnB3)* rescued them, highlighting neurodegeneration is dependent on γ secretase activity. This triple transgenic system engineered by Greeves and colleagues has particularly aided investigation into APP processing, as well identifying inhibitors of β and γ secretases that are potential targets for the treatment and/or prevention of AD.

Alternatively, direct expression of human $Aβ_{40}$ or $Aβ_{42}$ proteins through the secretory pathway is another approach to overproduce human Aβ peptides in the fly. This is achieved by fusion of the Aβ peptide sequence with a signal peptide at the N-terminus, ensuring its secretion from the cell (Finelli et al. 2004; Crowther et al. 2005). Such approach has enabled cell targeted expression of Aβ peptides and thus the ability to separately dissect the toxicity of $Aβ_{40}$ and $Aβ_{42}$ in the brain, pinpointing mechanisms of Aβ toxicity. For instance, Iijima and colleagues used this system to highlight only $Aβ_{42}$ peptides form Aβ deposits, despite both $Aβ_{40}$ and $Aβ_{42}$ peptides accumulating in the fly brain (Iijima et al. 2004). They also showed only overexpression of $Aβ_{42}$ in the nervous system resulted in dose dependent neurodegeneration that increased with age. Locomotor deficits, reduced survival, impaired short-term memory, as well as retinal degeneration were some of the phenotypes observed

upon overexpressing human $A\beta_{42}$ pan-neuronally (Finelli et al. 2004; Iijima et al. 2004) Furthermore, flies engineered to overexpress the $A\beta_{42}$ peptide sequence with FAD-related Artic mutation (E22G), known to increase the rate of $A\beta_{42}$ aggregation (Nilsberth et al. 2001), accelerated neurodegenerative phenotypes, which is consistent with the earlier onset of AD in humans harbouring this mutation (Crowther et al. 2005).

1.9.4. Modelling Tau Toxicity in *Drosophila*

In current fly models expressing $A\beta_{42,}$ neurofibrillary structures are not detected and therefore do not fully recapitulate the full spectrum of AD pathology as seen in the human brain. However, fly models to investigate tau pathology have also been created.

A single homolog of the human tau gene (*MAPT*) exists in *Drosophila*, sharing 46% identity and 66% similarity with corresponding human tau sequences (Giong et al. 2021). Despite modest sequence divergence, the *Drosophila* tau protein possess conserved tubulin binding repeats, enabling its interaction with neuronal microtubules and the actin cytoskeleton, as is the case with mammalian and human tau (Heidary & Fortini, 2001). Furthermore, several tau targeting kinases such as GSK-3β, CDK5 and MARK1 are conserved in the fly (Jackson et al. 2002; Shulman and Feany, 2003; Nishimura et al. 2004). Endogenous expression of fly tau is non-pathogenic, however overexpression of the fly tau in neurons or the eye induces apoptotic neuronal cell death (Chen et al. 2007).

Flies have been engineered to overexpress either human wildtype or Frontotemporal Dementia with Parkinsonism (FTDP) linked tau mutations (R406W, V337M) (Wittmann et al. 2001; Jackson et al. 2002). Overexpression of human wildtype or FTDP-mutant tau in the nervous system results in adult onset, progressive neurodegeneration, characterised by nuclear fragmentation and vacuolisation in the brain (Wittmann et al. 2001). Tau transgenic flies also exhibit early death and accumulation of abnormally phosphorylated and folded tau, however the formation of NFTs is not detected (Wittmann et al. 2001). The severity of these phenotypes is shown to increase dose dependently upon introduction of FTDP-mutant tau isoforms, such as R406W and V337M. In addition, targeted expression of wildtype or mutant human tau in the retina induced retinal degeneration, characterised by reduced size and rough appearance (Jackson et al. 2002).

In aiming to better replicate the full spectrum of AD pathology, Folwell and colleagues have created a fly model concomitantly expressing human $A\beta_{42}$ and wildtype tau protein, allowing mechanisms underlying their interaction to be explored. They demonstrated co-expression of $A\beta_{42}$ enhanced tau induced neurodegenerative phenotypes, such as behavioural deficits,

reduced survival and disruption of axonal transport, which were ameliorated upon treatment with Lithium Chloride, an inhibitor of the tau kinase GSK-3β. (Folwell et al. 2010). This highlighted GSK-3β may be involved in the mechanism by which $A\beta_{42}$ and tau interact to cause neuronal dysfunction. Furthermore, the exacerbating effects of $A\beta_{42}$ were independent of tau levels or its propensity to aggregate.

These represent some of the main *Drosophila* models for studying AD, however, as our understanding of AD grows, newer models emerge to encapsulate modern theories of AD pathology.

1.9.5. Modifiers of $A\beta_{42}$ and Tau Induced Toxicity

Drosophila models have been widely used in large scale genetic screens, revealing several modifiers of $A\beta_{42}$ and tau induced toxicity. Changes in locomotion, survival or rough eye phenotype are easily quantifiable indicators of neurodegeneration and commonly screened when assessing genetic modifiers of AD in flies. In two separate unbiased genetic screens, dominant modifiers of $A\beta_{42}$ induced toxicity were identified from screening a library of over-expression lines (EP elements) (Cao et al. 2008; Rival et al. 2009). Notably, both screens identified important roles of transition metals, copper (Cu^{2+}) (Cao et al. 2008) and iron (Rival et al. 2009) in modifying phenotypes of $A\beta_{42}$ overexpression i.e. rough eye phenotype or survival deficits. Cao et al identified a putative mutation in the Cu^{2+} transporter (ATP7) which enhanced $A\beta_{42}$ rough eye phenotype (Cao et al. 2008), whilst Rival and colleagues demonstrated the iron binding protein, ferritin, suppressed $A\beta_{42}$ survival deficits and reduced oxidate damage in the fly brain (Rival et al. 2009). In particular, Rival highlighted production of oxidative stress, by the Fenton reaction was a significant contributor to $A\beta_{42}$ toxicity (Rival et al. 2009).

In addition to pathways involved in metal ion homeostasis, Cao and colleagues identified several other genetic modifiers of the $A\beta_{42}$ rough eye phenotype, including *Drosophila* orthologs of carboxypeptidase D (CPD), the δ subunit of the Adapter Protein complex 3 (AP3), Adenosine Monophosphate (AMP) kinase γ subunit and SIN3A, implicating the secretory pathway, cholesterol metabolism and processes of chromatin regulation in mediating toxic effects of $A\beta_{42}$ (Cao et al. 2008).

In identifying modifiers of tau induced toxicity, several large-scale genetic screens have been conducted. In one of the first genetic modifier screens, investigating molecular mechanisms involved in tau induced neurodegeneration, Shulman and Feany took an unbiased approach,

screening a library of 2276 EP transposable elements, to identify dominant modifiers of tau induced rough eye phenotype. Kinases and phosphatases were among the largest group of modifiers to be identified, which included orthologs of kinases such as cyclin-dependent kinase 5 (CDK5) and GSK-3β (Shulman and Feany, 2003). These results emphasised the importance of tau phosphorylation in regulating tau toxicity. Others have since added to these findings, highlighting the role of PAR-1, the fly homolog of MARK in modifying tau toxicity (Nishimura et al. 2004), as well as mechanisms involved in ribonucleic acid (RNA) metabolism (Ambegaokar & Jackson, 2011). Direct candidate-based screens of conserved AD risk genes have also identified *Drosophila* orthologs of *CD2AP*, *FERMT*, *CELF1*, *CASS4*, *EPHA1*, *PTK2B*, *MADD* as modifiers of tau toxicity (Shulman et al. 2014; Dourlen et al. 2017).

In addition to identifying modifiers of $A\beta_{42}$ and tau toxicity, *Drosophila* have been employed in the functional characterisation of several important AD-associated genes. For instance, flies have demonstrated, mis-expression of ankyrin 2 (ANK2), the *Drosophila* ortholog of ankyrin 1 (ANK1), may drive AD like pathology, whereby its expression has been shown to regulate synaptic stability (Koch et al. 2008), as well as survival and memory (Higham et al. 2019). Furthermore, fly models have revealed mechanistic insight into the role of AD associated genes, *BIN1* and *PICALM*, in endo-lysosomal functions and glutamatergic transmission, respectively (Lambert et al. 2022; Yu et al. 2020). These studies provide clear examples that *Drosophila* models have provided valuable insight into features of AD pathology and specific modifiers.

1.10. Thesis Outline

The overarching aim of this study was to use *Drosophila* models in investigating glial specific roles of AD risk genes and elucidate potential mechanisms for which they contribute to AD pathogenesis. Approaches to explore glial roles of AD risk genes in *Drosophila* models have been outlined below.

1) To test the hypothesis that glial activity of AD risk genes contribute to a healthy ageing nervous system and longevity, a reverse genetic RNAi knockdown (KD) screen was performed. The screen employed a UAS/Gal4/Gal80^{ts} expression system (described in section: 1.9.1) to target gene KD of conserved AD risk genes, exclusively in glia at adult specific stages and then measured locomotor behaviour

and survival phenotypes. Knocking down AD risk genes whose activity is essential to glial functions is hypothesised to cause locomotor and/or survival deficits.

2) To further our understanding of PLCG2 role in glia, glial specific functions of the *Drosophila* ortholog, *small wing* (*sl)* and its substrates (PIP2) were characterised. This involved defining glial role of *sl* in viability, locomotor behaviour, survival, PIP2/PIP3 metabolism, as well as $A\beta_{42}$ accumulation, as to elucidate the contribution of glial *PLCG2/sl* in ageing and $A\beta_{42}$ related pathology. Both loss of function and gain of function phenotypes were assessed upon pan glial KD or transgenic overexpression of *sl*. Given hyperactivity of PLCG2 is protective of AD, it was hypothesised that reduced glial expression of the *PLCG2* ortholog, *sl* would be detrimental in models of amyloid pathology.

3) To determine how the PLCG2-P522R coding variant contributes to reduced risk of developing LOAD, transgenic fly models harbouring the human *PLCG2* wildtype vs AD protective P522R coding variant were created and functional differences modelled. For instance, glial specific roles in survival, locomotor behaviour, PIP2/PIP3 metabolism, as well as $A\beta_{42}$ driven pathology were characterised in flies expressing the common (P522) vs protective (R522) human PLCG2 AD variants. I proposed that glial expression of the AD protective R522 variant would be protective of amyloid related pathology.

Chapter 2 - Materials and Methods

2.1. Fly Stock Maintenance

Fly stocks were maintained at room temperature on a 'Cornmeal-Molasses-Yeast' diet (Table 2.1) and flipped into fresh food medium every 3 weeks. All stocks were maintained in either vials or plastic bottles. Flies used in experiments were incubated either at 18, 25 or 30 degrees Celsius with a 12:12 hours light dark cycle as outlined in experimental designs for each chapter. Specific details of the fly crossing schemes are also included within experimental designs for individual chapters.

Fly Food component		Amount per litre
Agar (MIN GEL 920, BTP DREWITT)		6.4 g
Brewer's Yeast (903312, MP biomedical)		23.5 g
Cornmeal (901411, MP biomedical)		58.8 g
Molasses (62-118, FLYSTUFF SLS)		58.8 g
Tegosept (p-hydroxybenzoic acid) (102341, MP biomedical)		1.3 g
Acid Mix (~4 ml)	Propionic Acid	1.6 ml
	Phosphoric Acid	162.8 µl
	ddH_2O	2.1 ml
Ethanol		6.5 ml
ddH_2O		To final volume

Table 2.1: Components used for the 'Cornmeal-Molasses-Yeast' diet that flies were maintained on.

2.2. Fly Stocks

Fly stocks obtained from Bloomington *Drosophila* stock center (BDSC) (NIH P40OD018537) and Vienna *Drosophila* Research Center (VDRC) (www.vdrc.at) were used in this study. Fly stocks used throughout this thesis have been listed with details of their genotype, source, stock number and reference (Table 2.2 and 2.3). Transgenic sl/PLCG2 lines, self-generated for the purpose of this thesis are clearly highlighted.

Stock Name	Genotype	Stock No
w^{1118}	w-; +/+; +/+	In house
RepoGal4	w-; +/+; RepoGal4/TM3, Sb^1, e-	BDSC #7415
TubulinGal80	w-; Tubulin-$Gal80^{ts}$; TM2/ TM6B, Tb^1,	BDSC #7108
yw	yw; +/+; +/+	In house
aos::$A\beta_{42}^{Arc}$	yw; UAS-aos::$A\beta_{42}^{Arc}$;	BDSC #33773
aos::$A\beta_{42}^{Arc}$ DB	w-; UAS-aos::$A\beta_{42}^{Arc}$; TM2,Ubx,e-; TM6B,Sb,e-	
LacZ	w-;;P{w[+mC]=UAS-lacZ.Exel}/TM6	BDSC #8530
sl CRIMIC	yw,slCRIMIC/FM7h;;	BDSC #81213
mCD8::RFP	w-;;UAS-mCD8::RFP	BDSC #27398
mCD8::GFP	w-;;UAS-mCD8::GFP	Lee and Luo, 1999
mCD8::GFP + $A\beta_{42}^{Arc}$	w-; UAS-aos::$A\beta_{42}^{Arc}$; UAS-mCD8::GFP	
PLCδ-PH::GFP	yw; L/CyO; UAS-PLCδ-PH::EGFP/TM6B, Tb^1	BDSC #39693
GRP1-PH::GFP	w-; P(tGPH)2; Sb^1/TM3, Ser^1	BDSC #8163
PTEN RNAi	w-;; UAS-P(GD13500)v35731	BDSC #35731
PLD3 RNAi	w-; UAS-P(KK107515)VIE-260B;	BDSC #109798
Pi3K RNAi	w-; UAS-P(KK102291)VIE-260B;	BDSC #107390
UAS-sl M1	w-;; UAS-sl ^{AttP2}/TM3, Sb^1, e-	Self-generated
UAS-PLCG2 WT M1	w-;; UAS-PLCG2-P522^{AttP2}/TM3, Sb^1, e-	Self-generated
UAS-PLCG2 R522 M2	w-;; UAS-PLCG2-R522 ^{AttP2}/TM3, Sb^1, e-	Self-generated
UAS-pJFRC5 M1	w-;; UAS-pJFRC5 ^{AttP2}/TM3, Sb^1, e-	Self-generated
UAS-sl + $A\beta_{42}^{Arc}$	w-; UAS-aos::$A\beta_{42}^{Arc}$; UAS-sl ^{AttP2}	Self-generated
UAS-PLCG2 WT + $A\beta_{42}^{Arc}$	w-; UAS-aos::$A\beta_{42}^{Arc}$; UAS-PLCG2-P522 ^{AttP2}	Self-generated
UAS-PLCG2 R522 + $A\beta_{42}^{Arc}$	w-;UAS-aos::$A\beta_{42}^{Arc}$; UAS-PLCG2-R522 ^{AttP2}	Self-generated
UAS-pJFRC5 + $A\beta_{42}^{Arc}$	w-;UAS-aos::$A\beta_{42}^{Arc}$; UAS-pJFRC5 ^{AttP2}	Self-generated

Table 2.2: List of general fly tools used.

Stock Name	Genotype	Source
GFPValium10 (TRiP CTRL I)	y,v;; P{UAS-GFPValium10}attP2	BDSC #35786
P(CaryP)attP2 (TRiP CTRL II)	y,v;; P(CaryP)attP2	BDSC #36303
KK CTRL	P{attP,y+,w3'}VIE-260B	VDRC #60101
Abi RNAi I	P{KK108071}VIE-260B	VDRC #100714
Abi RNAi II	y1, sc*, v1, sev21; P{TRiP.HMS01597}attP2	BDSC #36707
Acer RNAi	y1, sc*, v1, sev21; P{TRiP.HMC06306}attP2	BSCD #67205
Amph RNAi I	w^{1118}; P{GD1311}v7190	VDRC #7190
Amph RNAi II	y1, sc*, v1, sev21; P{TRiP.HMS01933}attP40	BDSC #39015
Ance RNAi I	y1, sc*, v1, sev21; P{TRiP.HMS03009}attP2	BDSC #36479
Ance RNAi II	y1, sc*, v1, sev21; P{TRiP.GLC01369}attP2	BDSC #51394
bru1 RNAi I	w^{1118}; P{GD8699}v41567	VDRC #41567
CG11710 RNAi I	P{KK102304}VIE-260B	VDRC #109760
CG11710 RNAi II	y1, sc*, v1, sev21; P{TRiP.HMC05087}attP40	BDSC #60093
CG18130 RNAi	w^{1118}; P{GD9516}v20599/TM3	VDRC #20599
CG34120 RNAi I	P{KK104441}VIE-260B	VDRC #100472
CG34120 RNAi II	P{KK111208}VIE-260B	VDRC #101700
CG34120 RNAi III	P{KK101831}VIE-260B	VDRC #100384
cindr RNAi	w^{1118}; P{GD8679}v38854	VDRC #38854
dor RNAi I	w^{1118}; P{GD5124}v41186	VDRC #41186
dor RNAi II	P{KK111208}VIE-260B	VDRC #105330
Eph RNAi	P{KK101831}VIE-260B	VDRC #110448
Ets98B RNAi I	P{KK107560}VIE-260B	VDRC #107292
Ets98B RNAi II	w^{1118}; P{GD4451}v10932	VDRC #10932
Fak RNAi I	P{KK101680}VIE-260B	VDRC #108608
Fak RNAi II	y1, v1; P{TRiP.HMS02792}attP40	BDSC #44075
Fit1 RNAi	y1, sc*, v1, sev21; P{TRiP.HMC02930}attP40	BDSC #44536
fw RNAi	P{KK109200}VIE-260B	VDRC #106656
Hasp RNAi	y1, sc*, v1, sev21; P{TRiP.HMC05997}attP40	BDSC #65101
Hs3st-A RNAi I	w^{1118}; P{GD2075}v4998	VDRC #4998
Hs3st-A RNAi II	w^{1118}; P{GD10001}v25571	VDRC #25571
Iap RNAi I	w^{1118}; P{GD4725}v12731	VDRC #12731
Iap RNAi II	P{KK109279}VIE-260B	VDRC #105767
LpR2 RNAi	y1, sc*, v1, sev21; P{TRiP.HMS03722}attP2	BDSC #54461
Mef2 RNAi I	w^{1118}; P{GD5039}v15550	VDRC #15550
Mef2 RNAi II	y1, v1; P{TRiP.JF03115}attP2	BDSC #28699
Mef2 RNAi III	y1, sc*, v1; P{TRiP.HMS01691}attP40	BDSC #38247
Nrx-IV RNAi I	P{KK102207}VIE-260B	VDRC #108128
Nrx-IV RNAi II	w^{1118}; P{GD2436}v9039	VDRC #9039
Ocrl RNAi	P{KK101922}VIE-260B	VDRC #110769
p130CAS RNAi I	w^{1118}; P{GD7492}v41479	VDRC #41479
p130CAS RNAi II	P{VSH330191}attP40	VDRC #330191
P32 RNAi I	P{KK101475}VIE-260B	VDRC #110239
P32 RNAi II	y1, sc*, v1, sev21; P{TRiP.HMS01059}attP2	BDSC #34585
PLD3 RNAi I	P{KK107515}VIE-260B	VDRC #109798
PLD3 RNAi II	y1, v1; P{TRiP.JF01595}attP2	BDSC #31122
sl RNAi I	P{KK101565}VIE-260B	VDRC #108593
sl RNAi II	y1, sc*, v1, sev21; P{TRiP.HMS00695}attP2	BDSC #32906
Wwox RNAi I	y1, v1; P{TRiP.HMC02942}attP40	BDSC #44546
Wwox RNAi II	y1, v1; P{TRiP.HMC03298}attP2	BDSC #51747
zyd RNAi I	w^{1118}; P{GD3723}v40988	VDRC #40988
zyd RNAi II	y1, v1; P{TRiP.JF01872}attP2	BDSC #25851
GFPValium10 (TRiP CTRL I)	y,v;; P(UAS-GFPValium10)attP2	BDSC #35786
P(CaryP)attP2 (TRiP CTRL II)	y,v;; P(CaryP)attP2	BDSC #36303
KK CTRL	P{attP,y+,w3'}VIE-260B	VDRC #60101
Abi RNAi I	P{KK108071}VIE-260B	VDRC #100714
Abi RNAi II	y1, sc*, v1, sev21; P{TRiP.HMS01597}attP2	BDSC #36707
Acer RNAi	y1, sc*, v1, sev21; P{TRiP.HMC06306}attP2	BSCD #67205

Table 2.3: List of RNAi transgenes used.

RNAi transgenes sourced from BDSC (Perkins et al. 2015) *or VDRC* (Dietzl et al. 2007)**.**

2.3. DRSC Integrative Orthologue Prediction tool (DIOPT)

DIOPT is an online predictive tool used to identify orthologs between species, in this instance *Homo sapiens* and *Drosophila*. DIOPT integrates results from multiple ortholog prediction tools and algorithms based on sequencing alignment, evolutionary relationships and protein-protein interaction networks (see Table 2.4) (Hu et al. 2011). This produces a final score indicating the number of tools that support a given gene-pair relationship. To identify conserved AD risk gene orthologs DIOPT version 8.5 was used, which assessed gene orthology from a set of 18 algorithms. Throughout the course of this thesis a newer version of DIPOT was released (version 9), which integrated 6 new algorithms – a total of 24 algorithms. The versions of DIOPT used to assess gene orthology throughout the thesis have been clearly indicated.

2.4. Molecular Biology

2.4.1. Squish Buffer Genomic DNA Extraction

For genotype profiling of individual flies, a single fly was anaesthetised and transferred to a microcentrifuge tube containing 50 µl of squishing buffer (10 mM Tris pH 8.2, 1 mM Ethylenediaminetetraacetic acid (EDTA), 25 mM NaCl). The fly was homogenised with a motorised pestle and then a further 100 µl of squish buffer was added. 1 µl of Proteinase K (4 µg/ml) was added to the homogenate, incubated for 1 hour at 37°C and then at 85°C for a further 10 minutes to stop the reaction. The homogenate was then centrifuged 15000 x g (Fisherbrand; 11516873) for 5 minutes to pellet the fly carcass and the supernatant was transferred to a fresh microcentrifuge tube. DNA extractions were stored at -20°C for no longer than 1 month. Around 1-2 µl of DNA extraction was used in PCR (Gloor et al. 1991).

2.4.2. Agarose Gel Electrophoresis

Gel electrophoresis was used to separate DNA fragments based on molecular size. 10 µl of PCR reaction mix were loaded into wells of a 1.5% agarose gel (1.5 g agarose in 100 µl TAE) and ran in TAE buffer at 100 volts. 1 Kb (Thermo Scientific, 11581625) or 100 base pair (bp) (Invitrogen, 11538766) molecular ladders were ran alongside the samples for molecular weight reference.

2.4.3. Collection of Fly Heads for Molecular Biology

Flies were anesthetised on CO_2 pads then separated into males and females. Using a sharp razor blade fly heads were severed at the intersection with the thorax, picked up with a fine paintbrush and transferred to a microcentrifuge tube prechilled on dry ice. Fly heads were immediately snap frozen and stored at -80°C for later use.

2.5. Molecular Cloning: Generation of Transgenic Flies

cDNA of the *Drosophila sl* gene and the human *PLCG2* gene harbouring the wildtype (P522) or protective coding variants (R522) were cloned into a 5XUAS-pJFRC5 vector to be injected into the fly embryo and produce transgenic fly lines. The pJFRC5-5XUAS-IVS-mCD8::GFP vector was gifted from Gerald Rubin (Addgene, plasmid #26218) (Pfeiffer et al. 2010).

2.5.1. Ampicillin Resistance LB Plates

500 ml of Luria-Bertani (LB) agar was made with LB broth (Thermo Fisher, 12780052) in ddH_2O plus agar as per instructions. The mixture was autoclaved then left to cool before adding ampicillin (amp) antibiotic resistance at 100 µg/ml.

2.5.2. Preparation of cDNA and Transformation to *E. coli* Competent Cells

Drosophila cDNA for *sl* cloned into pFlc-1 vector (Stapleton et al. 2002) (Drosophila Genomics Resource Center (DGRC), GOLD RE62235) arrived lyophilised on filter paper and was eluted in 50 µl of TE buffer. 50 µl of DH5α competent Escherichia coli (*E.coli)* cells (Thermo Fisher, 18263021) were mixed with the eluted sl cDNA and left on ice for 30 minutes, vortexed halfway through (15 minutes). The cells were then heat shocked for 2 minutes at 37ºC, transferred to 1 ml of prepared LB media and incubated for 1 hour at 37ºC with shaking. 100 and 200 ml of cell suspension was then plated on LB + amp resistance plates and left overnight in the 37ºC incubator for colonies to grow. The human PLCG2 plasmid pUASgHA.attB (Bischof et al. 2013) (DGRC, HSCD00506018) was provided as bacterial stab which was streaked across an LB + amp resistant plate. Plates were left in the 37°C incubator for colonies to grow overnight.

2.5.3. Primer and Vector Design

Primers were designed for amplification of *sl* and *PLCG2* cDNA with the addition of *NotI* and *XBaI* restriction sites to the 5' and 3' ends of the sequences respectively. Primer sequences are outlined in the Table 2.8 below. The forward primer design contained a linker sequence, *NotI* restriction site, Kozak sequence optimised for *Drosophila*, followed by the ATG start codon and hybridisation sequence to the cDNA of interest. The reverse primer design instead had a *XBaI* restriction site and no ATG start codon.

Product	Forward Primer	Reverse Primer
sl	TCAGCGGCCGCACAACCAAAATGAGCTGCTTTAGTGCGAT	GTATCTAGACTACGGTGCGGTAACATTTG
PLCG2	TCAGCGGCCGCACAACCAAAATGTCCACCACGGTCAATGT	GTATCTAGACTACGGTGCGGTAACATTTG

Table 2.4: Forward and reverse primer design for amplification of sl and PLCG2 cDNA and addition of NotI and XBaI restriction sites.

A modified pJFRC5 vector (~780 bp) (Pfeiffer et al. 2010) provided the backbone for which *sl* and *PLCG2* cDNA was cloned into (Figure 2.1). The pJFRC5 vector contained an amp resistance site, 5XUAS site, Hsp70 and SV40 sequences and an additional poly-linker region to facilitate cloning of transgenes. Hsp70 facilitates protein folding and assembly of polypeptides within the cell, whilst SV40 helps promote gene expression in cells transfected with plasmid. *Not1* and *XBaI* restriction sites allowed for insertion of *sl* and *PLCG2* cDNA which had been digested with the same restriction enzymes to make complementary sticky ends.

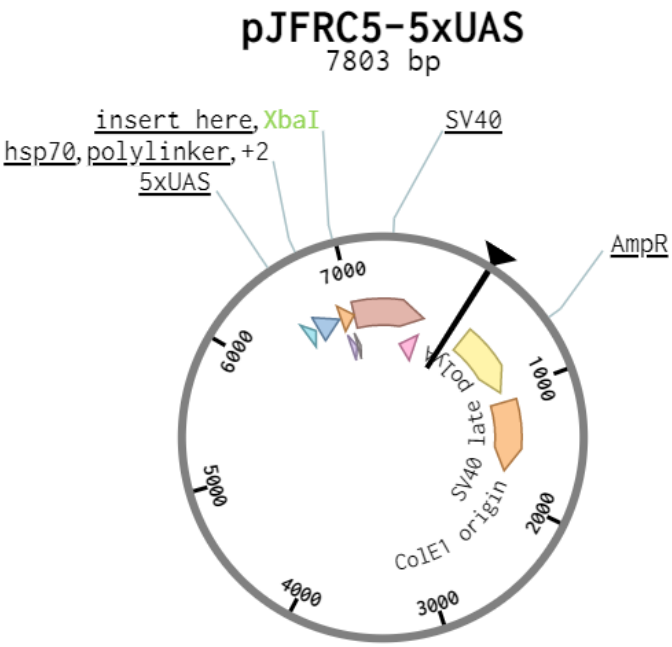

Figure 2.1: Empty pJFRC5 vector design. The empty pJFRC5 vector contains an amp resistance site, 5XUAS sites and a poly-linker site with NotI and XbaI restriction sites.

2.5.4. PCR Amplification of *sl* and *PLCG2* cDNA

NotI and *XBaI* restriction sites were added to the 5' and 3' ends of *sl* and *PLCG2* sequences following PCR amplification. 50 µl PCR reactions were prepared on ice according to Table 2.4. Four reactions were set for amplification of *sl* and *PLCG2* with template DNA concentrations at either 50 ng or 100 ng (2 reactions each). Samples were mixed by pipetting and briefly centrifuged. DNA amplification was performed using the benchtop PCR machines (Thermo, A37834) set at thermocycling conditions outlined in Table 2.9.

Component	Volume for 1 Reaction (µl)
5X Phusion HF buffer	10
10 mM dNTPs	1
10 µM Forward Primer	2.5
10 µM Reverse Primer	2.5
Template RNA	50/100 ng
DMSO	1.5
Phusion DNA polymerase	0.5
Nuclease free H_2O	Up to 50 µl final volume

Table 2.5: Components required for PCR reaction mix using Phusion High-fidelity DNA polymerase.

Step	Temperature (°C)	Time	
Initial Denaturation	98	30 seconds	
Denature	98	10 seconds	X30 cycles
Anneal	65*	30 seconds	
Extend	72	**2 mins (15-30sec/Kb)	
Final Extension	72	5 mins	

Table 2.6: Thermocycling conditions for amplification of sl/PLCG2 cDNA.

**Step 3 was set based on the predicted melting temperature (Tm) of the sl and PLCG2 primers. **Time in step 4 was based on the length of PCR product to be amplified; for every Kb in length and extension of 30 seconds was added.*

2.5.5. DNA Extraction

The amplified inserts were run on 1% agarose gel for 1 hour at 100 volts then visualised using a UV lamp. Bands of the correct size were cut out of the gel with razor blades and collected into microcentrifuge tubes for DNA extraction (Thermo Fisher, K220001) as per manufacturer's instructions.

2.5.6. Restriction Digest, Ligation and Transformation

1 µg of modified *sl* and *PLCG2* were digested with *NotI-HF* and *XhoI* restriction enzymes to create sticky ends. 1 µg of pJFRC5 vector was digested with the same restriction enzymes which produced complementary sticky ends for which *sl* and *PLCG2* were to be ligated. Alkaline phosphatase added to the vector digest prevented re-ligation of the vector backbone. sl and PLCG2 inserts were ligated into the pJFRC5 vector at a 5:1 ratio using T4 DNA ligase (New England Biolabs, M0202S). 50 ng of pJFRC5 vector and 121.7 ng of sl or PLCG2 inserts were mixed with 2 µl of T4 DNA ligase buffer, 1 µl of T4 DNA ligase and nuclease free H_2O up to 20 µl then left overnight at 18°C. 1 µl of ligation product was mixed with 50 µl of competent DH5α cells (Thermo Fisher, 18263021) placed on ice for 30 minutes, vortexing halfway through. Cells were then heat shocked for 2 minutes at 37°C before being transferred to 1 ml of prewarmed LB media and incubated for 1 hour at 37°C with shaking (100 RPM). 100 µl and 200 µl of cells were plated onto LB + amp resistance plates and were incubated at 37°C overnight for colonies to grow.

2.5.7. Colony PCR

Bacterial colonies were screened for their presence or absence of inserted DNA in the plasmid constructs. 16 colonies were picked with sterile pipette tips for both sl and PLCG2 transformants and streaked onto an area of LB + amp plate. The tip was then submerged into correspondingly labelled 1.5 ml microcentrifuge tubes with 100 µl sterile distilled H_20 to be used as templates for PCR amplification. Samples were boiled to lyse the cells then 16 µl was added to PCR master mix containing: 32 µl of 5X High fidelity Phusion buffer, 32 µl of 10 mM dNTPs, 8 µl of 10 µM forward and reverse primers, 4.8 µl of dimethyl sulfoxide (DMSO), 1.6 µl of Phusion Taq (New England Biolabs, M0530L) and nuclease free H_2O up to 160 µl. sl and PLCG2 primer sets targeted the inserted DNA for amplification. The size of the PCR amplicon was then determined by electrophoresis alongside a 1 Kb DNA molecular weight ladder (Thermo Scientific, 11581625) on a 1% agarose gel. The size of *sl* and *PLCG2* inserts were ~4 Kb.

2.5.8. Isolation of Plasmid DNA by Miniprep

Bacterial cultures made from inoculating 3 ml of LB + amp liquid media with selected colonies were grown overnight at 37°C, 250 RPM and then miniprepped. A 50% glycerol

stock was made with 500 µl of the overnight culture and 500 µl glycerol then stored at -80°C. The QIAprep Spin Miniprep kit (Qiagen, 27106) was used to isolate and purify plasmid DNA as per manufactures guide. The DNA was eluted in 30 µl of elution buffer opposed to 50 µl stated in the instructions.

2.5.9. Sequencing Verification

5 µl of 50 ng/µl plasmid DNA from selected colonies was mixed with 5 µl of 5 mM forward and reverse primers in separate tubes and sent for sequencing through the Sanger sequencing service at GENEWIZ (UK). Firstly, hsp70 and sv40 forward and reverse primers were used to verify the sequence flanking the insertion site of the plasmid. Sequences were verified using the sequence alignment tool on Benchling, a web-based research and development platform. Once confirmed, sl and PLCG2 primers were made to sequence across the full length of insert.

2.5.10. Site Directed Mutagenesis

4 µg of PLCG2 wildtype plasmid DNA cloned in the pJFRC5 vector was prepared and sent to Genscript (Netherlands, Leiden), to carry out the site-directed mutagenesis. A C>G base substitution was introduced at position 1564 bp of the PLCG2 insert (8519 bp of entire template sequence) to generate a copy of the AD associated protective coding variant (P522R).

2.5.11. Maxi Prep

Single colonies from transformed DH5α cells grown on LB + amp plates were selected to make overnight bacterial cultures for a Maxi Prep. A starter culture was made with 3 ml of LB liquid media supplemented with amp and incubated at 37°C at 250 RPM for 8-10 hours. 1.5 ml of the starter culture was expanded in 200 ml of LB liquid media plus amp and left overnight in the orbital shaker at 37°C, 250 RPM. A bacterial pellet was harvested from overnight cultures by centrifugation at full speed for 15-30 minutes at 4°C (length of centrifugation based on visible pellet formed), and then maxi-prepped as per manufacturer's instructions (Qiagen, 1262). DNA was eluted in 65 or 80 µl nuclease free H_2O for sl or PLCG2 constructs respectively.

2.5.12. *Drosophila* Embryo Injection

20 µg of DNA from sl, PLCG2 wildtype and P522R constructs were prepared in nuclease free H_2O and sent to BestGene (USA) for *Drosophila* embryo injection. UAS-sl and PLCG2 variants were incorporated into the genome by PhiC31 integrase mediated site-specific recombination. Successful transformants were identified and then single balanced. Insertions were targeted to both second and third chromosomes by injection into stocks BDSC 36304 and 8622 harbouring attp40 and attp2 landing sites respectively. 5 balanced transformants for each construct were shipped to us to be maintained.

2.6. Behavioural Phenotyping

2.6.1. Rapid Iterative Negative Geotaxis Assay

The Rapid Iterative Negative Geotaxis (RING) assay, adapted from (Gargano et al. 2005) was used to evaluate *Drosophila* locomotor behaviour, measuring negative geotaxis response. Empty narrow plastic vials (RING vial) were rinsed with ddH_2O and dried prior to use. Flies recovered from brief CO_2 anaesthesia for at least 24 hours were used in the assay and flipped from their food vial into a RING vial and sealed with a plug that sat flush with the top of the vial. All RING assays were performed at 22-25°C. Up to six RING vials were loaded into the apparatus and secured with the lid. The RING assay is set up as shown in Figure 2.2 and flies were left in their RING vials to acclimatise for approximately 10 minutes prior to running the assay. A table lamp distanced 30 cm away from the apparatus provided background illumination. The wooden box with RING vials enclosed is moved vertically along the metal rail. Negative geotaxis was elicited by dropping the box from a consistently defined height of 20 cm, causing the flies to be knocked down to the bottom of the tubes at a consistent impact force. The position of each fly in a single tube was photographed every second for 10 seconds upon eliciting negative geotaxis and the resulting images were used to determine the vertical position (Y coordinates) of the flies in a tube at 4 and 10 seconds. The average distance travelled by all flies in a single vial, averaged across five consecutive RING trials is considered 1 technical replicate.

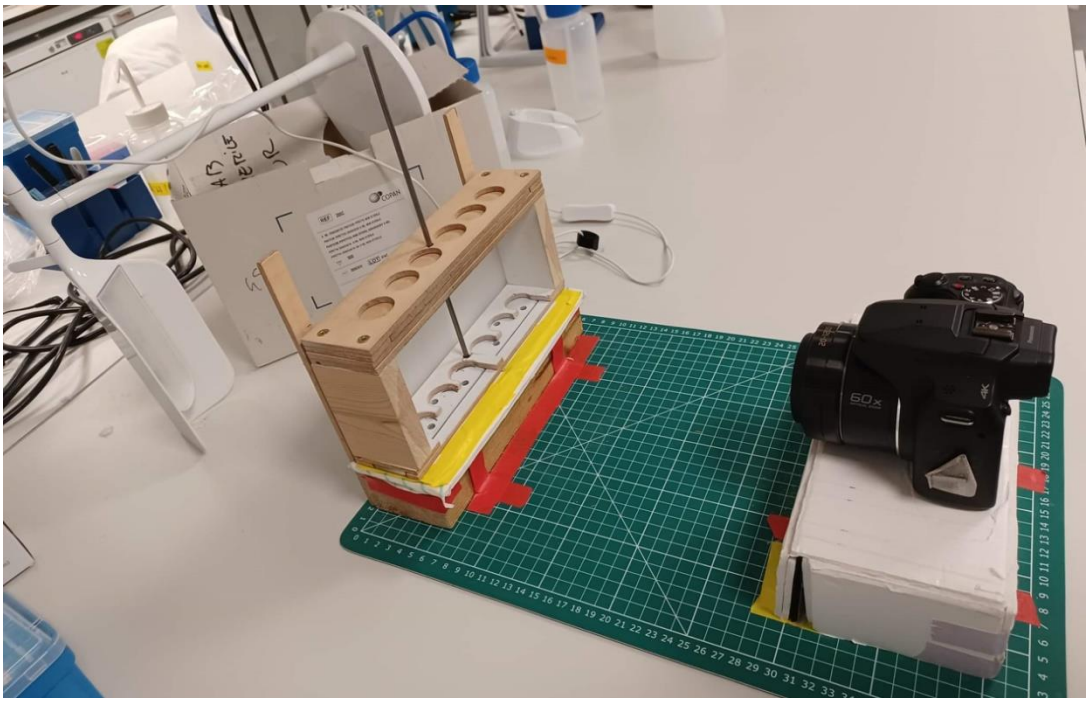

Figure 2.2: Setup of RING assay apparatus.

2.6.2. Semi-automated Image Analysis of Locomotor Behaviour

Digital images (.JPG) of the flies were opened with Fiji software and processed as follows. The image was cropped around the region of interest as selected by the rectangle tool, capturing the length of the vial, below the plug to the bottom of the vial. The cropped image was duplicated for reference and processed through a series of steps that were recorded as a macro for automation. The macro instructions were changing the image type to 8 bits, subtracting background with a rolling ball radius of 30 pixels, thresholding the image to (0,238) and setting the background to black. The processed image was then compared with the original and the pencil tool was used to erase the surrounding white edges (that were not flies), as well as manually segregate flies that were visibly overlapping as to prevent the software from recognising them as one particle. A scale was set at 80 mm by drawing a line down the length of the image and particles were analysed at a defined size of 0.20 mm to infinity. The centre of mass for each fly was reported as a list of X and Y coordinates with the highest position on the vertical axis listed first. Outlines of the particles analysed were also show as guide (Figure 2.3).

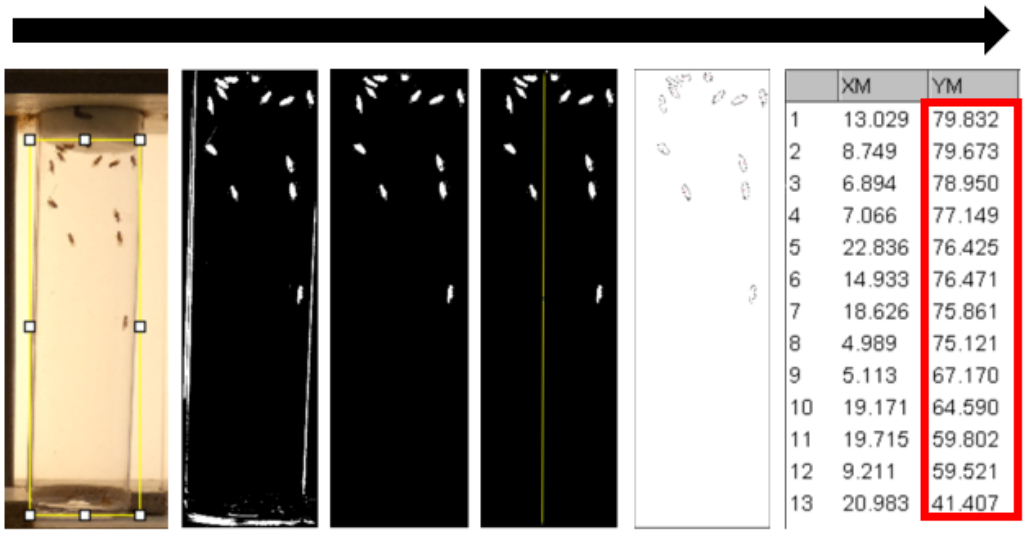

Figure 2.3: Sequence of steps for analysis of RING assay images.

Steps are as follows: Crop image to size of specified rectangular selection, run macro, removal of white edges and separation of adjoining flies, set scale, analyse particles, and record Y co-ordinates.

2.6.3. Lifespan assay

24 hours mated males and females were selected and transferred to narrow plastic vials containing ~3-5 ml of low yeast 'brown food' media at a density of 10-15 flies per vial. Approximately 10 vials per genotype of males and females were collected for each experiment. Flies were maintained at 30°C for their remaining lifespan and flipped into fresh food vials every 2-3 days. At each passage the number of deaths were recorded. Dead flies appeared motionless, shrivelled bodies, and legs curled. Flies that were stuck in the food but visibly moving or had escaped during flipping were marked as censored. A record was also made if any dead flies were transferred over to the new vial. Data were presented as survival curves and log rank tests were used for statistical comparisons.

2.7. Histological Techniques

2.7.1. Brain Dissections

Using dissection forceps, the proboscis was removed from the fly head, leaving behind a small opening between the retina. The whole fly was placed into a well of a 9 well glass dissection dish containing 200 µl premade 0.1% PTx solution (0.1% triton X-100 in phosphate buffered saline). The dish was kept on ice until all flies were prepared for the fixing step. PTx solution was discarded from the wells and heads were fixed in 4% PFA (16% formaldehyde in 0.1% PTx) for 15 minutes, rinsed with PTx 5 times over 30 minutes and then placed on ice ready for dissections. Whole fixed flies were placed within a black bottomed plate filled with solid agar and held in place with a dissection pin through the centre of the fly's thorax. Brains were dissected in ice cold 0.1% PTx and transferred to a well of the glass dissection dish for a second fix. After 15 minutes incubation in 4% PFA at room temperature (RT) with gentle rocking (50 RPM), brains were washed with 0.1% PTx 5 times over 30 minutes and kept on ice prior to immunostaining or mounting.

2.7.2. Immunohistochemistry

Following fixation, adult brains were blocked in 10% goat serum (Vector Laboratories S-100), diluted in 0.1% PTx (blocking solution), for 1 hour at RT with gentle rocking (50 RPM), then incubated with primary antibody at 4°C (see specific antibody stains for further detail). Following primary antibody incubation brains were washed in 0.1% PTx 5 times over 30 minutes at RT with gentle rocking, then an appropriate secondary antibody was added and left to incubate for 2 hours (no light exposure). Brains were rinsed with a series of 5X5 minute washes in 0.1% PTx before finally being mounted on microscope slides in Vectashield (Vector Laboratories, H-1000).

2.7.2.1. Amyloid Beta Staining

Brains were incubated at 4°C for two nights with anti-mouse $A\beta_{42}$ (Biolegend 6E10 803001, 1.5:500), diluted in blocking solution. Brains were then incubated with secondary goat anti-mouse AF568 (Thermo Fisher, A11004, 1:500), for 2 hours at RT with gentle rocking.

2.7.2.2. Repo/Elav/nc82 Staining

Anti-Repo (8D12; developed by Goodman, C), Elav (Elav-9F8A9, developed by Rubin, G) or nc82 (nc82, developed by Buchner, E) antibodies were obtained from Developmental studies Hybridoma Bank. Brains were incubated overnight at 4°C with 8D12 (1:500) ElaV-9F8A9 (1:500) or nc82 (1:100) diluted in blocking solution. Brains were then incubated with goat anti-mouse AF647 secondary (Thermo Fisher, A21244, 1:500) diluted in blocking solution for 2 hours at RT with gentle rocking.

2.7.2.3. Ref(2)P and FK2 Staining

Brains were incubated overnight at 4°C with either rabbit anti-Ref(2)P (Abcam 178440, 1:200) or mouse anti-polyubiquitinated proteins (FK2, Millipore 04-263, 1:200), diluted in blocking solution. Brains were then incubated with secondary goat anti rabbit AF648 (Thermo Fisher, A11008, 1:250), or secondary goat anti mouse AF568 (Thermo Fisher, A11019, 1:250) diluted in blocking solution.

2.7.3. Mounting

Brains were mounted on glass microscope slides (Epredia™ SuperfrostTM, Cat No: 12392098), aligned between two strips of double sided sticky tape. A coverslip was placed over the brains and gently pushed down to seal. Vectashield was added and drawn up through capillary action, covering the brains underneath the coverslip.

2.7.4. Confocal Microscopy

The spinning disc confocal microscope (Zeiss Axio Observer) was used to image adult fly brains at 20 and 63X objectives. The Zeiss was set up to take multichannel Z-stacks of brains according to the fluorescence being detected i.e. 488 nm, 568 nm and 647 nm. Post-acquisition, the Zen 2.6 (Blue edition), image software was used for image processing, which involved adjusting the fluorescence histogram according to the signal strength and making maximal orthogonal projections. Once desired settings were achieved, this was copied to each brain image in an experiment.

2.8. Image Analysis

Images from the Zeiss were saved and exported as TIFF files to be opened and analysed on the Fiji (ImageJ) software.

2.8.1. Area Threshold Analysis

Area threshold analysis was used for quantification of PIP2, Ref(2)P, FK2 and $A\beta_{42}$ in the fly brain. A scale was set using the reference scale bar (50 µm), then a region of interest (ROI) was drawn around the fly midbrain (minus optical lobes) and total area measured. A background fluorescence threshold was set (see Table 2.11) and the area above the set threshold was measured. This provided the area of fluorescence, which was divided by the total ROI area of the midbrain, calculating the relative area of fluorescence within the midbrain. The area of midbrain positive for PIP2, Ref(2)P, FK2 or $A\beta_{42}$ as indicated by fluorescence was reported as a percentage.

Target	Threshold setting
PIP2	(55,255)
PIP2 with $A\beta_{42}$	(15,255)
FK2	(14,235)
Ref(2)P	(30,90)
$A\beta_{42}$	(21,220)

Table 2.7: Threshold settings used to detect fluorescence corresponding to analytes PIP2, FK2, Ref(2)P and $A\beta_{42}$

2.8.2. Mean Gray Analysis

Mean gray analysis was used to quantify GFP intensity of the PIP2 and PIP3 reporters within the fly midbrain. Images were opened and analysed using the Fiji (ImageJ) software, and a region of interest was manually traced around the fly midbrain. The mean gray value within the region of interest was then measured.

2.9. Protein Quantification

2.9.1. Standard Protein Extraction

Radioimmunoprecipitation assay (RIPA) lysis buffer was used for standard protein extraction from *Drosophila* heads. 20 fly heads were homogenised with a motorised pestle in freshly prepared homogenisation buffer made of 1X cOmplete mini EDTA - free protease inhibitor cocktail (Roche, 04693159001) diluted in RIPA buffer (Thermo Fisher, 10017003). Tissue homogenate was centrifuged at 13.3 RPM for 10 minutes at 4°C and supernatant was collected into a fresh 1.5 ml microcentrifuge tube and stored on ice prior to determining protein concentration.

2.9.2. Soluble and Insoluble Amyloid Beta Extraction

Soluble and insoluble extraction buffers were prepared as follows, 50 mM HEPES pH 7.3, 5 µM EDTA and 1X cOmplete mini EDTA-free protease inhibitor for the soluble buffer and the same for the insoluble buffer with 5 mM of Guanidinium Hydrochloric acid added. 150 µl of soluble extraction buffer was added to 40 fly heads in a 1.5 ml microcentrifuge tube and homogenised with a motorised pestle for around 3 minutes (no whole fly heads remained), vortexed briefly on the table-top centrifuge and then incubated for 10 minutes at RT. Tissue homogenate was sonicated in a 4°C water bath for 4 minutes following a 30 second on/off cycle. Samples were then centrifuged at 17,000 x g for 5 minutes at 4°C and supernatant was transferred to a fresh 1.5 ml microcentrifuge tube labelled soluble fraction. The remaining pellet was homogenised with 55 µl of insoluble extraction buffer, vortexed briefly and then incubated for 10 minutes at RT. Samples were sonicated in a water bath set to 4°C for 4 minutes following the 30 seconds on/off cycle, and then centrifuged at 17,000 x g for 5 minutes at 4°C. The supernatant was collected in a fresh 1.5 ml microcentrifuge tube labelled insoluble fraction.

2.9.3. BCA Protein Assay

A 1:5 dilution of protein lysates was made in compatible protein extraction buffer. Bovine serum albumin standards were made up to manufacturer's instructions from the Bicinchoninic Acid (BCA) protein assay kit (Thermo Scientific, 10678484) and desired

volume of working reagent was obtained by mixing reagents A and B in a 50:1 ratio. 2 5 µl of standards and samples were plated in duplicate in a 96 well plate (Thermo Scientific, 10078850), followed by 200 µl of working reagent to each well. The plate was sealed, incubated at 37°C for 30 minutes and then read on the FLUOstar® Omega microplate reader (BMG Labtech) at absorbance of 562 nm.

2.9.4. Meso Scale Discovery Assay

Quantification of soluble and insoluble Aβ peptides (38,40, and 42), were determined using the V-PLEX Aβ peptide panel 1 (6E10) kit or the V-PLEX $Aβ_{42}$ peptide (4G8) kit provided by Meso Scale Discovery (MSD). MSD assays were run with guidance of Central Biotechnology Services, at Cardiff university. The Aβ peptide calibrator standards and kit reagents were prepared according to manufacturer's instructions prior to running the assay. Soluble and insoluble Aβ protein extractions (experimental samples) were diluted 1 in 5 and 1 in 10 in diluent 35 respectively and mixed thoroughly. MSD plates were blocked for 1 hour, washed in prepared wash buffer, then incubated for 2 hours with 25 µl of detection antibody solution and 25 µl of prepared samples, calibrators, or controls per well. 3 biological replicates per genotype with 2 technical replicates were plated in total. All incubations were performed at room temperature with the plate on a plate shaker. Plates were washed with a wash buffer and 150 µl of 2X Read buffer T was then added to each well prior to analyte levels being measured on the MESO QUICKPLEX SQ120. Analysis of analyte levels was then performed using the MSD Workbench 4.0 software. The concentration of Aβ peptide was normalised to the total protein concentration for each sample as determined by BCA assay. The final concentration of Aβ peptide was reported as pg/µg.

2.9.5. Western Assay

Protein lysates from 1 biological replicate per genotype were made up to a desired protein concentration per well (40 µg/well) with 4X Laemmli buffer, 10X reducing agent and topped to 70 µl with RIPA buffer. Protein extracts were denatured for 10 minutes at 95°C on a heat block. 30 µl of protein sample (1 technical replicate), was loaded into a precast 4-12% Bis-Tris gel (Thermo Fisher, NW04120BOX), in 1X SDS running buffer (Invitrogen, 13266499) and separated by electrophoresis for 1 hour at 100 volts. 5 µl of 250 Kilodalton (kDa) protein ladder marker (Thermo Scientific, 11832124), was ran alongside samples for size reference.

The gel was dry transferred to a nitrocellulose membrane (Invitrogen, IB23002), using the iBlot 2 (Thermo Fisher, IB21001).

2.9.6. Probing PLCG2 and Actin

The nitrocellulose membrane was blocked for 1 hour with 5% skimmed milk in 1X TBST (10X TBS with Tween-20 and ddH_2O) then probed with mouse anti-PLCG2 (Santa Cruz, sc-5283), diluted in blocking solution (1:2500) overnight at 4°C with shaking. The membrane was washed with TBST 5 times for 5 minutes and then incubated with IRDye 800CW Goat (polyclonal) anti-mouse IgG (H + L), (LI-COR biosciences, 926-32210) diluted in blocking solution (1:10000) at RT for 1 hour with rocking. The membrane was then washed 3 times for 5 minutes in TBST and imaged on the LI-COR Odyssey CLx imaging system. The membrane was re-probed with the anti-mouse actin loading control (Abcam, ab8226), diluted in blocking solution (1:5000) overnight at 4ºC with shaking.

2.10. Statistical Analysis

Statistical analysis was performed on GraphPad Prism (version 9.3.1). Data were checked first for normality using the Shapiro-Wilk test to decide between a parametric or non-parametric test. Statistical significance was calculated in each data set from a combination of t-tests, Kruskall-Wallis test, one-way and two-way Analysis of Variance (ANOVAs) or Log rank, Mantel-cox tests with *post hoc* multiple comparison analysis.

Chapter 3 - Screening Glial Roles of Conserved Alzheimer's Disease Risk Genes in *Drosophila*

3.1. Introduction

3.1.1. Genetic Risk of LOAD

Second to age, genetics constitutes a significant risk factor for developing LOAD, with heritability of 58-79% (Sims et al. 2020). GWAS, whole genome and exome sequencing have led the way in identifying single nucleotide polymorphisms (SNPs) underlying LOAD pathology. Several lowly penetrants, highly frequent genetic variants have been found from large meta-analysis studies comparing SNPs across several thousand AD case and control individuals. Since the advent of GWAS, over 75 genetic risk loci have been identified (Lambert et al. 2013; Kunkle et al. 2019; Bellenguez et al. 2022), implicating pathways such as cholesterol and lipid metabolism, immune response, endosomal vesicle cycling, and Aβ and tau processing in the pathogenesis of AD (Jones et al. 2010; Hardy et al. 2014; Sims et al. 2020). Many of the SNPs identified lie in non-coding regions and so the most proximal gene to the SNP locus is typically predicted as the AD risk loci. This presents a major challenge in translating genetic risk association into molecular insight, requiring a means to effectively triage the sheer number of genes that emerge from AD GWAS, assessing their contribution in biological processes that are implicated in AD. Since the majority of AD risk loci are enriched in microglia, including *CD33*, *CR1*, *ABCA7*, *INPP5D*, *PLCG2* and *TREM2* etc. (Efthymiou & Goate, 2017), there is a compelling case to dissect how AD associated genes influence microglial biology and thus discover ways of therapeutically modulating microglia function for the benefit of AD pathogenesis.

3.1.2. Using *Drosophila* to Screen AD Genetic Risk

To progress our understanding in the genetic and molecular underpinnings of AD pathogenesis, a range of *in vivo* and *in vitro* models have been created. These explore pathological hallmarks of toxic protein aggregates such as Aβ and tau but also the role of various AD associated risk genes and how they contribute mechanistically to AD pathology (Karch and Goate, 2015; Drummond and Wisniewski, 2017). Whilst mammalian models exhibit great physiological and genetic similarities to humans, ethical restrictions, long lifespan and being laboriously intensive to work with makes them challenging for use in large scale genetic screens. Alternatively, human iPSCs can provide a more representative, authentic model of the complex genetic architecture of human neurodegenerative diseases, which are suitable for high throughput screens. However, 2D cultures do not fully encapsulate a 3D physiological brain environment like *in vivo* models.

Drosophila models however provide a low cost, genetically tractable *in vivo* system, with lower genetic redundancy, enabling simpler genetic analysis compared with the more complex mammalian model system. Furthermore, flies are relatively easier to breed and maintain. With over 15,000 genes and 65% homologous to human disease genes (Pandey & Nichols, 2011), *Drosophila* can be used to model disease phenotypes of conserved orthologs, dissecting molecular pathways underlying disease pathogenesis. For instance, flies have helped uncover roles of the Parkinson's related autosomal dominant genes *Pink1* and *Parkin* in mitophagy (Clark et al. 2006). Extensive characterisation of Pink1 and Parkin loss of function mutants in *Drosophila* have revealed abnormal mitochondrial morphology, apoptotic muscle degeneration, increased sensitivity to oxidative stress and male sterility (I. E. Clark et al. 2006). Functional screening in *Drosophila* have also implicated a number of AD associated genes in tau mediated neurotoxicity (Shulman et al. 2014; Dourlen et al. 2017). Fly models have also been used to study AD risk genes, for instance *BIN1* and *PICALM*, which has revealed mechanistic insight into their roles in early endosomal defects and glutamatergic transmission respectively (Lambert et al. 2022; Yu et al. 2020).

As a number of AD associated genes are well conserved in flies, it is possible to explore their functions in a simpler *in vivo* model system. The range of genetic tools available to *Drosophila* enables genetic manipulation of conserved AD risk genes through gene KD, KO or overexpression and the ability to assess gene function in any given cell type or at any life stage. Additionally, a number of assays conducive to high throughput screening have been developed for *Drosophila* to test learning and memory, CNS functioning, neuronal firing, and axonal regeneration/degeneration etc. The shortened lifespan of *Drosophila* also permits larger scale survival studies which are just not feasible in mammalian models. Furthermore, external features such as bristles, wings and the compound eye give rise to visible mutant phenotypes, ideal for use as phenotypic markers in mutagenesis studies (St Johnston, 2002). For instance, the fly compound eye represents a well characterised neuronal structure that is permissible to neurodegenerative phenotypes such as the rough eye phenotype, characterised by reduced size and rough appearance. The rough eye phenotype is sensitive to genetic modifications such as expression of mutant forms of tau or $A\beta_{42}$, whereby the severity of rough eye phenotype correlates to the degree of photoreceptor cell loss (Tan and Azzam, 2017). The rough eye phenotype has provided an ideal readout for screens, such as identifying modifiers of tau neurotoxicity. Such modifier screens have revealed several candidate tau kinases and phosphatases involved in controlling tau induced toxicity, such as GSK-3β, CDK5, protein kinase A (PKA), protein phosphatase 2A (PP2A) and many more (Shulman and Feany, 2003; Jackson et al. 2002).

Overall, *Drosophila* models prove valuable for large scale genetic screening, which is ideal for investigating roles of several conserved AD risk genes.

Several AD risk genes are highly enriched in microglia and therefore it will be important to deduce their glial specific functions. *Drosophila* has functional glial cells, which make up ~10% of the total cell brain population (Freeman, 2015). The six glial subtypes of the *Drosophila* nervous system: wrapping glia, perineural glia, sub-perineural glia, cortex glia, ensheathing glia and astrocytic glia, share many functional and anatomical features with their mammalian counterparts (outlined in Chapter 1; section: 1.9.2). Although *Drosophila* do not possess the brain resident, immune associated microglial cells found in mammals, they have an equivalent glial subtype called ensheathing glia which adopt similar phagocytic functions. Ensheathing glia engulf degenerating axons through the Draper pathway which is conserved with the mammalian MEGF10 pathway (MacDonald et al. 2006). Furthermore, the glial engulfment receptor Draper was found to protect against Aβ toxicity in a fly AD model, indicating conservation of glial mediated Aβ clearance mechanisms across mammals and flies (Ray et al. 2017). *Drosophila* glia therefore provide a representative system for studying glial specific functions of conserved AD risk genes.

3.1.3. Aims and Hypotheses

This chapter outlines a novel reverse genetic screen which aims to evaluate the functional importance of AD risk gene activity in glia throughout age. To test the hypothesis that glial AD risk gene activity contributes to a healthy ageing nervous system and longevity in adult flies, changes in locomotor behaviour and survival were examined upon RNAi mediated KD of Drosophila risk gene orthologs, exclusively in glia. It was hypothesised KD of AD risk genes important to glial functions will result in locomotor and survival deficits. By determining the importance of risk gene activity in glia throughout age, we hope to form a more comprehensive understanding of how such genes contribute to AD pathology.

3.1.4. Experimental Design

3.1.4.1. Genetic Approach

This chapter details a reverse genetic screen, utilising RNAi mediated KD of fly orthologs of AD risk genes identified up to 2019. Fly orthologs of human AD risk genes were identified

through DIOPT (version 8.5) (see explanation in Materials and Methods section 2.3). Expression of UAS-RNAi transgenes against conserved AD risk genes were targeted to glia cells using the pan glial driver, reversed polarity (Repo) Gal4. Furthermore, as AD is an age associated adult disease and to avoid phenotypes associated with disrupted glial development, RNAi expression was temporally restricted to adult stages (1-2 days post eclosion (d.p.e) by co-expression of a temperature sensitive Tubulin-Gal80^{ts} (Tub-Gal80^{ts}). Gal80 acts as a Gal4 repressor, binding as a dimer to Gal4, such that Gal4 can no longer activate transcription downstream of the UAS (Ma and Ptashne, 1987; Lee and Luo, 1999). Gal80 has been modified to allow for temperature regulated activity (Gal80^{ts}). At temperatures 18°C or below, Gal80^{ts} binds and represses Gal4 expression, whereas at temperatures 29°C or higher, a conformational change in Gal80 causes it to dissociate from Gal4 (McGuire et al. 2004). At these permissive temperatures Gal4 can bind to UAS and activate transgene expression (refer to Figure 1.10).

Temperature sensitive, pan-glial driver stocks, with Tub-Gal80^{ts} on the second chromosome and RepoGal4 on third were made for the purpose of this screen. Female virgins from the temperature sensitive, pan-glial driver stock were crossed to males containing RNAi transgenes constructed under control of the UAS promoter. Crosses were reared at 18°C to suppress Gal4 transcriptional activity, then the F1 progeny were selected 1-2 d.p.e and transferred to 30°C as to induce glial specific AD risk gene KD, exclusively in adulthood (Figure 3.1).

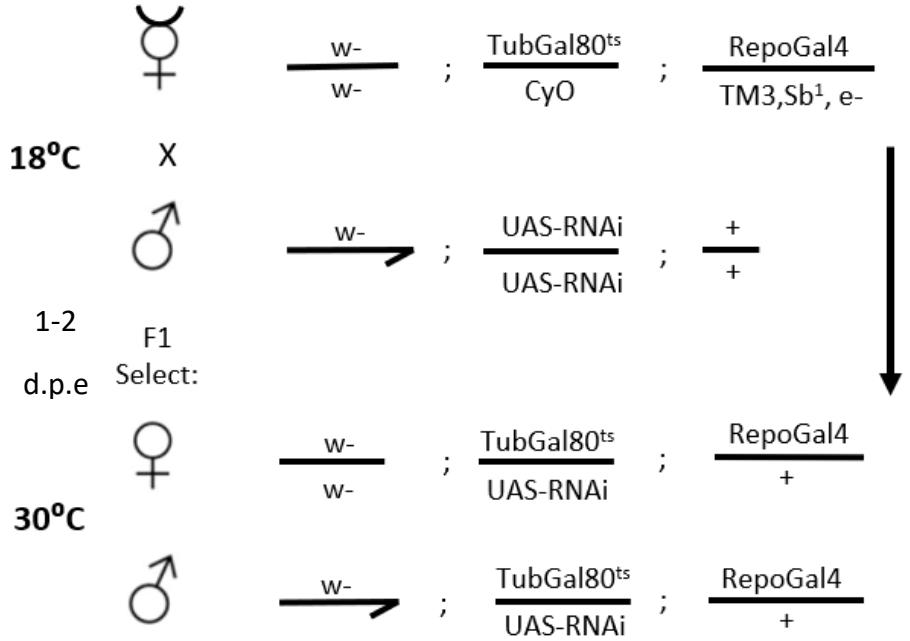

Figure 3.1: Crossing scheme for adult specific gene KD in glia.

The Gal80^{ts}/Gal4 inducible expression system allowed temporal regulation of glial specific gene KD. UAS-RNAis were expressed at adulthood specific stages when the progeny was transferred to 30°C temperatures at 1-2 d.p.e. Example crossing scheme for UAS-RNAi on second chromosome.

UAS-RNAi stocks were acquired either from VDRC or BDSC. The collection of RNAis sourced from VDRC are comprised of VDRC phiC31 RNAi Stocks (KK) and GD libraries, which contain long hairpin fragments of 300-400 bp inverted repeats, cloned into pMF3 (GD) or pKC26 (KK) vectors. The GD collection contains P-element based transgenes, resulting in random integration, whereas the KK collection targets transgenes to 30D or 40D3 landing sites via phiC31 mediated site directed insertion (Vissers et al. 2016). The 60101 line served as a control for the KK family of RNAis covering genomic insertions at both 40D3 and 30B3 landing sites. With no equivalent control for the GD library of randomly inserted RNAi transgenes, comparisons for GD RNAis were made with the 60101 line as to provide a UAS control. The UAS-RNAi alone could have also been used to control for RNAis of the GD library. Alternatively, the Transgenic RNAi project (TRiP) collection of RNAis sourced from BDSC are cloned into a series of Vermilion-AttB-Loxp Intron-UAS-MCS (VALIUM) vectors for phiC31 mediated genomic integration at attP landing sites on second (attP40) or third chromosomes (attP2) (Perkins et al. 2015). P(CaryP)attP2 and GFPValium10 were used as

controls for TRiP RNAis supplied from BDSC. GFP Valium10 expresses GFP under UAS control in the same Valium10 vector the RNAis were generated into, whilst P(CaryP)attP2 is an RNAi landing site control for transgene integration taking place on the third chromosome. As the majority of RNAis screened from the TRiP collection were 3rd chromosomal insertions, the attP2 landing site was an appropriate control. All RNAi constructs are designed to KD gene expression under UAS control.

3.1.4.2. Behavioural Phenotyping and Lifespan Assay

To have a holistic view of how glial AD risk gene activity impacts nervous system functioning throughout the fly's lifespan, locomotion was assessed at 2 weeks and 4 weeks post RNAi expression, reflecting mid and end stages of adulthood. Locomotion behaviour in *Drosophila* was assessed using an adaptation of the RING assay first described by (Gargano et al. 2005). The RING assay provides a rapid approach to assaying negative geotaxis response in multiple groups of flies in parallel. Negative geotaxis measures how quickly a fly climbs upwards once being tapped to the bottom of a vial. Such behaviour is part of the flies innate escape response and declines with age (Gargano et al. 2005). Also, across many neurodegenerative models including Alzheimer's, Parkinson's, Huntington's, and motor neuron diseases such as Amyotrophic lateral sclerosis (ALS), *Drosophila* show signs of locomotor impairment (Moloney et al. 2010; (Feany and Bender 2000,; Romero et al. 2008; Casci and Pandey 2015).

A similar RING assay design was replicated for the purpose of this screen with improvement to repeatability. The RING assay was used to identify AD risk genes that modify negative geotaxis behaviour and thus determine contribution of glial risk gene activity in the maintenance of nervous system functioning throughout age. The locomotive performance of flies was calculated from the average distance flies travelled up the vial in 10 seconds, post initiation of negative geotaxis, across five consecutive RING trials. A single RING trial was defined by a single round of inducing negative geotaxis and recording locomotor behaviour (see Chapter 2; section: 2.6.1). Flies were split into 10-20 flies per vial and around 5-10 vials per genotype were assayed; one vial equals 1n. Locomotor behaviour was compared to appropriate RNAi controls and statistical differences assessed by one-way ANOVA's with Sidak's multiple comparisons test.

Conducting a complete longevity screen for multiple RNAi lines targeting over 30 AD associated genes was beyond the scope of this screen. However, the difference in number of flies assayed at 2-week and 4-week behavioural timepoints provided an indication of the

impact glial AD risk gene KD had on viability. Where significant loss of viability was seen, complete survival studies for candidate genes were performed in male and female flies using an n ~100 flies per genotype.

A timeline of experiments conducted in this chapter, as well as a summary of timepoints and total n used for each experiment has been outlined below (Figure 3.2 and Table 3.1).

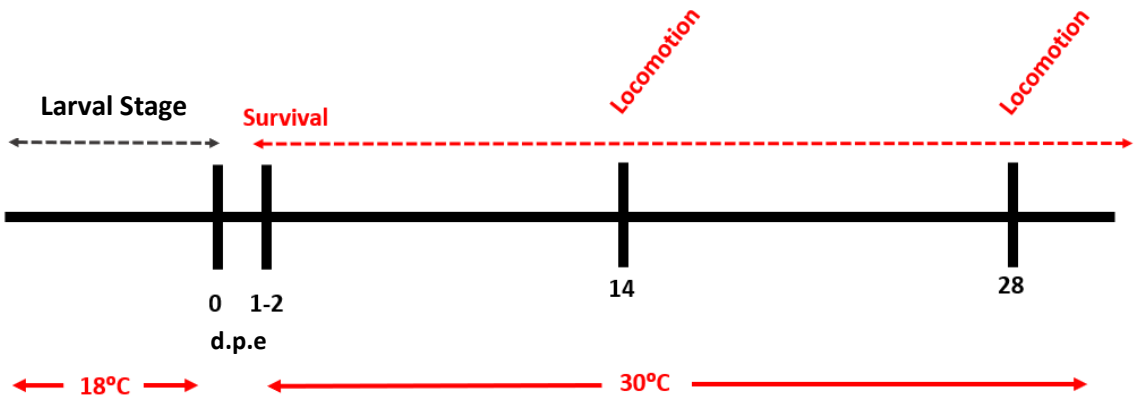

Figure 3.2: Timeline of experimental procedures.

Female virgins of glia specific driver were crossed to UAS-RNAi construct for conserved AD risk gene. Parental cross was kept at 18˚C throughout egg lay and rearing of F1 progeny. Adult male files, selected for RING assay experiments were maintained at 30˚C for a period of 4 weeks, recording locomotion behaviour at 2-week intervals. Where flies had survived to the 4-week timepoint locomotion data have been included. Percent survival of each genotype to 4 weeks was also recorded.

Experiment/Group	Total n	
	2 weeks	4 weeks
Locomotion	2-10n per genotype, males only	2-10n per genotype, males only
Survival	60-100 females and males combined	

Table 3.1: Summary of experimental assays. Number and sex of flies used for each experiment at respective timepoints.

3.2. Results

3.2.1. Computational Analysis of AD Risk Gene Orthologs in Flies

Human AD risk genes selected across several independent GWA studies and recent AD literature were analysed for genetic conservation in flies using DIOPT (version 8.5) (Lambert et al. 2013; Cruchaga et al. 2014; Witoelar et al. 2018; Kunkle et al. 2019; Schwartzentruber et al. 2021). DIOPT scores were calculated upon a set of 18 algorithms, indicating the level of gene conservation between species (human and flies), where the maximum score is 18 and the lowest being 1. 27 AD risk genes were found to have a direct ortholog in *Drosophila,* with varying degrees of conservation (see Table 3.2). AD risk genes *TREM2*, *CD33*, *MS4A6A*, *CLU* and *ZCWPW1* did not have a conserved ortholog. Conserved AD risk genes in flies were taken forward as candidates for the reverse genetic screen. DIOPT scores were used as a guide for gene homology and all genes with a conserved ortholog were included in the screen (even those with low DIOPT scores (≤4). In cases where candidate genes had a low DIOPT score consideration into the translatability of the results were to be taken, making sure to verify human risk gene orthologs through rescuing phenotypes with expression of the human cDNA.

Human Risk Gene Candidate	Fly homologue	DIOPT
ABCA7	CG34120	4
ABI3	Abi	5
BIN1	Amph	12
CELF1	bru1	14
TRIP4	CG11710	15
NME8	CG18130	3
PLD3	CG9248	15
CD2AP	cindr	8
CR1	Hasp	4
TP53INP1	DOR	4
EPHA1	Eph	6
SPI1	Ets98B	1
PTK2B	Fak	8
PICALM	Lap	14
FERMT2	Fit1	14
CR1	Fw	2
HS3ST1	Hs3st-A	6
SORL1	LpR2	2
MEF2C	Mef2	11
CNTNAP2*	Nrx-IV	13
INPP5D	Ocrl	13
CASS4	p130CAS	5
C1QBP*	P32	13
PLCG2	sl	10
SLC24A4	zyd	7
WWOX	Wwox	14
ACE	Acer	10
	Ance	10

Table 3.2: AD risk genes and their conserved Drosophila ortholog.

*List of AD risk genes conserved in Drosophila; comprised mostly of GWAS identified AD risk loci. Other AD relevant genes that did not come out of GWA studies are marked with *. The best conserved fly homologue of the AD risk loci has been reported based on DIOPT scores (version 8.5). DIOPT scores are to be used as guide for gene homology where the level of gene conservation between human and fly genes is indicated by a score out of 1. A score below 4 is considered poor conservation.*

3.2.2. The Development and Optimisation of RING Apparatus and Assay

Locomotion is an easily quantifiable phenotype in flies, providing a readout of overall CNS function. Typical assays that observe *Drosophila* behavioural responses to gravity involve tapping down individual vials to initiate negative geotaxis in flies (Ali et al. 2011;Benzer 1967). As flies ascend walls of the vial the number of flies to successfully pass a defined height after a defined number of seconds is counted. Whilst this method, is quick to set up and assay, with no need for specialised equipment, it is labour intensive and time consuming, producing significant variation in the force applied to initiate negative geotaxis between trials. RING assay was developed to provide a more sensitive, reproducible, and high throughput approach to measuring adult fly locomotor behaviours (Gargano et al. 2005).

In order to create a consistent assay that was amenable for simultaneous screening of multiple genotypes, thus fitting with the scale of the planned screen, I chose to adapt a similar RING apparatus previously described by (Gargano et al. 2005). The initial apparatus design (Figure 3.3A), built from card, held six cylindrical vials but was flimsy and an inconsistent force was applied between trials.

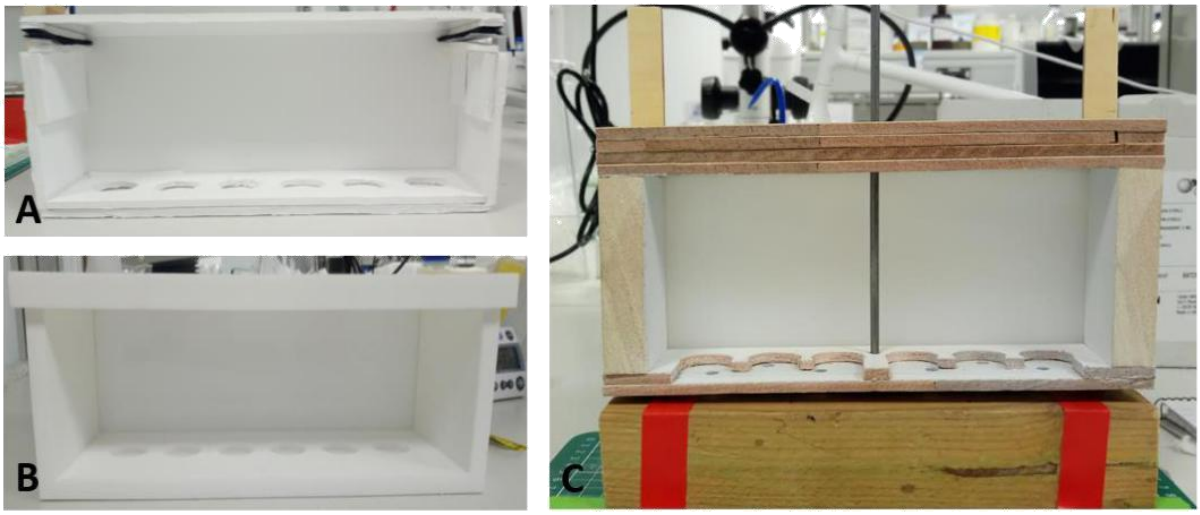

Figure 3.3: Three prototypes of RING apparatus.

A) Initial design made from foamboard with velcro to fasten the lid shut. B) 3D printed box design, made from a hard resin and an acrylic plastic sheet slotted at the back to allow uniform backlighting. C) Final prototype comprised of wooden box and stand. Metal rod runs through the middle of the box and two wooden guides are fixed to the posterior of the wooden platform. For this third prototype, the box is dropped from the same height for each RING trial (20 cm).

The second prototype was 3D printed in a hard plastic (Figure 3.3B), making the box more robust. Also, as 3D printed the design could be rebuilt precisely by other groups if desired. However, from a pilot test the design illustrated the importance of having a consistent force to initiate negative geotaxis across independent RING trials (Figure 3.4). On the first trial, flies travelled an average distance of 38 mm in 4 seconds which was double the average distance climbed by flies in the second trial 18 mm. The variation in average distance travelled between RING trials was due to inconsistent downward forces applied to initiate negative geotaxis. Inconsistent forces of negative geotaxis across assays therefore skewed the overall distance travelled recorded after n seconds.

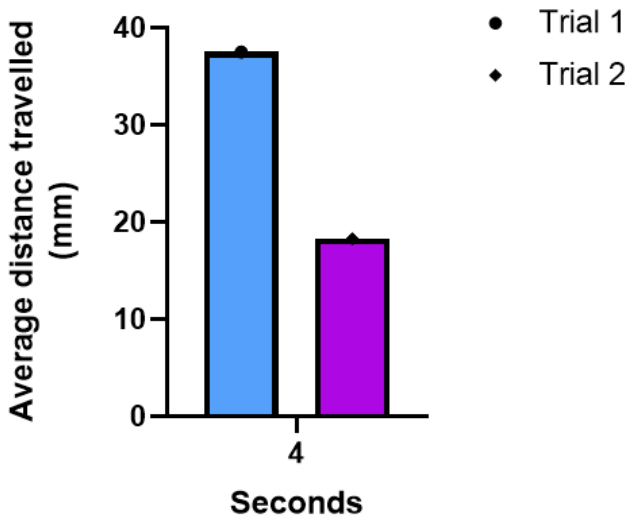

Figure 3.4: Comparison of Drosophila w- locomotion performance tested in two separate RING assay trials.

Average distance travelled (mm) by flies in 4 seconds, averaged across five consecutive RING trials. The RING assay was performed on separate days for female w- flies, 7 d.p.e. 18 flies per vial, assayed five times produced 1n. Statistics were not computed on these data sets as this was an n of 1.

The third design (Figure 3.3C) incorporated a physical constant into the experimental approach. Dropping the box from a set height (20 cm), allowed the constant force of gravity to initiate negative geotaxis in all flies. A vertical metal rod was used as a runner for the box, plus two wooden guides to help keep the box in place when hitting the platform.

3.2.3. Pan Glial Expression of Gal4 Does not Cause Locomotor Defects

After optimisation of the RING assay design, experiments then set out to determine if in absence of any UAS-reporters, the Gal4 and Tub-Gal80 gene expression machinery used in this study have any detrimental impact upon locomotion. Throughout this study, Repo-Gal4 was used to drive UAS-RNAi expression under regulation of temperature sensitive Tub-Gal80, exclusively in glia. The Tub-Gal80; Repo-Gal4 driver crossed to a w- background provided a technical control to ensure the Tub-Gal80 and Repo-Gal4 machinery did not themselves elicit a strong locomotor phenotype. If so, the screen may result in finding modifiers of this non-specific phenotype i.e. suppression of Gal4 expression, rather than biologically meaningful changes in glia functions.

Assessment of locomotor behaviour in wildtype flies (w-) vs the pan-glial driver only control (Tub-Gal80; RepoGal4) firstly highlighted that the distance travelled linearly correlates with assay duration (Figure 3.5), where flies travel further in 10 seconds than 4. In the first 4 seconds, the pan-glial driver only control had travelled further than age-matched wildtype flies (w-), 54 mm vs 41 mm respectively (Two-way ANOVA with Bonferroni's multiple comparison test; n=6-7, *p=0.0396). However, by 10 seconds the majority of flies from each genotype reached the top of the vial and there was no significant difference in average distance travelled (Two-way ANOVA with Bonferroni's multiple comparison test; n=6-7, ns: p>0.9999). This demonstrated, while the pan glial driver only control may climb quicker compared to wildtype flies (w-), the Tub-Gal80 and Repo-Gal4 machinery does not elicit any visible locomotion deficits (Two-way ANOVA with Bonferroni's multiple comparison test; n=6-7; Time: $F(1, 11) = 43.17$, ****p<0.0001, Genotype: $F(1, 11) = 3.526$, ns: p=0.1105, TimeXGenotype: $F(1, 11)= 3.526$, ns: p=0.0872).

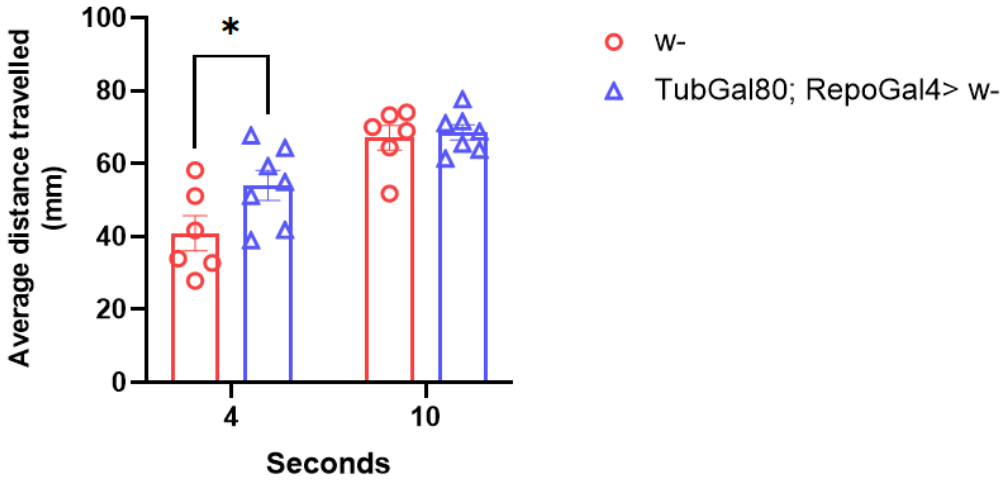

Figure 3.5: Locomotor behaviour of pan glial driver only control.

*Comparison of locomotion performance in males at 14 d.p.e. between wildtype flies (w-) and the pan glial driver only control (Tub-Gal80; Repo-Gal4). Plotted average distance travelled in 4 and 10 seconds, post negative geotaxis, averaged across 5 consecutive RING trials. Two-way ANOVA with Bonferroni's multiple comparison test; n=6-7, *p=0.0396. Error bars represent ±SEM.*

3.2.4. Validating Genetic Tools for Locomotion Screen of AD Risk Genes

Optimal time points for analysis of fly locomotive behaviour and effect of genetic background on performance in the RING assay were next determined. A time-course of heights climbed over 10 seconds was plotted for all control lines being used in the screen (Figure 3.6). Control lines included the glia specific temperature sensitive driver machinery (Tub-Gal80; Repo-Gal4) and RNAi specific controls made by the two stock centres each RNAi were sourced from.

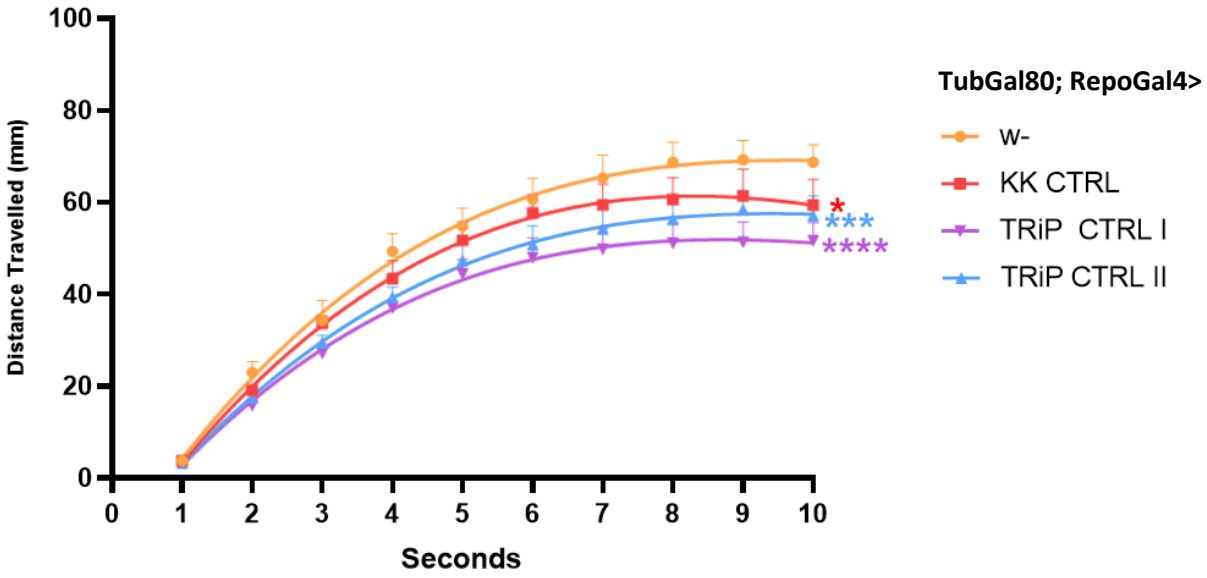

Figure 3.6: Locomotion time-course of control genetic backgrounds over RING test duration.

*Average distance travelled each second across 10 seconds, in male flies of respective control backgrounds, at 14 d.p.e. A n of 40-45 flies were assayed from 3 biological replicates. Area under the curve followed by one-way ANOVA with Sidak's multiple comparison test was used to calculate statistical differences in locomotor behaviour compared to the glial temperature sensitive driver only control (w-), *p=0.0279, ***p=0.0006, ****p<0.0001. Error bars represent ±SEM.*

The locomotion time-course of control genetic backgrounds, at 14 d.p.e (Figure 3.6), highlights locomotion performance throughout test duration differs significantly between genotype (Area under the curve followed by One-way ANOVA test; n=3; F= 35.75, p<0.0001). *Post hoc* analysis with Sidak's multiple comparison test indicates differences lie between the glial driver only control (w-) and each of the RNAi controls, KK control (*p=0.0279), P(CaryP)attP2 control (***p=0.0006) and GFPValium10 control (****p<0.0001). There was also a significant difference in locomotor performance between the VDRC RNAi control line (KK control) and the Bloomington RNAi control line (GFP Valium10) (**p=0.0020), however no significant differences between the P(CaryP)attP2 and GFP Valium10 controls (p=0.1336) which were both sourced from BDSC.

Whilst the distance travelled throughout test duration differed across independent controls, there were clear trends in locomotion behaviour across the 10 second period. For example, the time-course highlights the greatest overall distance travelled by the flies occurs in the

first 4 seconds (the most linear part of the graph) and that around 5-7 seconds the height climbed begins to plateau. By 8 seconds flies have typically reached the highest point and at 10 seconds this height has become saturated.

These optimisation experiments for RING assay analysis and screen design demonstrate that the machinery used for glia specific KD does not alter fly motor behaviour as expected, with no clear locomotor deficits at 14 d.p.e. However, machinery required to make UAS-RNAi constructs such as vectors and transgene elements may play party to the differences in locomotor behaviour observed between the glial specific driver and each RNAi control line. Regardless to this finding, optimal timepoints for RING data analysis were deduced; 4 and 10 seconds. Reporting heights climbed at 4 seconds serves as a good indicator of any genes that enhance or suppress locomotor activity. Comparing the distance travelled in the first 4 seconds would also provide greater sensitivity over measuring distance travelled between 4 and 10 second timepoints. As the final timepoint, 10 second analysis of heights climbed will enable identification of modifiers that cause exceptionally strong locomotor deficits.

3.2.5. RNAi Screen of Candidate AD Risk Genes Using Optimised RING Assay

48 independent RNAi lines targeting these conserved AD risk genes were selected and screened for locomotor behaviour, using the optimised RING assay (see section: 3.2.2). Where possible multiple RNAis for each gene were tested to ensure off target effects or inefficient RNAi KD did not mislead identification of potential screen hits.

3.2.5.1. Screened Locomotor Behaviour at 2 Weeks

Locomotor performance was first assessed in flies 2 weeks post RNAi induction, recording distance travelled at 4 and 10 seconds post negative geotaxis (Figure 3.7). The glial driver only control (w-) and individual RNAi controls (KK CTRL, TRiP CTRL I, TRiP CTRL II), showed no deficits in locomotor behaviour, reaching average heights of 70 mm, 60 mm, 58 mm and 59 mm, respectively after 10 seconds (full duration of the assay). As previously shown in optimisation experiments the glial driver only control performed better compared to RNAi background controls, travelling on average 10 mm further in 10 seconds (One-way ANOVA with Sidak's multiple comparison test; n=5-10, F=13.04, w- vs KK CTRL: **p=0.0061, w- vs TRiP CTRL I: ****p<0.0001, w- vs TRiP CTRL II: ***p=0.0006). However,

there was no significant differences in distance travelled between individual RNAi background controls (One-way ANOVA with Sidak's multiple comparison test; n=5-9, F=13.04, KK CTRL vs TRiP CTRL I: ns: p=0.9635, KK CTRL vs TRiP CTRL II: ns: p>0.9999, TRiP CTRL I vs TRiP CTRL II: ns: p=0.9601). Average distance travelled upon expression of individual RNAis were therefore compared to each of their respective age-matched RNAi controls i.e. RNAis sourced from VDRC were compared to the KK control, whereas RNAis sourced from BDSC were compared to the GFPvalium10 vector control (TRiP RNAi I), which expresses GFP under UAS control in the Valium10 vector.

Locomotor deficits were observed upon glial KD of *CG9248/PLD3* (RNAi: 109798), *cindr/CD2AP* (RNAi: 38854), *Mef2/MEF2C* (RNAi: 15550), *zyd/SLC24A4* (RNAis: 40988, 25851) and *Ance/ACE* (RNAi: 36479), whereby the average distance travelled in 10 seconds was significantly lower compared to their respective RNAi controls. These flies travelled average distance of 42 mm, 43 mm, 47 mm, 37 mm, 19 mm, 12 mm, and 28 mm respectively (One-way ANOVA with Sidak's multiple comparison test; KK CTRL comparisons: n=1-10, F=12.62, CG9248 I: ***p=0.0003, cindr: *p=0.0452, Mef2 I: ****p<0.0001, zyd I: ****p<0.0001. TRiP CTRL I comparisons: n=1-10, F=13.04, Ance: ****p<0.0001, zyd II: ****p<0.0001). 4 out of the 6 RNAis to exhibit locomotor deficits at 10 seconds also showed reduction in locomotor performance as early as 4 seconds. These included genes for *cindr/CD2AP* (RNAi: 38854), *Mef2/MEF2C* (RNAi: 15550), *Ance/ACE* (RNAi: 36479) and *zyd/SLC24A4* (RNAi: 40988, 25851) (One-way ANOVA with Sidak's multiple comparison test; KK CTRL comparisons: n=1-10, F=8.818, cindr: *p=0.0234, Mef2 I: ****p<0.0001, zyd I: ****p<0.0001. TRiP CTRL I comparisons: n=1-10, F=8.818, Ance: ****p<0.0001, zyd II: ****p<0.0001). On the other hand, glial KD of *Acer/ACE* (RNAi: 67205) improved locomotor behaviour, increasing average distance travelled by 15 mm compared to the TRiP RNAi control (TRiP CTRL I) (One-way ANOVA with Sidak's multiple comparison test; n=1-10, F=13.04, ***p=0.0002). This demonstrated LOF of *Acer/ACE* in glia may have early protective effects in nervous system functioning.

Overall, analysis of screened locomotor behaviour at 2 weeks revealed a number of AD risk genes important to glial mediated neurological dysfunction.

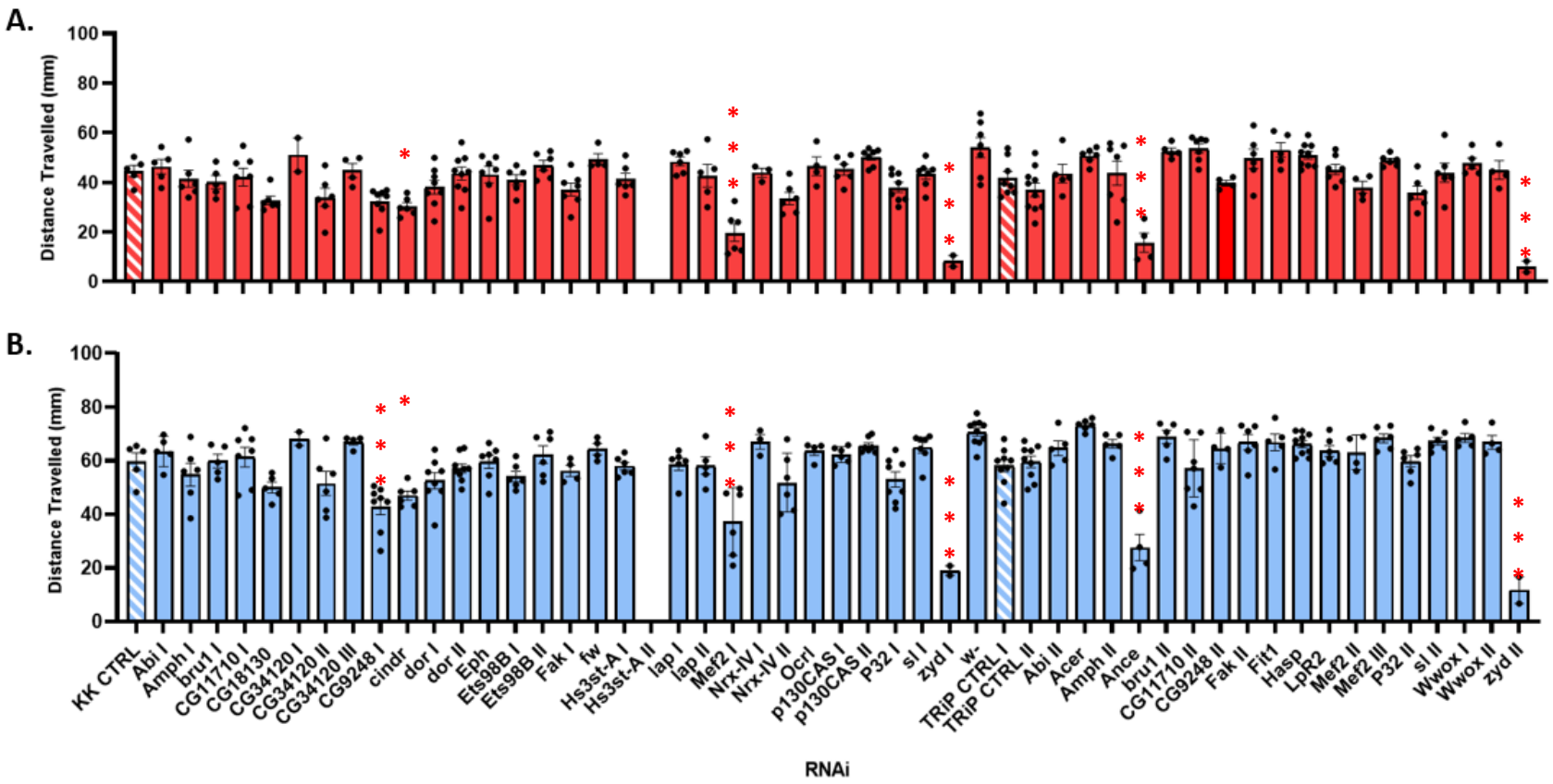

Figure 3.7: Screened locomotion performance at 2 weeks post eclosion.

Average distance travelled at A) 4 and B) 10 seconds post negative geotaxis in male flies following glial KD of conserved AD risk genes, at 2 weeks. Individual data points correspond to the average distance travelled by flies in a single vial, averaged over 5 consecutive RING trials, which equates to n=1. A total n=2-10 vials were analysed at 2 weeks and statistical differences in distance travelled were calculated from One-way

*ANOVA with Sidak's multiple comparisons test. Statistical differences are marked by asterisks A) Left to right: cindr: *p=0.0280, Mef2 I: ****p<0.0001, zyd I: ****p<0.0001, Ance: ****p<0.0001, zyd II: ****p<0.0001. B) Left to right: CG9248 I: ***p=0.0003, cindr: *p=0.494, Mef2 I: ****p<0.0001, zyd II: ****p<0.0001. Error bars represent ±SEM.*

3.2.5.2. Screened Locomotor Behaviour at 4 Weeks

With AD being an age associated disorder it is feasible that an observed phenotype may only occur in relatively elderly flies and so locomotion performance was remeasured at 4 weeks; a timepoint reflective of later adulthood stage.

Assessment of average distance travelled post 4 weeks RNAi induction clearly demonstrated locomotor behaviour senesces in flies, with all RNAis exhibiting at least a 10% reduction to average distance travelled from the initial 2-week timepoint (Figure 3.8). The KK control exhibits a more severe decline in locomotor behaviour compared to TRiP RNAi background controls (70% vs 40%). Locomotion behaviour recorded at 4 weeks is much more variable than at 2-week timepoints demonstrated by the increase in average standard deviation of the TRiP RNAi background control (2 weeks: 6.9, 4 weeks: 19). It was also clear that a number of genotypes were not viable to this 4-week timepoint, as indicated by no recorded locomotion data. 41% of the RNAis tested experience a 50% decline in locomotion behaviour, similar to their respective RNAi background controls. Glial KD of *DOR/TP53INP1* (RNAi: 105330), *Eph/EPHA1* (RNAi: 110448) and *p130CAS/CASS4* (RNAi: 330191) however, display somewhat conserved locomotor behaviour at 4 weeks, showing significant increase in average distance travelled by 10 seconds to their respective RNAi background control (One-way ANOVA with Sidak's multiple comparison test; KK CTRL comparison n=1-10; F= 2.519, DOR RNAi I: **p=0.0039, Eph RNAi: *p= 0.0238 and p130CAS RNAi II: **p= 0.0024).

Analysis of screened locomotor behaviour at 4-week timepoints highlighted glial expression of some AD risk genes negatively impacts nervous system functioning in aged models, where their KD in glia slowed age related locomotor decline.

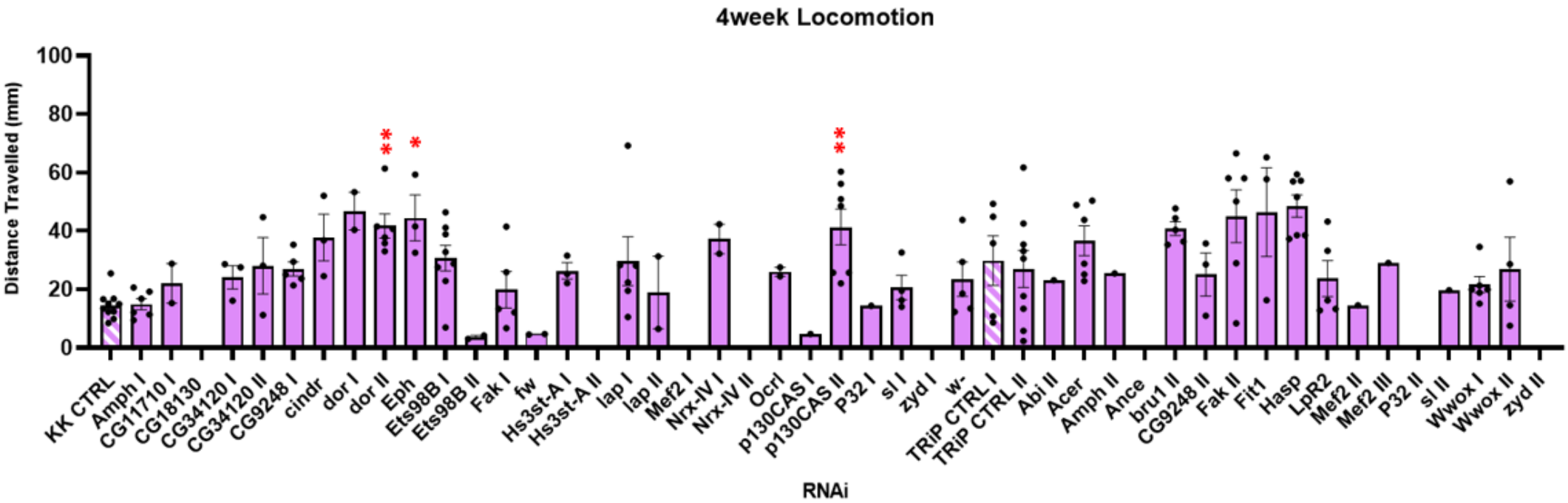

Figure 3.8: Screened locomotion performance remeasured at 4 weeks upon KD of conserved AD risk genes.

*Average distance travelled 10 seconds post negative geotaxis in male flies, following glial KD of conserved AD risk genes, at 4 weeks. Individual data points correspond to the average distance travelled by all flies in a single vial, averaged across five consecutive RING trials (n=1). A total n=1-10 vials were analysed at 4 weeks and statistical differences in average distance travelled were calculated from One-way ANOVA with Sidak's multiple comparisons test. Statistical differences are marked by asterisks, left to right: DOR RNAi II: **p= 0.0039, Eph RNAi: *p= 0.0238, p130CAS RNAi II: **p= 0.0024). Error bars represent ±SEM.*

3.2.6. Glial Knockdown of Some AD Risk Genes Alter Survival

Upon ageing flies out to 4-week locomotor timepoints, several RNAis were not able to be tested due to premature death, highlighting that glial KD of some AD risk genes may influence survival. Instead of conducting complete survival assays for all RNAis, the percent survivorship of flies between 2-week and 4-week locomotor timepoints was used as a proxy to determine which genes may be important to longevity. The percent survival was calculated from the difference between number of flies tested in RING behavioural assays at 2-week vs 4-week timepoints.

For each genotype the percentage of flies surviving to 4-week locomotion timepoints was calculated and graphed (Figure 3.9). RNAi controls showed an average survival rate of 56%. The percent survival for each RNAi varies considerably to this, with glial KD of AD risk genes showing to either enhance or reduce survival rate compared to respective RNAi background control. A stringent 5% survival rate was decided to threshold genes that displayed marked reduction in survival comparative to their RNAi controls. 7 candidate genes demonstrated 0% survival rate to 4 weeks upon glia specific loss, those being *CG18130/NME8* (RNAi: 20599), *Hs3st-A/HS3ST1* (RNAi: 25571), *NrX-IV/CNTNAP2* (RNAi: 9039), *P32/C1QB* (RNAi: 11023 and 34585), *zyd/SLC24A4* (RNAi: 40988 and 25851), *Ance/ACE* (RNAi: 36479) and *Mef2/MEF2C* (RNAi: 15550 and 38274). The RNAi targeting P32 (RNAi: 110239) also showed notably reduced survival rates upon glial KD, lying just below the 5% survival rate threshold.

Overall results demonstrated that glial expression of some AD risk genes may be important to longevity, such that their reduced expression in glia can cause survival deficits.

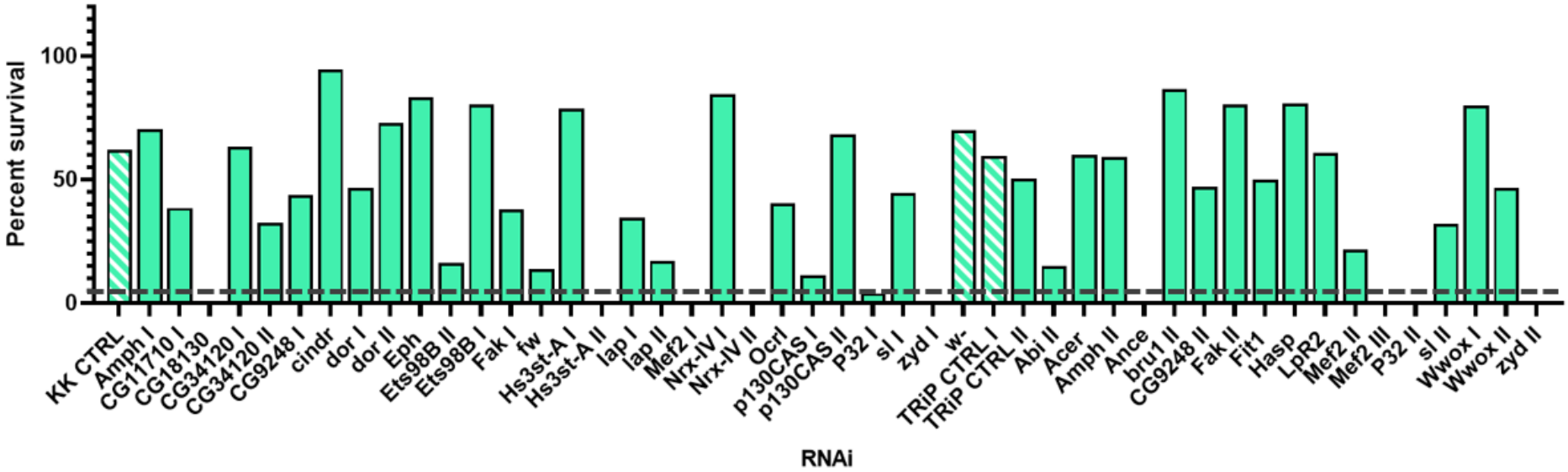

Figure 3.9: Percentage survival of Drosophila to 4 weeks from glial RNAi KD screen.

The percentage of male flies that survived to 4-week ages, calculated from the difference in number of flies initially tested at 2-weeks locomotion timepoints and those tested at 4 weeks. n= 15-270 (taken as the number of flies assayed from each group at the 2-weeks timepoint). Percent survivorship below the 5% threshold mark was considered significant.

3.2.7. Validating Locomotion and Survival Phenotypes of Screen 'hits'

Having identified glial expression of some AD risk genes could be implicated in nervous system functioning and survival of adult flies, validation of repeatable locomotor and survival phenotypes using multiple RNAis available for the gene of interest was completed next. Glial KD of genes yielding significant locomotor deficits at 2-week timepoints were reviewed. The availability of RNAis largely dictated the extent of which genes could be validated.

Glial KD of *CG9248/PLD3*, *Ance/ACE* and *Mef2/MEF2C* were tested for repeatable locomotor phenotypes at 2-week timepoints (Figure 3.10). The fly gene phospholipase D family member 3 (pld3), formerly known as CG9248, is orthologous to mammalian PLD3, and is a membrane associated protein involved in phosphoinositide metabolism (Gaudet et al. 2011). Repeated comparison of locomotor behaviour upon glial KD of *pld3/PLD3* (RNAi: #109798) with age matched KK RNAi control revealed no significant difference in average distance travelled by 10 seconds (Unpaired t-test; two tailed, t=0.04609, df=28, ns: p=0.9636). Since locomotor deficits upon glial KD of *pld3/PLD3*, observed from the initial screen were not replicated, it is unlikely glial expression of *pld3* plays a role in glial mediated neuronal dysfunction.

Next, locomotor behaviour upon glial KD of *Ance/ACE* was retested. Ance is the fly ortholog of mammalian angiotensin converting enzyme (ACE) which possess endopeptidase activity. In contrast to mammalian ACE which canonical role is in the Renin angiotensin system (RAS), Ance is required for normal development (metamorphosis) and reproduction of *Drosophila* (Siviter et al. 2002). Comparison of average distance travelled in 10 seconds with age matched TRiP RNAi background control (TRiP CTRL II) demonstrated repeatable locomotor deficits with Ance RNAi I (#36479), where glial KD resulted in flies travelling significantly shorter distances (28 mm) compared to the TRiP RNAi background control (58 mm) (One-way ANOVA with Sidak's multiple comparison test; n=4-5, F=26.49, ***p=0.0005). However, testing another independent RNAi of Ance (Ance RNAi II: #51747) revealed discrepancy in locomotor behaviour, where the average distance travelled by flies expressing Ance RNAi II vs TRiP RNAi background control were comparable (One-way ANOVA with Sidak's multiple comparison test; n=4-5, F=26.49, ns: p=0.2112). This conflicting result between independent RNAis targeting the same gene highlighted the need to verify Ance RNAi gene targets.

Finally, repeatable locomotor deficits upon glial KD of Mef2 (RNAi: #15550) were verified. *Myocyte enhancing factor 2* (*Mef2*) belongs to the MADs-box family of transcription factors and is orthologous to *MEF2C* in humans. From the initial screen of RNAis, glial KD of *Mef2*

with RNAi I (RNAi: #15550) highlighted a significant locomotor deficit at 2 weeks (Figure 3.8C). This locomotor phenotype was repeated, where glial KD of *Mef2* was shown to reduce average distance travelled in flies by 37 mm compared to age matched KK RNAi control (Unpaired t-test, two-tailed; n=5, t=6.259, df=8, ***p=0.0002). Other Mef2 RNAis (RNAi II: #28699 & RNAi III: #38247) did not display locomotor deficits at 2 weeks in both the initial screen and in phenotype validation. However, retesting locomotor behaviour at a later timepoint (3 weeks), demonstrated glial KD of *Mef2* with RNAi II (RNAi: #28699) resulted in impaired locomotor function, where flies travelled on average 20 mm less than age matched RNAi control (TRiP CTRL II) (Mixed effect analysis with Dunnett's multiple comparison test; n=3-5, **p=0.0017). Repeatable locomotor deficits upon glial KD of *Mef2* with two independent RNAis, strongly implicates glia expression of *Mef2* is important for maintaining nervous system functioning with age.

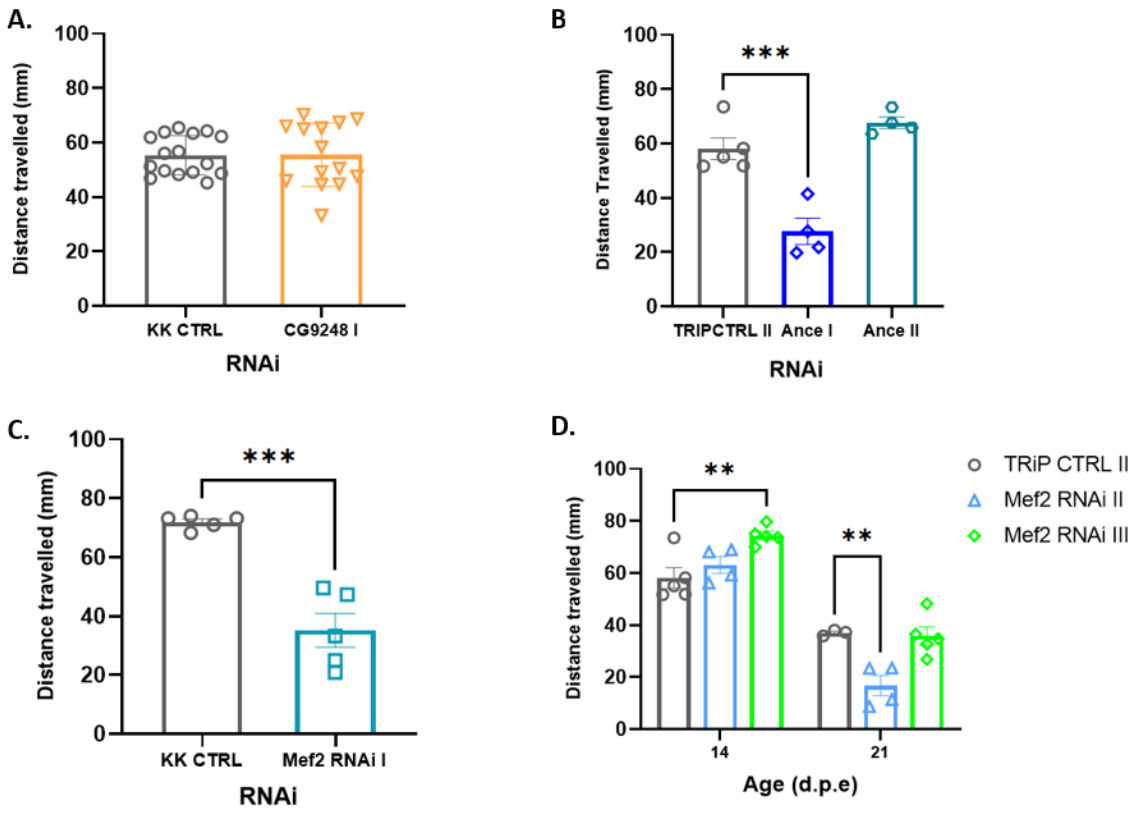

Figure 3.10: Validated locomotor phenotypes for initial RNAi hits.

*A&B) Average distance travelled 10 seconds post negative geotaxis in male flies following glial KD of A) pld3 B) Ance and C) Mef2 at 2 weeks, compared to respective RNAi background controls. A single data point (n=1) corresponds to the average distance travelled by all flies in a single vial, averaged across 5 consecutive RING assays. Statistical differences were calculated by either A&C) Unpaired t-test or B) one-way ANOVA with Dunnett's multiple comparison test, where significance is marked by asterisks B) ***p=0.0005, C) ***p=0.0002. D) Time-course of locomotor performance in male flies testing multiple independent RNAis against Mef2. Plotted average distance travelled, 10 seconds post negative geotaxis, at 14 and 21 d.p.e. Mixed effect analysis with Dunnett's multiple comparisons test; Mef2 RNAi III: **p=0.0021 (14 d.p.e) and Mef2 RNAi II: **p=0.0017 (21 d.p.e). Error bars represent ±SEM.*

Next, repeatability of survival phenotypes, identified in section 3.2.6 were tested by conducting full survival assays with multiple RNAis available for the gene of interest. From the initial screen, viability defects were noted upon glial expression of Hs3st-A RNAi II (RNAi: #25571), CG18130 RNAi (RNAi: #20599), Mef2 RNAi I & II (RNAi: #15550 &

#38247), P32 RNAi I & II (RNAi: #110239, #34585) and Ance RNAi I (RNAi: #36479), where the percentage survival to 4-week locomotor timepoints was 5% or less. Full survivorship of flies expressing these RNAis were recorded and compared to appropriate controls (Figure 3.11).

Repeatable survival deficits in Hs3sT-A RNAi II, CG18130 RNAi, Mef2 RNAi I and Ance RNAi I expressing flies were observed. The survivorship of flies expressing Hs3sT-A RNAi II, CG18130 RNAi and Mef2 RNAi I was markedly shorter compared to the glial driver only control (w-), with flies exhibiting median lifespan of 6, 22 and 21 days respectively compared with 32 days of the control (Log-rank, Mantel-Cox test; Hs3sT-A RNAi II: n=203-275, χ^2= 656, df=1, ****p<0.0001; CG18130 RNAi: n=90-122, χ^2= 170.4, df=1, ****p<0.0001; Mef2 RNAi I: n=105-224, χ^2= 273.5, df=1, ****p<0.0001). Lifespan of flies expressing Ance RNAi I was also markedly reduced compared to that of the TRiP RNAi background control for attP2 transgene insertion, with a difference in median lifespan of 16 days (Log-rank, Mantel-cox test; n=106-191, χ^2= 227.6, df=1, ****p<0.0001).

Severe viability defects observed upon glial expression of P32 RNAis (RNAi: #110239, #34585) in the initial screen were not repeated, however modest differences in survival were observed. Log-rank, Mantel-cox test reported a statistical difference between survivorship of flies expressing P32 RNAi I vs the glial driver only control (w-) (Log rank, Mantel-cox test; n= 150-156, χ^2= 25.69, df=1, ****p<0.0001), however, the difference in median lifespan was only 2 days and not considered substantial. Flies expressing the P32 RNAi II also showed a 2-day difference in median lifespan when compared with the TRiP RNAi background control, however, Log rank, Mantel-cox test did not report a statistical difference in survival here (Log-rank, Mantel-cox test; n=106-182, χ^2=2.062, df=1, ns: p=0.1510). *P32* encodes an evolutionary conserved mitochondrial protein and is orthologous to the human AD risk gene *C1QBP*. Knocking down *P32/C1QBP* in glia did not give rise to survival deficits in two independent RNAis and therefore unlikely glial expression of *P32/C1QBP* is involved in survival of adult flies.

Comparative analysis of survival in additionally sourced RNAis revealed conflicting survival phenotypes for glial KD of Hs3st-A, Ance and Mef2. Additional RNAis of Hs3st-A (RNAi I: #4998 and RNAi III: #28618) did not lead to severe survival deficits. Instead, survival curves presented only minor deviation in survival compared to respective controls; glial driver only (w-) and TRiP RNAi background control (TRiP CTRL II). The median lifespan was 33 and 30 days respectively in Hs3st-A RNAi I and III expressing flies, which was comparable to the median lifespan of their respective controls (w-) and (TRiP RNAi II) at 32 and 33 days (Log-rank, Mantel-cox test; Hs3st-A RNAi I: n=193-322; χ^2=10.51, df=1, **p<0.0012; Hs3st-A

RNAi III: n=106-147; χ^2=31.90, df=1, ****p<0.0001). Clear differences in survival phenotypes observed indicate possible off target effects of the Hs3st-A RNAi II (RNAi: #25571) and thus the unlikely contribution of glial *Hs3sT-A/HS3ST1* expression in survival of adult flies. Differences in survival phenotypes were also observed between tested Ance RNAis, where the median lifespan of Ance RNAi I expressing flies was 17 days, whilst for Ance RNAi II expressing flies, the median lifespan was 30 days. Compared to the TRiP RNAi background control, Ance RNAi II expressing flies displayed a similar survival trajectory, where Log-rank, Mantel-cox test reported only slightest of differences (Log-rank, Mantel-cox test; 106-193; χ^2= 6.845, df=1, **p=0.0089). Similarly, other RNAis of Mef2 (RNAi II: #28699, RNAi III: #38247) did not exhibit strong survival deficits, where their median lifespan was 33 and 30 days respectively compared to the median lifespan of the TRiP RNAi background control at 33 days (Log-rank, Mantel-cox test; Mef2 RNAi II: n=106-118, χ^2=4.891, df=1, *p=0.0270; Mef2 RNAi III: n=106-217, χ^2= 22.09, df=1, ****p<0.0001).

Data from phenotypic validation studies revealed verifiable locomotor or survival phenotypes with Mef2 RNAi I (#15550), Ance RNAi I (#36479), Hs3st-A RNAi II (28618) and CG18130 RNAi (#20599). Results also highlighted phenotypic differences in both locomotion and survival between independent RNAis tested that targeted the same gene. To have greater confidence in locomotor and survival phenotypes observed upon glial KD of these AD risk genes, further investigation is needed for each RNAi implicated in the screen.

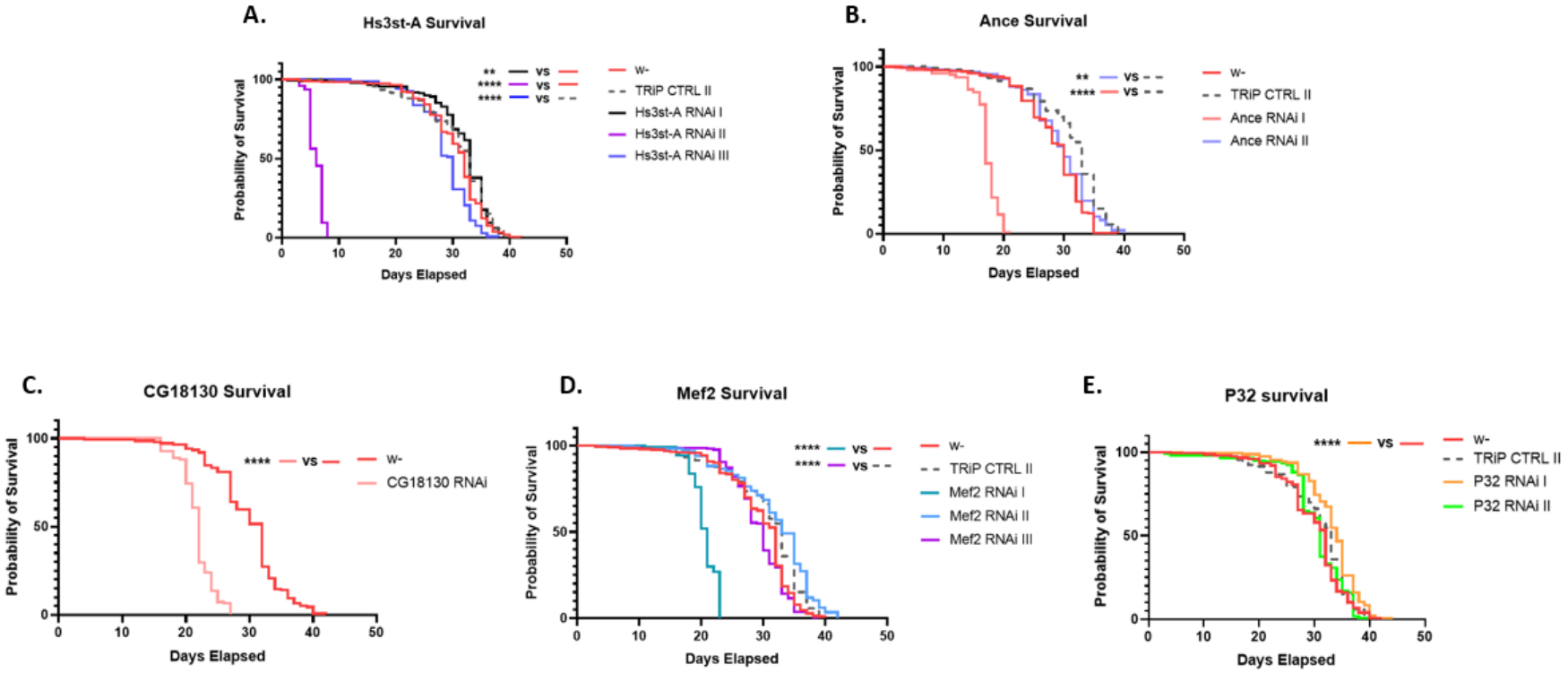

Figure 3.21: Survival assays of initial screen hits.

*Various RNAis against A) Hs3st-A, B) Ance, C) CG18130, D) Mef2 and C) P32 were tested for repeat survival phenotypes. RNAis expression was targeted to glia during adulthood where flies were maintained at 30°C for their remaining lifespan and deaths were recorded every 2-3 days (see Chapter 2; section: 2.5.3). Log-rank, Mantel-cox test for combined survival of males and 24hr mated females A) Hs3st-A RNAi I: **p=0.0012, Hs3st-A RNAi II: ****p<0.0001, Hs3st-A RNAi III: ****p<0.0001 B) Ance RNAi I: ****p<0.0001, Ance RNAi II: **p=0.0089 C) CG18130 RNAi: ****p<0.0001 D) Mef2 RNAi I: ****p<0.0001, Mef2 RNAi III: ****p<0.0001 E) P32 RNAi I: ****p<0.0001. For all survival experiments, n> 106 deaths were counted per condition.*

3.3. Discussion

This chapter details a reverse candidate KD screen of conserved AD risk genes, identifying genes that expression in glia likely contributes to nervous system functioning and/or survival in adult flies.

In total 48 RNAi lines were screened, knocking down 27 AD risk genes exclusively in glia at adult specific stages. Knocking down *Ance/ACE* (RNAi: #36479), *Mef2* (RNAi: #15550) and *zyd* (RNAi: #40899, #25851) in glia resulted in significant deficits to both locomotion and survival, highlighting their expression in glial potentially plays important roles in the overall fitness/health of the fly. Deficits in locomotor behaviour were verified in *Ance/ACE* (#36479) and Mef2/MEF2C (#15550) RNAi expressing flies at 2 weeks and Mef2/MEF2C (#28699) at 3 weeks, implicating glial expression of these genes could be involved in the maintenance of nervous system functions throughout age. Additionally, survival phenotypes were replicated in CG18130/NME8 (#20599) and Hs3st-A/HS3ST1 (#25571) RNAi expressing flies, whereby flies exhibited significantly shorter lifespan compared to their respective controls. This is indicative of these genes' potential involvement in survival. Overall, this data supports further exploration into *Ance/ACE*, *Mef2/MEF2C*, *CG18130/NME8*, *Hs3st-A/HS3ST1* and *zyd/SLC24A* genes, which expression in glia demonstrates a potential contribution to physiological ageing.

3.3.1. AD Risk Genes that Modify Locomotor Behaviour and/or Survival

3.3.1.1. zyd/SLC24A4

Pan-glial KD of *zydeco (zyd)* exhibited seizure phenotypes upon initiating negative geotaxis, resulting in notable locomotor deficits ($p<0.0001$). Also, several flies did not survive to 2-week locomotor timepoints, indicating reduced survivorship upon glial KD of zyd.

Zyd is orthologous to human *solute carrier 24* member 4 (*SLC24A4*) (DIOPT score: 7) and encodes a conserved plasma membrane glial transporter involved in potassium dependent exchange of sodium and calcium (Melom & Littleton, 2013). In the adult fly brain, zyd is predominately expressed in a specific subset of glia called cortex glia, where the potassium Na^{+}/Ca^{2+} (NCKX) exchanger it encodes is located within the membrane microdomain. Cortex glia in flies most closely resemble satellite glia in humans (Melom and Littleton 2013; Lago-

Baldaia et al. 2020). The human ortholog, SLC24A4 is expressed in glia cells such as astrocytes, schwann cells, and oligodendrocyte precursors, however is also very highly expressed in retinal neurons (Uhlén et al. 2015). The role of zyd in nervous system functioning is likely due its ability to control neuronal excitability through regulation of glial Ca^{2+} oscillations. Dysregulation of glial Ca^{2+} oscillations in zyd mutants causes neuronal hyperactivity, inducing seizures in flies (Melom & Littleton, 2013). Melom and Littleton demonstrated pan-glial KD of zyd by two independent RNAis resulted in temperature sensitive seizures in the third instar larvae and was semi lethal in adults, supporting the seizure phenotypes and early death phenotype we observed. Given zyd mutants have been reported to exhibit increased susceptibility to seizures (mechanical and temperature induced), locomotion impairments seen in our assay likely represent ‘’bang’’ (mechanically), inducible seizures. Whilst the role of zyd/SLC24A4 in the pathogenesis of AD has not yet been fully elucidated, its influence on neuronal function through controlling glial Ca^{2+} transients is likely to contribute. Furthermore, involvement of zyd/SLC24A4 in glial Ca^{2+} cytosolic export may be critical to glial function, whereby a build of intracellular Ca^{2+} is cytotoxic, making the cells more vulnerable to death.

The SNP (rs10498633) was first identified in a 2013 AD risk GWAS, linking the *SLC24A4* locus with AD (Lambert et al. 2013). Whilst zyd mutants display seizure like phenotypes, no link between the human ortholog SLC24A4 and seizures have yet been identified. During the course of this thesis study, fine mapping has revealed another gene *RIN3* (Ras and Rab interactor 3) within the *SLC24A4* locus, which is now thought to be the causal gene. RIN3 also directly interacts with two other AD risk loci, *BIN1* and *CD2AP* in the early endocytic pathway (Schwartzentruber et al. 2021). With the genetics of this locus still being determined, it is important to understand how all genes within this locus might contribute to AD. Since we and others evidence an important role for zyd in glial modulation of neuronal function, it would be worth investigating how zyd expression in glia impacts fly models of AD.

3.3.1.2. CG18130/NME8

Glial KD of *CG18130*, orthologous to human AD risk gene *NME/NM23 family member 8* (*NME8)* (DIOPT score: 3) significantly reduced survivorship of adult flies ($p<0.0001$).

In flies, functions of CG18130 are largely unknown but speculated to be involved in ciliary motility of *Drosophila* sperm (Lage et al. 2019), where its ortholog *NME8* has been shown to bind microtubules and play a key role in ciliary motility (Duriez et al. 2007). Scope data

reveals little expression of CG18130 within the adult fly brain, suggesting its role in glia may be unlikely. Similarly, its human ortholog, NME8 is not highly expressed in the nervous system, displaying very low expression in oligodendrocytes (Uhlén et al. 2015). NME8 and members of its family (NME/NM23) have however been associated with neurodegenerative disease (Kim et al. 2002; Lahiri et al. 2013). In a 2013 AD GWAS, *NME8* was highlighted as the closet loci to the SNP rs2718058 (Lambert et al. 2013) and has since been replicated in a more recent European Alzheimer and Dementia Biobank GWA study (Bellenguez et al. 2022). Whilst there has not been much reported on NME8s involvement in AD, a study assessing association of the NME8 polymorphism (rs2718058) and AD biomarkers revealed a potential role of the SNP in lowering brain neurodegeneration: delaying cognitive decline, elevation of tau levels in the CSF and hippocampal atrophy (Liu et al. 2014). Other SNPs in *NM8E* (rs2722372), have also been linked to Aβ accumulation in patients (Seo et al. 2020), indicating this gene has interesting potential in AD pathology. NME8s interaction with microtubules, which supports ciliary movements may well underlie its contribution to AD, given microtubule instability is an important factor of tau pathophysiology. Microtubules are an important structural component of the glial cytoskeleton, where its interaction with the actin cytoskeleton is necessary for the establishment and maintenance of cell shape, migration and division, intracellular transport, and intercellular interactions (Dugina et al. 2016). Microtubules have been shown to control actin cytoskeletal organisation (Small and Kaverina 2003) and therefore impairment of microtubule function may promote dysregulation of actin dynamics, which would ultimately impair glial cell functions such as migration and phagocytosis. Exploring how NME8 AD associated polymorphisms interact with microtubules and thus influence glial cell functions such as migration and phagocytosis would be an interesting direction for future experiments.

3.3.1.3. Mef2/MEF2C

The screen implicated glial expression of *Mef2* in both glial mediated neurological dysfunction and survival, where knocking down *Mef2* in glia led to deficits in both locomotor behaviour ($p<0.0002$, $p<0.0017$) and survival ($p<0.0001$).

Drosophila Myocyte enhancing factor 2 (Mef2), encodes a transcription factor involved in transcriptional regulation of a number of genes, primarily required for muscle development (Bour et al. 1995). It is also responsible for gene expression in other tissues including neural tissue (Assali et al. 2019). Mef2s expression in Keynon neurons for instance has been linked to the development of the mushroom body in the fly brain, which is pivotal to learning

and memory (Crittenden et al. 2018). Moreover, Mef2 is a core transcriptional component of the innate immune response of the adult fly (Clark et al. 2013).

Drosophila Mef2 is orthologous to mammalian *MEF2C* (DIOPT: 11), sharing conserved functions. N-terminal sequences that encode the DNA binding domains, MEF and MADs, exhibit ~80% identity between *Drosophila Mef2* and the four mammalian *MEF2* members, indicating evolutionary conservation in DNA sequences bound by MEF2 (Molkentin and Olson 1996; Potthoff and Olson 2007). Furthermore, Mef2 has been shown to transcriptionally activate orthologous gene sets in flies and mice (Lilly et al. 1995; Lin et al. 1997). Both Mef2 and MEF2C are expressed in glial cells of the adult fly and human brain, respectively. In particular, MEF2C in humans is enriched in microglia cells, where it has been shown to regulate inflammatory microglial responses that are critical to AD pathogenesis (Deczkowska et al. 2017).

MEF2C was first linked to AD in a 2013 GWA study, however, has lost genome wide significance in more recent studies (Kunkle et al. 2019; Bellenguez et al. 2022). Nonetheless, MEF2C plays an important role in synapse development, facilitating learning and memory (Barbosa et al. 2008), as well as transcriptional activation of BDNF, which promotes neuronal survival (Lyons et al. 2012; Azman and Zakaria 2022). Reduced BDNF expression has been linked to AD pathogenesis through modulation of tau and Aβ induced toxicity (Tapia-Arancibia et al. 2008; Jiao et al. 2016). These roles of MEF2C make it an interesting gene to study its contribution in AD and thus warrants further investigation.

3.3.1.4. Hs3st-A/HS3ST1

Glial expression of Hs3st-A may be implicated in adult fly survival, where its KD showed to significantly reduce survivorship ($p<0.0001$).

The *heparan sulphate 3-O sulfotransferase A* (*Hs3st-A*) gene encodes a heparan sulphate (HS) modifying enzyme, which is abundantly expressed in neurons of the adult fly brain. The HS modifying enzyme transfers a sulphate group to the 3-O position of glucosamine residues of HS, producing a rare 3-O-sulphated HS. Little is known about the role of Hs3st-A in the fly nervous system, however is important for intestinal stem cell homeostasis in the adult midgut. Depletion of Hs3st-A results in increased intestinal stem cell proliferation and tissue homeostasis loss (Guo et al. 2014). Loss of homeostatic mechanisms likely contributes to a decrease in glial cell health and capacity to carry out functions. It was further

shown Hs3st-A depleted enterocytes were unhealthy and prone to death, adding to the role of Hs3st-A in cell health (Guo et al. 2014).

In mammals, there is a diverse family of HS3ST enzymes with *HS3ST1* having been linked to AD risk in a Norwegian cohort (SNP: rs6448807) (Witoelar et al. 2018). Seven HS3STs have been characterised in humans for which they exhibit cell type and tissue dependent expression levels. *HS3ST1* itself, has strong expression within the cerebellar cortex and primary visual cortex with other members of the HS3ST family expressed in elderly human hippocampus. In particular, *HS3ST2* has been proven to be overexpressed in the hippocampus of AD patients (Witoelar et al. 2018). 3-O-sulphation of HS has been implicated in underlying processes of AD pathogenesis. For example, one study demonstrated a key role of 3-O sulphation in the interaction of tau and heparan sulphate and thus the cellular uptake of tau (Zhao et al. 2019). Understanding how 3-O-sulphation of HS impacts glial functions and ultimately how this contributes to progression of AD is certainly an interesting area for further investigation.

3.3.1.5. Ance/ACE

Locomotor and survival deficits were observed upon glial KD of *Ance* (RNAi #36904) demonstrating a potential role of glial *Ance* in the maintenance of nervous system functions and survival.

Drosophila angiotensin converting enzyme (*Ance*) is a single domain homolog of the mammalian angiotensin I converting enzyme (*ACE*) (DIOPT: 10) which both function as endopeptidases (Siviter et al. 2002). Ance is expressed throughout embryogenesis and is known to play roles in development and reproduction in flies, such that mutant alleles of Ance cause lethality at pupae/larval stages and impair spermatogenesis (Siviter et al. 2002; Hurst et al. 2003). A variety of peptides, with and without amidated C-termini can be hydrolysed by Ance, however, none that show structural resemblance to angiotensin I, bradykinin or the hemoregulatory peptide, N-acetyl Ser–Asp–Lys–Pro, which are known substrates of mammalian ACE (Siviter et al. 2002). In the adult fly brain, Ance expression in glia is low, however it is possible, secretion of this endopeptidase from glia is required to control the breakdown of important signalling messengers in the fly CNS, for instance neurotransmitters. Neurotransmitters are pivotal to neural transmission, such that dysfunction in their metabolism would have implications on nervous system functioning and ultimately result in cell death.

In humans, ACEs expression is predominantly neuronal and is found elevated in AD brains (Miners et al. 2009). For some years, ACE's involvement in AD has been a puzzle (Lehmann et al. 2005; (Arregui et al. 1982), where only recently more robust genetic evidence has supported its association in AD (Kunkle et al. 2019; Bellenguez et al. 2022). Increased levels and activity of ACE in brains has been associated with Aβ load and disease severity, whereby ACE's activity is increased in a physiological response to Aβ accumulation (Miners et al. 2009). Several studies support ACE's functions in Aβ degradation, whereby inhibiting ACE's catalytic activity has shown to promote Aβ accumulation (Hemming and Selkoe 2005; Hu et al. 2001). Angiotensin II, the product of ACE also mediates a number of neurological processes in AD, such as inhibiting acetylcholine release which implicates cognition and is now a new target for AD intervention (Kehoe, 2018). The AD associated ACE variant (R1279Q), has also been recently associated with $A\beta_{42}$ accelerated neurodegeneration, adding further evidence of its importance in AD (Cuddy et al. 2020). ACEs role in glia is less well understood however warrants further investigation. Given the differences to substrate specificity between fly *Ance* and mammalian *ACE*, further investigations in a model system closer to humans such as mice or human iPSC may be more representative.

Based on literature, current human genetics, and verifiable phenotypes, *Mef2/MEF2C, Ance/ACE* and *CG18139/NME8* stand out as the most promising candidate genes for follow up studies. These candidate genes are potentially involved in glial processes that maintain healthy brain status throughout age and support the animal's survival. Determining the importance of these risk genes in AD models would be an interesting avenue to follow, such as their ability to modify $A\beta_{42}$ or tau toxicity.

3.3.2. Overview of Screening Strategy

A reverse candidate screen was a quick and efficient way to triage several conserved AD risk genes uncovered by GWAS, assessing their role in glia throughout age. Benefits of taking an RNAi mediated KD approach to explore gene function was the availability in RNAis, ability to temporally regulate their expression and bypass embryonic lethal phenotypes. However, the disadvantages to RNAi technology are the possibility for off target effects or varying degrees of gene KD, which may mislead findings of potential screen hits (Qiu, 2005). We tried to mitigate for this by testing multiple RNAi lines and maintaining flies throughout adulthood at optimum temperature for maximal RNAi transgene expression (30ºC). In some cases, testing multiple RNAis targeting the same gene yielded different

phenotypes, such as with Hs3st-A, reducing confidence in the phenotype being a true reflection of the gene's KD. Genetic background was controlled for both KK and TRiP RNAi lines using the appropriate UAS-vector only and landing site controls (discussed in section: 3.1.4.1). Future experiments, however, may wish to consider the addition of UAS/+ controls for validation of phenotypes arising from GD RNAi lines, which were generated through random insertion. Given genetic background can have a prominent influence on behavioural assays such as locomotion or survival, it would be important to validate these controls. It is also recommended future experiments validate screen 'hits' by sourcing knock-out/knock-in mutant lines to confirm phenotypes observed, but also verify gene KD with an antibody or qPCR. Additionally, rescuing locomotor or survival deficits observed with the predicted human ortholog will play party to identifying homology between the fly and human AD risk gene in question, confirming translatability of the data.

Screening for locomotive phenotypes provided a rapid, initial readout of whether glial expression of these AD risk genes influenced nervous system functions during aging. The third iteration of our RING assay, adapted from the initial RING assay designed by the Grotewiel lab provided a quick and efficient way to screen locomotor phenotypes in multiple flies. Having the constant force of gravity initiating negative geotaxis aided reproducibility and reliability of the data. Notably, scoring locomotion behaviour at 2 weeks provided greater consistency and reproducibility in data over 4-week locomotion timepoints. Variability in locomotor behaviour at 4-week timepoints was likely attributed to a larger proportion of flies having reached late adulthood or died, which significantly reduced the n being tested and thus statistical power.

Locomotor behaviour, however, is not the only phenotype that can be screened in *Drosophila*. Alternatively, survival, learning and memory, sleep and rough eye phenotypes can also be assessed for these AD risk genes (Dourlen et al. 2017; Jeon et al. 2020). Genes influencing multiple phenotypic readouts such as reduced survival, impaired locomotion and increased neuronal cell death would be interesting for follow up studies. It is worth noting, relatively few genes gave strong locomotor phenotypes in the screen. The absence of amyloid in these experiments may influence the penetrance of phenotypes. For instance, these genes may be expendable in normal ageing but essential for handling additional stress associated with amyloid or tau pathology.

During the course of the screen several genes have fallen in and out of GWAS significance, as well as changes to best the predicted fly/human ortholog, following updates to the DIOPT algorithm. Conducting functional studies for these genes such as the screen outlined in this

chapter helps bridge the gap between sequence to consequence and shed all important light on the role these risk genes may play in AD pathogenesis.

Chapter 4: Glial Function of *small wing/PLCG2* in *Drosophila* Models of Ageing and Alzheimer's Disease

4.1. Introduction

Advances in modern genomic profiling has seen a surge in the number of genetic loci being mapped and associated with complex diseases such as AD, but has left us bridging the gap between statistical association and biological mechanisms that underpin disease risk. Often it is unclear, due to the non-coding nature of GWAS SNPs which is the causal variant or which gene is being regulated, whereas protein coding variants can tell us much more about disease pathology. Coding variants have facilitated the discovery of important biological processes associated with neurodegenerative diseases. For instance, autosomal dominant mutations within genes *PSEN 1&2* and *APP*, have linked early onset AD with altered APP processing, where production of the longer, more aggregation prone $A\beta_{42}$ peptide is favoured (Suzuki et al. 1994; de Strooper et al. 1998; Hardy and Selkoe 2002).

The reverse genetic screen conducted in the previous chapter was suitable for triaging multiple genetic AD risk loci conserved in *Drosophila*, assessing their basic biological functions in ageing glia biology. However, a more direct candidate-based approach using multiple screening techniques is better suited for the functional characterisation of AD risk genes that have known coding variants such as PLCG2. KD or KO of a gene of interest is a quick and direct approach to determining its basic biological functions. This approach has precedent in determining native functions of neurodegenerative disease associated genes. For example, gene KD has been used to uncover important biological processes of the Parkinson's disease related gene *Pink1*, revealing a critical function in mitochondrial bioenergetics and selective mitophagy (Dagda et al. 2009; Ziviani et al. 2010). In this chapter, the glial role of AD associated gene, *PLCG2,* will be explored in ageing and $A\beta_{42}$ associated pathology, upon RNAi mediated gene KD of the conserved *Drosophila* ortholog, *small wing* (*sl*).

4.1.1. PLCG2 Variants are Associated with Reduced Risk of LOAD

The PLCG2 locus was recently associated with AD, where the rare coding variant P522R (rs72824905-G, minor allele; p.P522R) was identified at genome wide significance from an exome microarray sequencing study (p= 5.38 × 10-10, odds ratio= 0.68, minor allele frequency (MAF) cases = 0.0059, MAF controls = 0.0093). The P522R variant was attributed to reduced risk of developing late onset AD (Sims et al. 2017). Several other genetic aberrations have also been discovered in the PLCG2 locus linking its dysfunction with other

diseases such as cancer and inflammatory disorders (Figure 4.1). For instance, hypermorphic mutations have been linked to inherited antibody deficiency and immune dysregulation (PLAID) and in some cases autoinflammation (APLAID). Additionally, in humans, PLCG2 signalling has been implicated in a number of haematological malignancies such as chronic lymphocytic leukaemia, diffuse large B cell lymphoma, Hodgkin's lymphoma, and myelodysplastic syndrome (Jackson et al. 2021).

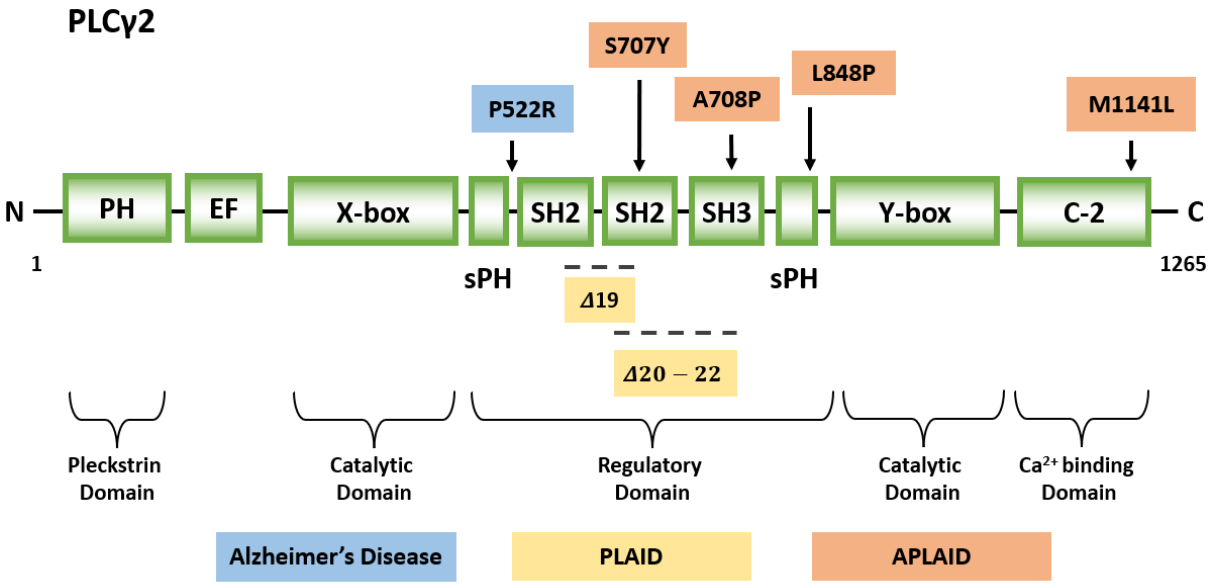

Figure 4.1: Structural domains and disease associated mutations of PLCG2.

The X-Y box regions make up catalytic domains which lie either side of the regulatory domain. The regulatory domain is comprised of a single PH domain split between two tandem Src homology-2 (SH2) domains and one Src homology-3 (SH3) domain. The EF hands and Ca^{2+} binding domains lie at the N and C terminal ends respectively. PLAID-causing genomic deletions (Δ 19 and Δ20-Δ22), APLAID-associated somatic mutations (S707Y, L848P, A708P) and the protective P522R mutation in AD are located in the regulatory domain of PLCG2. The M1141L APLAID somatic mutation however lies in the C-2 Ca^{2+} binding domain.

The R522 variant in *PLCG2* is one of few protective coding variants in AD and has been found to have protective association with other neurodegenerative diseases such as dementia with Lewy bodies and frontotemporal dementia. Besides protecting against other forms of dementia, the R522 variant in PLCG2 was also evidenced to increase likelihood of

longevity (Lee et al. 2019). The impact of the R522 variant in glia is discussed further in the next chapter.

PLCG2 is an intracellular phospholipase belonging to the PLC-γ subfamily of a much wider family of PLC enzymes (Nakamura & Fukami, 2017) (discussed further in Chapter 1; section: 1.6.1). Typically located at the cytoplasm, PLCG2 gets recruited to the membrane upon activation by receptor or non-receptor tyrosine kinases, where it hydrolyses membrane associated PI(4,5)P2 into secondary messengers IP3 and DAG (Figure 4.2) (S.G. Rhee and Choi 1992). In addition, by regulating PI(4,5)P2 hydrolysis, PLCG2 influences PI3-kinase (PI3K) dependent generation of PI(3,4,5)P3, for which PI(4,5)P2 is the substrate of PI3K (Rhee and Bae 1997). Following PLCG2 mediated hydrolysis of PIP2, secondary messengers IP3 and DAG are released which control intracellular Ca^{2+} flux and protein kinase c (PKC) activation respectively. In turn, downstream signalling pathways MAPK/ERK, NF-κB and NFAT associated with cell survival, proliferation, differentiation, phagocytosis, and inflammatory responses are regulated (Takalo et al. 2020). Alternatively, PIP3 is the major effector of the PI3K-AKT signalling axis which controls cell survival, growth, and autophagy (Datta et al. 1999, Porta et al. 2014; Soto-Avellaneda and Morrison 2020) (Figure 4.2).

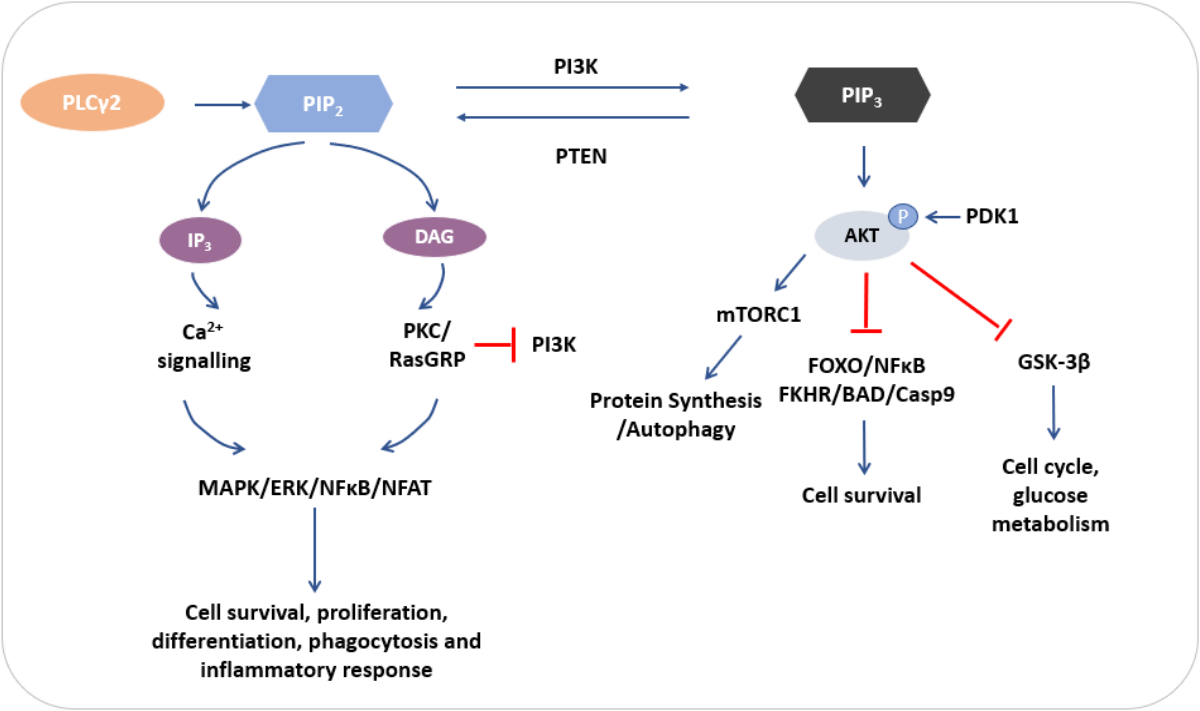

Figure 4.2: Metabolism and downstream signalling of phosphoinositols PIP2 (PI(4,5)P2) and PIP3 (PI(3,4,5)P3.

Phospholipase c gamma 2 (PLCG2) catalyses the hydrolysis of PIP2 into inositol triphosphate (IP3) and diacylglycerol (DAG) which the former induces calcium release from the endoplasmic reticulum and the latter activates protein kinase c (PKC). Secondary messengers IP3 and DAG control pathways, MAPK, ERK, NF-κB and NFAT that are involved in cell survival, phagocytosis, proliferation, and inflammatory response. PIP3 is the main effector of the PI3K/AKT pathway, whereby PIP3 activates AKT through inducing AKT co-localisation with PDK1. AKT itself has a number of downstream targets that regulate critical events such as apoptosis, cell proliferation, protein synthesis and autophagy.

In the periphery, PLCG2 importantly regulates immune cell functions of B cells, NK cells, mast cells, macrophages, and platelets where it is expressed (Wang et al. 2000). Loss of PLCG2 function impairs B cell development and maturation, with defects in B cell receptor, signal transduction and Ca^{2+} signalling (Hashimoto et al. 2000). In the CNS, PLCG2 is however predominantly expressed in microglia, with upregulation of PLCG2 messenger RNA (mRNA) being reported in cortical tissue of LOAD patients (Allen et al. 2016). Transgenic mice with mutations in EOAD associated genes (*APP* and *PSEN1*) and mouse models overexpressing the human tau-4R/2N isoform also show upregulation of PLCG2 mRNA (Castillo et al. 2017; (Matarin et al. 2015). In such cases, PLCG2 upregulation in affected

regions of AD brains is likely owing to the extensive microgliosis that is consequent to neurodegeneration.

In microglia, PLCG2 has been shown to function downstream of transmembrane associated receptor TREM2, to mediate lipid metabolism, phagocytosis, and cell survival (Andreone et al. 2020). PLCG2 also transduces signals downstream of TLR activation to regulate inflammatory responses in microglia such as cytokine production (Andreone et al. 2020). The fact PLCG2 and TREM2 belong to the same signalling network is particularly interesting given TREM2 is also an AD risk gene, where loss of function variants have been associated with increased risk of LOAD (Sims et al. 2017). Given PLCG2 signalling facilitates many diverse functions of microglia, it has therefore become an attractive target for therapeutically modulating microglial function in AD.

4.1.2. The Fly Ortholog of *PLCG2*; *small wing*

Flies have a single conserved ortholog of human *PLCG2*, called *small wing* (*sl*) which name was given as result of mutants displaying reduced wing sizes (Emori et al. 1994; Thackeray et al. 1998). DIOPT (version 9) predicts *sl* as the best ortholog for human *PLCG2*, scoring 12/24 in the assessed algorithms (see section … for more detail on algorithms). Ancestrally, PLC enzymes represent an important family of enzymes which have been identified in *Drosophila,* highlighting evolutionary conservation of phosphoinositide (PI) signalling. Other PLC proteins encoded by the *Drosophila* genome include NorpA and Plc-21c which are categorised under the PLC-β subfamily and expressed in neuronal cells of the eye and CNS respectively (Bloomquist et al. 1988; Shortridge et al. 1991). *In vivo* functions of NorpA have been characterised in phototransduction, whereas Plc-21c functions have been implicated in olfaction and flight.

Sl, the first and only PLCG homolog to be identified in flies in 1915 by Bridges was mapped to 14B-C of the X chromosome (Emori et al. 1994). Although sl is expressed in early developmental stages and most highly during embryogenesis, homozygous null mutants are both viable and fertile (Emori et al. 1994). Nonetheless, sl null mutants exhibit developmental defects such as mildly rough eye phenotype, development of extra Rabdomere 7 (R7) photoreceptors and characteristically smaller wings to wild type which can contain patches of ectopic veins (Thackeray et al. 1998). sl regulates cell growth and differentiation processes through MAPK pathways, downstream of Epidermal Growth Factor (EGF) and insulin receptor activation (Murillo-Maldonado et al. 2011). During photoreceptor development, sl

negatively regulates the MAPK cascade whereby loss of sl activity results in overactivation of this pathway and development of extra R7 photoreceptors (Thackeray et al. 1998). In stimulating cell growth, sl is found to also work downstream of the insulin receptor, promoting MAPK activation to an extent that supports cell growth (Murillo-Maldonado et al. 2011).

The single isoform of sl shares 38% sequence identity and 57% sequence similarity with human PLCG2 and 40% identity, 57% similarity with PLCG1, indicating PLCG homologs in mammals have evolved from one common ancestor, sl. Whilst the overall aa sequence of sl shows general similarity to mammalian PLCGs, protein domains shared across the two species are highly homologous. In particular, the X and Y catalytic regions required for PI substrate specificity and regulatory SH2 and SH3 domains that permit specific protein: protein interactions unique to PLCG isoforms are conserved between *Drosophila* and mammals (Figure 4.3), (Manning et al. 2003). SH2 sequences have phosphotyrosine binding activity enabling association with various receptor protein tyrosine kinases such as the EGF receptor, platelet derived growth factor receptor and fibroblast growth factor receptor, whilst the SH3 domain is required specifically in PLCG activation of PI3K (Moran et al. 1990; Ye et al. 2002). The homology between sl and PLCG protein domains indicates their overall mode of activation and cellular function is conserved across *Drosophila* and mammals. Some variations in protein structure however do exist such as a shorter C terminal region of sl, as well differences in tyrosine phosphorylation sites. *Drosophila* lack two out the three tyrosine's in PLCG1 that become phosphorylated upon activation. These differences may indicate unique functions to PLCG1 and 2 that are not included in sl, such as subtle differences in the role of tyrosine phosphorylation in enzyme activation (Manning et al. 2003). Nonetheless, given the similarity in catalytic and regulatory protein domains, sl is thought to catalyse PI(4,5)P2 turnover coupled to receptor tyrosine kinases through SH2 binding, the same as mammalian PLCGs.

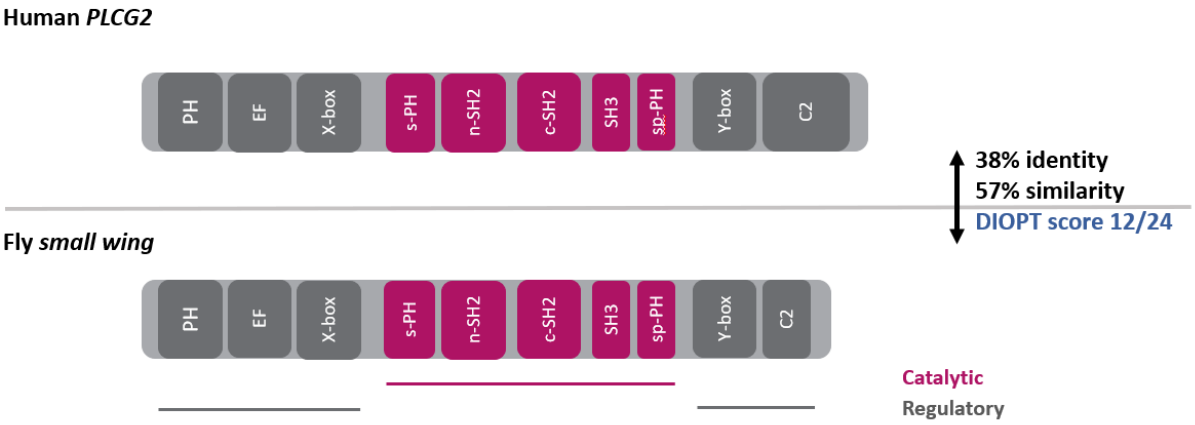

Figure 4.3: Protein domain homology between human PLCG2 and Drosophila small wing (sl).

The catalytic and regulatory domains show overall similarity between the two PLCG homologs (PLCG2/sl). The C2 domain of Drosophila sl protein is shorter compared to human PLCG2. The regulatory domain of sl comprises of two SH2 and one SH3 domain split between a single PH domain and is located between X-Y regions, which is characteristic of γ-type PLCs.

Whilst studies have characterised the role of sl during development, biological functions of sl throughout adulthood have been largely unexplored, specifically glial cell functions. Notably, PLCG2 plays important roles in glial mechanisms that are known to be conserved in *Drosophila,* for instance phagocytosis (MacDonald et al. 2006; Tasdemir-Yilmaz and Freeman 2014). It will therefore be interesting to explore whether sl, the conserved ortholog of PLCG2, equally mediates diverse glia functions in *Drosophila* throughout ageing and AD pathology.

4.1.3. The aos::$A\beta_{42}^{Arc}$ Model in *Drosophila*

The amyloid cascade hypothesis stipulates Aβ peptide is the main initiator of AD pathophysiology where its deposition in the brain parenchyma is the leading event to a cascade of toxic events (Hardy and Selkoe 2002). Aβ has since become an attractive target for therapeutic intervention. Out of the two predominant Aβ species produced from the amyloidogenic pathway ($A\beta_{40-42}$), $A\beta_{42}$ is considered the more neurotoxic peptide given its

propensity to oligomerise and form fibrils which can in turn aggregate into amyloid plaques. *Drosophila* can offer a powerful *in vivo* model to rapidly explore $A\beta_{42}$-induced toxicity, with various models already generated (see Chapter 1; section: 1.9.3). Transgenic expression of human $A\beta_{42}$ in the fly provides a direct approach to exploring phenotypes associated with $A\beta_{42}$ induced toxicity, where models display age and dose dependent molecular and behavioural phenotypes such as Aβ accumulation, neuronal hyperexcitability, defective mitochondrial function, rough eye phenotypes, locomotor dysfunction and reduced lifespan(Finelli et al 2004; Iijima et al 2004).

The UAS-aos::$A\beta_{42}^{Arc}$ transgenic fly model, sourced from BDRC (33773) was used in this study to model $A\beta_{42}$ induced toxicity. Flies express the human $A\beta_{42}$ peptide with the highly pathogenic familial "Artic'' Swedish mutation (E693G) (Martin et al. 1995), fused to the *Drosophila* argos secretory signal (aos) peptide (Casas-Tinto et al. 2011). The aos directs the $A\beta_{42}$ peptide through the secretory pathway to promote extracellular secretion (Figure 4.4). The secretory signal itself is then cleaved off during processing in the golgi apparatus. Neuronal expression of aos::$A\beta_{42}^{Arc}$ in flies results in diffuse formation of amyloid deposits and degenerative phenotypes such as locomotor, survival, learning and memory deficits and rough eye (Casas-Tinto et al. 2011; Ray et al. 2017). Furthermore glial targeted expression of aos::$A\beta_{42}^{Arc}$ was found to phenocopy neuronal expression, with flies similarly exhibiting accumulation of Aβ deposits, impaired locomotor activity and reduced survivorship (Ray et al. 2017). Ray and colleagues also demonstrated altering glial phagocytic activity through KD of the major glial engulfment receptor Draper was able to modify amyloid pathology in flies (Ray et al. 2017). Glial overexpression of human aos::$A\beta_{42}^{Arc}$ in flies will therefore help identify genetic modifiers of glial $A\beta_{42}$ induced toxicity. In experiments described in this chapter flies expressing aos::$A\beta_{42}^{Arc}$ were used to investigate the role of conserved AD risk gene, sl/PLCG2 in modifying $A\beta_{42}$ associated pathology. In this instance, the UAS-Gal4 binary expression system was used to drive expression of both sl RNAi and $A\beta_{42}$ production in glia.

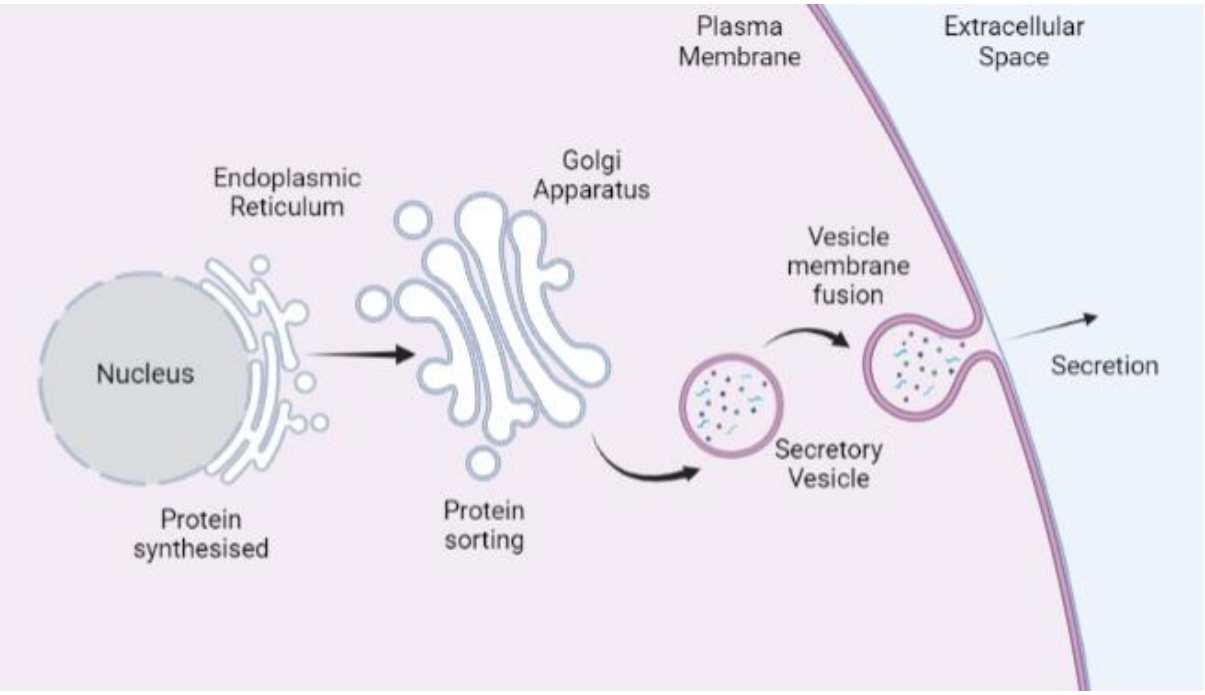

Figure 4.4: Mechanism of aos::Aβ$_{42}^{Arc}$ peptide production and secretion.

The argos secretion signal peptide directs the Aβ$_{42}$ peptide through the secretory pathway, transporting the peptide from the endoplasmic reticulum to the Golgi apparatus where it is processed (aos is cleaved off) and packaged into vesicles then transported to the plasma membrane. The secretory vesicle fuses with the plasma membrane and contents are exocytosed out into the extracellular environment.

4.1.4. Aims and Hypotheses

Experiments in this chapter aimed to characterise the basic biological function of the *Drosophila PLCG2* ortholog, *sl* and its substrates (ie: PIP2) in glia. Furthermore, given the important functions of PIP2 and PIP3 in glial biology and evidence of their imbalance in neurodegenerative diseases, such as AD and PD (Volpatti et al. 2019), experiments also aimed to address how their metabolism contributes to glia biology throughout age, as well as Aβ$_{42}$ related pathology. Finally, this study set out to define and characterise the glial role of sl in contributing to the onset and progression of Aβ$_{42}$ associated pathology, upon glial specific KD. Given hyperactivity of PLCG2 is protective of AD, it was hypothesised that reduced glial expression of the *PLCG2* ortholog, *sl* would be detrimental in models of Aβ$_{42}$ pathology.

4.1.5. Experimental Design

The glial role of *sl/PLCG2* throughout ageing and $A\beta_{42}$ associated pathology was assessed following RNAi mediated KD, exclusively in adulthood. Glial specific KD of sl was achieved by the pan glial driver Repo-Gal4 and restricted to adulthood using the temperature sensitive Tubulin-Gal80 promoter, which repressed Gal4 transcription during development. In such cases, crosses were reared at 18°C to limit protein expression during development and then transferred to 30°C, 1-2 d.p.e to induce sl KD in glia, as well as drive maximal $A\beta_{42}$ expression during adulthood stages. Multiple phenotypes in viability, survival, locomotor behaviour, PIP2/PIP3 metabolism were screened to characterise the basic biological role of sl in glia. Similar phenotypic parameters, as well as assessment of $A\beta_{42}$ handling (accumulation and clearance), were then used to determine if glial sl modifies phenotypes of $A\beta_{42}$ induced toxicity. In this instance, the UAS-Gal4 binary expression system was used to drive expression of both sl RNAi and $A\beta_{42}$ production in glia. Initial experiments to characterise glial targeted expression of aos::$A\beta_{42}^{Arc}$ in flies also included immunohistochemistry, survival, and locomotor behaviour.

4.1.5.1. CRIMIC cassette

The CRISPR Mediated Integration Cassette (CRIMIC) promotor trap tool was used to determine cellular expression of sl in the adult fly brain. The CRIMIC tool hijacks a gene endogenous promoter i.e. sl, allowing expression of Gal4 in its place (Lee et al. 2018). This elegant system can be used to assess gene expression patterns at a tissue and cellular level or even test for rescue of mutant phenotypes by driving the corresponding UAS-cDNA. The CRIMIC cassette (pM37) is comprised of a splice acceptor, coding sequences of the viral T2A peptide, followed by Gal4, a 3XP3-GFP marker and a 3' polyadenylation (polyA) signal, flanked by two Flippase Recognition Targeg (FRT) sites (Figure 4.5). The polyA signal prematurely terminates transcription of the gene in which the cassette is inserted, generating an effective null allele which renders the gene product non-functional. The viral T2A ribosomal skipping site facilitates production of an untagged Gal4 protein in all cells where the gene is endogenously expressed (Diao et al. 2015).

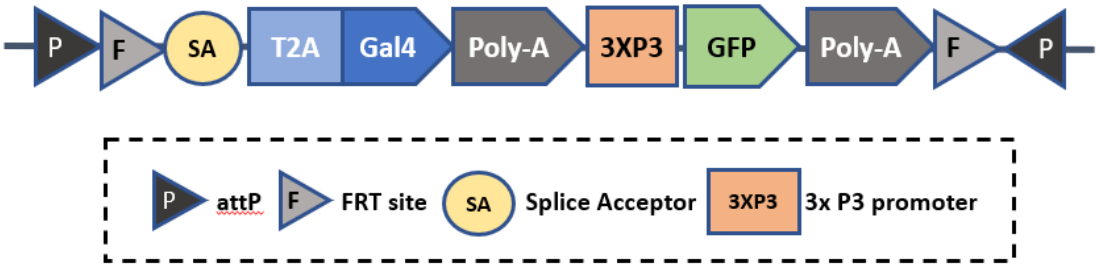

Figure 4.5: Structure of the CRIMIC (CRISPR Mediated Integration Cassette) (pM37) cassette.

To determine which cell endogenously express sl, the sl CRIMIC line was crossed with flies expressing a UAS promoter, driving expression of a phospholipid membrane tethered red fluorescent protein (mCD8::RFP) (Figure 4.6). Males, homozygous for sl CRIMIC transgene were selected for use in experiments.

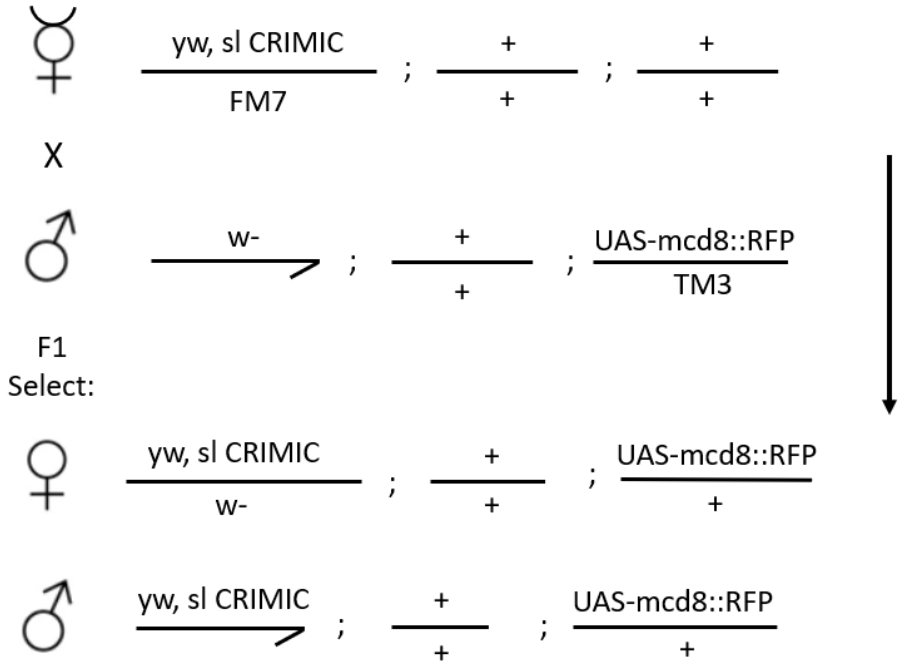

Figure 4.6: X chromosome crossing scheme for the generation of flies expressing the UAS-RFP marker under control of sl endogenous promoter.

4.1.5.2. Phosphoinositol Specific Fluorescent Reporters

To visualise cellular PI(4,5)P2 and PI(3,4,5)P3 dynamics, novel chimeric GFP reporters that selectively recognise PH domains PLCδ1 and GRP1 were used to detect PI(4,5)P2 (herein PIP2) and PI(3,4,5)P3 (herein PIP3) species respectively in the fly brain, under confocal microscopy. These phosphoinositol specific fluorescent reporters were used to explore the cellular distribution and changes in PIP2 and PIP3 levels *in vivo*, following manipulation of their metabolism. Manipulation of PIP2/PIP3 metabolism was achieved through glial targeted KD of lipid metabolising enzymes such as sl, PI3K, PTEN and PLD3. Furthermore, the PIP2 specific reporter could be regulated via the cell type specific Gal4-UAS expression system, allowing for glial specific distribution and abundance of PIP2 to be deduced.

For the purpose of this study a PIP2, RepoGal4 stock was established, by recombining the UAS-PLCδ-PH::GFP reporter with the pan glial driver, Repo-Gal4, on the third chromosome (Figure 4.7). Virgin females from this driver stock were crossed with males containing UAS-transgenes. Crosses were reared 6 days at 25°C, then switched to 30°C upon removal of parents, as to drive maximal expression of the phosphoinositol specific reporter simultaneous to glial gene KD from development. The distribution and abundance of PIP2 or PIP3 in the fly brain were visualised under the confocal microscope at 7 d.p.e and their levels in the midbrain quantified by area above set threshold or mean gray analysis (see Chapter 2; sections: 2.8.1 and 2.8.2).

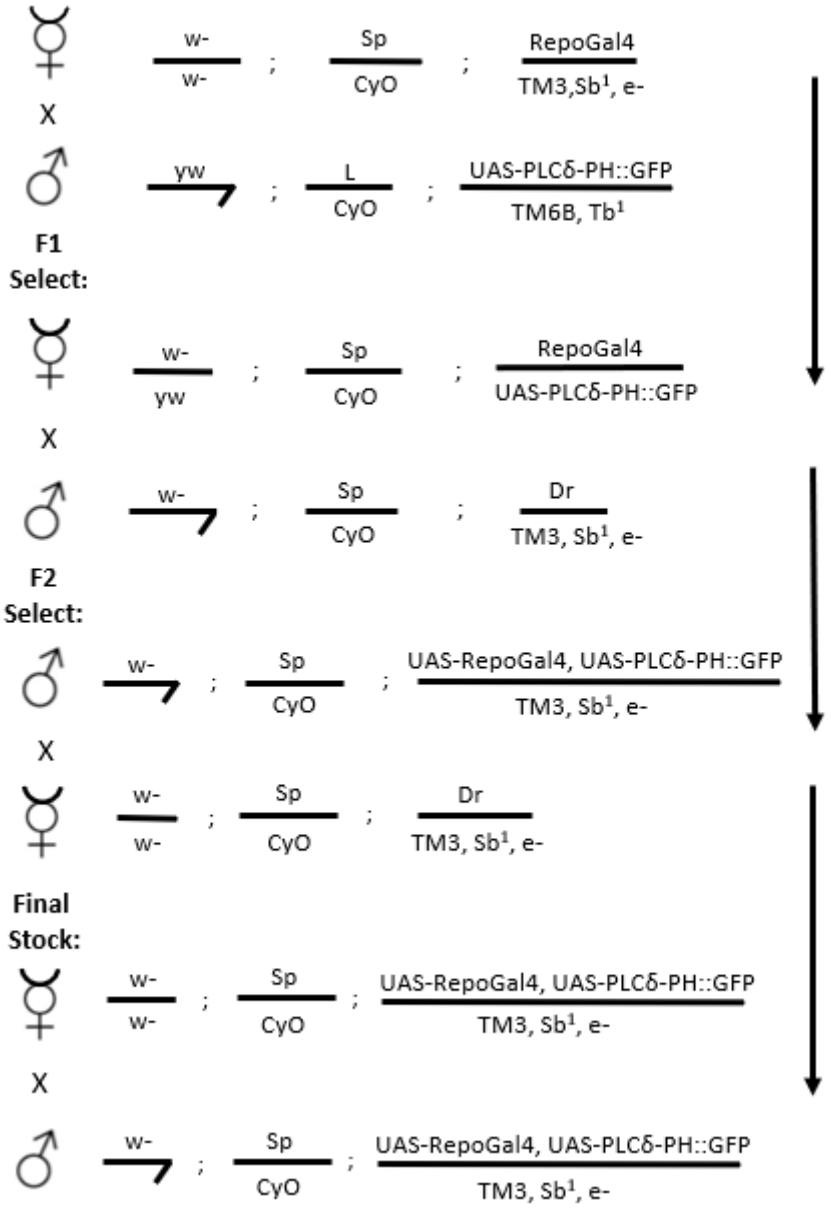

Figure 4.7: Crossing scheme to recombine RepoGal4 and UAS-PLCδ-PH::GFP on third chromosome.

A timeline of experiments conducted in this chapter, as well as a summary of timepoints and total n used for each experiment has been outlined below (Figure 4.8 and Table 4.1).

Experiment/Group	Without $A\beta_{42}$	With $A\beta_{42}$
sl localisation	≤10 brains per genotype, females only	N/A
Wing sizes	≤10 wings per genotype, combined females and males	N/A
qPCR	20 heads per biological replicate (total replicates 3) combined female and male	N/A
Survival	101-146, combined females and males	105-159, females only
Locomotion	27-135 (14 d.p.e), 28-75 (21 d.p.e), males only	95-194 (14 d.p.e), 119-131 (21 d.p.e), males only
PIP2/PIP3	≤10 brains per genotype, combined females and males	≤10 brains per genotype, combined females and males
MSD assay	N/A	40 heads per biological replicate (total replicates 3) combined females and males
Aβ immunostaining	N/A	≤10 brains per genotype, combined female and male

Table 4.1: Summary of experimental procedures including number and sex of flies used for each group, with and without $A\beta_{42}$.

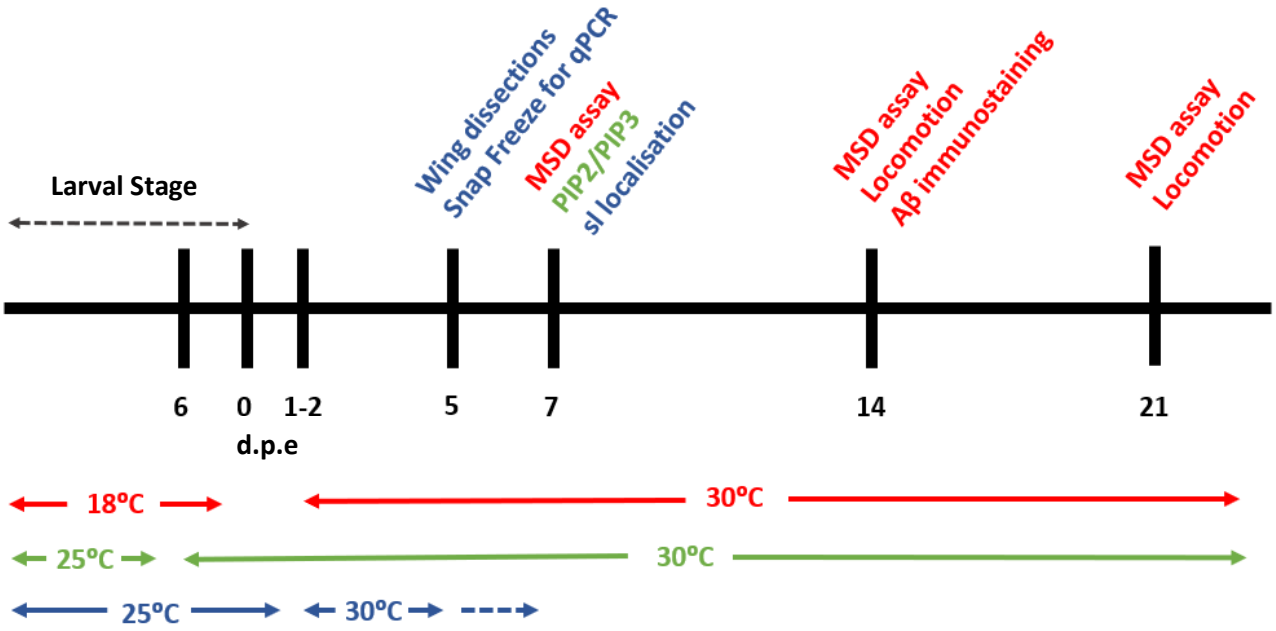

Figure 4.8: Timeline of experimental procedures.

Timepoints each assay were conducted and the temperatures flies were bred or aged at for each (see corresponding colours).

4.2. Results

4.2.1. *Small Wing* is Expressed Throughout Neurons and Glia in the Adult Fly Brain

The R522 variant found in the *PLCG2* loci has been linked to reduced LOAD risk, making PLCG2 an important candidate gene to study AD relevant functions in flies. The DIOPT ortholog prediction tool calculates sl as the best conserved fly homolog for PLCG2 with 12 out of 24 independent algorithms supporting this prediction. Protein alignment of PLCG2 and sl highlight an overall similarity in the aa sequence with 57% of the residues related and a high degree of homology in regions characteristic of the PLCG subtypes such as the X and Y regions essential for catalytic activity and the Z region, containing SH2 and SH3 domains (Emori et al. 1994).

In the human and mammalian brain, PLCG2 is highly enriched in microglia cells and so it was logical to determine the expression pattern of sl in the adult fly brain, particularly within glial cells. Firstly, publicly available single cell RNAseq data for the adult fly brain was used to examine the cell type specific expression profile of sl. The fly cell atlas provides single cell resolution of gene expression profiles from over 250 annotated cell types across 15 individually dissected tissues including whole head. Within the whole head, 81, mostly neuronal cell types, have been annotated (Li et al. 2022). Using the online *SCope* analysis tool, single cell transcriptomic profiles for genes of interest can be uncovered, where each dot represents a single cell (http://scope.aertslab.org). Glial and neuronal cells were identified based on *Repo* and *Elav* expression and annotated in red and blue respectively. *Sl* expression, (shown in green) appears to be more predominantly expressed in neurons compared to glial cell populations. (Figure 4.9).

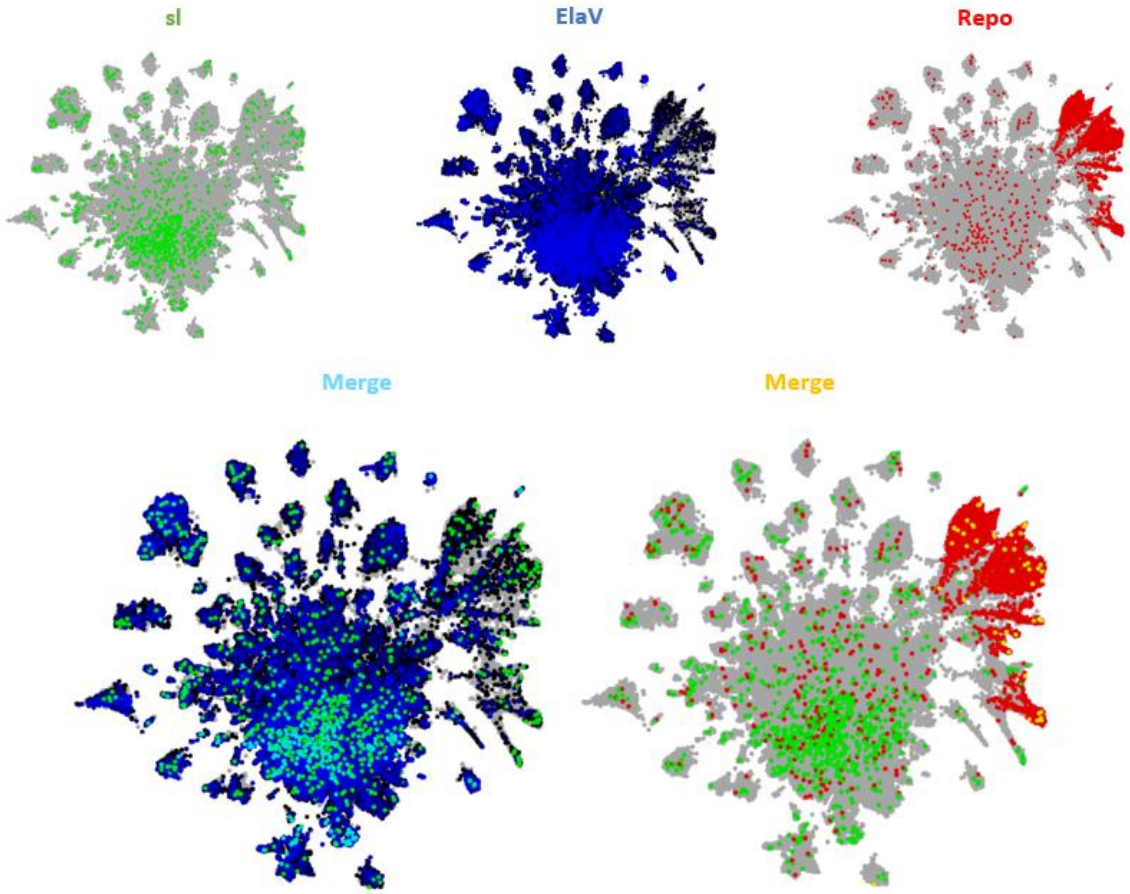

Figure 4.9: sl is expressed in neuronal and glial cell populations of the adult fly brain.

Single cell transcriptomic profiles of sl (green), Elav (blue) and Repo (Red) in the adult fly brain is indicated, where each dot represents a single cell. Merged images correspond to sl expression in Elav/Repo expressing cell populations. Turquoise depicts the overlap of sl expression within neuronal (Elav expressing) cells whilst yellow depicts the overlap of sl expression in glial (Repo expressing) cells.

To further characterise this *in vivo,* the sl CRIMIC promoter trap (described in section: 4.1.5), was used to drive expression of UAS-mCD8::RFP, with expression of the red fluorescent reporter (RFP) indicating cells where sl is endogenously expressed.

The insertion of the CRIMIC cassette into chromosome X (14B17, X:16352221) of the endogenous sl gene disrupts protein function, resulting in an effective null allele. The sl CRIMIC line was crossed with flies expressing a UAS promoter driving expression of a phospholipid membrane tethered red fluorescent protein (mCD8::RFP). This allowed visual inspection of cell type specific *sl* expression patterns in the brains of adult flies by confocal microscopy. Visual inspection of endogenous *sl* expression revealed high distribution of RFP within the mushroom bodies and the protocerebral bridge of the adult fly brain (as indicated

by arrow heads) (Figure 4.12). These regions are known to play important roles in memory and learning, as well as locomotor related functions and sleep regulation (Akalal et al. 2006; Lin et al. 2013; Tomita et al. 2021). Although *sl* expression appears to be concentrated to these brain regions, the distribution of RFP throughout the fly brain highlights wider expression of *sl* outside of the mushroom body (Figure 4.10).

To better define cell types of interest in which *sl* was expressed, brains were immunostained with antibodies specific for neurons (Elav) and glia (Repo). Immunostaining of sl CRIMIC adult fly brains with anti-Repo or Elav (shown in purple), revealed the sl promoter is active in both glial and neuronal cells, although has a greater neuronal expression, similar to what the SCope data showed (Figure 4.10).

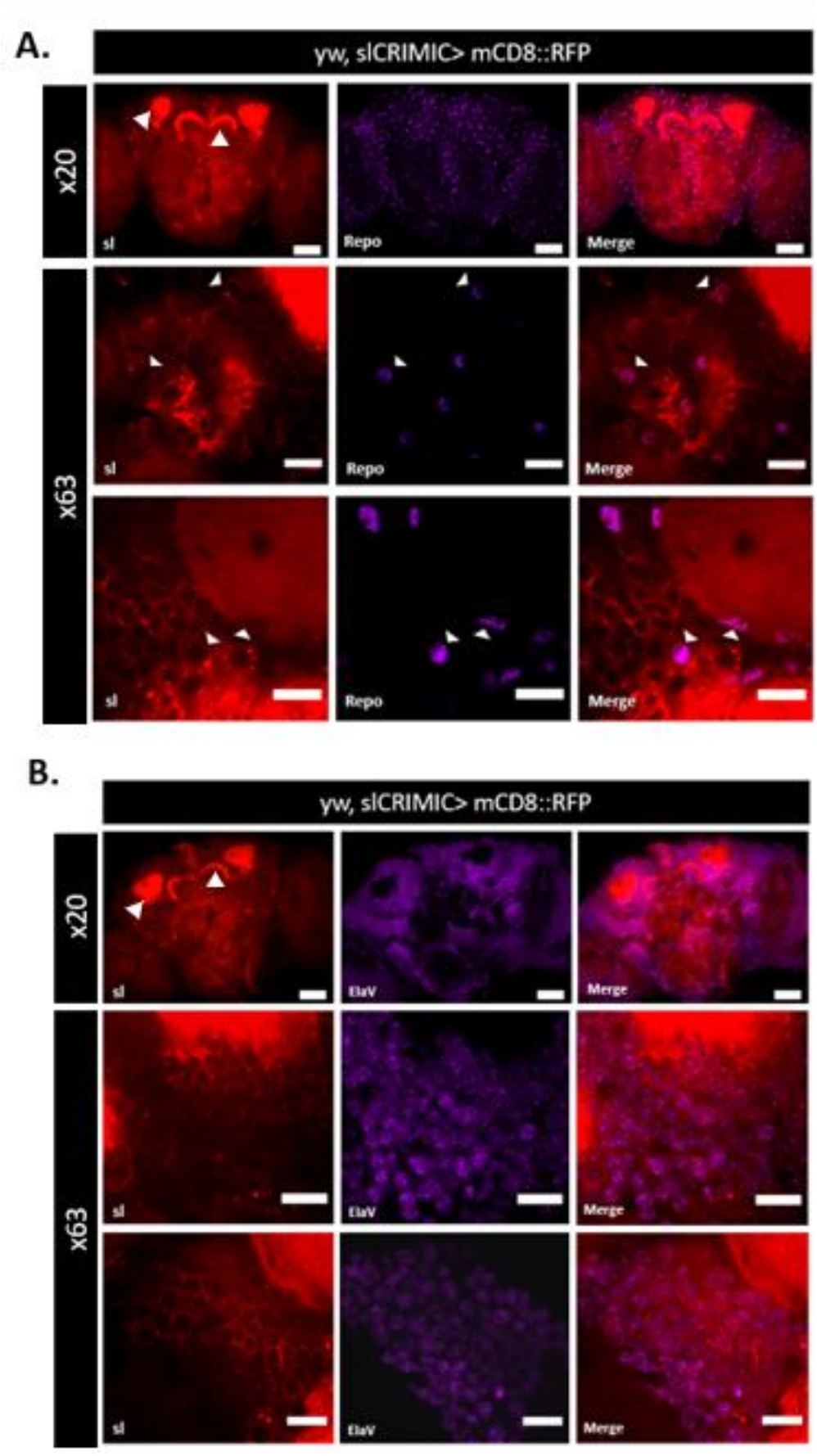

(see figure legend on next page)

Figure 4.10: Immunofluorescence images depicting sl expression pattern in the adult fly brain.

Representative images depict endogenous sl expression (Red) across the entire brain (x20) (Scale bar = 50 µM) and at the cell body layer (x63) (Scale bar = 10 µM) in both Repo (A) and Elav (B) (purple) positive cells. sl CRIMIC drives mCD8::RFP expression in cells where sl is endogenously expressed whilst co-staining with anti-Repo (A) and Elav (B) is used to depict glial and neuronal cell populations respectively.

4.2.2. sl CRIMIC Null Mutant Exhibit a Small Wing Phenotype

Small wing is important in wing development, promoting cell growth in the wing through insulin and EGF/MAPK signalling pathways (Murillo-Maldonado et al. 2011). Loss of function sl mutants have characteristically smaller wings than wildtype flies (Thackeray et al. 1998). To determine whether sl CRIMIC mutants exhibit developmental wing defects similar to those characterised in nulls, the wing size was quantified in homozygous sl CRIMIC females and males. As sl is located on the X chromosome and with females in general having larger wing sizes to males, the wings of females and males were measured and analysed separately, accounting for any sex specific phenotypic differences. The boundary between L4, L5 veins and the posterior cross vein (PCV) (highlighted in Figure 4.11A), was measured for consistency. Visual inspection of the wings indicated reduction in overall wing size. Follow up measurement of wing area revealed sl CRIMIC mutants exhibited around 30% reduction in wing area compared to control yw wildtype flies (the same background as CRIMIC mutants). In females, the average wing area decreased from 0.13 mm^2 to 0.07 mm^2 and in males the average wing area went from 0.09 mm^2 to 0.06 mm^2 (Figure 4.11B&C), (Unpaired t-test; n=10, Females: t=12.91, df=18, Males: t=13.29, df=18, Females and Males: ****$p<0.0001$). This demonstrates sl CRIMIC mutants successfully disrupted sl function and therefore an appropriate tool to be used in further exploration of sl loss of function phenotypes, as well as rescue experiments to test orthology with human PLCG2.

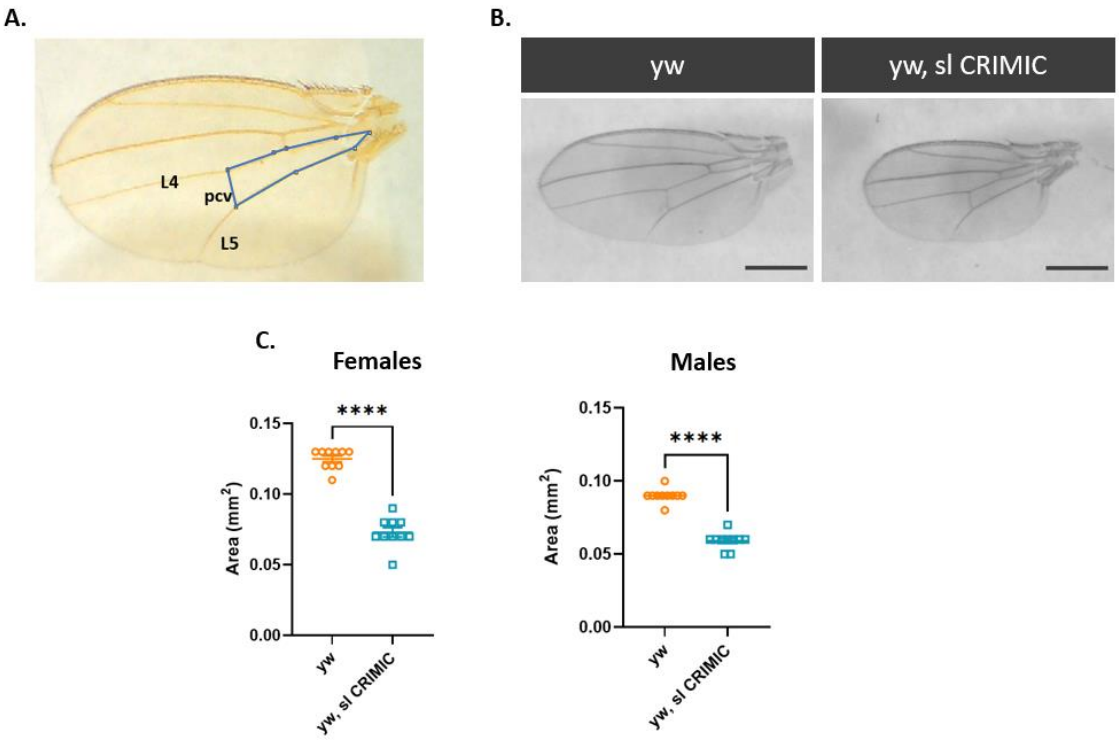

Figure 4.11: Measured area in wings of sl CRIMIC mutants.

*A) Region of interest (highlighted blue) between the L4, L5 and posterior cross vein measured in the right wing. B) Representative images of male wings in control (yw) versus sl 'null' mutants (sl CRIMIC), scale bar (1.5 mm) C) Graph showing measured area (mm^2) of the region of interest in n=10 right wings of female and male flies for control (yw) versus sl mutants (sl CRIMIC); unpaired t-test; n=10, females: t=12.91, df=18, ****p<0.0001, males: t=13.29, df=18, ****p<0.0001.*

4.2.3. *small wing* Knockdown Recapitulates small wing Phenotype

Besides null mutant lines, RNAi tools for sl are also available, enabling cell type and temporal exploration of glia specific loss of function phenotypes resulting from sl KD. Two independent sl RNAi tools from the VDRC KK and TRiP RNAi collections were characterised for loss of function, small wing phenotypes. Each sl RNAi targeted non overlapping sequences of exonic regions within the sl transcript (Figure 4.12).

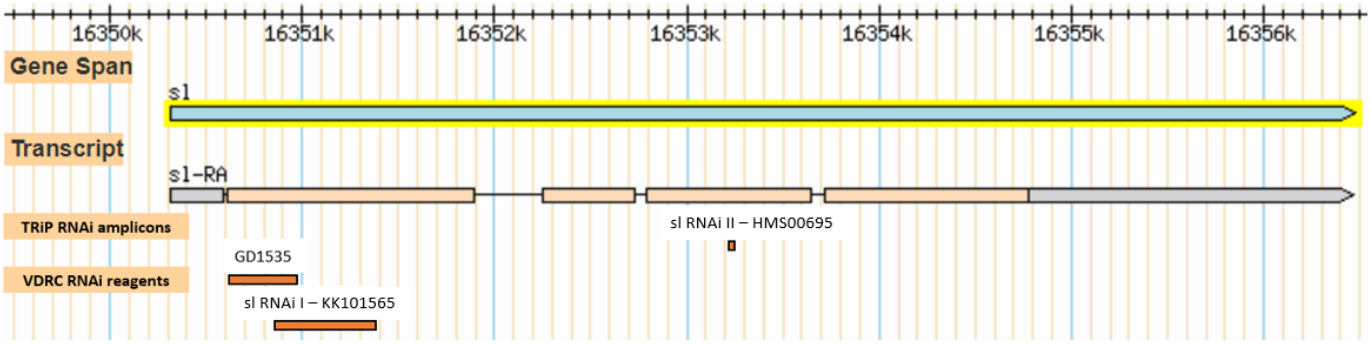

Figure 4.12: small wing RNAi tools.

Acquired RNAi stocks KK101565 (sl RNAi I) and HMS00695 (sl RNAi II) from VDRC and Bloomington TRiP RNAi collections respectively to be used in the following experiments, with the region of sl transcript targeted by each RNAi sequence depicted.

Knowing that loss of function sl mutants exhibit smaller wings to wildtype flies (yw), sl RNAis were validated for the small wing phenotype upon comparison with an empty vector background control (UAS-GFPvalium10), (noted as GFP). UAS-GFPValium10 expresses GFP under UAS control in the VALIUM10 vector and can used to control for TRiP generated RNAis in both the VALIUM10 or VALIUM20 vectors. The small wing phenotype was used as a phenotypic indicator for reduced sl expression, indicating which sl RNAis impacted sl function and were thus suitable for use in follow up experiments in this chapter. Under control of the Tubulin-Gal4 promoter, which is ubiquitously expressed in somatic cells, both sl RNAis (IDs: 105893 and 32906) recapitulated a small wing phenotype (Figure 4.13A&B). Expression of the KK sl RNAi (sl RNAi I; ID: 105893), reduced area measured on average by 13% in males (from 0.076 mm^2 to 0.066 mm^2) compared to the empty vector background control and in females, the average area measured reduced by 14% (from 0.116 mm^2 to 0.099 mm^2) (One-way ANOVA with Dunnetts multiple comparison test; Females: n=7-10,

F=71.81, ***p=0.0001; Males: n=9-10, F=56.37, ***p=0.0008). The TRiP sl RNAi (sl RNAi II; ID:32906) reduced the average wing size even further, with males exhibiting a 17% decrease in area measured (from 0.076 mm^2 to 0.063 mm^2) comparative to the empty vector background control and in females the average wing area decreased by 20% (from 0.116 mm^2 to 0.091 mm^2) (One-way ANOVA with Dunnett's multiple comparison test; Females: n=7-10, F=71.81, ****p<0.0001; Males: n=9-10, F=56.37, ****p<0.0001). Of additional note, expression of the empty vector background control in males reduced the average wing size compared to yw male flies by around 15% (from 0.090 mm^2 to 0.076 mm^2) (One-way ANOVA with Dunnett's multiple comparison test; n=9-10, F=56.37, ****p<0.0001).

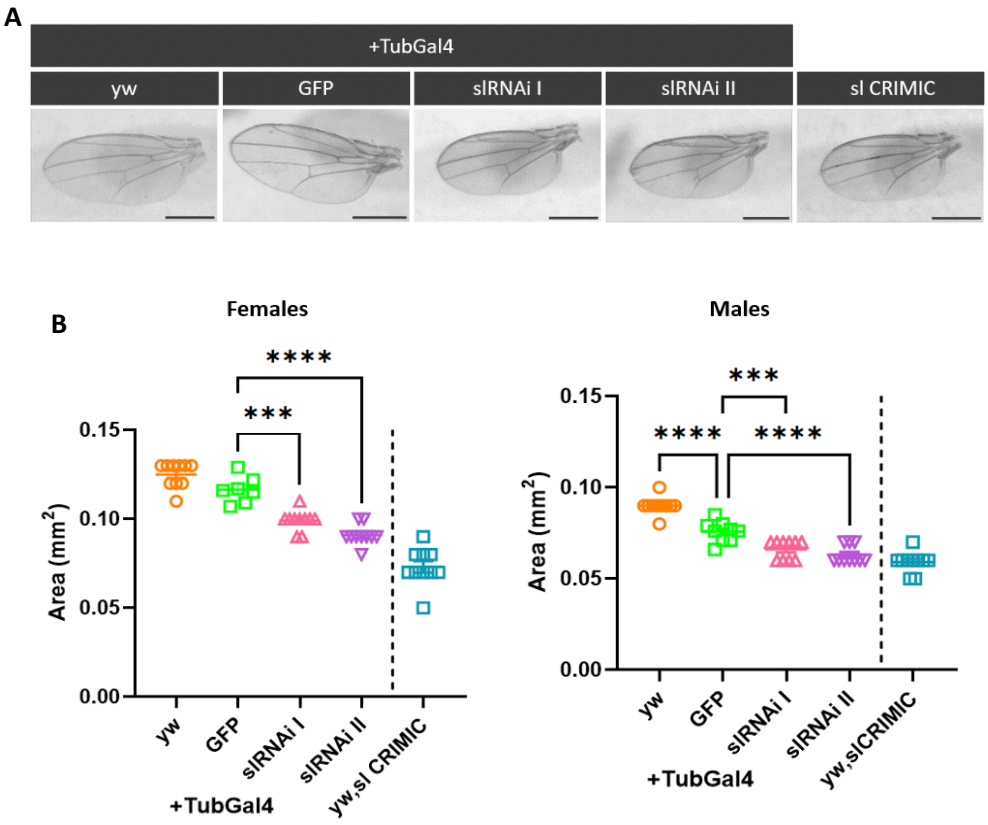

Figure 4.13: Small wing phenotype upon ubiquitous sl KD.

*A) Representative images of male wings for wildtype (yw), empty vector background control (GFP) and two independent sl RNAis (sl RNAi I & II) under control of the ubiquitous tubulin promoter. Male wings of a sl 'null' mutant (sl CRIMIC) have been included for positive comparison of small wing phenotype (Scale bar: 0.6 mm). B) Graph of measured area (mm^2) for the selected region of interest (See Figure 4.13A) in the right wings of each genotype, female and male flies (One-way ANOVA with Dunnett's multiple comparison test; slRNAi I (ID:105893): Females: n=7-10, F=71.81, ***p=0.0001; Males: n=9-10, F=56.37, ***p=0.0008, sl RNAi II (32906): Females: n=7-10, F=71.81, ****p<0.0001; Males: n=9-10, F=56.37, ****p<0.0001, GFP: Males: n=9-10, F=56.37, ****p<0.0001).*

4.2.4. PLCδ-PH:GFP and GRP1-PH::GFP Reporters Enable Dynamic Modelling of PIP2 and PIP3 Lipid Profiles *in vivo*

Transgenic flies with novel chimeric GFP reporters fused to PLCδ and GRP1 PH domains have been developed for *in vivo* visualisation of PIP2 and PIP3. Experiments were first conducted to optimise the use of these fluorescent phosphoinositol reporters for visualisation of PIP2 and PIP3 in the fly brain.

To define glial distribution of PIP2 in the fly brain, the pan glial driver Repo-Gal4 was used to target expression of the UAS-PLCδ-PH::GFP reporter to glial cells. Glial distribution of PIP2 was diffuse over the fly midbrain and optic lobes (x20) and visualised at the cell membrane (x40). Furthermore, the GFP signal of the reporter was strong enough without the need for antibody staining (Figure 4.14).

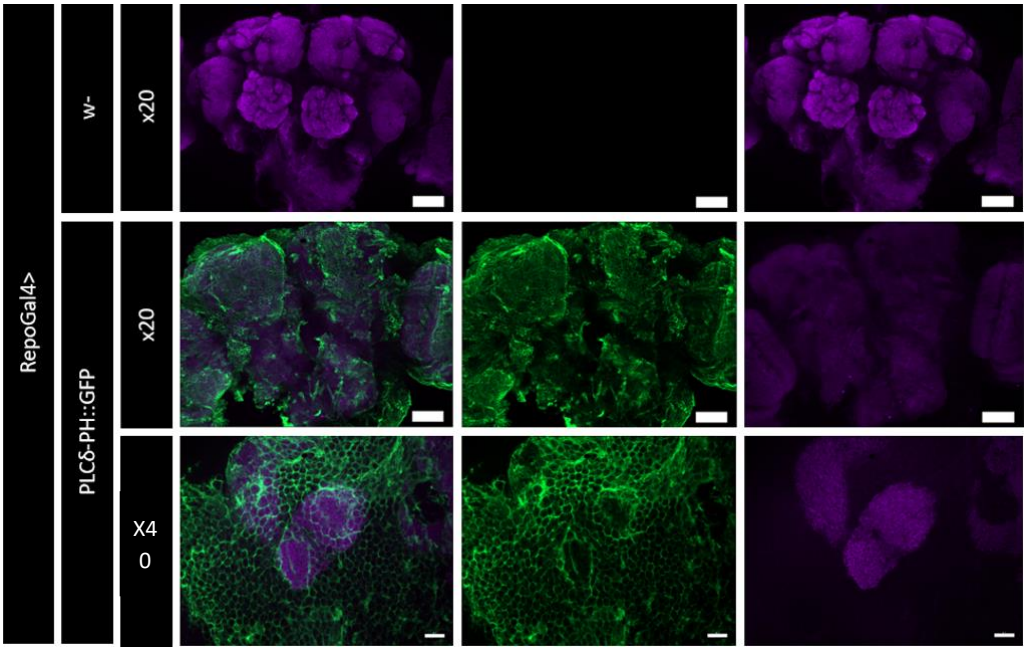

Figure 4.14: Glial PLCδ-PH::GFP reporter expression in the adult fly brain.

Representative confocal images of the adult fly brain (x20) (scale bar 50 µm) with and without PLCδ-PH::GFP reporter expression targeted exclusively to glia cells using the Repo-Gal4 promoter. Glial distribution of PIP2 is visualised in green and presynaptic zones labelled with the bruchpilot antibody nc82 are shown in purple for contrast. The cell body layer of the mushroom body (x40) is shown for brains expressing the PLCδ-PH::GFP reporter, demonstrating GFP expression localised to cell membranes (scale bar 10 µm).

To define the distribution of PIP3 throughout the fly brain, a GFP reporter fused to the GRP1 PH domain (GRP1-PH::GFP) was expressed under transcriptional control of the ubiquitous alphaTub84B promoter. GFP fluorescence of the PIP3 reporter is comparatively weaker to that of the PIP2 reporter and is constitutively expressed throughout the brain. Areas enriched with PIP3 are marked by brighter GFP foci (see arrowheads). To confirm this was not autofluorescence, brains of w- vs the PIP3 reporter alone were compared and distinctive differences in levels of GFP fluorescence were observed (Figure 4.15).

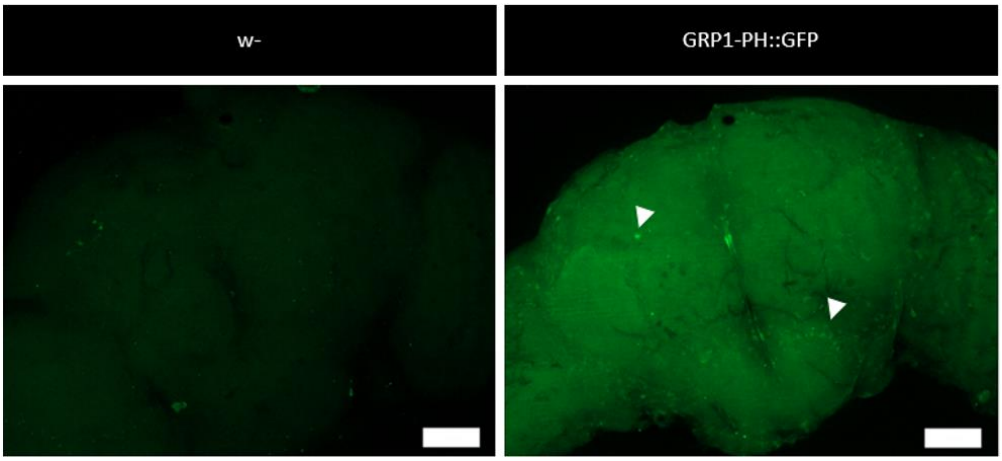

Figure 4.15: Ubiquitous GRP1-PH::GFP expression in the adult fly brain.

Representative confocal images of adult fly brains with and without ubiquitous GRP1-PH::GFP reporter expression (x20) (scale bar 50 µm), where GFP fluorescence depicts PIP3 distribution throughout the fly brain. Arrowheads mark regions of increased GFP fluorescence, indicating higher abundance of PIP3 localised to these areas.

Both genetically encoded PI reporters were viable and expressed sufficiently in the adult fly brain to allow for quantification via confocal microscopy. The next experiments set out to determine whether these genetic tools have utility as a means to detect and quantify changes in PIP2/PIP3 distribution and levels in response to genetic perturbation of key enzymes in their metabolism.

To further characterise the utility of the UAS-PLCδ-PH::GFP reporter, various enzymatic targets of known function in PIP2 metabolism such as PTEN, PLD3 and PI3K were manipulated through RNAi mediated KD. Glial PIP2 distribution and baseline GFP intensity

were confirmed following co-expression of the UAS-PLCδ-PH::GFP reporter with UAS-LacZ, serving as a Gal4 titration control. In brains expressing UAS-LacZ, PIP2 distribution is widespread indicated by GFP throughout the midbrain and optic lobes (Figure 4.16B). The pattern of PIP2 distribution in the UAS-LacZ control is similar to that of the Repo-Gal4 driver only control (w-). Both PTEN and PLD3 contribute to the formation of PIP2. PTEN dephosphorylates PIP3 to produce PIP2, whilst PLD3 produces phosphatidic acid an activator of phosphatidylinositol-4-phosphate kinase (PI4K), which itself phosphorylates PI4P, producing PIP2. Upon glial specific KD of PTEN and PLD3, a reduction in the percentage area GFP above set threshold was expected, due to reduced ability to form PIP2 from PTEN and PLD3 dependent pathways. However, there was no overall change in the area percentage of GFP in the midbrain compared to the UAS-LacZ control despite seeing focal regions of increased GFP (see arrowheads: Figure 4.16B) (Kruskal-Wallis test with Dunn's multiple comparison test; n=10-44, LacZ vs PTEN: ns: >0.0009 and LacZ vs: ns: >0.0009). These results indicate overall abundance of glial PIP2 in the midbrain is not altered following reduced glial expression of PTEN or PLD3 (Figure 4.16C).

Alternatively, PI3K is involved in the generation of PIP3 upon phosphorylation of its substrate PIP2. Upon glial KD of PI3K we anticipated a rise in the area GFP above set threshold, as less PIP2 substrate is used for PI3K dependent PIP3 generation. The area percentage of GFP measured in the midbrain however was strikingly reduced upon glial KD of PI3K, highlighting a significant depletion in PIP2, which was unexpected (Kruskal-Wallis test with Dunn's multiple comparison; n=10-44, PI3K: ****p<0.0001) (Figure 4.16C).

These characterisation experiments demonstrate that the UAS-PH-PLCδ::GFP reporter can be a useful tool for defining the cellular distribution of PIP2, as well as recording dynamic changes to PIP2 flux in an *in vivo* model system.

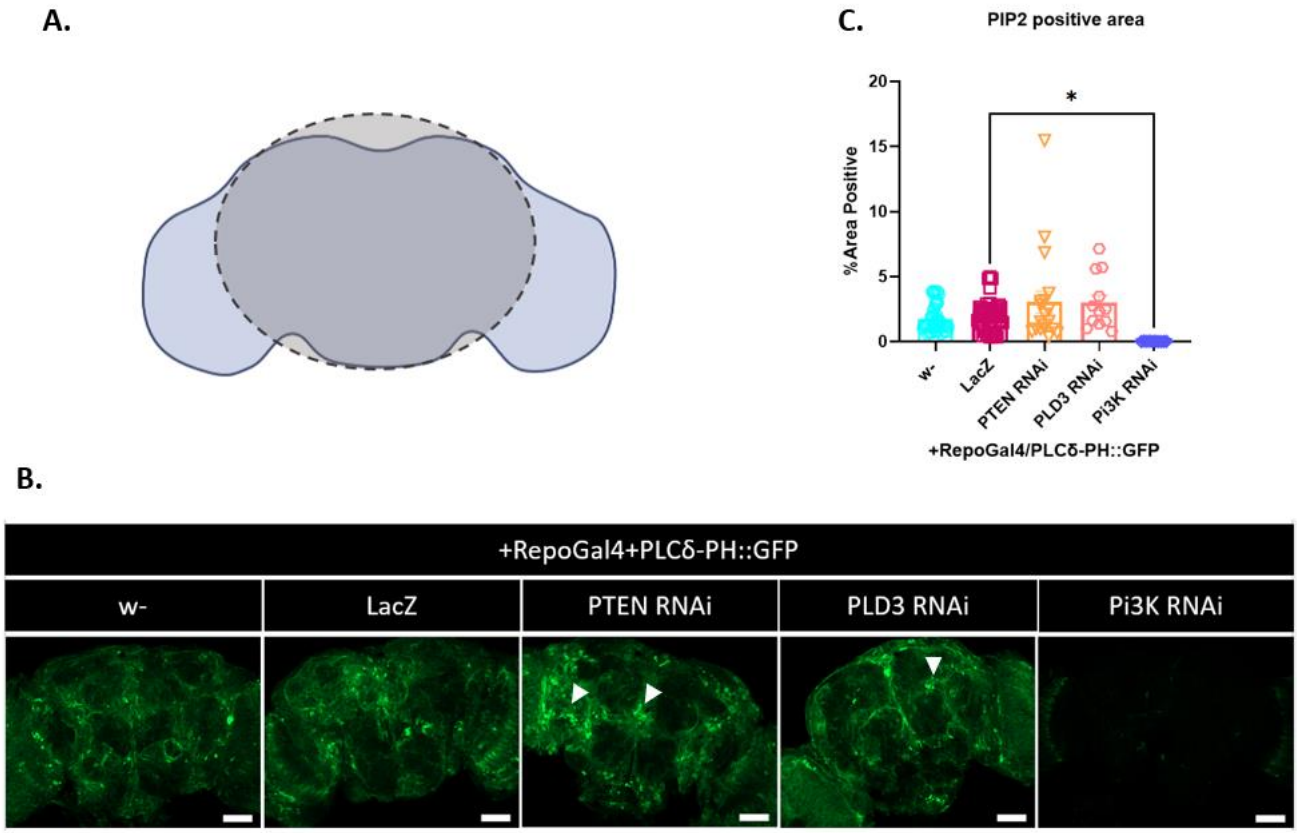

Figure 4.16: Measuring changes in PIP2 metabolism using the PLCδ-PH::GFP reporter tool.

*A) Grey shaded ellipse (dashed) outlines the region of interest (midbrain) for image analysis. B) Representative maximum orthogonal projections of dissected brains (7 d.p.e) for genotypes shown (x20). The pan-glial driver Repo-Gal4 targeted glial specific expression of the PIP2 specific reporter (UAS-PLCδ-PH:GFP) in the following genetic backgrounds: w-, LacZ (UAS control), PTEN RNAi, PLD3 RNAi and PI3K RNAi (Scale bar: 50 µm). Glial distribution of PIP2 is depicted by GFP fluorescence (green), where GFP intensity positively correlates with PIP2 abundance. Arrowheads mark areas of intense PLCδ-PH::GFP reporter expression, indicating higher levels of PIP2. C) The percentage of midbrain positive for PLCδ-PH::GFP expression in genotypes indicated, quantified by area threshold analysis. A total of n=44 (w-), n=42 (LacZ), n=19 (PTEN), n=12 (PLD3) and n=10 (PI3K) brains were analysed from a mixed sex population and statistical differences were calculated by Kruskal-Wallis test with Dunn's multiple comparison test. Significant differences presented as ****p<0.0001. Error bars represent ± SEM.*

4.2.5. Glial sl Knockdown Regulates PIP2 but not PIP3

PLCG2 and its conserved *Drosophila* homolog, sl catalyse membrane turnover of PIP2 into IP3 and DAG secondary messengers. Manipulating PLCG2/sl activity has therefore a direct impact on PIP2 metabolism whereby hyper-functional PLCG2 mutations are associated with depleted PIP2 levels, indicating a potential pathogenic mechanism for AD (Maguire et al. 2021). Given PIP2 plays critical roles in actin remodelling, endocytosis, and phagocytosis, as well as being an important cell signal transducer, it is feasible that perturbations in PIP2 metabolism will subsequently impair important glial functions shared between microglia and their fly counterparts.

Having confirmed Repo-Gal4 driven expression of the UAS-PLCδ-PH::GFP reporter enabled visualisation of dynamic changes in glial membrane PIP2 within the fly brain, we next set out to characterise changes seen in response to downregulating glial sl activity by RNAi (Figure 4.17A). GFP expression of the PIP2 reporter was bright enough without the need to enhance the signal with anti-GFP immunostaining. In brains of wildtype (w-) flies, glial PIP2 distribution is fairly uniform and widespread throughout, similar to PIP2s distribution pattern seen in brains expressing the UAS control (LacZ) for Gal4 titration. Quantifying the % area of GFP in the midbrain by measuring fluorescence above a set background threshold displays no difference between wildtype (w-) and UAS-LacZ control flies (Figure 4.17B) (One-way ANOVA with Dunnett's multiple comparison test; n=10-11, F=14.99, ns: p=0.7814), indicating PIP2 abundance is equivalent between the two control genotypes. Following glial KD of sl there was however ~60% increase in the area of GFP measured above the set background threshold compared to the UAS-LacZ control (One-way ANOVA with Dunnetts multiple comparison test; n=10-11; F=14.99, *** p=0.0003) (Figure 4.17B), highlighting an overall increase in PIP2 within the midbrain upon reduced sl activity in glia, as anticipated. Regions /in the midbrain exhibiting increased GFP fluorescence can be seen in representative confocal images (see arrowheads: Figure 4.17A). These regions are around 5 µm in diameter, similar to the size of cell bodies, indicating levels of PIP2 may be elevated in cell bodies following glial KD of sl.

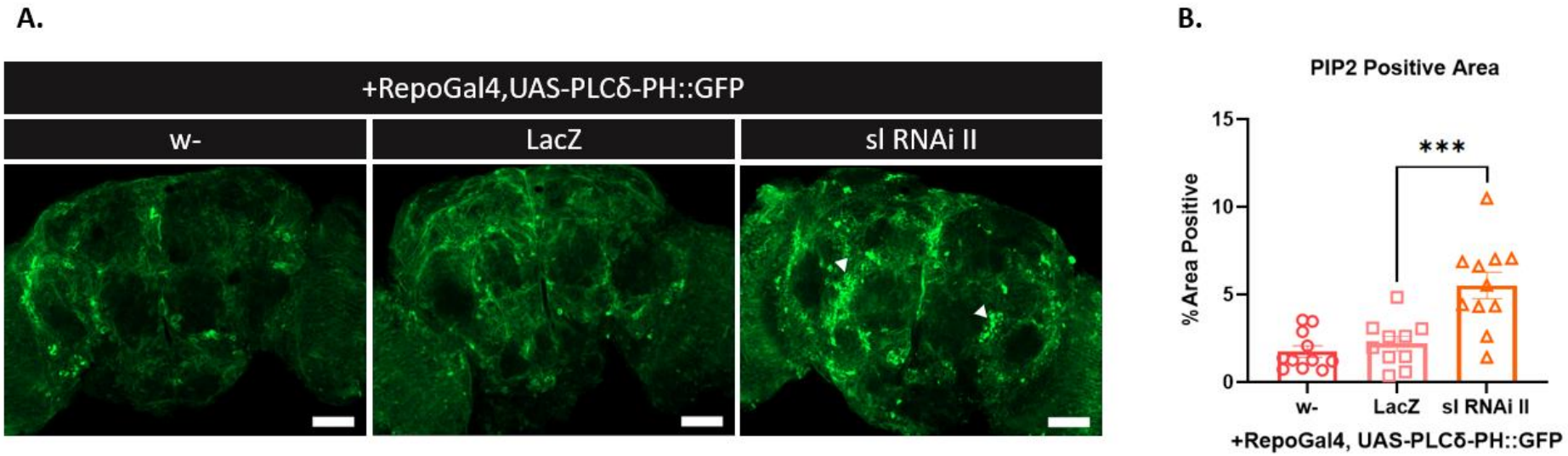

Figure 4.17: Characterisation of glial PI(4,5)P2 membrane dynamics following glial sl KD.

*A) PIP2 specific reporter (UAS-PLCδ-PH::GFP) was recombined with the pan glial driver RepoGal4 and crossed to the following genetic backgrounds w- (wildtype), LacZ (UAS control) and sl RNAi II (ID:32906), from which brains were dissected 7 d.p.e and imaged via confocal microscopy. Representative maximum orthogonal projections are shown (x20) (Scale bar: 50 µm). GFP fluorescence depicts glial localisation of PIP2, whereby GFP signal intensity positively correlates with PI(4,5)P2 levels. Arrowheads mark regions of increased GFP intensity upon glial sl KD. B) Chart showing the % of midbrain positive for PLCδ-PH::GFP expression in genotypes indicated, quantified by area threshold analysis in n=11 (w-), n=10 (LacZ) and n=11 (slRNAi) dissected brains from a mixed sex-population. % coverage of PLCδ-PH::GFP expression in the midbrain increased significantly following glial sl KD compared to the UAS-LacZ control. One-way ANOVA with Dunnett's multiple comparison test and significant differences were shown as: *** p=0.0004. Error bars represent ±SEM.*

Given PIP3 can be formed from phosphorylation of PIP2 by PI3K, altering PIP2 membrane dynamics can thus indirectly impact PIP3 synthesis. As PIP2 accumulated following the reduction of glial sl expression, a simultaneous increase in PIP3 was anticipated, through increased availability of its precursor. Following glial specific KD of sl, changes to PIP3 abundance and localisation were probed using the ubiquitously expressed GRP1-PH::GFP reporter.

In the brains of wildtype flies (w-), PIP3 was distributed ubiquitously at low abundance, as depicted by the widespread but weak GFP signal from the GRP1-PH reporter (Figure 4.18A). Although weaker than the signal from the PLCδ-PH::GFP reporter, the GRP1-PH::GFP reporter in the brains of wildtype flies (w-) could be visualised without the need for immunostaining. The distribution of PIP3 reporter was diffuse throughout the fly brain, opposed to the regional distribution of PIP2 reporter, therefore PIP3 levels in the midbrain was measured through GFP intensity instead of % GFP area. Visual comparison of GFP fluorescence in the midbrain of wildtype (w-) vs UAS-control (LacZ) flies appeared similar. However, analysis of GFP intensity in the midbrain by mean gray analysis revealed a subtle decrease in PIP3 levels in the UAS-LacZ control group, indicating minimal reduction to PIP3 following expression of a UAS site (Figure 4.18B) (One-way ANOVA with Dunnett's multiple comparison test; n=10-13, F=6.330, w- vs LacZ: *p=0.0239). The UAS-LacZ control was thus used to define baseline GFP intensity of the GRP1-PH::GFP reporter for which the UAS-sl RNAi could be compared.

Upon glial specific KD of sl, GFP intensity in the midbrain appeared to diminish compared to the UAS-LacZ control (Figure 4.18A) however, the overall difference as quantified by mean gray analysis highlighted no significant change in GFP intensity (Figure 4.18B) and thus no change in PIP3 levels following reduced glial sl activity. Secondary to no difference in abundance, there was also no change in PIP3 localisation, remaining uniformly distributed throughout the entire midbrain and optic lobes.

These findings demonstrate, as anticipated, glial sl activity regulates PIP2 turnover similar to its human homolog PLCG2. Moreover, this is without compensatory changes to PIP3 biosynthesis.

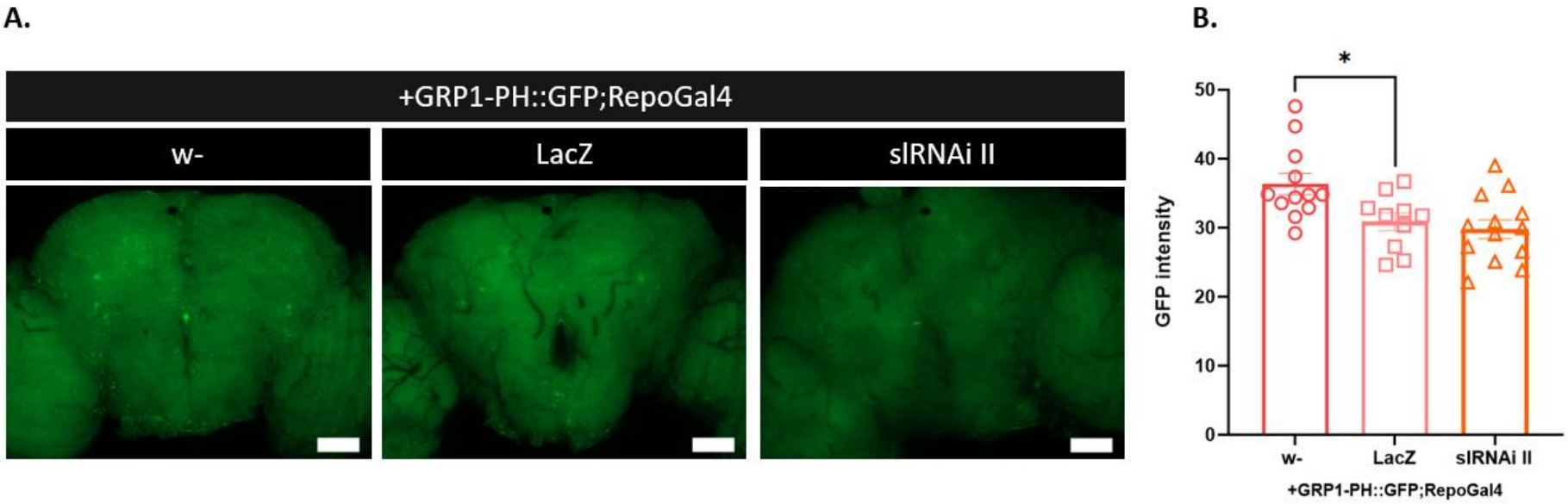

Figure 4.19: PI(3,4,5)P3 dynamics remain unaltered following glial sl KD.

*A) The following genetic backgrounds w-, LacZ and slRNAi II were each crossed to an established driver stock containing the PI(3,4,5)P3 specific reporter (GRP1-PH::GFP) and pan glial driver (Repo-Gal4) then brains of F1 progeny were dissected at 7 d.p.e. Representative maximum orthogonal projections are shown for each genotype (x20) (Scale bar: 50 µm). Distribution of the GRP1-PH::GFP reporter (green), is ubiquitous with fluorescence corresponding to levels of PI(3,4,5)P3. B) Chart displaying quantification of GFP intensity in the midbrain measured by mean gray analysis for n=12 (w-) n=10 (LacZ) and n=13 (slRNAi II) dissected brains of a mixed sex population for genotypes indicated. One-way ANOVA with Dunnett's multiple comparison test and significant differences were annotated as *p=0.0239). Error bars represent ±SEM.*

4.2.6. Glial Knockdown of small wing does not Impact Locomotor Function or Survival

Ubiquitous expression patterns of sl mRNA throughout development, that are notably higher during embryonic stages indicates sl supports universal cellular processes throughout embryogenesis, in particular cell proliferation and differentiation (Emori et al. 1994) . sl null mutants, although viable, show mild defects in eye and wing development (Thackeray et al. 1998). How sl expression throughout adulthood contributes to biological processes such as longevity and behaviour has not yet been explored, especially glial specific sl expression. To understand the basic biological importance of sl in glia throughout age, survival and locomotor phenotypes were assessed upon glia specific KD. sl KD was achieved using the sl RNAi (ID 32906), which was to be used in follow up Aβ experiments.

First survival phenotypes upon glial sl KD were assessed in female flies mated 24 hours (Figure 4.20A). Lifespan of the glial driver only control (w-), exhibits a smooth trajectory and median lifespan of 29 days when aged at 30°C. With a median lifespan of 31 days, the TRIP RNAi control for attP2 insertion site (TRIP CTRL II) demonstrates a slightly longer survival rate than the glial driver only control by just 2 days (Log Rank Mantel-Cox test; n=53-90, χ^2=9.414, **p=0.0022). Survivorship of flies expressing the sl RNAi II, were compared to the TRiP RNAi control (TRIP CTRL II), controlling for effects of transgene insertion at the attP2 site. Glial sl KD did not significantly alter lifespan of adult flies, as a difference in median survival by only 2 days was observed between flies expressing the sl RNAi II and the TRiP RNAi control (29 vs 31) (Log rank Mantel-Cox test; n=53-60, χ^2=0.5605, ns p=0.4541). The survival trajectory following glial sl KD was also similar that of the glial driver only control (w-), which shared a median lifespan of 29 days (Log Rank Mantel-Cox test; n=60-90, χ^2=1.707, ns: p=0.1913).

To assess gross neurological function, locomotor behaviour in male flies aged 14 d.p.e was assessed (Figure 4.20B). Flies expressing the Repo-Gal4 driver alone (w-) travelled on average a distance of 71 mm in 10 seconds, which was 12 mm further than the TRiP RNAi control group (TRiP CTRL II) (One-way ANOVA with Tukey's multiple comparison test; n=13-14, F=14.43, ****p<0.0001). Distance travelled following glial KD of sl (sl RNAi II) was compared to locomotor behaviour of the TRiP RNAi control group (TRiP CTRL II), revealing no deficit in locomotor function upon glial KD of sl. In fact, flies expressing glial sl RNAi II travelled on average 8 mm further compared with aged-matched TRiP RNAi control (TRiP CTRL II) (One- way ANOVA with Tukey's multiple comparison test; n=6-14, F=14.43, * p=0.0159). However, in comparison with the Repo-Gal4 driver only control, glial KD of sl showed no significant difference in locomotor function whereby the average distance

travelled was 71 mm and 67 mm respectively (One-way ANOVA with Tukey's multiple comparison test; n=6-13, F=14.43, ns: p=0.4709).

Overall, these results demonstrate glial KD of sl is not detrimental to survival nor locomotor function of the adult fly.

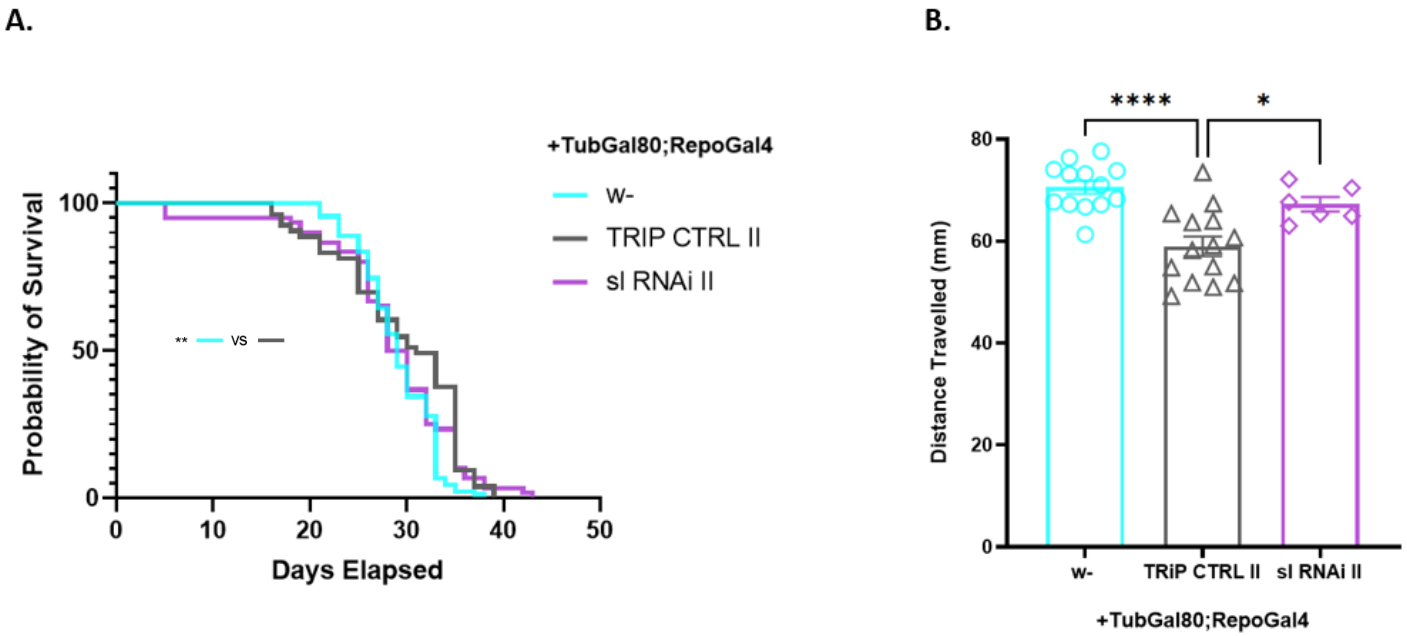

Figure 4.20: Glial KD of sl does not impact survivorship or locomotor function.

A) Lifespan trajectories and B) locomotor performance in flies expressing w-, sl RNAi II (ID: 32906) or the respective TRiP RNAi control (P(CaryP)attP2) (noted as TRiP CTRL II) targeted to glia using the RepoGal4 driver, repressible by the temperature sensitive Tubulin Gal80 machinery. A) Survivorship of 24 hours mated females were recorded for each genotype indicated and statistically analysed using Log Rank Mantel-Cox test (n=53-90). B) Average distance travelled (mm) in 10 seconds, following negative geotaxis for male flies at 14 d.p.e. Individual data points represent the average distance travelled of all flies in a single vial averaged over five consecutive RING trails (1n). A total of n=6-14

*vials were analysed and statistical differences calculated by One-way ANOVA with Tukey's multiple comparison test and statistical differences are shown as, ****p<0.0001, and *p=0.4709. Error bars represent ±SEM.*

4.2.7. Glial Expression of aos::$A\beta_{42}^{Arc}$ Results in Widespread Extracellular Aβ Accumulation

We next aimed to assess if sl contributed to pathology associated with AD, firstly aiming to establish a useful model of amyloid pathology. To test utility of fly models expressing human aos::$A\beta_{42}^{Arc}$ in glial and its ability to induce AD relevant pathological phenotypes, several quantifiable phenotypes were assessed, such as image-based detection of amyloid, sensitive immune-assays (MSD), as well as locomotor behaviour and survival assays.

The *Drosophila* aos fused at the N-terminus of the human $A\beta_{42}^{Arc}$ peptide should direct extracellular secretion following packaging of the peptide into vesicles from the golgi apparatus (Figure 4.4). At 14 d.p.e. glial expression of human aos::$A\beta_{42}^{Arc}$ resulted in widespread accumulation of $A\beta_{42}$ deposits across the fly brain, detected by immunostaining with the 6E10 antibody that is widely used for detection of amyloid plaques in mice and humans. Amyloid deposits were absent from the brains of non $A\beta_{42}$ expressing flies (w-), as expected (Figure 4.21).

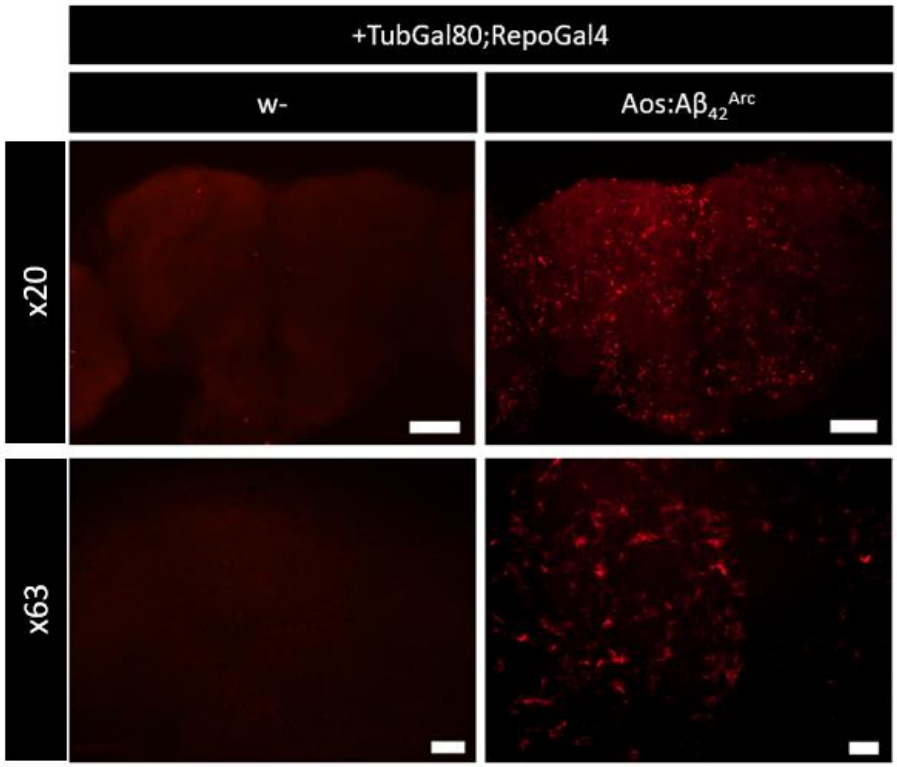

Figure 4.21: Glial targeted aos::$Aβ_{42}^{Arc}$ peptide results in widespread amyloid accumulation.

Representative maximum orthogonal projections of brains immunostained with 6E10 (anti-Aβ) at 14 d.p.e. Widespread accumulation of Aβ deposits is seen throughout the whole brain (x20) upon glial targeted expression of aos::$Aβ_{42}^{Arc}$, compared to non-amyloid expressing flies (w-) (Scale bar: 50 μm). Magnification to the cellular level (x63) highlights individual Aβ deposits and their fibrillar like morphology (Scale bar: 10 μm).

To further explore the cellular/intercellular localisation of these amyloid deposits and confirm the aos indeed directed extracellular secretion of the Aβ peptide, a membrane tethered mCD8::GFP reporter was co-expressed with aos::$Aβ_{42}^{Arc}$ to depict localisation of Aβ in relation to glial cell membranes. Expression of mCD8::GFP and aos::$Aβ_{42}^{Arc}$ were driven by the pan glial promoter Repo-Gal4 and brains were immunostained with the 6E10 antibody for Aβ at 14 d.p.e. mCD8::GFP outlined glial cell membranes in green and $Aβ_{42}$ deposits were depicted in red (Figure 4.22). $Aβ_{42}$ deposits appear in close proximity to the extracellular side of the glial cell membrane but do not fully overlap (see arrowheads: Figure 4.22), indicating $Aβ_{42}$ is secreted extracellularly and not retained in the cell.

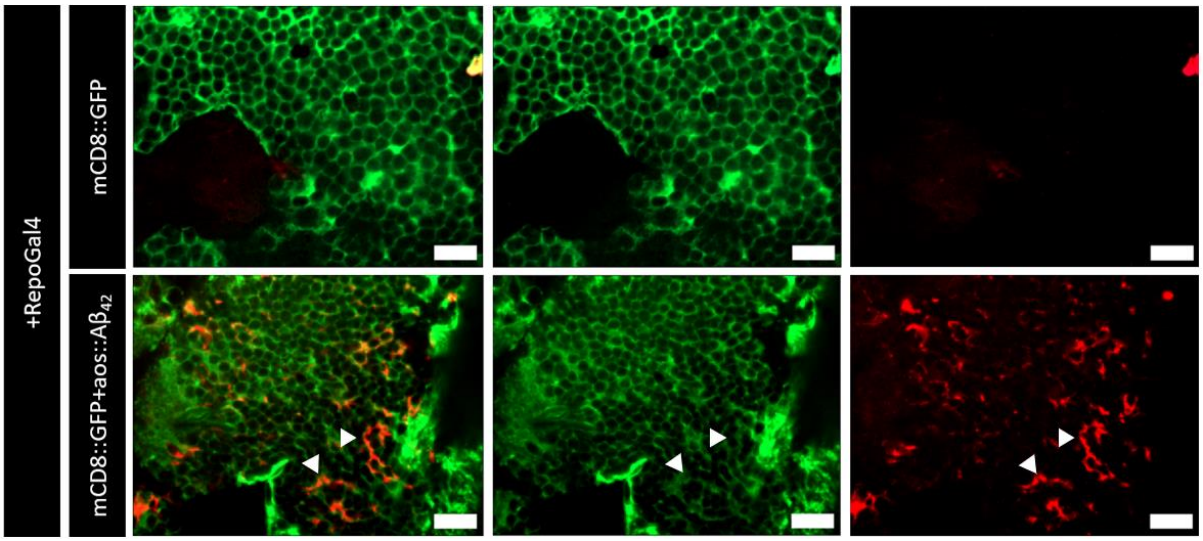

Figure 4.22: aos directs extracellular secretion of the Aβ$_{42}$ Arc peptide expressed in glia.

Repo-Gal4 driven expression of membrane tethered GFP (mCD8::GFP) and co-expression of aos::Aβ$_{42}^{Arc}$. Representative z stack slice to depict localisation of Aβ$_{42}$ deposits, (red) immunostained with 6E10, in relation to glial cell membranes (green) (x63). Overlay of the two channels (green and red), demonstrates extracellular localisation of the Aβ$_{42}$ peptide (see arrowheads) (Scale bar: 10 µm).

These findings provide evidence that glial expression of aos::Aβ$_{42}^{Arc}$ drives accumulation of physiologically relevant extracellular amyloid deposits throughout the fly brain. Also data supports glial expression of aos::Aβ$_{42}^{Arc}$ can be used to model Aβ$_{42}$ associated pathology in following experiments addressing how sl interacts with Aβ$_{42}$ associated pathology.

Having confirmed $A\beta_{42}$ accumulates extracellularly, the highly sensitive MSD assay was next used to quantitatively define concentrations of soluble and insoluble $A\beta_{42}$ in the fly brain at 14 d.p.e, upon pan-glial expression of aos::$A\beta_{42}^{Arc}$. The MSD assay uses electrochemiluminescence to detect and quantify levels of target protein in a given sample. The plate is designed with carbon electrodes and involves the addition of a sulpho-tagged detection antibody. When electricity is passed through the plate, the captured label emits light proportionally to the amount of protein being detected. In AD brains, amyloid can be found in both soluble and aggregated insoluble forms (Esparza et al. 2016). Initially, the MSD Aβ peptide panel plate (6E10) was used to validate the exclusive production of $A\beta_{42}$ peptide fragments and no other fragment lengths of 38 or 40 aa. The peptide panel plate used a multi-well format to detect Aβ species 38, 40 and 42 aa in length.

Soluble forms of $A\beta_{42}$ were readily detectable in fly heads at 14 d.p.e, in those expressing aos::$A\beta_{42}^{Arc}$ (Two-way ANOVA with Sidak's multiple comparison test; n=3; Genotypes $F(1,12)=4.61$, $p<0.0001$; Aβ species $F(2,12)=41.97$, $p<0.0001$; Interaction Genotype X Aβ species $F(2,12)=41.97$, $p<0.0001$) significant (****$p<0.0001$) (Figure 4.23A). Guanidinium insoluble fractions of $A\beta_{42}$ were also detected in aos::$A\beta_{42}^{Arc}$ expressing flies, demonstrating disease relevant aggregated forms of Aβ peptide present in the brain after 14 d.p.e (Figure 4.23B). Notably two of the three biological replicates fell above the assay detection limits and therefore statistics could not be computed for this part of the data. Nonetheless, this finding was indicative that insoluble aggregates can form in this model.

Altogether, the Aβ peptide panel confirmed presence of soluble amyloid and gave indication of insoluble, aggregated forms of $A\beta_{42}$ peptide could accumulate. The MSD panel ruled out production of smaller Aβ fragment sizes 38 and 40, suggesting cleavage of the Aβ peptide was specific to 42 aa in length.

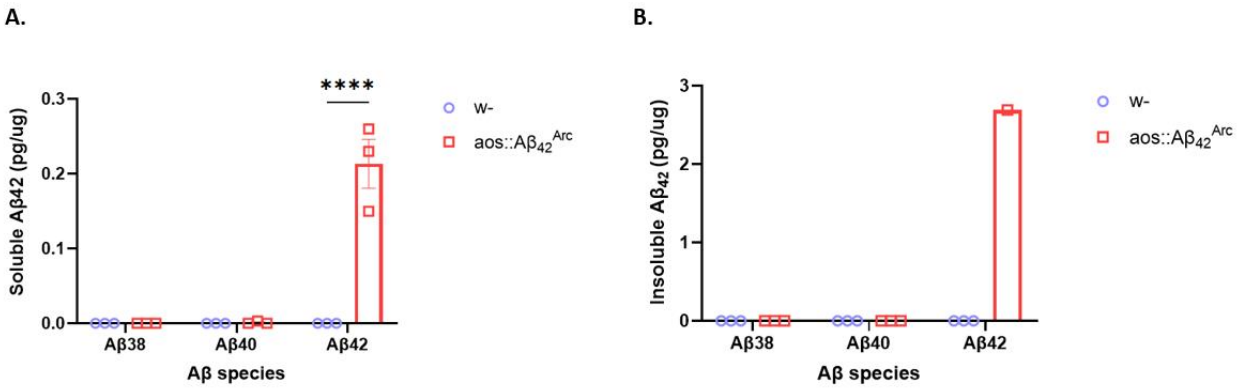

Figure 4.23: Detection of soluble and insoluble Aβ$_{42}$ species upon glial expression of aos::Aβ$_{42}^{Arc}$.

*Quantification of soluble (A) and insoluble (B) concentrations of Aβ species 38, 40 and 42 in fly head extracts normalised to total protein concentration (pg/ug) at 14 d.p.e for three independent biological replicates. Comparison of glial expressing Aβ flies (aos::Aβ$_{42}^{Arc}$) versus non Aβ expressing flies (w-). Bars of the chart present data from independent biological replicates ±SEM (n=3 with 40 flies in each set) with significant differences annotated ****p<0.0001.*

4.2.8. Glial Expression of aos::Aβ$_{42}^{Arc}$ Impairs Survival and Locomotor Behaviour

Having confirmed glial expression of aos::Aβ$_{42}^{Arc}$ induced disease relevant Aβ$_{42}$ pathology in the fly brain by 14 d.p.e, I next set out to define the impact of its accumulation, measuring two quantifiable phenotypes of adult *Drosophila* physiology such as lifespan and behaviour.

Firstly, to assess the impact of marked Aβ$_{42}$ accumulation on survival in adult *Drosophila*, aos::Aβ$_{42}^{Arc}$ was expressed throughout glial cells, exclusively in adulthood specific stages using the pan-glial driver Repo-Gal4 repressible by the temperature sensitive Gal80 machinery. Upon eclosion at 18°C, flies were maintained at 30°C throughout their remaining lifespan, as to drive maximal Aβ$_{42}$ expression. Male and female survivorship were first assessed independently. It was noted male flies exhibited a stronger survival deficit upon glial expression of aos::Aβ$_{42}$ compared to females, with males having a median lifespan of 16 days and females 30 days. Nonetheless both sexes exhibited a statistically significant shortening of lifespan compared to the UAS-LacZ control, which median lifespan was 38

days (Log Rank, Mantel-Cox test; Female: n=61-84, χ^2=99.73, df=1, ****p<0.0001, Male: n=42-77, X^2=78.05, df=1, ****p<0.0001). As both sexes demonstrated strong survival deficits upon glial aos::$A\beta_{42}$ expression, the survival of male and females were combined. Combined survivorship of male and female flies expressing aos::$A\beta_{42}$ in glia still demonstrated a significant reduction in survival compared to the UAS-LacZ control, whereby the median lifespan was 21 days.(Figure 4.24A) (Log Rank, Mantel-Cox test; combined n=103-161, χ^2=135.8, df=1, ****p<0.0001). This indicated accumulation of $A\beta_{42}$ from glial sources is detrimental to the survival of adult flies both in males and females by an average of 17 days.

Having demonstrated glial expression of aos::$A\beta_{42}^{Arc}$ results in survival deficits, the impact on locomotor behaviour was assessed next (Figure 4.24B). Locomotor performance of male flies, measured by distance travelled up the vial in 10 seconds post initiation of negative geotaxis were examined at 7, 14 and 18 d.p.e. Locomotor performance of glial expressing aos::$A\beta_{42}^{Arc}$ flies were compared to that of age matched UAS control (LacZ). LacZ expressing control flies performed consistently over the 18 days, travelling an average distance of 69 mm. In flies expressing aos::$A\beta_{42}^{Arc}$ in glia, a small decline in locomotor performance was observed between 7 and 14 d.p.e, going from an average distance travelled of 72 mm to 59 mm. By 18 d.p.e, there was a further decline in locomotor performance whereby flies travelled only 35 mm. At 18 d.p.e, aos::$A\beta_{42}^{Arc}$ expressing flies exhibited a significant decline in locomotion performance compared to the age matched UAS-LacZ control, where distance travelled after 10 seconds is reduced nearly 2-fold, from 72 mm to 35 mm (Figure 4.24B) (Two-way ANOVA with Sidak's multiple comparison test; n=5, F=18.84, DFn=1, DFd=8, ****p<0.0001).

In conclusion, deficits to survival and locomotor functions indicate glial expression of aos::$A\beta_{42}^{Arc}$ must be toxic to the fly, manifesting through in early death and CNS dysfunctions.

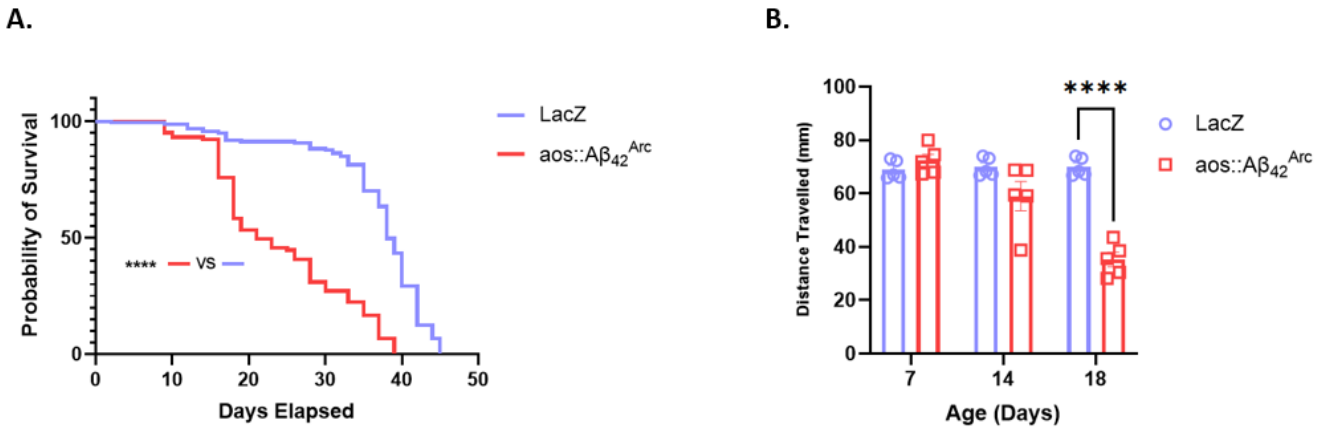

Figure 4.24: Glial expressed aos::Aβ$_{42}^{Arc}$ induces survival and locomotor deficits.

*Lifespan trajectories (A) and locomotor performance (B) of aos::Aβ$_{42}^{Arc}$ expressing flies (red) versus UAS-LacZ control flies (lilac) using the pan-glial driver Repo-Gal4 for targeted glia expression during adulthood. A) Survivorship of male and 24 hours mated females were combined for statistical analysis using Log Rank, Mantel-cox test (n=103-161) where statistical significance is indicated as ****p<0.0001. B) Histogram of plotted average distance travelled (mm) in 10 seconds, following analysis of negative geotaxis performance in male flies for timepoints indicated (7, 14 and 28 d.p.e) using the RING apparatus (described in Chapter 3). Individual data points represent the average distance travelled of all flies in a single vial averaged over five consecutive RING trails (1n). A total of n=5 vials were analysed for each genotype and statistical differences were calculated by two-way ANOVA with Sidak's multiple comparison test, revealing a strong statistical difference ****p<0.0001. Error bars represent ±SEM.*

4.2.9. Glial Knockdown of sl Rescues Aβ$_{42}$ Survival Related Deficits but not Locomotion Impairment

To determine whether glial sl expression modifies glial phenotypes of Aβ$_{42}$ toxicity, changes to Aβ$_{42}$ associated survival and locomotor deficits were assessed. Flies were generated to co-express UAS-sl RNAi and the human UAS-aos::Aβ$_{42}^{Arc}$ peptide. Using temperature sensitive Gal80 to control Repo-Gal4 driven expression of sl RNAi, KD of sl was targeted to glial cells exclusively in adulthood stages. Flies were reared at 18°C (prohibitive temperature for Gal4 activity) and upon eclosion, flies were selected and transferred to 30°C (permissive temperature for Gal4 activity). Survival assays were conducted on female flies mated 24 hours (Figure 4.25A) whilst locomotor assays were tested in male flies at 14 and 21 d.p.e (Figure 4.25B).

Quantification of survival demonstrated that wildtype flies (w-) live significantly longer than flies of the $A\beta_{42}$ expressing RNAi control group (GFP-Valium10 (GFP)+ $A\beta_{42}$) with median survival declining by 6 days (37 to 31) (Log Rank, Mantel-Cox test; n=105-136, χ^2=79, ****p<0.0001). In this instance, the GFP-Valium10 empty vector background control was used to appropriately control for the number of UAS sites in RNAi lines generated under the TRiP collection. Glial KD of sl, significantly improved survival associated deficits of glial aos::$A\beta_{42}^{Arc}$ expression, increasing the median survival of the $A\beta_{42}$ expressing RNAi control group (GFP+ $A\beta_{42}$) by 7 days (Log Rank, Mantel-Cox test; n=105-159, χ^2=129.8, ****p<0.0001). In fact, glial sl KD rescued the survivorship back to wildtype (w-) where median lifespan was 38 and 37 days respectively (Log Rank, Mantel-Cox test; n=105-159, χ^2=0.7019, ns: p=0.4022).

As reduced sl expression in glia ameliorated $A\beta_{42}$ dependent lifespan deficits, the impact of glial sl expression on $A\beta_{42}$ associated locomotor deficits was examined next. Since glia provide neurotrophic support and regulate neuronal activity, it was important to address whether glial sl expression contributed to $A\beta_{42}^{Arc}$ associated neurological dysfunction, using the RING locomotion assay.

Locomotor behaviour was examined at 14 and 21 d.p.e (Figure 4.25B). At 14 d.p.e locomotor performance was consistent across all genotypes with the average distance climbed for each group around 66 mm. At 21 d.p.e, locomotor performance expectedly declined across all genotypes by at least 16%, however the decline was more prominent in flies co-expressing $A\beta_{42}$. At 21 d.p.e, the average distance travelled by the $A\beta_{42}$ expressing RNAi control group (GFP+ $A\beta_{42}$) is significantly reduced compared with age-matched, non-$A\beta_{42}$ expressing flies (w-) (Mixed effect analysis with Tukey's multiple comparison test; n=7-13, Age: F(1,26)=55.44, ****p<0.0001; Genotype F(2,28)=3.040, ns: p=0.0639; AgeXGenotype interaction: F(2,26)=3.377, *p=0.0497; w- vs GFP+ $A\beta_{42}$: **p=0.0047). However, the average distance travelled between the $A\beta_{42}$ expressing RNAi control and glial sl KD group (slRNAi+$A\beta_{42}$) is comparable, 35 mm and 36 mm respectively, demonstrating reduced glial sl expression does not modify $A\beta_{42}$ associated locomotor deficits (Mixed effect analysis with Tukey's multiple comparison test; n=7-13, GFP+$A\beta_{42}$ vs sl RNAi II +$A\beta_{42}$: ns, 0.9777).

In summary, these findings indicate reduced glial sl expression ameliorates $A\beta_{42}$ induced survival deficits but not locomotor impairment.

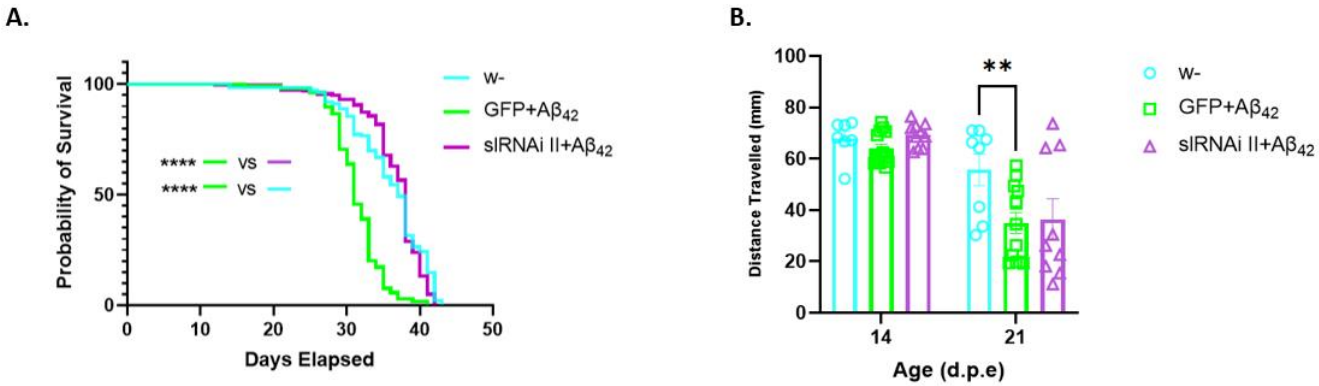

Figure 4.25: Glial small wing KD ameliorates $A\beta_{42}$ induced survival deficits but not locomotor impairment.

*A) Lifespan trajectories and B) locomotor performance in non- $A\beta_{42}$ expressing flies (w-) (cyan) and flies co-expressing human aos::$A\beta_{42}^{Arc}$ (noted as $A\beta_{42}$) with either slRNAi II (ID 32906) (purple), or the respective TRiP RNAi control (GFP-Valium10) (noted as GFP) (green), using the pan-glial Repo-Gal4 driver. A) Kaplan-Meier plot showing survivorship of 24 hours mated females were recorded for each genotype indicated and statistically analysed using Log Rank, Mantel-cox test (n=105-159). Statistical differences are annotated as ****p<0.0001. B) Chart showing average distance travelled (mm) in 10 seconds, following analysis of negative geotaxis performance for male flies at timepoints indicated (14 and 21 d.p.e) using the RING apparatus. Individual data points represent the average distance travelled of all flies in a single vial averaged over five consecutive RING trials (1n). A total of n=7-13 vials where analysed and statistical differences calculated by mixed effects analysis with Tukey's multiple comparison test and statistical differences are shown as **p=0.0047. Error bars represent ±SEM.*

4.2.10. Glial Specific sl Knockdown does not Alter Total $A\beta_{42}^{Arc}$ Load in the Brain

Glial sl activity contributed to $A\beta_{42}$ associated early death phenotypes but not behavioural deficits. The contribution of glial sl activity on amyloid accumulation was therefore determined next. Aβ immunostaining was first used to define the distribution of amyloid in

control vs transgenic flies after 14 d.p.e, where we begin to see pathology manifest in early death and locomotor deficits. As anticipated, amyloid was absent from the brain of non-transgenic glial driver only control flies (w-) but detected in transgenic flies expressing $A\beta_{42}$. After 14 d.p.e, $A\beta_{42}$ deposits concentrated around cortical regions of the brain in $A\beta_{42}$ expressing RNAi control flies. Similarly, to age matched RNAi control, amyloid accumulation remained in cortical regions of the brain upon glial KD of sl (Figure 4.26A&B), where visually there is no striking difference in total amyloid load between RNAi control and sl KD brains.

Subtle changes in Aβ load and the ratio of soluble vs insoluble Aβ fractions cannot be accurately detected by imaging. The MSD immunoassay provided a more sensitive means for quantifying changes in Aβ load following glial KD of sl at 14 d.p.e, defining levels of both total soluble and insoluble $A\beta_{42}$. Similar to experiments described above, the Aβ peptide panel plate (6E10) was used to quantify levels of soluble and insoluble $A\beta_{42}$ in fly brains following glial sl KD. As anticipated, in non $A\beta_{42}$ expressing flies (w-) no soluble or insoluble $A\beta_{42}$ was detected. In brains of $A\beta_{42}$ expressing RNAi control flies (GFP+ $A\beta_{42}$) there was a clear presence of soluble $A\beta_{42}$ and an even higher abundance of insoluble $A\beta_{42}$ (One-way ANOVA with Tukey's multiple comparison test; n=3, Soluble: F=18.02, ** p=0.0052, and Insoluble: F=11.72, ** p=0.0098). Glial sl KD did not influence total amyloid burden in the fly brain at 14 d.p.e, with levels of soluble and insoluble $A\beta_{42}$, remaining comparable to the aged matched $A\beta_{42}$ expressing RNAi control group (Figure 4.26A) (One-way ANOVA with Tukey multiple comparison test; n=3, Soluble: F=18.02, ns: p=0.9864, Insoluble: F=11.72, ns: p=0.7818). The ratio of insoluble to soluble $A\beta_{42}$ was also comparable between flies expressing the $A\beta_{42}$ RNAi control and sl RNAi II, indicating reduced glial expression of sl does not shift the ratio of insoluble vs soluble $A\beta_{42}$ (Figure 4.26C) (One-way ANOVA with Tukey's multiple comparison test; n=3, F=3.045, ns: p=0.8837).

In summary, this data demonstrates glial sl KD does not contribute to changes in load or solubility of $A\beta_{42}$ in the brain at 14 d.p.e and therefore extends lifespan independent of amyloid pathology.

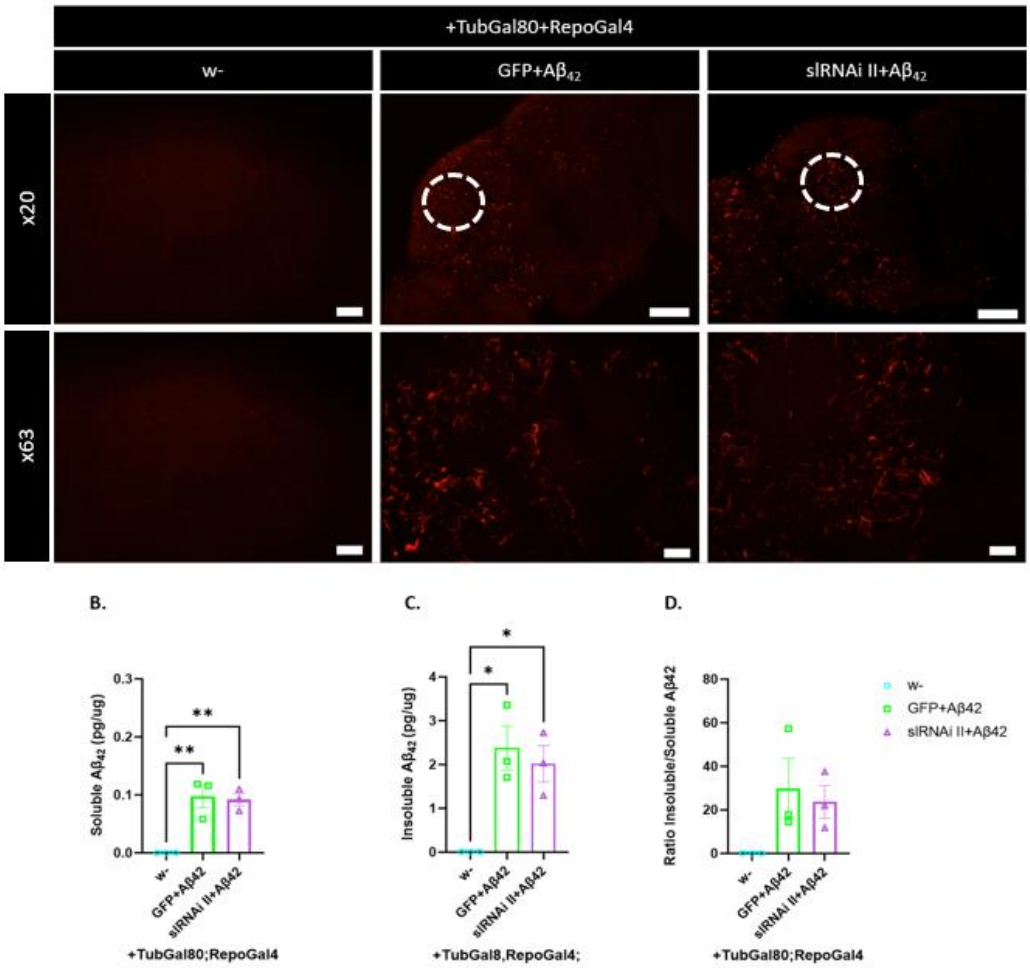

Figure 4.26: Glial small KD does not alter total Aβ$_{42}$ load in the brain.

*Aβ$_{42}$ pathology depicted in the fly brains (A) or whole heads (B-D) at 14 d.p.e for genotypes as follows; w-, GFP+ Aβ$_{42}$ and sIRNAi II+ Aβ$_{42}$ (ID: 32906), under control of the pan glial driver Repo-Gal4. A) Representative maximal orthogonal projections of brains immunostained with the 6E10 anti-amyloid antibody from a mixed population of female and male brains. Dotted circles outline Aβ deposits (red) in the cortical brain region (Scale bar: 50 µm) and magnification of the cellular level (x63) depicted individual Aβ$_{42}$ deposits and their fibril like morphology (Scale bar: 10 µm). B-D) Quantified soluble (B) and insoluble (C) concentrations of Aβ$_{42}$ normalised to total protein concentration (pg/µg) in extracts from fly heads and calculated insoluble: soluble ratio (D) deduced from three biological replicates with n=40 flies in each set. Statistical differences calculated by one-way ANOVA with Tukey's multiple comparison test are displayed **p≤ 0.001 and *p≤0.05. Error bars represent ±SEM.*

Although reduced glial sl expression did not alter total $A\beta_{42}$ burden or solubility in the brain at 14 d.p.e, it is feasible that its activity may modify dynamics of amyloid accumulation at earlier or further aged timepoints. To test this, total soluble and insoluble $A\beta_{42}$ were measured at two additional timepoints (7 d.p.e and 21 d.p.e) (Figure 4.27A, B&C). As the MSD Aβ peptide panel plate (6E10) used in initial experiments confirmed the transgenic aos::$A\beta_{42}^{Arc}$ model produced only $A\beta_{42}$ species (See Figure: 4.23A&B), further investigations used an MSD plate specific to detection of the $A\beta_{42}$ species (4G8).

As expected, no soluble or insoluble $A\beta_{42}$ was detected in the glial driver only control group (w-) at either 7 or 21 d.p.e. For flies expressing $A\beta_{42,}$ both soluble and insoluble forms of $A\beta_{42}$ were detected at 7 and 21 d.p.e. At 7 d.p.e there was a higher proportion of soluble $A\beta_{42}$ detected in fly heads compared to 21 d.p.e where heads exhibited higher proportions of insoluble $A\beta_{42}$ (Figure 4.27A&C). In $A\beta_{42}$ expressing RNAi control flies (GFP+$A\beta_{42}$) the proportion of insoluble $A\beta_{42}$ detected had increased by approximately two-fold from 7 d.p.e to 21 d.p.e (Figure 4.27B), indicative of $A\beta_{42}$ aggregation. These results demonstrate a clear shift in the ratio of soluble to insoluble $A\beta_{42}$ with age, starting with more soluble, monomeric forms of $A\beta_{42}$ in earlier adulthood which progressively forms insoluble, $A\beta_{42}$ aggregates in later stages (Mixed effects analysis with Sidak's multiple comparison test; n=2-3, Age: $F(1,5)=14.19$, * $p=0.0131$, Genotype: $F(2,6)=9.667$, * $p=0.133$, Interaction Age X Genotype: $F(2,5)= 3.888$, ns $p=0.0958$).

Whilst an increase to insoluble pools of $A\beta_{42}$ was evident with age, glial KD of sl did not alter the total soluble or insoluble $A\beta_{42}$ being produced compared to the age matched $A\beta_{42}$ expressing RNAi control group (GFP+$A\beta_{42}$) at 7 d.p.e or 21 d.p.e (Mixed effects analysis with Tukey's multiple comparison test; n=2-3, GFP+$A\beta_{42}$ vs sl RNAi II+$A\beta_{42}$; soluble 7 d.p.e: ns, $p=0.9546$, 21 d.p.e: ns, $p=0.9347$, insoluble 7 d.p.e: ns, $p=0.9232$, 21d.p.e: ns, $p=0.7045$). This highlighted reduced sl expression in glia did not modify progression of amyloid accumulation throughout age. There was also no significant difference to the calculated ratio of insoluble: soluble $A\beta_{42}$, with the proportion of insoluble $A\beta_{42}$ remaining comparable in both glial sl KD and $A\beta_{42}$ expressing RNAi control groups at 7 and 21 d.p.e (Mixed effects analysis with Tukey's multiple comparison test; n=2-3, GFP+$A\beta_{42}$ vs sl RNAi II+$A\beta_{42}$; 7 d.p.e: ns, $p=0.6147$, 21 d.p.e: ns, $p=0.4505$). These findings indicate that glial sl KD does not significantly alter the dynamics of amyloid pathology with age, with no significant difference in either total load or solubility of $A\beta_{42}$.

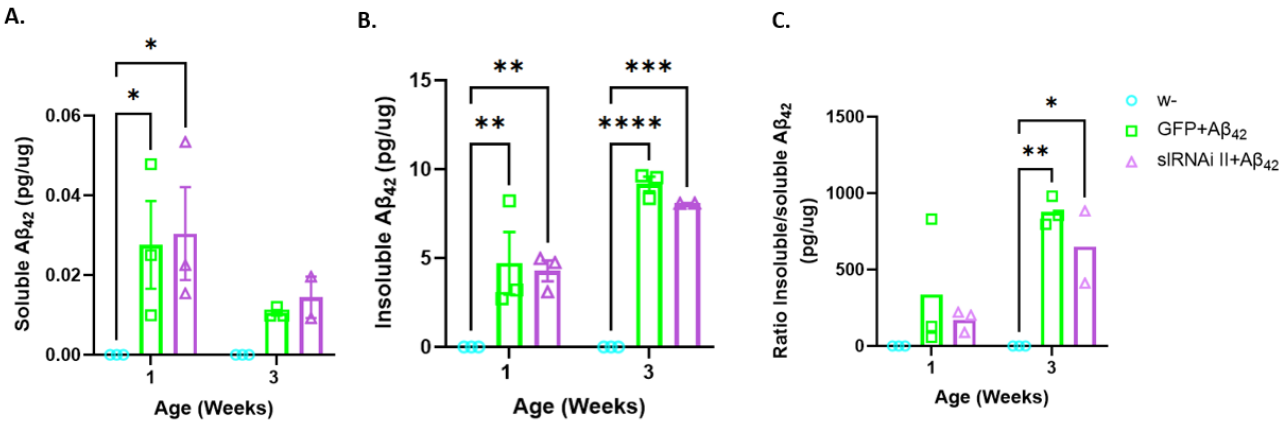

Figure 4.27: Accumulation and solubility of Aβ42 throughout age, following glial KD of sl.

*Quantified levels of Aβ42 from soluble (A) and insoluble (B) extracts of fly heads for the following genotypes; w-, GFP+ Aβ42, slRNAi II+ Aβ42 at 7 and 21 d.p.e, where glial targeted expression is achieved using the Repo-Gal4 driver. Total soluble (A) and insoluble (B) concentrations of Aβ42 were normalised to total protein concentrations (pg/ug) and Insoluble: Soluble Aβ42 (C) was calculated accordingly. One-way ANOVAs with Tukey's multiple comparisons was performed on three independent biological replicates where n=40 for each set. Statistical differences are annotated as; *p≤0.05, **p≤0.01, ***p≤0.001 and ****p≤0.0001. Error bars represent ±SEM.*

4.2.11. Glial sl does not Alter PIP2 Membrane Dynamics in Response to Amyloid Accumulation

In AD brains, PIP2 levels are found to be decreased with studies showing elevation of oligomeric Aβ results in PIP2 depletion (Arancio, 2008). The relationship between PIP2 and Aβ42 expression in glial sl KD models was therefore explored. Glial specific expression of the PLCδ-PH::GFP reporter (refer to Figure 4.14) combined with anti-Aβ immunostaining allowed visualisation of the distribution and abundance of glial PIP2 in brains, in response to amyloid accumulation following glial sl KD.

Changes in levels and distribution of glial PIP2 were investigated in response to amyloid accumulation and combined KD of glial sl (Figure 4.28A&B). The LacZ+ Aβ42 group served as a Gal4 titration control, without interfering with GFP fluorescence of the PLCδ-PH::GFP reporter. The distribution of PIP2 is widespread throughout the brain of the glial driver only

control group (w-). Whilst a similar pattern of PIP2 distribution can be observed in the LacZ+ $A\beta_{42}$ control group, a significant decrease to the PLCδ-PH::GFP reporter signal is observed when compared to the glial driver only control (w-) (One-way ANOVA with Dunnett's multiple comparison test; n=10-13, ****p<0.0001), demonstrating presence of extra UAS sites dilutes expression of the PLCδ-PH::GFP reporter. As glial sl KD previously demonstrated to elevate levels of glial PIP2 in the midbrain (refer to Figure 4.17), levels of glial PIP2 were expected to similarly increase in the combined presence of $A\beta_{42}$. However, the measured percentage area of GFP above the set threshold in the midbrain showed no difference compared to the LacZ+$A\beta_{42}$ control group, highlighting levels of glial PIP2 was not altered by glial sl KD and combined $A\beta_{42}$ expression (Figure 4.28B) (One-way ANOVA with Dunnett's multiple comparison test; n=10-13, ns=0.1635).

At higher magnifications (x63) it was possible to determine $A\beta_{42}$ localisation in relation to the glial distribution of PIP2. In $A\beta_{42}$ expressing flies, a correlation between $A\beta_{42}$ deposits and levels of glial membrane PIP2 was observed, such that glial membranes in close contact with $A\beta_{42}$ deposits exhibited lower levels of PIP2, as indicated by dimmer GFP signal (see arrowheads: Figure 4.28A). Upon glial sl KD this correlation between Aβ localisation and glial PIP2 abundance did not change. Furthermore, the abundance of Aβ deposits appear consistent between glial sl KD and the aged matched Aβ expressing UAS-control group (LacZ+ $A\beta_{42}$), with no gross differences in total Aβ load, supporting previous results showing reduced glial sl expression does not alter total amyloid load (refer to Figure 4.26)

A.

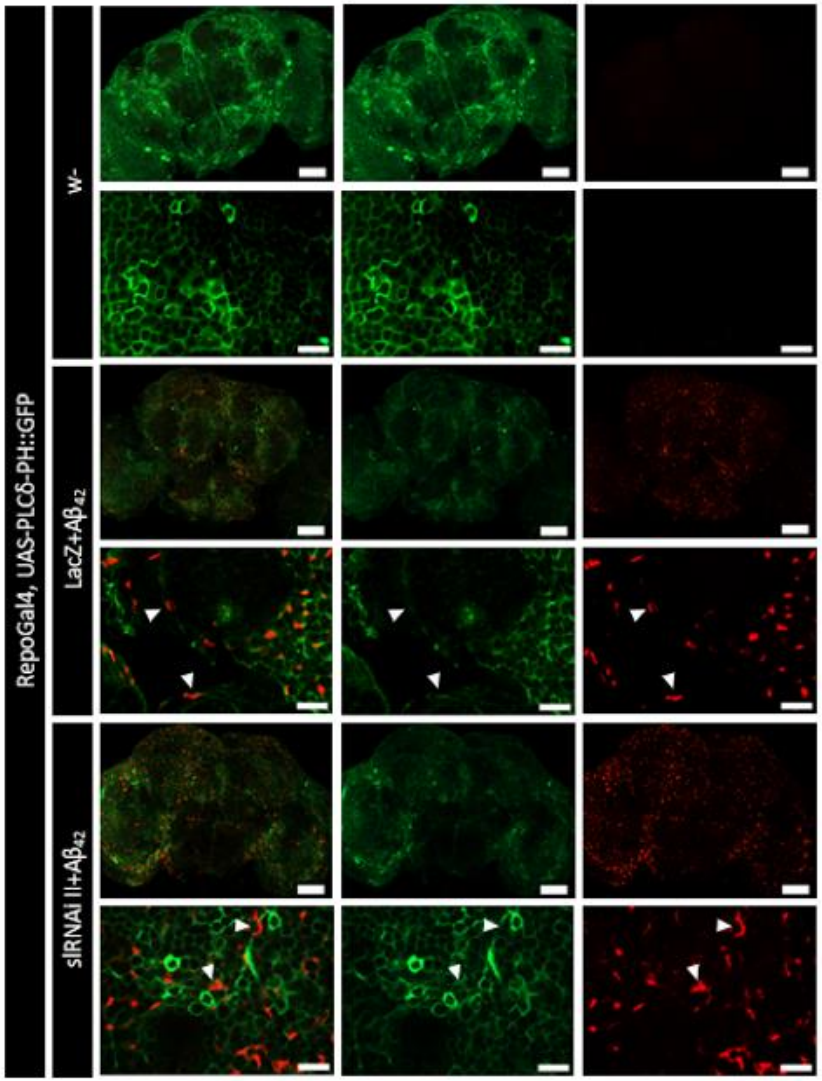

B.

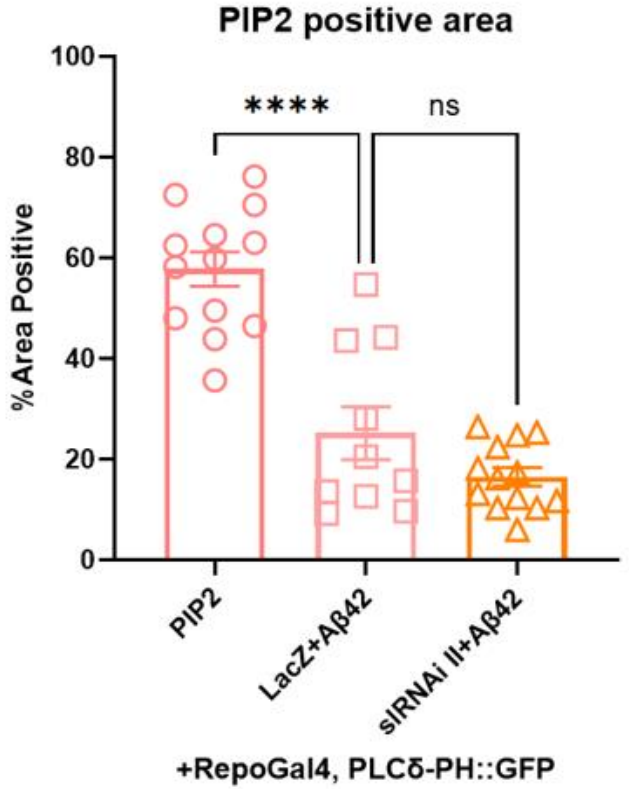

(See figure legend on next page)

Figure 4.28: Characterisation of glial specific PIP2 dynamics in brains exhibiting $A\beta_{42}$ pathology.

*A) Glial targeted expression of the PIP2 specific reporter (UAS-PLCδ-PH::GFP) together with w-, LacZ+$A\beta_{42}$ or slRNAi II+$A\beta_{42}$. Representative maximum orthogonal projections of whole brains (x20) and the cell body level (x63) immunostained with 6E10 anti-Aβ antibody, 7 d.p.e (Scale bar: 50 µm and 10 µM for x20 and x63 magnification images respectively). Localisation of the PLCδ-PH::GFP reporter depicts the distribution of PIP2 in glia, whilst GFP intensity positively correlates with PIP2 abundance. $A\beta_{42}$ deposits are shown in red. Arrowheads demonstrate glial membranes depleted in PIP2 and their close association with $A\beta_{42}$ deposits. B) Measured % coverage of GFP in the midbrain for genotypes indicated, quantified by area above set background. A total of n=14 (w-), n=13 (LacZ+ $A\beta_{42}$) and n= 18 brains from a mixed sex population were analysed with statistical differences calculated by one-way ANOVA with Dunnett's multiple comparison test and significant differences reported as ****p<0.0001. Error bars represent ±SEM.*

4.2.12. Elevation to PIP3 Following Glial Knockdown of sl in Response to $A\beta_{42}$ Accumulation

Next, the ubiquitously expressed GRP1-PH::GFP reporter was used to quantify changes in PIP3 membrane dynamics in response to $A\beta_{42}$ accumulation. The glial driver only control (w-) confirmed low expression of PIP3 at basal levels in brains absent of amyloid pathology, with a weak GFP signal observed across the entire midbrain and optic lobes (Figure 4.29A). In $A\beta_{42}$ expressing control brains (LacZ+$A\beta_{42}$), there is a gross increase in GRP1-PH::GFP reporter fluorescence with the presence of small bright GFP foci around 5 µm in size, sparsely distributed around the brain (see dashed circles: Figure 4.29A). However, in quantifying GFP intensity of the midbrain, no significant difference in mean grey value was recorded following expression of $A\beta_{42}$, indicating PIP3 levels did not significantly change in response to $A\beta_{42}$ accumulation (One-way ANOVA with Sidak's multiple comparison test; n=6-12, F=7.784, ns: p=0.5280).

In response to glial KD of sl, a slight increase in GFP intensity was measured compared to its respective $A\beta_{42}$ expressing control (LacZ+$A\beta_{42}$) (Figure 4.29B) (One-way ANOVA with Sidak's multiple comparison test; n=6-12, F=7.784, *p=0.0256), indicating a moderate rise in PIP3 levels. This rise in PIP3 abundance following reduced glial sl expression is independent of $A\beta_{42}$ load, as there is no obvious difference to number of amyloid deposits measured by qualitative comparison of anti-Aβ immunostaining between glial sl KD and LacZ groups.

Lastly, in determining the correlation between $A\beta_{42}$ accumulation and PIP3 membrane dynamics, we observe that the distribution of amyloid deposits does not correlate well with PIP3 expression, whereby regions rich in $A\beta_{42}$ accumulates do not fully overlap with points of higher GFP intensity and vice versa (see arrowheads: Figure 4.29A). This could be further confirmed by higher magnification images (not shown here). Overall, these findings evidence that PIP3 levels elevate upon glial KD of sl in response to $A\beta_{42}$ build up.

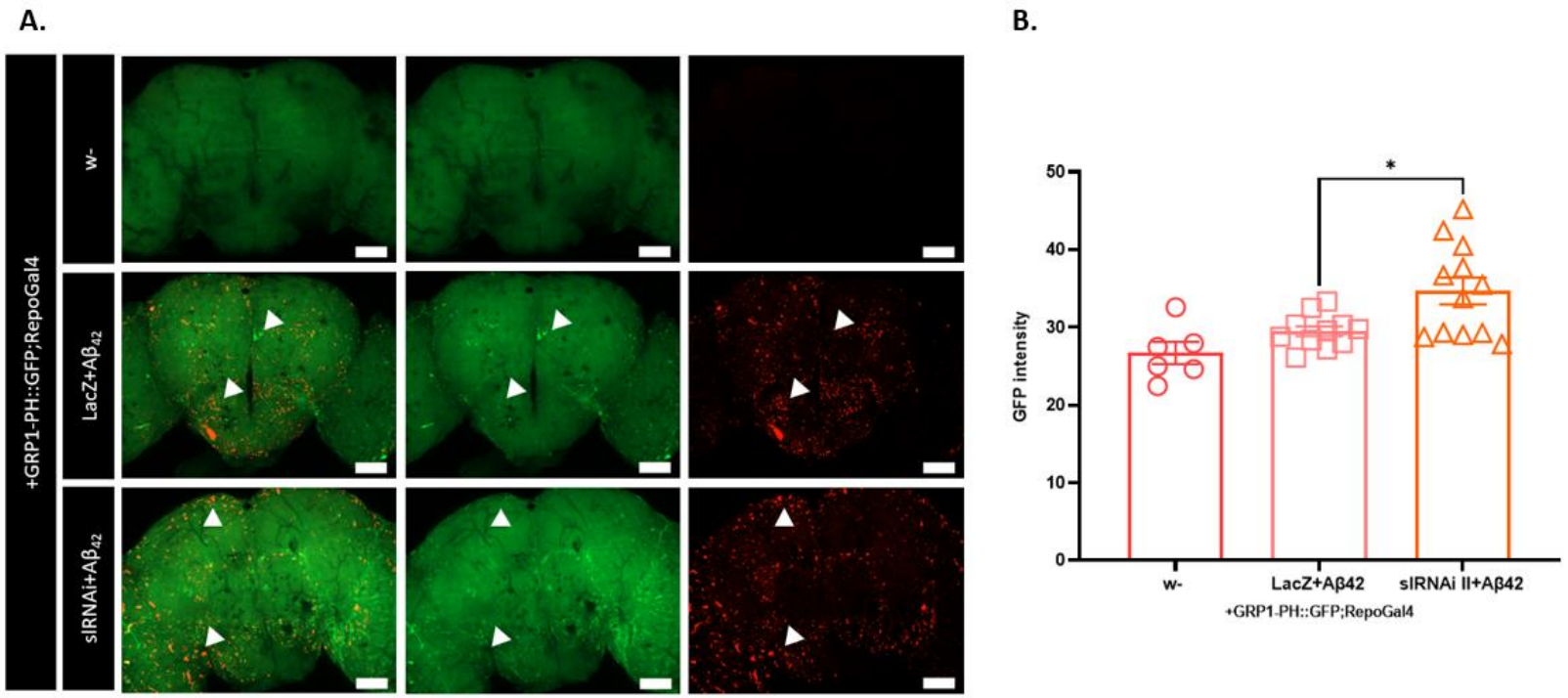

Figure 4.29: Characterisation of PIP3 dynamics in brains exhibiting $A\beta_{42}$ pathology.

*A) Representative maximal orthogonal projections of brains 7 d.p.e expressing the PIP3 specific reporter (GRP1-PH::GFP) alongside glial targeted expression of w-, LacZ+ $A\beta_{42}$ or sIRNAi II+ $A\beta_{42}$ (x20) (Scale bar: 50 µm). GFP fluorescence (green) depicts the distribution and abundance of PIP3 throughout the brain, with regions of increased GFP fluorescence outlined by dashed circles. There is little to no overlap between PIP3 distribution and localisation of $A\beta_{42}$ deposits as indicated by arrowheads. Brains were immunostained with the 6E10 antibody, depicting Aβ accumulates (red). B) Measured GFP intensity of the GRP1-PH::GFP reporter in the midbrain measured by mean grey analysis of n=6 (w-), n=12 (LacZ+$A\beta_{42}$) and n=12 (sIRNAi+$A\beta_{42}$) brains from a mixed sex-population. Statistical differences were calculated by one-way ANOVA with Sidak's multiple comparison test and significant differences were reported as * p=0.0256. Error bars represent ±SEM.*

4.2.13. Glial sl Knockdown Does not Modify Proteostatic Mechanisms

Aberrant accumulation of toxic protein aggregates is hypothesised to contribute to many neurodegenerative diseases including AD, whereby improving proteostatic mechanisms involved in protein quality control and turnover could offer therapeutic benefit (Vilchez et al. 2014). Autophagy is one mechanism regulating protein homeostasis in the cell for which its dysregulation is recognised to contribute to AD pathogenesis (Nixon 2013; Nilsson et al. 2014; Vilchez et al. 2014; Lee et al. 2022).

Phosphoinositides have been implicated in many aspects of the autophagic process, from its initiation of autophagosome biogenesis to maturation. In particular, PI(3,4,5)P3 controls activation of the mTOR pathway which in turn negatively regulates autophagy (Dall'Armi et al. 2013). As PLCG2/sl plays an important role in PI metabolism, the glial role of sl in autophagic mediated removal of protein aggregates was explored.

Protein ubiquitination is an important process involved in marking proteins for degradation. Furthermore, Ref(2)P, the fly ortholog of p62, is an important regulator of protein aggregation in the adult brain, where it binds ubiquitinated protein aggregates marking them for autophagic degradation. Accumulation of Ref(2)P positive or ubiquitinated protein aggregates can be indicative of defects in autophagy or proteasomal function. Levels of Ref(2)P and polyubiquitinated (FK2 antibody positive) protein aggregates were thus quantified in the adult fly brain, using specific antibodies Ref(2)P and FK2, which recognise Ref(2)P and polyubiquitinated positive protein aggregates respectively.

Ref(2)P and polyubiquitinated protein structures were characterised for the first time in a glial model of aos::$A\beta_{42}^{Arc}$ expression. Ref(2)P positive structures were detected following immunostaining with anti-Ref(2)P and were observed both in brains of wildtype and $A\beta_{42}$ expressing flies, demonstrating the presence of Ref(2)P positive aggregates were not exclusive to amyloid pathology (Figure 4.30A). Surprisingly, there was no difference in abundance of Ref(2)P positive structures between wildtype and $A\beta_{42}$ expressing flies (Figure 4.30B) (Kruskal-Wallis test with Dunn's multiple comparison; n=8-11, ns: p>0.9999). Furthermore, Ref(2)P positive structures were observed to be similar in size and shape. However, a significant increase in Ref(2)P positive structures was unexpectedly observed in the $A\beta_{42}$ expressing RNAi control group (GFP+$A\beta_{42}$) (Figure 4.30A). This was quantified by a 46.5% increase in Ref(2)P positive structures in the midbrain when compared to non $A\beta_{42}$ expressing flies (w-) (Figure 4.30B) (Kruskal-Wallis test with Dunn's multiple comparison test; n=8-11, *p=0.0121). Ref(2)P positive structures were also distinctly brighter and larger

here. Significantly fewer Ref(2)P positive structures were visualised in the brain upon glial sl KD when compared to the $A\beta_{42}$ expressing RNAi control group (GFP+$A\beta_{42}$), where an 11% decrease in Ref(2)P positive structures in the midbrain was measured (Figure 4.30A&B) (Kruskall-Wallis test with Dunn's multiple comparison test; n=8-17, ****p<0.0001).

In addition to detection of Ref(2)P positive protein aggregates, polyubiquitinated protein aggregates were also detected in the adult fly brain by immunostaining with anti-FK2. Polyubiquitinated protein aggregates were present in all genotypes at 14 d.p.e (Figure 4.30A), with a greater % coverage of FK2 positive structures in $A\beta_{42}$ expressing fly brains compared to the glial driver only control (w-), as determined by area above set threshold (Figure 4.30C) (Kruskal-Wallis test with Dunn's multiple comparison test; n=10-11, ****p<0.0001). Nonetheless, there were fewer polyubiquitinated protein aggregates in brains of the $A\beta_{42}$ expressing RNAi control group (GFP+$A\beta_{42}$) compared to $A\beta_{42}$ alone, which was likely due to Gal4 titration (Kruskal-Wallis test with Dunn's multiple comparison test; n=10-11, *p=0.0237). Measuring changes in ubiquitination upon glial sl KD was thus appropriately controlled by comparison with the $A\beta_{42}$ expressing RNAi control group (GFP+$A\beta_{42}$). Visually, there appeared to be more polyubiquitinated protein aggregates following glial sl KD (Figure 4.30A), however quantification of FK2 positive area in the midbrain demonstrated no significant difference (Figure 4.30C) (Kruskal-Wallis test with Dunn's multiple comparison; n=10-11, ns: p=0.4466), indicating glial sl does not modify protein ubiquitination. Further exploration is required however to dissect whether FK2 labelling in these brains co-localises with $A\beta_{42}$ aggregates.

Characterising levels of autophagy markers Ref(2)P and ubiquitin in models of glial aos::$A\beta_{42}^{Arc}$ expression demonstrated an increase in ubiquitinated protein aggregates but no change in levels of Ref(2)P, which was unexpected. Furthermore, reduced expression of sl in glial, did not alter ubiquitination of protein aggregates, indicating sl does not likely contribute to autophagic mediated removal protein aggregates. Levels of Ref(2)P positive aggregates where significantly reduced in brains exhibiting sl KD in glia, however, given the unexpected rise in Ref(2)P of $A\beta_{42}$ expressing RNAi control flies, the interpretation of this response is not so clear and requires further validation (see Discussion).

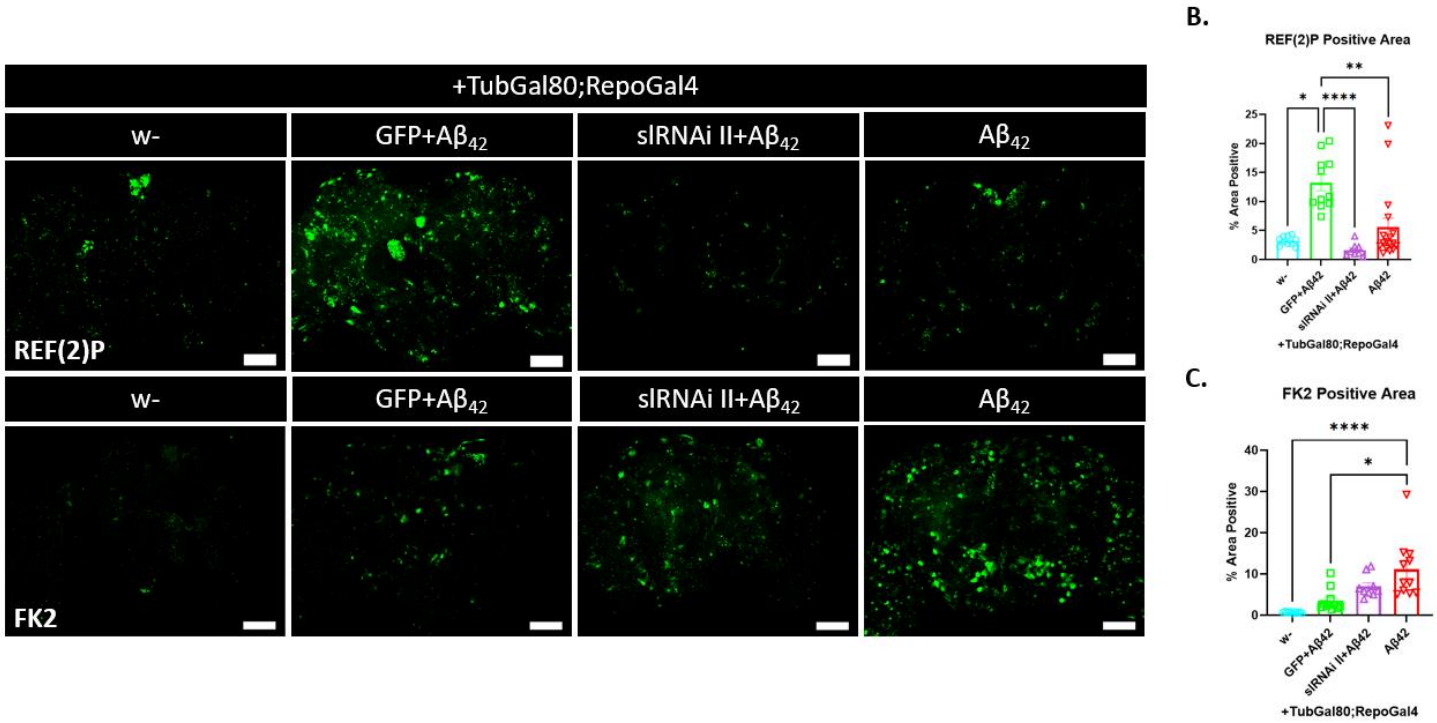

Figure 4.30: Localisation and expression of Ref(2)P and FK2 in brains exhibiting Aβ42 pathology.

*A) Representative maximum orthogonal projections of brains immunostained with anti-Ref(2)P and anti-FK2 at 14 d.p.e (x20). Repo-Gal4 repressible by the temperature sensitive Tubulin-Gal80 was used to drive glial targeted expression of transgenes exclusively at adulthood stages. Ref(2)P and FK2 accumulates (green), are visible throughout the brain (Scale bar: 50 µm). B&C) Chart showing % area of Ref(2)P B) and FK2 C) positive protein structures in the midbrain of genotypes indicated, measured by area set above threshold. Statistical differences were calculated by Kruskal-Wallis test with Dunn's multiple comparison test. Statistical differences were reported as follows B) *p=0.0121, ****p<0.0001, **p=0.0080 and C) ****p<0.0001 and *p=0.0237.*

4.3. Discussion

For this chapter*, Drosophila* have been used as a genetically tractable *in vivo* system enabling glial specific functions of the AD risk gene *PLCG2* to be explored through the conserved homolog, *small wing*. This study elaborated on known biological functions of sl, addressing specific roles in glial biology and PIP2/PIP3 metabolism, as well as evaluating the glial role of sl in $A\beta_{42}$ associated pathology. Experiments in this chapter also characterised phenotypes associated with glial $A\beta_{42}$ expression. Potential mechanisms underlying the glial role of sl in ameliorating $A\beta_{42}$ associated pathology will be discussed further.

4.3.1. Modelling Cellular Functions of Human *PLCG2* with Fly Ortholog *sl*

The *Drosophila sl* gene is the predicted ortholog of human AD associated *PLCG2*, with a DIOPT score of 12/24. Exploiting the GAL4/UAS binary system available to flies enabled exploration of sl basic biological function, in a cell autonomous manner, using an RNAi mediated KD approach. sl KD with RNAi (#32906) gave rise to expected phenotypes, such as small wings and elevation of PIP2, providing strong evidence gene KD was effective. Since completion of this study, sl KD has been independently verified through qPCR by Daniel Maddison (results shown in Appendix 8.1). After 7 d.p.e, ubiquitous expression of sl RNAi II (RNAi: 32906) resulted in ~40% KD of *sl*. The level of sl knockdown may be proportional to the small wing phenotype as null mutants display smaller wing sizes (~30% reduction) (Thackeray et al. 1998) compared to the partial knockdown with sl RNAis (~15% reduction) (see Figure 4.13). It will be important however to validate observed phenotypes of sl KD with available sl null and hypomorphic mutants (Thackeray et al. 1998). Alternatively, experiments could also be designed using the CRIMIC system as a means to study sl loss of function phenotypes.

Results presented in this chapter highlight under physiological conditions glial sl activity is not critically essential to the overall health of adult flies, whereby reduced glial sl expression does not compromise viability, longevity, nor general nervous system functioning. Similarly, sl loss of function mutants were viable, with no known impact to survival or nervous system functions, however they do exhibit mild morphological defects to wing and eye development (Mankidy et al. 2003). The mild phenotypes of sl LOF mutants is surprising given the marked

effects of PLCG2 LOF in mice which although viable have profound defects in B cell development and functions, including defective B cell receptor signalling (Hashimoto et al. 2000; Wang et al. 2000). Additionally, in iPSC derived microglial models, loss of PLCG2 function has been shown to reduce cell survival downstream of TREM2 activation (Andreone et al. 2020). That said both sl and PLCG2 share important roles in cellular development and growth. With there being only one isoform of sl, it is likely such additional functions of PLCG2 have emerged throughout evolution.

Human iPSC derived microglia models have highlighted the importance of PLCG2 activity in regulating diverse microglial functions, such that loss of PLCG2 function impairs cell survival, phagocytic activity, and lipid metabolism downstream of TREM2 activation (Andreone et al. 2020). However, flies do not possess a conserved ortholog of TREM2, and so TREM2 dependent PLCG2 functions in glia cannot be modelled in the fly system. Nonetheless, TREM2 activation of PLCG2 involves phosphorylation through Syk, a non-receptor tyrosine kinase that is evolutionary conserved in *Drosophila. Drosophila* possess a single syk-related molecule called Shark which interacts with the major glial engulfment receptor Draper, homologous to the mammalian MEGF10 glial phagocytic receptor. Shark activity is essential for Draper mediated phagocytosis of axonal debris and neuronal corpses in glia (Ziegenfuss et al. 2008). As core components of the glial engulfment signalling pathway are conserved between *Drosophila* and mammals, the role of sl on glial engulfment was investigated in an independent study ran by another PhD student (Freya Storer; data not shown). These experiments showed reduced glial expression of sl decreased axonal clearance, aligning with *in vitro* data where PLCG2 KO impairs phagocytic activity (Andreone et al. 2020).

Furthermore, PLCG2 is known to regulate Ca^{2+} signalling through IP3 mediated release of intracellular Ca^{2+} stores such as the endoplasmic reticulum. Future experiments, measuring real-time changes in intracellular Ca^{2+} flux could provide another readout of glial sl function, whereby various GcaMP tools are available for live calcium imaging in the intact fly brain (Delestro et al. 2020). Specifically, a GcaMP tool localising to the endoplasmic reticulum would provide readout of receptor mediated Ca^{2+} release from the ER.

PLCG1 and PLCG2 both have distinct expression profiles, where PLCG1 is ubiquitously expressed and PLCG2 expression is restricted to certain immune cells derived from the hematopoietic lineage. In the brain, PLCG2 is predominantly expressed in microglia and also found in granule cells of the dentate gyrus (Magno et al. 2019). Through transcriptomic data, harnessed from the online *SCope* tool, and confocal based gene-localisation studies, sl expression was confirmed in both neuronal and glial cells of the fly brain. Our studies demonstrate, in the adult brain sl expression is more neuronal than glial, however as PLCG2

is preferentially expressed in microglia (Magno et al. 2017), this study aimed to capture the role of its fly ortholog, sl, exclusively in glia. The ubiquitous expression pattern of sl is however more similar to that of PLCG1 expression than PLCG2. It is probable sl adopts functions of both PLCG1 and 2 due to the reduced genetic redundancy of flies, explaining why the expression pattern of *sl* is not restricted to glial cells.

4.3.2. Phosphoinositol Metabolism in Glial Biology

Phosphoinositides, PIP2 and PIP3 are central to many cellular processes such as cell signalling, adhesion, membrane trafficking and actin-cytoskeletal rearrangement, which are important to microglia functions such as motility and phagocytosis (Czech, 2000). Phosphoinositol signalling importantly regulates microglial actin remodelling and phagocytosis, where PIP3 is involved in phagocytic cup formation and cell polarisation and PIP2 facilitates phagosome formation (Desale & Chinnathambi, 2021).

Measuring glial specific levels of PIP2 and PIP3 in *in vivo* tissues by biochemical assays is limited due to the presence of these molecules in other cell types such as neurons and the vasculature etc. However, the availability of phosphoinositol specific GFP reporters in *Drosophila*, some of which can be regulated by the cell type specific GAL4/UAS expression system, have allowed monitoring of PI(4,5)P2 and PI(3,4,5)P3 changes in flux, as well as their distribution within the fly brain, under confocal microscopy. This study is the first described use of these fluorescent reporters in an *in vivo* system, characterising membrane dynamics of important phosphoinositols PI(4,5)P2 and PI(3,4,5)P3 in the adult fly brain. The PLCδ1-PH::GFP reporter, constructed under UAS control was targeted to glial cells using the Repo-Gal4 driver, revealing localisation of PIP2 at glial membranes. Contrastingly, expression of the GRP1-PH::GFP reporter was ubiquitous, albeit much weaker than the PLCδ-PH::GFP reporter, possibly reflecting the lower abundance of PIP3 in unstimulated conditions. Only upon stimulation do levels of PIP3 reach significant detection (Halet, 2005). To further validate the specificity of the PIP2/PIP3 reporters *in vivo*, PIP2/PIP3 specific antibodies could be acquired to check co-localisation with the GFP fluorescence from the reporters.

Use of these reporters have previously been demonstrated in *in vitro* studies where the PLCδ-PH::GFP reporter similarly shows to localise to PIP2 found predominately in the plasma membrane and less so at other internal organelle membranes (Stauffer et al. 1998;

Varnai & Balla, 1998). Additionally, the PLCδ-PH::GFP reporter has been shown to rapidly translocate into the cytosol upon breakdown of PIP2 after stimulation with angiotensin II (Varnai & Balla, 2006). Alternatively, for imaging PIP3 dynamics several probes have been identified such as Brunton tyrosine kinase (BTK-PH-GFP), protein kinase B, (AKT-PH-GFP) and Arf nucleotide opener (ARNO-PH-GFP), however the GRP1-PH domain is considered the most specific probe for detecting PIP3 *in vitro*. Other probes such as AKT-PH::GFP do not have the same degree of selectivity, as they also recognise a derivative of PIP3, PI(3,4)P2 (Klarlund et al. 1997). The GRP1-PH domain has been reported to successfully monitor PIP3 generation in living cells translocating from the cytosol to the plasma membrane following activation of the PI3K pathway (Venkateswarlu et al. 1998).

In a variety of cell types, the PLCδ-PH::GFP reporter has been used to monitor PIP2 hydrolysis upon PLC activation by agonists or the Ca^{2+} ionophore ionomycin. Upon PLC activation the PLCδ-PH::GFP reporter translocates from the plasma membrane into the cytosol, revealing a decrease in membrane PIP2 (Halet, 2005). Experiments described in this chapter used the PLCδ1-PH::GFP reporter to monitor changes in metabolism of glial PIP2 following glial targeted KD of conserved lipid metabolising enzymes in the fly. As expected, an increase in membrane PIP2 following glial KD of the *PLCG2* ortholog, *sl* was evidenced. However, following glial KD of PI3K, an enzyme involved in the conversion of PIP2 to PIP3, levels of PIP2 were significantly depleted. A decline in membrane PIP2 following KD of PI3K was unexpected but could be attributed to enzymatic regulatory mechanisms overcompensating the initial rise in PIP2 that you would expect from reduced expression of PI3K. Testing other independent PI3K RNAis would help confirm this unexpected observation of reduced PIP2 following PI3K KD.

Whilst this data has demonstrated a role of sl in PIP2 metabolism, levels of PIP3 were not directly altered by glial sl expression. Nonetheless, PI metabolism involves a complex network of phosphatases, kinases and phospholipases with several feedback loops keeping PI levels tightly regulated (Figure 4.2). Disruption to one gene, such as *sl/PLCG2* may therefore be insufficient to significantly alter PIP3 levels when there exist compensatory enzymatic mechanisms regulating the intracellular balance of PIP2 and PIP3. For instance, PI3K and PTEN work antagonistically in the interconversion of PI(4,5)P2 and PI(3,4,5)P3 species. PI(3,4,5)P3 can be generated from PI3K dependent phosphorylation of PI(4,5)P2 and PTEN can subsequently convert PI(3,4,5)P3 back to its precursor PI(4,5)P2 by dephosphorylation. Alternatively, other mechanisms also exist in the turnover of PI(3,4,5)P3 in flies, such as the conversion of PI(3,4,5)P3 to PI(3,4)P2 by the ciliary inositol polyphosphate-5-phosphatase (INPP5E) (Kisseleva et al. 2000).

Whilst these studies have used a semi-quantitative approach to measure levels of PIP2 and PIP3, such as area threshold and mean gray value, alternative approaches are available such as PIP specific ELISAs. Such approaches have been used to provide a more quantitative measure of PIP levels, for instance PIP2 specific ELISAs measured depleted levels of PIP2 following expression of a hypermorphic PLCG2 variant (Maguire et al. 2021). Nonetheless, these measures are based on total levels of a specific phosphoinositol species from whole brain homogenate and do not offer the cellular resolution that these fluorescent phosphoinositol reporters can provide. Single cell lipidomics, using highly specialised mass spec technology, however, can provide single cell analysis of lipidomic profiles (Li et al. 2021).

4.3.3. Phosphoinositol Metabolism in AD

Several lines of evidence indicate dysregulated balance of PIP2 and PIP3 in neurodegenerative diseases including AD. For instance, in AD brains PIP2 levels are decreased (Stokes & Hawthorne, 1987) and presenilin mutations linked to familial AD have been shown to cause imbalances in PIP2 metabolism (Landman et al. 2006). Furthermore, APOE-ε4 carriers have reduced levels of PIP2 and increased expression of the PIP2 degrading enzyme, synaptojanin, which is thought to contribute to APOE-ε4 associated cognitive deficits in AD (Zhu et al. 2015). Lowered levels of PI3K subunits (p85 and P110) have also been found in AD brains, indicating decreased generation of PIP3 from its precursor PIP2 (Moloney et al. 2010). Finally, GWAS has identified a number of AD risk genes linked to phosphoinositol metabolism such as *INPP5D*, *PLD3, CD2AP*, *PICALM* and *SLC24A4* (Tan et al. 2019; Sims et al. 2020)

No study to date has monitored changes in PIP2/PIP3 dynamics in an Aβ model following glial KD of sl/PLCG2. Given the critical role of PIP2 and PIP3 in regulating key glial functions such as phagocytosis, motility and signalling which become compromised in Aβ pathology, this was an important concept to address. In the combined presence of $A\beta_{42}$, glial sl KD did not alter levels of PIP2 in glia. This was unexpected since initial experiments had demonstrated under physiological conditions (no $A\beta_{42}$ expression) glial sl KD increased levels of PIP2 in glia. Alternatively, glial sl KD elevated PIP3 in response to $A\beta_{42}$ accumulation. This was specific to Aβ models as glial sl KD alone did not alter PIP3 metabolism, suggesting PIP3 may be contributing to the amelioration of $A\beta_{42}$ associated survival deficits following glial KD of sl.

PIP3 is an important secondary messenger of the PI3K/AKT pathway which has been implicated in AD. PIP3 activates AKT which itself has a number of downstream targets, such

as GSK-3β, Bad, Bax and caspase 9 that have been linked to survival and apoptotic mechanisms (Datta et al. 1999; Franke et al. 1997). PIP3s contribution in the pathogenesis of AD is dependent on the downstream target of AKT. For instance, GSK-3β activity, which is involved in tau hyperphosphorylation is inhibited upon phosphorylation by AKT (Hermida et al. 2017). Increasing AKT activity upon elevation of PIP3 would therefore reduce GSK-3β mediated tau hyperphosphorylation that would otherwise lead to increased microtubule instability, NFT formation and ultimately cell death and dementia.

Conversely, AKT stimulates mTOR signalling, which there is evidence of higher mTOR activity in AD brains (An et al. 2003; X. Li et al. 2005; Oddo, 2012). mTOR signalling regulates a number of downstream events, one of those being autophagy which is inhibited by the mTORC1 complex (Kim and Guan 2015). Pharmacological reduction of mTOR signalling with rapamycin in brains of 3X Tg-AD mice reduced levels of soluble Aβ and tau by increasing autophagic induction (Caccamo et al. 2010). Increased AKT/mTOR signalling upon a rise in PIP3, could therefore reduce autophagic induction, resulting in increased accumulation of Aβ and tau. Nonetheless, in our model of $A\beta_{42}$ toxicity, fly brains showed no signs of reduced autophagic induction following glial sl KD, highlighted by the consistent levels of autophagic markers, Ref(2)P and polyubiquitinated proteins, measured in the brain compared to controls.

Given the diverse and contrasting effects of PIP3 through the PI3K/AKT pathway, epistatic studies will be important to dissect which downstream target(s) of AKT are upregulated/downregulated in models of $A\beta_{42}$ toxicity following glial sl KD. This would provide some insight to underlying mechanisms of glial sl KD protective effects.

Furthermore, these experiments interestingly demonstrated that $A\beta_{42}$ may influence glial membrane PIP2 composition, such that membranes in contact with $A\beta_{42}$ deposits exhibited lower levels of PIP2 (Figure 4.30). This corresponds with previous *in vitro* studies demonstrating elevation of Aβ oligomers leads to loss of membrane PIP2 in cultured neurons (Berman et al. 2008). Together this suggests $A\beta_{42}$ impedes PIP2 metabolism which in turn may contribute to the toxicity of Aβ, given the critical roles of PIP2 in phagosome formation, a mechanism important for the removal of toxic $A\beta_{42}$ aggregates.

4.3.4. Glial Models of $A\beta_{42}$ Expression Exhibit Pathological Phenotypes

Glial production of $A\beta_{42}$ is a fairly unique and underexplored phenomena compared to that of neuronal $A\beta_{42}$ expression. Whilst neurons have been primarily viewed as the main source of Aβ production in the brain, it is worth noting APP expression has also been detected in glial cell types such as oligodendrocytes, astrocytes, and microglia (LeBlanc et al. 2002). Nonetheless, the model used in this study secretes $A\beta_{42}$ into the extracellular space.

Experiments in this chapter aimed to firstly characterise glial expression of the human $A\beta_{42}$ peptide carrying the highly pathogenic Swedish Artic mutation (Glu22Gly), N-terminally fused to the aos sequence (aos::$A\beta_{42}^{Arc}$), (Martin et al. 1995; Casas-Tinto et al. 2011). The glial model characterised in this chapter exclusively produced Aβ peptide of 42 aa in length, secreted extracellularly and gave rise to quantifiable phenotypes representative of neurodegeneration. This included phenotypes such as marked $A\beta_{42}$ accumulation within the brain by 14 d.p.e, locomotor deficits at 18 d.p.e and reduced survival. These phenotypes matched those previously described by Ray et al. (2017), which uses a similar aos::$A\beta_{42}^{Arc}$ peptide expressed in glia. Furthermore, as evidenced through MSD assays the aos::$A\beta_{42}^{Arc}$ model displays similar dynamics of amyloid build up and aggregation with age to other rodent and human brain models, providing evidence of a valuable translational aspect of this fly model. We and others have therefore demonstrated glia are an efficient system in driving $A\beta_{42}$ toxicity.

Currently these experiments have used the binary UAS/GAL4 expression system to drive sl KD and production of $A\beta_{42}$ both in glia. The caveat to this being that manipulating sl expression in glia may in turn impede the glial processing of $A\beta_{42}$ and or its secretion, since both sl RNAi and $A\beta_{42}$ are being expressed by the same cell type. Furthermore, glial mediated production of Aβ is not main physiological source of Aβ in the brain. Future experiments should consider the use of a dual expression system (QUAS/QF2 with UAS/GAL4), which would allow independent manipulation of sl in glia, in tandem with neuronal production of $A\beta_{42}$.

4.3.5. Glial Knockdown of sl Rescues $A\beta_{42}$ Related Survival Deficits

Results from this chapter evidence that glial sl activity may help drive $A\beta_{42}$ dependent degeneration such that reduced expression of sl in glia ameliorates $A\beta_{42}$ survival deficits. This is independent of amyloid pathology as total $A\beta_{42}$ load or turnover was not altered

throughout age, as shown by $A\beta_{42}$ quantification with MSD assays. Under physiological conditions, glial sl activity did not modify survival, demonstrating a specific interaction with sl and Aβ toxicity. Additionally, this interaction only modified $A\beta_{42}$ survival related deficits and no other phenotypes of $A\beta_{42}$ induced toxicity such as locomotor deficits, indicating specific regulation of survival related pathways.

Sl has been demonstrated to negatively regulate the MAPK cascade whereby loss of sl results in its overactivation (Thackeray et al. 1998). Among MAPK cascades, the RAS/RAF/MAPK/ERK pathway has been shown to play a crucial role in cell survival, particularly that of tumour cells (Guo et al. 2020) It could be that reduced expression of sl in glia leads to activation of the MAPK/ERK pathway, making cells less vulnerable to death. Another pathway that is key in regulating survival is the PI3K/AKT pathway, whereby several downstream targets have been linked to pro-survival and anti-apoptotic effects of AKT activation, such as GSK-3β, Bad, Bax, caspase-9 and transcription factors such as cAMP response element binding protein (CREB), Forkhead1 and NFκB (Datta et al.1999; Franke et al. 1997; Khwaja 1999). PIP3 is the main effector of PI3K/AKT signalling and as demonstrated in this chapter is elevated upon glial KD of sl in a model of $A\beta_{42}$ toxicity. It could therefore be possible under stressed responses (i.e. amyloid pathology), reduced sl expression in glia increases AKT dependent activation of pro-survival and anti-apoptotic mechanisms, resulting in the protection of $A\beta_{42}$ related survival deficits. An interaction between sl and downstream PI3K/AKT signalling could be further explored with PI3K inhibitors such as wortmannin or LY294002, that inhibit PIP3 mediated activation of AKT (Vlahos et al. 1994; McNamara and Degterev 2011). Future experiments could inhibit PIP3 activation of AKT using these compounds to establish whether increased PI3K/AKT signalling contributes to the preserved survival seen with reduced sl expression in glia in models of $A\beta_{42}$toxicity. Furthermore, western blotting or qPCRs could be used to detect upregulation/downregulation of various downstream targets of AKT following glial sl KD, and therefore help determine which pathways may contribute to its protective effects against $A\beta_{42}$ related early death phenotype.

4.4. Conclusion

This chapter demonstrates the optimisation and use of i) an effective, quantifiable model of glial driven amyloid pathology and ii) a genetically encoded, cell type specific fluorescent reporter system for measuring PIP2 and PIP3 distribution in *in vivo* models. Overall, data in this chapter has allowed us to conclude that reduced glial expression of sl is protective of

early death associated with glial $A\beta_{42}$ expression, independent of Aβ pathology. This was opposite to our initial hypothesis that reduced expression of glial sl would be detrimental to amyloid related pathology. Confirming KD phenotypes with a sl null mutant will be important in validating these findings. Finally, I have demonstrated PIP3 may play a contributory role in alleviating $A\beta_{42}$ survival deficits following glial sl KD, however epistatic studies will be required to confirm this.

Chapter 5: Modelling Alzheimer's Disease Associated PLCG2 Variant in *Drosophila*

5.1. Introduction

Whole genome and exome sequencing has paved the way for identifying novel rare variants with large effect on disease. With there being greater conservation and characterisation in protein coding regions of the genome, discovery of variants within the exome offers greater insight into disease pathology than the non-protein coding portion of the genome. In identifying rare AD associated variants, whole exome microarrays have been particularly valuable, identifying three novel rare coding variants in microglial enriched genes, *TREM2*, *ABI3* and *PLCG2*. The rare coding variant P522R found in the PLCG2 locus was a particularly interesting discovery, being linked to reduced risk of developing LOAD (rs72824905: p.Pro522Arg, P = 5.38 × 10-10, odds ratio= 0.68, MAF cases = 0.0059, MAF controls = 0.0093) (Sims et al. 2017).

In chapter 4, an RNAi mediated gene KD approach was used to explore glial roles of the fly PLCG2 ortholog, sl. Given the AD-protective P522R variant is a gain of function mutation, studying glial functions relating to *sl* overexpression would better reflect genetically gene activity of a hypermorphic variant rather than gene KD. Even better, transgenic fly models that express human *PLCG2* and AD-protective variant (P522R), would offer greater insight into human risk gene activity and how the genetic variant contributes to aspects of AD pathogenesis such as $A\beta_{42}$ induced toxicity.

5.1.1. The P522R AD Associated Protective Coding Variant

The P522R coding variant in the *PLCG2* gene was first identified for its association in reducing risk of developing LOAD (rs72824905/p. P522R, P=*5.*38×10^{-10}) and has since been associated with lowered risk for other neurodegenerative diseases such as dementia with Lewy bodies and frontotemporal dementia as well as being linked to pro-longevity (van der Lee et al. 2019). A C>G point mutation within exon 17 of the *PLCG2* gene results in an aa change from proline to arginine at position 522 (Sims et al. 2017) (Figure 5.1). This missense variant is found in the sPH domain of the *PLCG2* gene which structurally is positioned close to the TIM barrel that houses the active site, catalytic residues and Ca^{2+} binding site. The sPH domain is part of the auto-inhibitory region of the *PLCG2* gene for which a mutation here could impact PLCG2s activity (Menzies et al. 2017). A change in aa charge, from neutral to positive but also an increase in size alters the local loop structure in which residue 522 is found. It is thought new protein interactions between the new aa

(arginine) and other protein domains are introduced, effecting the resulting protein structure (Menzies et al. 2017; Maguire et al. 2021). Computational modelling revealed the C terminal SH2 domain, neighbouring the sPH domain is also significantly altered in terms of position and structure, whereby the mutated SH2 domain is shifted to the left. This change in flexibility and position of the SH2 domain is thought to modulate PLCG2 function, such as modulating intracellular Ca^{2+} release (Maguire et al. 2021). Increased hydrogen bonding as a result of the subsequent aa change from proline to arginine is also thought to have implications on the protein function (Maguire et al. 2021).

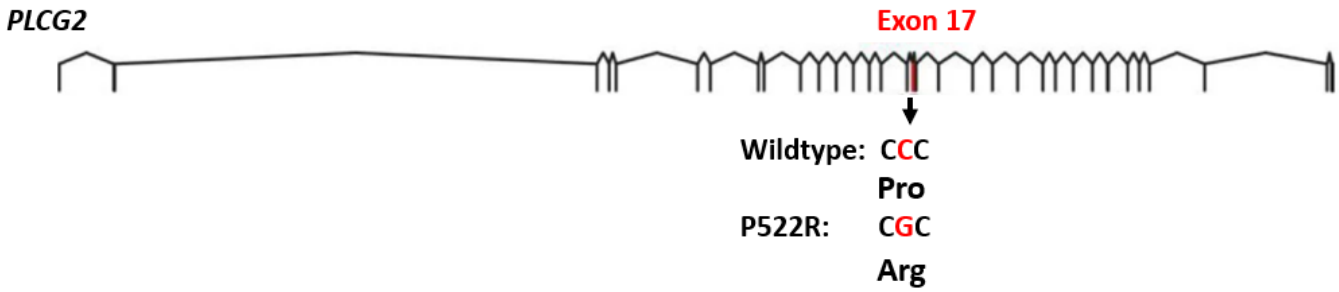

Figure 5.1: Location of the AD associated P522R coding variant in the PLCG2 transcript.

A C>G base substitution results in the aa change from Proline to Arginine at position 522 of exon 17 in the PLCG2 transcript.

PLCG2 importantly regulates immune cell functions and in the CNS is preferentially expressed in microglia cells. Functional studies in microglial cell models show the PLCG2-P522R variant has a small hypermorphic effect, mildly increasing PLCG2 enzymatic activity which results in PIP2 substrate depletion, accumulation of IP3 and DAG and increased calcium signalling in response to stimuli such as Fc receptor binding or Aβ oligomers (Magno et al. 2019; Maguire et al. 2021). The P522R AD protective variant promotes protective functions associated with TREM2 signalling such as enhancing cell survival, phagocytosis, and lipid metabolism (Takalo et al. 2020). The effect of the P522R variant on phagocytic activity however is still somewhat controversial. In contrast to Takalo et al, Maguire and colleges demonstrated that the P522R variant significantly reduced phagocytic activity in mouse macrophage and microglia models as well as human iPSC derived microglia. Notably, this study used higher doses of phagocytic target compared to Takalo and colleagues, indicating that in response to chronic stimuli, the P522R variant serves to

reduce phagocytic activity. Chronic activation of microglia and subsequently increased phagocytosis of neurons has been postulated to accelerate progression of AD pathology, therefore reduced phagocytic activity and subsequent phagocytosis of damaged yet viable neurons and synapses may contribute to the protective effect attributed to the P522R variant. Maguire and colleagues also reported enhanced endocytic clearance of Aβ oligomers in R522 variant expressing iPSC microglia (Maguire et al. 2021). Additionally, the R522 variant was shown to induce an acute inflammatory response in bone marrow derived macrophages (BMDMs) from knockin (KI) mice, secreting pro-inflammatory cytokines such as TNF-a, IL-6 and IL-1β cytokines. In contrast, nitric oxide levels are considerably lowered, which supports the cells against NO induced apoptotic cell death (Takalo et al. 2020).

Whilst these studies elaborate on various supportive immune related functions attributed to the P522R coding variant, the impact of this mutation on microglia responses to AD pathology still remains limited. Claes and colleagues sought to address this by expressing the P522R variant in human microglia of a chimeric 5XFAD transgenic mouse model. This study identified increased antigen presentation genes in human microglia that are otherwise suppressed in AD patient brains, as well as the recruitment of CD8+ T cells in P522R KI AD mouse models (Claes et al. 2022). Further enhancing knowledge of how the P522R variant influences microglial responses throughout ageing and AD related pathology is important for understanding how this genetic variant contributes to reduced AD risk.

To date, cell and mouse models have greatly contributed to our understanding of human *PLCG2* gene functions and structural/functional changes conferred by the AD associated P522R variant. However, *Drosophila* can provide a simpler *in vivo* system that facilitates complex *in vivo* functional analysis, being able to rapidly assess genetic interactions through epistatic analysis. As well, *Drosophila* are a genetically tractable system with shorter lifespan to mammalian models and have a range of genetic tools available to study gene functions. For instance, *in vivo* fluorescent phosphoinositol specific reporters to study dynamic changes in PI(4,5)P2, the substrate of PLCG2. This makes flies a fitting model system for the following functional genetic studies of the human *PLCG2* gene and its AD associated protective variant.

5.1.2. Aims and Hypotheses

The primary aim of this chapter was to create transgenic *Drosophila* models of the human *PLCG2* gene and AD risk gene variant (P522R), as to model microglial relevant functions of the human *PLCG2* gene, as well as functional changes caused by the AD-associated hypermorphic variant. This study aimed to assess functional conservation between the fly *sl* and human *PLCG2* ortholog. Given the overall sequence similarity and functional domain homology between the fly *sl* and human *PLCG2* genes (see Chapter 4), it was hypothesised that sl and human PLCG2 would be functionally analogous in phenotypes measured such as survival, locomotion, PIP2/PIP3 dynamics and $A\beta_{42}$ driven pathology. It was also predicted expression of human *PLCG2* would rescue sl loss of function phenotypes, such as small wings.

Through modelling the common vs protective AD associated PLCG2 variants (P522 vs R522) in *Drosophila,* we aimed to further understanding of how the R522 protective variant impacted glial responses and thus contributed to reduced risk of LOAD. It was hypothesised that glial expression of the R522 AD protective variant would be protective of $A\beta_{42}$ associated pathology, such as $A\beta_{42}$ induced survival and locomotor deficits, as well as reduce total amyloid deposition and accumulation in the brain.

5.1.3. Experimental Design

For this study, *sl* and human *PLCG2* (with P522 and R522 variant) genes were cloned into the 5XUAS-pJFRC5 plasmid, for which DNA was incorporated into the fly genome by site-directed insertion, generating transgenic flies. Expression of human PLCG2 variants was confirmed by western blotting. Survival, locomotor behaviour and influence on PIP2 and PIP3 metabolism were assessed following glial expression of sl and PLCG2 variants; wildtype (P522) vs AD linked (R522). The influence of sl and PLCG2 variants expression in glia on $A\beta_{42}$ associated pathology was also assessed, observing changes in quantifiable phenotypes of $A\beta_{42}$ induced toxicity, such as survival and behavioural deficits, as well as amyloid accumulation in the brain.

5.1.3.1. Assessment of PIP2 and PIP3 Dynamics

Previously described PIP reporters (PLCδ-PH::GFP and GRP1-PH::GFP) (see Chapter 4), were used to visualise the distribution of PI(4,5)P2 (PIP2) and PI(3,4,5)P3 (PIP3) within the fly brain, as well as monitor changes in flux, following overexpression of sl and human PLCG2 variants (P522 vs R522) in glia. Specifically, the PLCδ-PH::GFP reporter reported glial specific changes in PIP2 as was regulated by the pan glial driver Repo-Gal4. Flies were reared for 6 days at 25ºC to support egg lay and then switched to 30ºC, as to drive maximal protein expression. At 7 d.p.e fly brains were dissected, fixed, and imaged by confocal microscopy. The distribution of PIP2 and PIP3 were deduced upon visual inspection of GFP signal throughout the midbrain, whilst changes to PIP2/PIP3 flux was quantified through area threshold and mean gray analysis of the GFP signal intensity.

Changes in PIP2/PIP3 dynamics in the fly brain were also measured in response to combined $A\beta_{42}$ accumulation and overexpression of sl and human PLCG2 variants in glia. PIP2 and PIP3 specific reporters in brains counterstained with anti-Aβ, enabled visualisation of these changes under confocal microscopy. At 7 d.p.e brains were dissected, fixed, stained for Aβ and imaged, revealing the distribution of PIP2 and PIP3 in relation to $A\beta_{42}$ deposits. Area above set threshold and mean gray analysis of GFP signal in the midbrain also revealed gross changes in PIP2 and PIP3 levels in response to $A\beta_{42}$ accumulation and combined glial overexpression of sl and human PLCG2 variants.

5.1.3.2. Assessment of Alzheimer's Disease Associated Phenotypes

Additionally, to address whether increased glial expression of sl and PLCG2 variants impacted healthy brain ageing, locomotor behaviour and survival provided easy to measure phenotypic readouts for overall health of the flies throughout age. Furthermore, deficits in locomotion and survival were used as phenotypic markers of $A\beta_{42}$ induced toxicity. The effect of overexpressing glial sl and human PLCG2 variants on modifying $A\beta_{42}$ related survival and locomotor deficits was measured. Male and female flies were assayed separately for both locomotion and survival experiments, however, upon finding no significant phenotypic differences between sexes, results were pooled together for final statistical analysis by Log-rank, Mantel-cox test.

To further assess the glial role of sl and PLCG2 variants on driving $A\beta_{42}$ pathology, the accumulation of $A\beta_{42}$ in the brain was assessed following anti-Aβ immunostaining at

14 d.p.e. Image analysis of $A\beta_{42}$ deposition (see Chapter 2; section: 2.7.1), provided a semi quantitative measure of total Aβ burden within the brain.

5.1.3.3. Assessment of Wing Phenotypes

Wing rescue experiments utilised trojan Gal4 machinery of the sl CRIMIC mutant to drive expression of UAS-sl, UAS-hPLCG2-P522, or UAS-hPLCG2-R522 in place of endogenous sl gene expression. Rescue experiments aimed to demonstrate that the fly *sl* and human *PLCG2* genes were functionally conserved through the rescuing of small wing loss of function phenotypes, such as recovering wing size back to wildtype with expression of human PLCG2 cDNA. In this instance, the right wing was dissected from male flies, heterozygous for sl CRIMIC transgene on X chromosome with expression of the UAS-sl, UAS-hPLCG2-P522 or UAS-hPLCG2-R522 on third. The boundary between the L4, L5 and PCV was consistently measured in each genotype across 10 wings.

A timeline of experiments conducted in this chapter with a summary of timepoints and total n used for each experiment has been outlined below (Figure 5.2 and Table 5.1).

	N=	
Experiment	**Without $A\beta_{42}$**	**With $A\beta_{42}$**
PLCG2 Western Blotting	20 heads per genotype, combined female and male	N/A
Wing sizes	6-10 wings, males only	N/A
PIP2/PIP3	9-34 (PIP2), 9-22 (PIP3), combined females and males	8-34 (PIP2), 9-13 (PIP3), combined females and males
Survival	182-265 combined females and males	182-260 combined females and males
Locomotion	58-122 combined females and males	68-108 combined females and males
Aβ immunostaining	N/A	7-12 brains combined female and males

Table 5.1: Summary of experimental procedures.

For each group (with and without $A\beta_{42}$), the highest and lowest total n and sex of flies used across each experiment has been recorded.

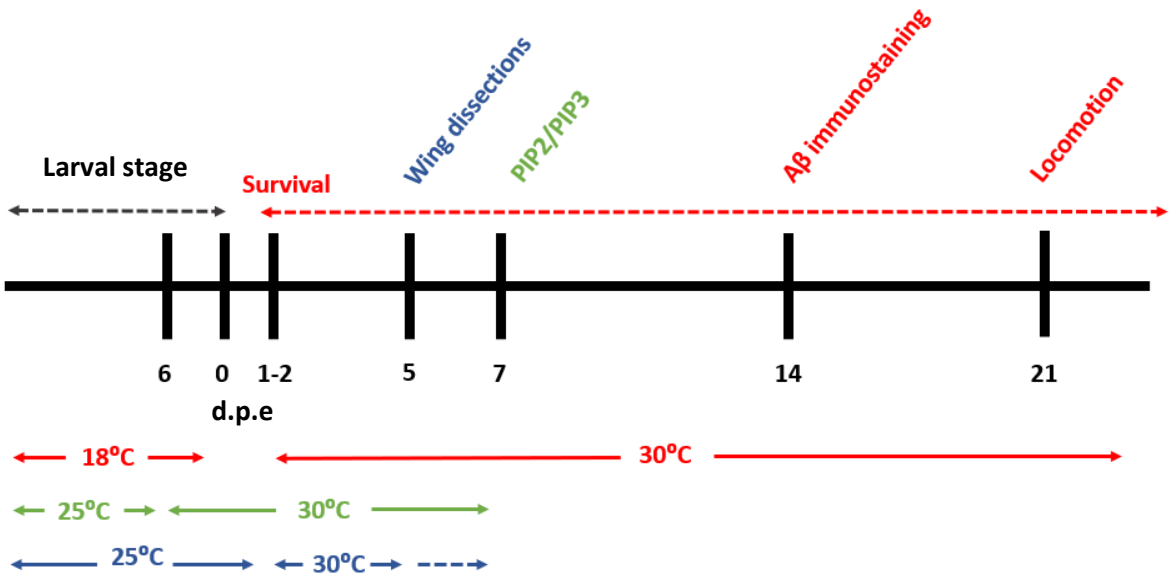

Figure 5.2: Timeline of experimental procedures.

Timepoint (d.p.e) which each assay was conducted including the temperatures flies were bred and aged at for each experiment (see corresponding colours).

5.2. Results

5.2.1. *sl* and *PLCG2* Genes were Subcloned into the 5x UAS-pJFRC5 Vector

To explore glial specific sl gain of function effects, as well as glial functions of the conserved human *PLCG2* gene in *Drosophila*, sl overexpression models and transgenic flies expressing human *PLCG2* were first generated (see full methodology in Chapter 2; section: 2.4). To subclone *sl* and *PLCG2* genes from pFlc-1 (source: DGRC) and pUASgHA.attB vectors (Bischof et al. 2013) respectively into the 5xUAS pJFRC5 vector, modified from the pJFRC5-5XUAS-IVS-mCD8::GFP plasmid (Addgene plasmid #26218) (Pfeiffer et al. 2010), *sl* and *PLCG2* cDNA was first amplified with forward and reverse primers specifically designed to add *XbaI* and *NotI* restriction sites to the 5' and 3' ends of the sequence. These restriction sites were identified within the multiple cloning site of the pJFRC5 vector and did not cut within the sequence of *sl/PLCG2* gene. Forward primers contained the *NotI* restriction site and reverse primers incorporated restriction site for *XbaI*. Primer sequences were as follows **sl forward primer:** 5' TCA-GCGGCCGC-ACAACCAAA-ATG-AGCTGCTTTAGTGCGAT 3'. **PLCG2 forward primer:** 5' TCA-GCGGCCGC-ACAACCAAA-

ATG-TCCACCACGGTCAATGT 3'. **sl reverse primer:** 5' GTA-TCTAGA-CTA-GTAAAACTTGCTGTTGCAGT, **PLCG2 reverse primer:** 5' GTA-TCTAGA-CTA-CGGTGCGGTAACATTTG 3'. After amplification, the presence of sl and PLCG2 amplicons at 4 Kb were confirmed by gel electrophoresis and DNA was extracted from the gel to undergo restriction digestion (Figure 5.3).

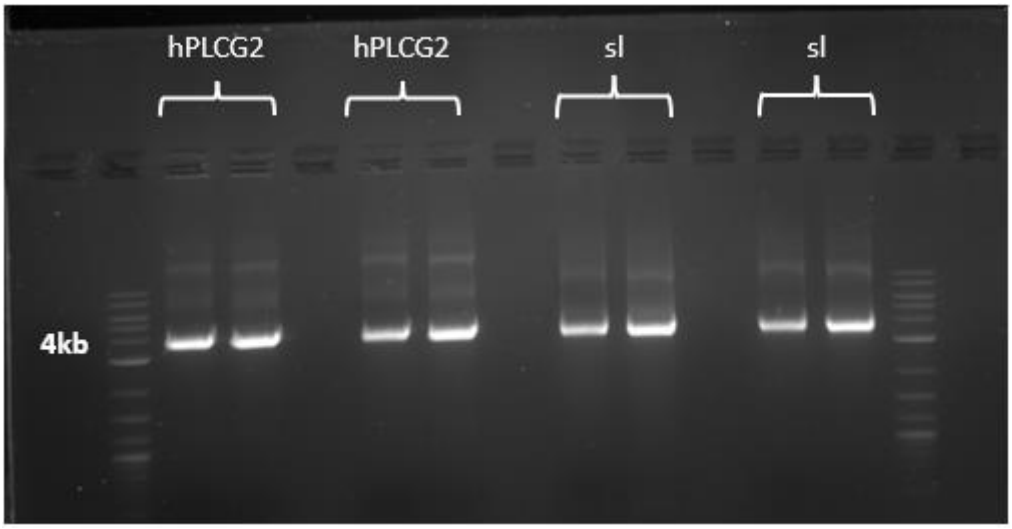

Figure 5.3: Human PLCG2 and fly sl amplicons.

Resulting amplicon of human PLCG2 and sl cDNA are ~4 Kb following addition of XbaI and NotI restriction sites. A 1 Kb DNA ladder was used as a molecular weight reference.

Complementary sticky ends between *sl*, *PLCG2* gene inserts and the pJFRC5 vector were created upon digestion with the same *XbaI* and *NotI* restriction enzymes, enabling ligation of *sl* and *PLCG2* cDNA in to the new pJFRC5 vector. Ligation products were transformed into DH5α cells and spread over amp resistant plates. Bacterial uptake of the pJFRC5 plasmid enabled colonies to grow on amp resistant plates, as the pJFRC5 plasmid contained the amp resistant gene. Successful *sl* and *PLCG2* transformants were selected upon screening up to 16 colonies for each, identifying plasmids that had successfully incorporated the *sl/PLCG2* genes. Bacterial DNA from 16 colonies were amplified with sl/PLCG2 primer sets and the presence of *sl/PLCG2* was verified through gel electrophoresis. Successful transformants are ~4 Kb, reflecting the size of the plasmid with *sl* or *PLCG2* gene insert. 6 transformants were identified containing *PLCG2* and 3 transformants with *sl* (Figure 5.4).

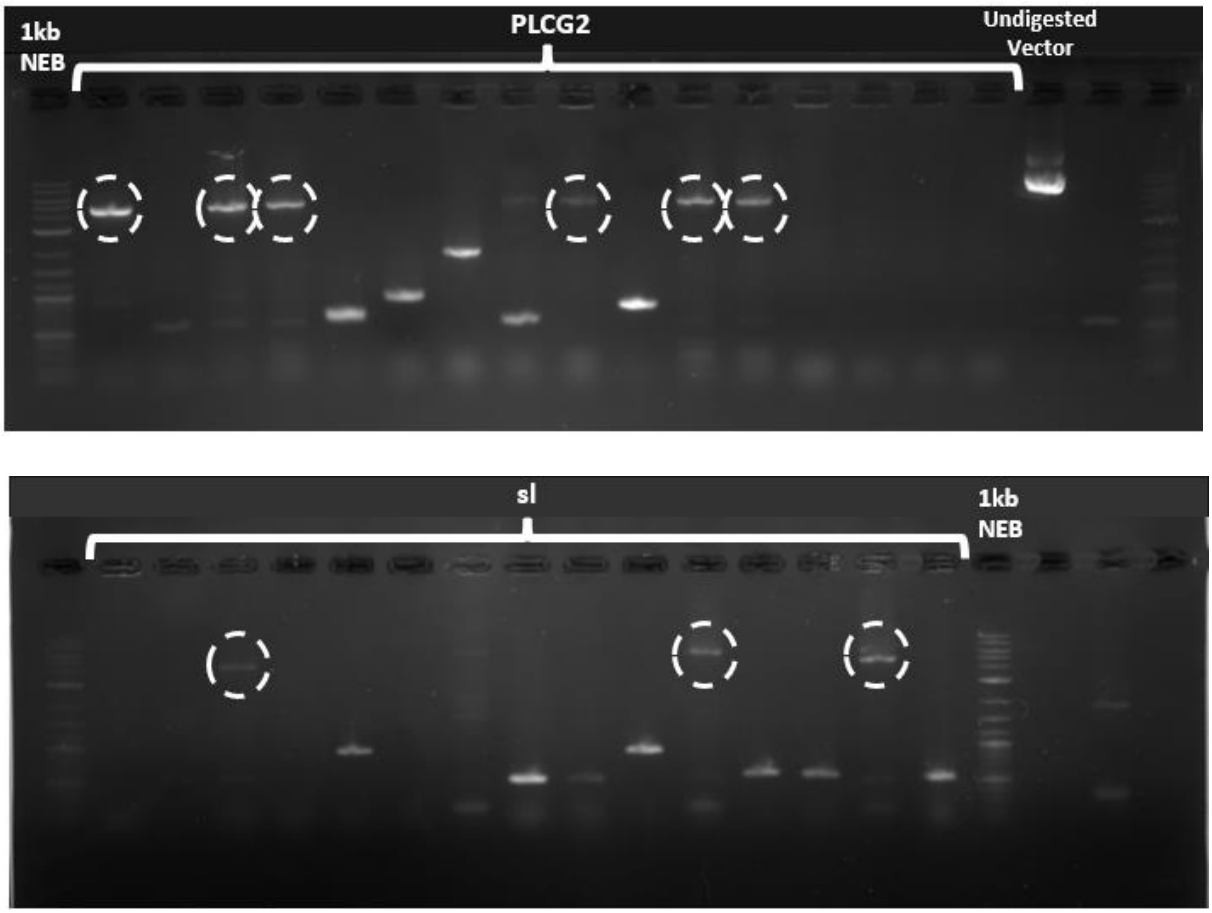

Figure 5.4: Colony PCR screen for human PLCG2 and sl transformants.

Amplified DNA of 16 colonies selected from potential sl and PLCG2 transformants separated by gel electrophoresis. Successful transformant are highlighted by dashed circles.

Bacterial DNA from corresponding colonies were isolated, purified via mini prep and sequence verified. Sequencing primers read along the entire length of *sl* and *PLCG2* gene inserts with reads aligning to sl/PLCG2 sequence templates, indicating the correct sl and PLCG2 sequences had been cloned into the pJFRC5 vector (Figure 5.5).

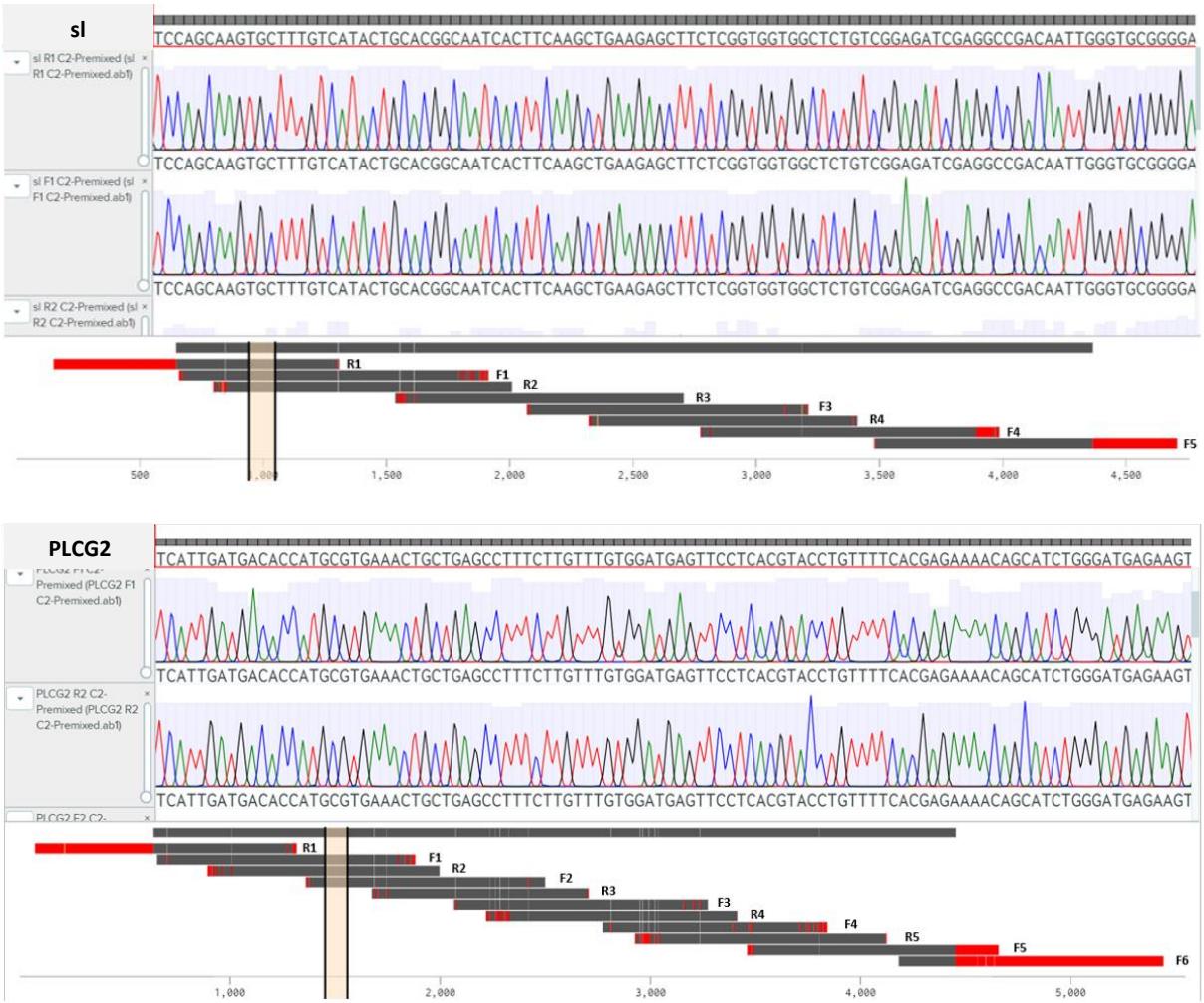

Figure 5.5: Sequence verification of cloned sl and human PLCG2 plasmids.

Chromatograms produced from Sanger sequencing show DNA sequences from cloned A) sl and B) PLCG2 plasmids. Sequencing primers designed to read across the length of A) sl and B) PLCG2 transcripts from selected transformants show alignment of sl and PLCG2 DNA sequences with inputted sequences for sl and PLCG2. Sequence alignment was confirmed using Benchling.

5.2.2. Site Directed Mutagenesis Induces C>G Nucleotide Change in Wildtype PLCG2 Sequence

Transgenic flies harbouring the PLCG2 AD protective coding variant (R522) were created to model *in vivo* functional changes associated with the variant. The protective R522 variant was generated via site directed mutagenesis of the wildtype *PLCG2* gene that had been cloned into the pJFRC5 vector. Site directed mutagenesis was completed by a commercial vendor (Genescript). A C to G base substitution at position 8534 bp of the entire plasmid

sequence (11568 bp), resulted in the aa change of proline to arginine at position 522AA, which modelled the nucleotide and protein change of the AD associated protective PLCG2 variant (C,G/p.P522R). The PLCG2 plasmid map, annotated with C>G base substitution is shown below (Figure 5.6 A) for which sequencing confirmed introduction of the R522 variant (Figure 5.6 B).

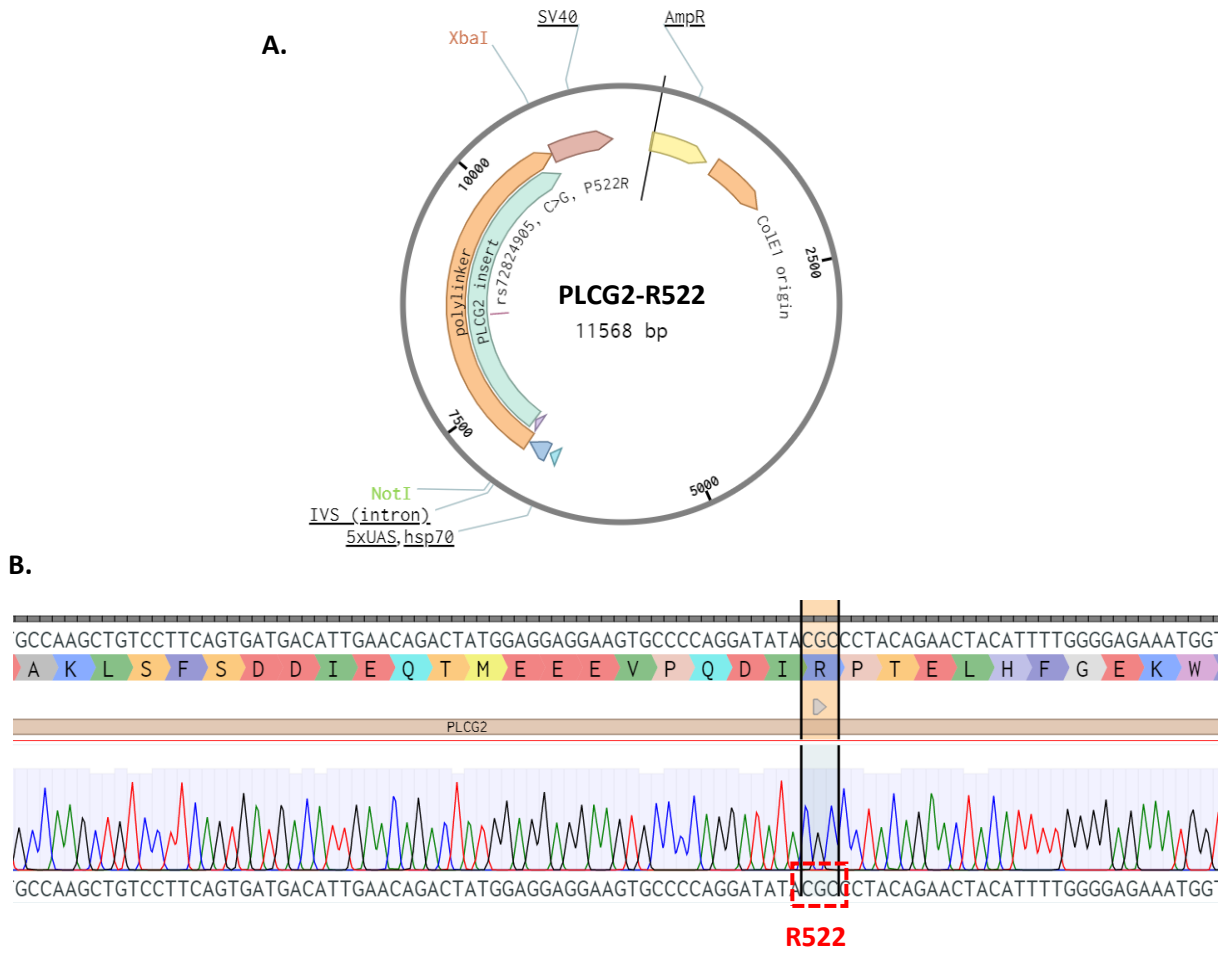

Figure 5.6: Generation of the PLCG2-P522R protein coding change.

A) Plasmid map of the pJFRC vector with the PLCG2-R522 variant insert (11568 bp). B) Chromatogram of DNA sequence reveals a single nucleotide change to guanine following the site directed mutagenesis of the wildtype PLCG2. The resulting codon now codes for an arginine aa at position 522 of the aa sequence.

5.2.3. Expression of Human PLCG2 in *Drosophila* Head Lysates

Transgenic flies were generated upon embryo injection of cloned plasmids, performed by commercial service (BestGene. USA). Small wing and human PLCG2 variants (P522/R522), cloned into the 5XUAS-pJFRC5 vector and the 5XUAS-pJFRC5 vector alone were injected via PhiC31 integrase mediated insertion into chromosome 2 and 3 using attP40 and attP2 landing respectively. This generated ~5 transformants for each gene. Insertion of the empty pJFRC5 vector alone acts as a control for landing site specific effects as well as Gal4 titration. Flies were received in a balanced w^{1118} genetic background and successful integration of the mini-*white*$^{+}$ labelled transgenes initially confirmed by presence of red eyes.

Pan glial expression of human PLCG2 in fly heads was then confirmed by western blotting, probing with anti-human PLCG2 antibody (Figure 5.7).

Bands slightly higher than the 155 kDa, which is the molecular weight of PLCG2 were observed in lanes with protein lysate from PLCG2 expressing fly heads; both P522 and R522 variants. Interestingly, no band was detected in the lane with protein lysate from sl expressing fly heads, suggesting the human PLCG2 antibody was not compatible with the *Drosophila sl* gene. As expected, there was no 155 kDa band detected for negative controls w- and pJFRC5 vector, given these flies did not have a copy of the *PLCG2* gene. The human microglia clone 3 cell line (HMC3) were selected as a positive control as they should express PLCG2 under physiological conditions, however unexpectedly no band for PLCG2 was detected in protein lysate extracted from these cells. Bands at 46 kDa were observed in each lane following re-probing with Actin antibody, a housekeeping gene that is expressed within both flies and cells. Levels of actin expression indicated equal amounts of protein had been loaded for each genotype.

The detection of PLCG2 protein in our transgenic fly models confirmed successful integration of PLCG2 into the fly genome.

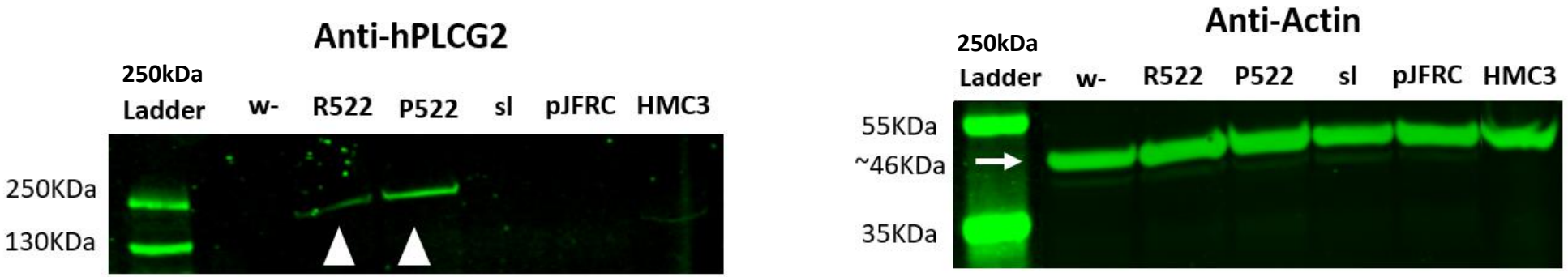

Figure 5.7: Detection of human PLCG2 protein.

A) Western blotting of human PLCG2 in whole brain lysates of Drosophila expressing the Repo driver only control (w-), PLCG2 variants (P522 and R522), the fly ortholog small wing or the pJFRC5 vector for which transgenes had been cloned into (control). Protein lysate from human microglial cells 3 (HMC3) were loaded as a positive control. PLCG2 protein (~155 kDa) is detectable in lysates from flies expressing P522 and R522 variants (see arrowhead). B) Re-probed membrane with anti-Actin reveals equal protein loading across all wells.

5.2.4. Human PLCG2 Rescues Loss of Function small wing Phenotype

As previously characterised (see Chapter 4; section: 4.2.2), sl CRIMIC mutants give rise to visibly smaller wings than wildtype (yw) flies, matching the expected phenotype of sl null mutants (Thackeray et al. 1998). The CRIMIC cassette works as a promoter trap, expressing Gal4 in place of the endogenous gene, creating effective null or severe loss of function alleles (Lee et al. 2018). Rescue of this mutant phenotype can be tested using the sl CRIMIC line to drive expression of the corresponding UAS controlled cDNA such as sl or its human PLCG2 orthologue. In this instance, the sl CRIMIC mutant was used to verify functional conservation between human PLCG2 and fly sl genes, anticipating a return to normal wing size if PLCG2 and sl are functional conserved. The ability to rescue the small wing phenotype back to wildtype size was assessed following expression of sl and human PLCG2 variants (P522/R522). UAS-transgenes were expressed in a sl CRIMIC mutant background resulting in Gal4 driven expression of the transgene throughout sl endogenously expressed cells. Wings from males carrying one copy of sl CRIMIC on X chromosome with UAS-transgene of interest on third were dissected and the area between L4, L5 and PCV measured (as in Chapter 4).

As anticipated, the empty pJFRC5 vector control did not rescue the wing size back to wildtype (yw), with wings on average having a 37% smaller area compared to wildtype flies (11.7 mm^2 compared to 29 mm^2) (Kruskal Wallis test with Dunn's multiple comparisons test; n=6-10, pJFRC5 vs yw: *p=0.0220). Instead wing sizes from flies expressing the pJFRC5 vector were more comparable with that of the sl null mutant flies (sl CRIMIC), (11.7 mm^2 compared to 7.1 mm^2) (Kruskal Wallis test with Dunn's multiple comparisons test; n=6-10, ns: p>0.9999). Alternatively, expression of sl cDNA led to a rescue in wing size, with no significant difference in wing area compared to wildtype (yw) (26.3 mm^2 vs 29 mm^2) (Kruskal-Wallis test with Dunn's multiple comparison test; n=6-10, ns: p>0.9999). Finally, expression of human PLCG2 P522 cDNA also recovered the wing size of sl CRIMIC mutants, whereby wings exhibited an average size of 37.1 mm^2, a 21% increase in area compared to wildtype (yw) (29 mm^2) (Kruskal-Wallis test with Dunn's multiple comparison test; n=6-10, ns: p>0.9999). Interestingly, partial lethality was observed in males following sl CRIMIC driven expression of the PLCG2 wildtype variant (P522), where only 10% of males were recovered. Furthermore, expression of the PLCG2 hypermorphic variant (R522) was not viable in males and thus no wing measurements were recorded following expression of PLCG2-R522 cDNA.

In summary, small wing loss of function phenotype is rescued upon expression of sl and the common P522 variant of human PLCG2 cDNA, indicating they are functionally analogous, both regulating cell growth in the wing. Unexpectedly the hypermorphic R552 allele was not viable when expressed by the sl CRIMIC promoter trap, potentially indicating a role for PIP2 in early development that is disrupted by overactivity of the AD associated protective PLCG2 variant.

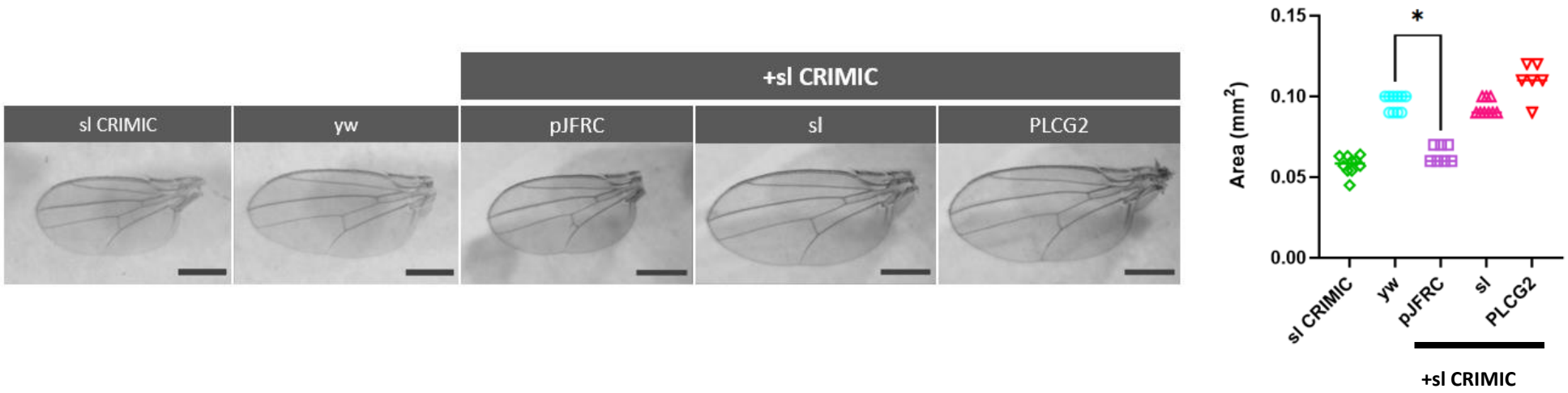

Figure 5.8: Rescue of small wing phenotype.

*A) Representative images of wing sizes taken from sl CRIMIC mutants and wildtype flies (yw) and flies expressing transgenes pJFRC5, sl and PLCG2 P522 under control of the sl CRIMIC driver (Scale bar 0.6 mm). B) Graph displaying the area (mm^2) measured for the selected ROI (boundary between L4, L5 and PC veins) from the right wing of each genotype in male flies. Asterisk represent significant values calculated from Kruskal-Wallis test with Dunn's multiple comparison test; n= 6-10, yw vs pJFRC: *p<0.0220). Error bars represent ±SEM.*

5.2.5. PIP2 and PIP3 Response to Glial Expression of sl and Human PLCG2 Variants in Aged Models

PIP2 is the primary substrate of PLCG2 catalysis, producing secondary messengers IP3 and DAG, and serving as a substrate for PI3K dependent PIP3 formation. PLCG2 can therefore directly and indirectly contribute to the levels of PIP2 and PIP3. By manipulating PLCG2 enzymatic activity we can therefore expect to alter physiological PIP2 and PIP3 dynamics. As such, changes to PIP2/PIP3 distribution and overall flux were examined following glial overexpression of sl/PLCG2 or expression of the hyper-functional PLCG2-R522 variant.

5.2.5.1. Response of PIP2 Dynamics

Pan-glial expression of the UAS-PLCδ-PH::GFP reporter highlighted glial specific distribution of PIP2 throughout the fly brain, and intensity of the GFP reporter provided an indication to PIP2 levels. In this case the GFP signal from the PLCδ-PH::GFP reporter was strong enough and did not require anti-GFP immunostaining.

The GFP signal of the PLCδ-PH reporter diminished in the empty pJFRC5 vector control, where a 3-fold decline in GFP intensity was recorded compared to the wildtype control, which expressed only the PIP2 reporter in glia (Kruskal-Wallis test with Dunn's multiple comparisons; n=9-34, ****p<0.0001) (Figure 5.9 A&B). Such a marked reduction in GFP signal was not expected with the empty pJFRC5 vector control, but likely attributed to Gal4 titration. An effect observed when more than one UAS binding site is present, as Gal4 transcriptional activity is diluted across a greater number of UAS sites (Fischer et al. 1988). As the pJFRC5 vector was the backbone for which sl and human PLCG2 variants were inserted, this was the most suitable control, providing baseline fluorescence of the PLCδ-PH::GFP reporter .

Following glial overexpression of sl, both the distribution and GFP intensity of the PLCδ-PH reporter in the fly midbrain remained comparable to that of the empty pJFRC5 vector control (Kruskal-Wallis test with Dunn's multiple comparison test; n=9-34, ns: p>0.9999), indicating no change in the localisation or total levels of glial specific PIP2 in the fly midbrain (Figure 5.9 A&B). Additionally, glial expression of human PLCG2 demonstrated a similar pattern of glial PIP2 distribution to that of the pJFRC5 vector control, with GFP distributing uniformly throughout the midbrain (Figure 5.9A). The % area of GFP, above background threshold showed no significant difference between the human PLCG2 wildtype variant (P522) and the

pJFRC empty vector control (Kruskal-Wallis test with Dunn's multiple comparison test; n=9-34, ns: p>0.9999) (Figure 5.9B). This demonstrated glial expression of human PLCG2 did not influence glial specific PIP2 localisation or abundance in an ageing fly model. Furthermore, comparison of brains expressing PLCG2 vs its ortholog sl in glia, revealed no differences in the glial distribution of PIP2 or its abundance, as measured by % area above threshold (Kruskal-Wallis test with Dunn's multiple comparison test; n=9-34, ns: p=0.0844), highlighting functional conservation between the two genes.

The impact of PLCG2 hyper-functionality on glial PIP2 distribution and abundance was also examined by comparison of PLCG2 wildtype (P522) vs hypermorphic (R522) variant expression in glia. PIP2 substrate depletion was anticipated following glial expression of the R522 variant *in vivo* (Maguire et al. 2021). Fly brains expressing the PLCG2 wildtype (P522) and hypermorphic (R522), variants in glia both exhibited a widespread distribution of the PLCδ-PH::GFP reporter, indicating the gain of function R522 variant does not alter glial specific PIP2 distribution in the fly midbrain (Figure 5.9A). Furthermore, measured GFP intensity of the PLCδ-PH reporter was comparable between glial expression of the wildtype vs hypermorphic PLCG2 variants (Kruskal-Wallis test with Dunn's multiple comparison test; n=9-34, ns: p=0.6375) (Figure 5.9B). The gain of function R522 variant therefore did not modify the glial specific distribution or abundance of PIP2 in aged *Drosophila* model.

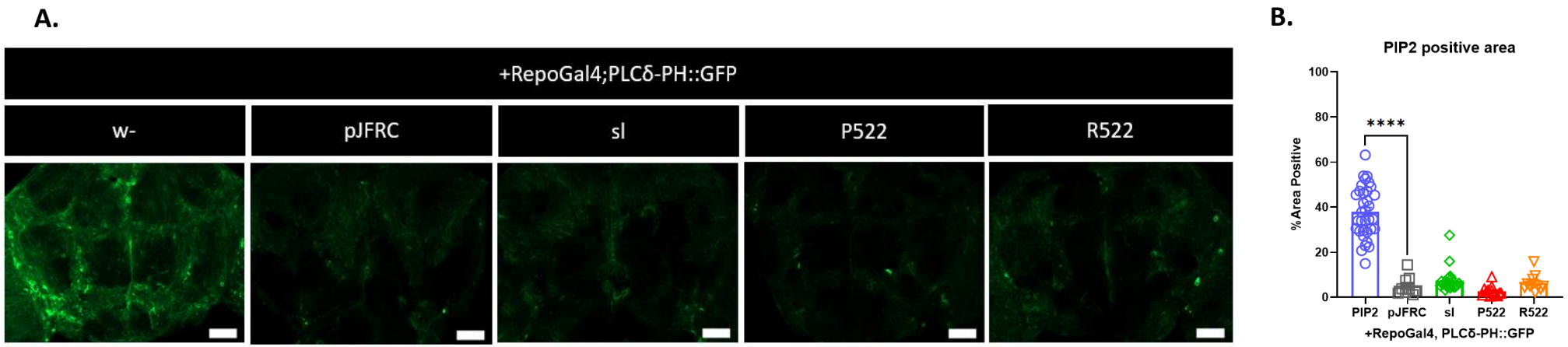

Figure 5.9: Glial expression of sl and human PLCG2 variants do not alter PI(4,5)P2 dynamics in the brain of aged Drosophila models.

*A) Representative confocal images of fly brains dissected 7 d.p.e. co-expressing the PLCδ-PH::GFP reporter in the following genetic backgrounds: w-, pJFRC5 (vector control), sl and human PLCG2 variants (P522 and R522) where the pan glial driver Repo-Gal4 was used to target glial specific expression (x20) (Scale bar: 50 µm). B) Percentage area of PIP2 in the midbrain of flies expressing w-, pJFRC5 vector, sl and human PLCG2 variants (P522 and R522) in glia, measured by area above the threshold. Kruskal-Wallis test with Dunn's multiple comparisons; n=9-34, ****p<0.0001. Error bars represent ±SEM.*

5.2.5.2. Response of PIP3 Dynamics

Next, changes to PIP3 distribution and abundance were visualised following glial overexpression of sl and human PLCG2 variants (P522 vs R522), using the GRP1-PH::GFP reporter that specifically detects PIP3. Widespread distribution of PIP3 throughout the fly brain was visualised following ubiquitous expression of GRP1-PH::GFP reporter, however, displayed a much weaker signal in comparison to the PLCδ-PH::GFP reporter.

The GRP1-PH::GFP reporter exhibited a similar pattern of distribution in the empty pJFRC5 vector control compared to the w- control that expressed the PIP3 specific reporter alone (Figure 5.10A). This indicated the pJFRC5 vector does not alter PIP3 distribution. Mean gray analysis also recorded no marked changes in GFP intensity (One-way ANOVA with Sidak's multiple comparison test; n=9-22, F=3.200, ns: p=0.1607) (Figure 5.10B), suggesting the pJFRC5 vector itself does not influence PIP3 levels, as expected. GFP intensity observed with pJFRC5 vector could therefore be used as a baseline control to compare sl overexpression and expression of human PLCG2 variants in glia.

Distribution of the GRP1-PH::GFP reporter remains ubiquitous throughout the fly brain following glial overexpression of sl and human PLCG2 variants (P522 and R522), (Figure 5.10A), indicating no change to PIP3 localisation when manipulating sl/PLCG2 activity in glia. Following glial overexpression of sl, total abundance of PIP3 is comparable to the empty pJFRC5 vector control, as shown by no significant difference in measured GFP intensity (One- way ANOVA with Sidak's multiple comparison test; n=9-22, F=3.200, ns: p=0.9382), (Figure 5.10B). Additionally, measured GFP intensity in the midbrain showed no significant difference between glial expression of human PLCG2 and the empty pJFRC5 vector control (One-way ANOVA with Sidak's multiple comparison test; n=9-22, F=3.200, ns: p=0.03087), (Figure 5.10B). It can therefore be inferred overexpression of sl and expression of the human PLCG2 wildtype variant does not lead to alterations in PIP3 levels in an aged fly model.

Distribution and intensity of the GRP1-PH::GFP reporter was additionally compared between the wildtype (P522) and hypermorphic (R522) PLCG2 variants. No difference in localisation of the GRP1-PH::GFP reporter was observed and calculation of mean gray value further reported no significant differences to the GFP intensity (One-way ANOVA with Sidak's multiple comparison test; n=9-22, F=2.049, ns: p=0.8258), (Figure 5.10 A&B). These findings indicated the R552 variant does not result in changes to PIP3 distribution or abundance in the fly brain.

From these findings we can therefore infer that, in an aged *Drosophila* model there is no change in the localisation and abundance of PIP2 or PIP3 in the brain upon increased sl/PLCG2 expression in glia. Furthermore, the hypermorphic R522 variant did not modify the localisation or abundance of PIP2 and PIP3 in the brain of an aged *Drosophila* model.

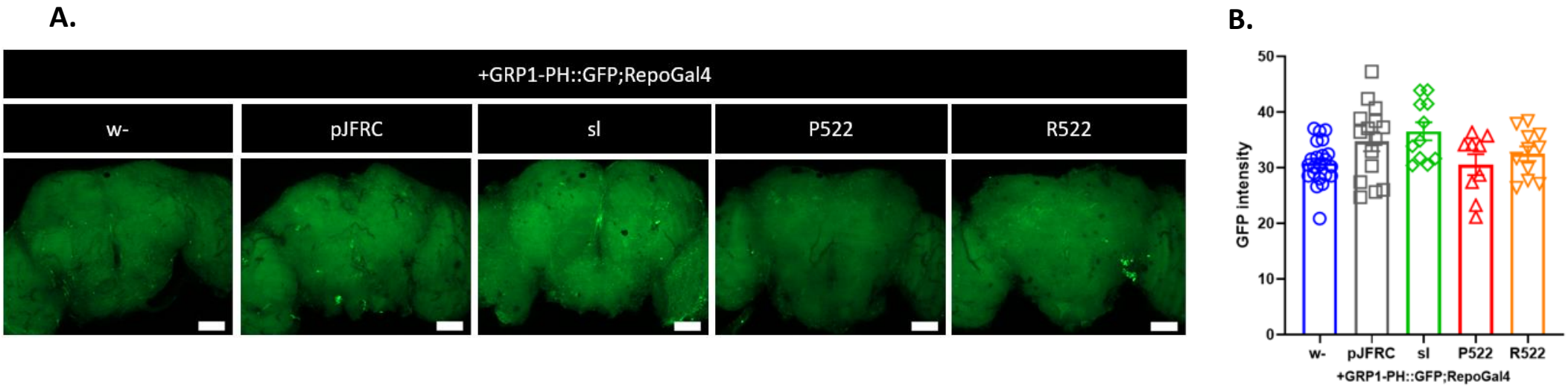

Figure 5.10: Glial expression of sl and human PLCG2 variants (P522 and R522) do not alter PI(3,4,5)P3 dynamics in the brain of aged Drosophila models.

A) Representative confocal images of fly brains dissected 7 d.p.e. co-expressing the GRP1-PH::GFP reporter in the following genetic backgrounds: w-, pJFRC5 (vector control), sl and human PLCG2 variants (P522 and R522), where the pan glial driver Repo-Gal4 was used to target glial specific expression (x20) (Scale bar: 50 µm). B) GFP intensity of the GRP1-PH::GFP reporter in brains expressing w-, pJFRC5 vector, sl and human PLCG2 variants (P522 and R522), in glia, measured by mean gray analysis of the midbrain. Error bars represent ±SEM.

5.2.6. Glial Expression of sl and Human PLCG2 Variants does not Impair Healthy CNS Ageing

Glial specific KD of sl did not impact survival or locomotor behaviour in adult flies under physiological conditions (see Chapter 4, Figure 4.17). Survival and locomotor phenotypes were therefore assessed following glial overexpression of sl or human PLCG2 variants (P522 vs R522), to deduce the impact on overall health and nervous system functioning throughout age.

Locomotion performance was evaluated using the RING assay described in previous experiments, providing a broad readout of CNS function. Negative geotaxis climbing behaviour was analysed in both female and male flies at 21 d.p.e, reflecting mid-stages of adulthood (Figure 5.11A). The distance travelled at 10 seconds was recorded for each genotype following glial overexpression of sl and human PLCG2 variants (P522 and R522). No difference in the average distance travelled between w- and pJFRC5 control groups were observed (One-way ANOVA with Sidak's multiple comparison test; n=5-10, F=3.992, p>0.9999), highlighting the pJFRC5 empty vector did not itself alter locomotor behaviour of the flies. Differences in locomotor performance upon glial expression of sl or PLCG2 variants can therefore be taken as a direct effect of increased sl or PLCG2 variant expression themselves.

Flies over-expressing glial sl and human PLCG2-P522 variant travelled average distances of 66 mm and 73 mm respectively in 10 seconds, which were comparable to the locomotor performance of flies carrying the pJFRC5 empty vector alone (68 mm) (One-way ANOVA with Sidak's multiple comparison test; 5-10, F=3.992, ns: p=0.8718, ns: p=0.3584). This indicated glial expression of sl or human PLCG2 do not themselves cause strong locomotor deficits and thus do not impact nervous system functioning in a healthy aged *Drosophila* model. Flies expressing the human PLCG2-P522 variant in glia travelled on average a slightly greater distance in 10 seconds than expression of its ortholog, sl (~9%) (One-way ANOVA with Sidak's multiple comparison test; n=5-10, F=3.992, * p=0.0438). Flies expressing the PLCG2-R552 variant travelled the greatest distance on average at 74 mm, however, this was comparable with that of the distance travelled by flies expressing wildtype PLCG2-P522 variant (73 mm) (One-way ANOVA with Sidak's multiple comparison test; n=5-10, F=3.992, ns: p=0.9983). The PLCG2-R522 variant therefore did not alter CNS functioning under physiological aged conditions.

The effect glial overexpression of sl and human PLCG2 variants (P522/R522) has on survival was next assessed in both female (24 hours mated) and male flies that were aged at

30ºC (Figure 5.11B). No clear survival deficits were observed in flies expressing the Repo-Gal4 driver alone (w-), with flies exhibiting a smooth survival trajectory and median lifespan of 40 days. A subtle difference in median lifespan was noted in flies carrying the pJFRC5 empty vector, increasing by 2 days compared to expression of the pan-glial driver only control (w-) (Log-Rank, Mantel-Cox test; n=191-265, χ^2=7.942, df=1, **p=0.0048). For consistency of genetic background glial expression of the pJFRC5 vector alone served as control for transgene expression of sl and human PLCG2 variants (P522/R522).

Log-rank Mantel-cox test showed a statistical difference in survival trajectories between flies carrying the empty pJFRC5 vector and glial over-expression of sl, despite median lifespan being comparable at 42 days (Log-rank Mantel-cox test; n=182-191, χ^2= 10.05, df=1, **p=0.0015). The difference in survival curves was however, not significant according to the Gehan-Breslow-Wilcoxon test (Gehan-Breslow-Wilcoxon test; n=182-191, χ^2= 7.942, df=1, ns: p=0.0795). Differences in statistical significance depending on the statistical test performed suggests overall increased glial expression of sl has no significant impact on survival in a physiological aged model.

Glial over-expression of the human PLCG2 wildtype variant also demonstrated a comparable survival trajectory with the empty pJFRC5 vector control, with a median lifespan of 42 days. No significant difference between flies expressing the pJFRC5 vector and the wildtype PLCG2 variant was reported (Log-rank mantel-cox test: pJFRC5 vs PLCG2-P522; n=182-191, χ^2= 0.08999, df=1, ns: p=0.7642), indicating glial over-expression of human PLCG2 in *Drosophila* did not impact survival, under physiological conditions. Comparison of survival between expression of PLCG2 and its ortholog sl showed significance with Log-rank Mantel-cox analysis but was non-significant in Gehan-Breslow-Wilcoxon test. This highlighted overall no marked differences in the contribution these conserved genes play on survival (Log-rank Mantel-cox test; n=182, χ^2= 9.755, df=1, **p=0.0018, and Gehan-Breslow-Wilcoxon test; n=182, χ^2=3.310, df=1, ns: p=0.0689).

Glial over-expression of the PLCG2-R552 variant exhibited a slightly shortened median lifespan of 40 days in comparison to 42 days of the empty pJFRC5 vector control and wildtype PLCG2-P522 variant. Whilst the difference in survival trajectories were reported to be significant, a minor difference in median lifespan of 2 days does not indicate a large survival deficit upon expression of the PLCG2-R522 variant in *Drosophila* (Log-rank Mantel-cox test: pJFRC5 vs PLCG2-R522; n=184-191, $\chi2=3.854$, df=1, *p=0.0499). Furthermore, the subtle difference in survivorship between expression of the common vs rare PLCG2 variants (P522 vs R522) indicates that under physiological conditions the gain of function R522 variant does not contribute to large changes in survival (Log-rank Mantel-cox test: PLCG2-P522 vs PLCG2-R522; n=182-184, $\chi2=5.172$, df=1, *p=0.0230).

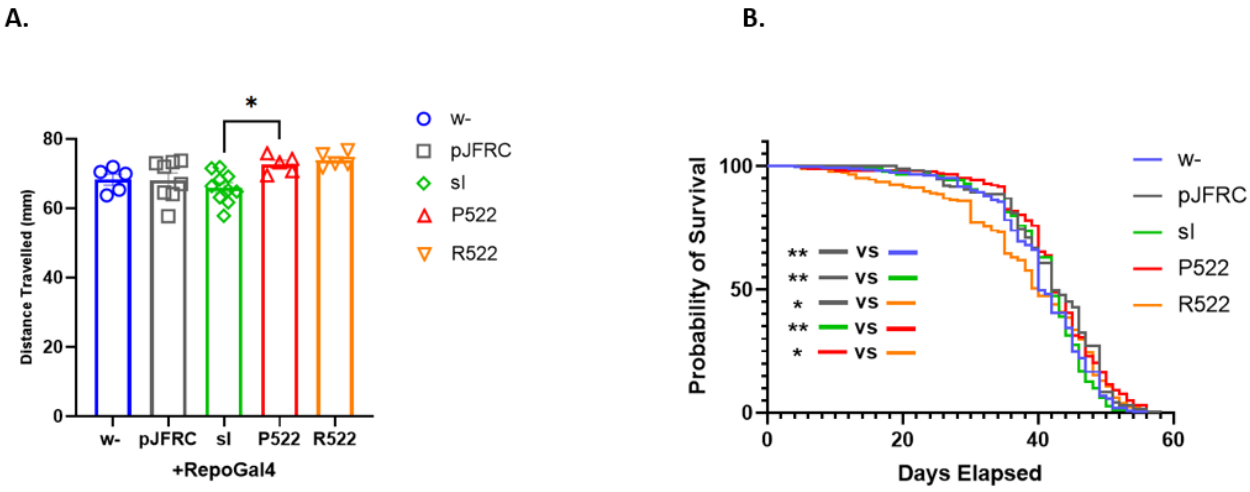

Figure 5.11: Survivorship and locomotion are maintained upon expression of sl and human PLCG2 variants in glia.

*A) Locomotor behaviour and B) survival trajectories following Repo-Gal4 driven expression of w-, empty pJFRC5 vector, sl and human PLCG2 variants (P522 and R522). A) Average distance travelled (mm) in 10 seconds post negative geotaxis recorded for both female and male flies at 3-week timepoints. Individual data points represent the average distance travelled by all flies in a single vial averaged over five consecutive RING trials (1n). A total of n=5-10 vials were analysed and statistical differences calculated with One-way ANOVA with Sidak's multiple comparison test. Statistical differences are marked with asterisks (*p=0.0438). Error bars represent ±SEM. B) Survival curves for female (24 hours mated) and male flies combined when aged at 30ºC, n=182-265. Statistical significance was calculated from Log-rank, Mantel-Cox test and are indicated by asterisks (from top to bottom: **p=0.0048, **p=0.0015, *p=0.0499, **p=0.0018, *p=0.0230).*

5.2.7. Modifying $A\beta_{42}$ Induced Survival and Locomotor Deficits

Aβ is the predominant pathologic protein in AD, where its production, deposition and clearance are important factors affecting AD progression and prognosis. In flies, glial expression of the human $A\beta_{42}$ peptide results in shortened lifespan and locomotor deficits (see Chapter 4, Figure 4.21). I previously showed reduced expression of glial sl ameliorated $A\beta_{42}$ induced survival deficits but did not alter associated locomotor impairment (see Chapter 4, Figure 4.22). Here, I assessed whether glial overexpression of sl altered $A\beta_{42}$ associated pathology, by measuring survival and locomotor phenotypes. Additionally, to explore the AD protective PLCG2-P522R mutations role in $A\beta_{42}$ pathology, I compared survival and locomotor phenotypes of the common-wildtype (P522) vs rare-protective (R522) PLCG2 variants in *Drosophila* models of glial $A\beta_{42}$ induced toxicity.

Using the RING assay, negative geotaxis behaviour in male and female flies (pooled together), was assessed at 21 d.p.e (Figure 5.12A). At 21 d.p.e, Repo-Gal4 driver only control flies (w-) travel an average distance of 68 mm in 10 seconds, significantly further than $A\beta_{42}$ expressing control flies (pJFRC5+ $A\beta_{42}$) which travel only 45 mm (One-way ANOVA with Sidak's multiple comparison test; n=5-12, F=6.213, ***p=0.0006). The reduction in locomotor behaviour by 33% is indicative of glial mediated neurological dysfunction in the pJFRC5 empty vector $A\beta_{42}$ expressing control group. As the pJFRC5 empty vector background recapitulates amyloid phenotypes previously described (see Chapter 4; Figure 4.21) it was chosen as an appropriate control for evaluating sl and human PLCG2 variants effect on modifying $A\beta_{42}$ related locomotor phenotypes.

First, locomotor behaviour of flies overexpressing sl and human PLCG2 variants in glia were evaluated. Transgenic glial overexpression of sl declined locomotor behaviour on average by 7%, with flies travelling an average distance of 42 mm (One-way ANOVA with Sidak's multiple comparison test; n=5-12, F=6.213, ns: p=0.9681). Glial overexpression of PLCG2 variants P522 and R522, however improved locomotor behaviour whereby the average distance travelled in 10 seconds increased by 6 and 13% respectively (51 mm and 48 mm) (One-way ANOVA with Sidak's multiple comparison test; n=5-12, F=6.213, ns: p=0.9681, ns: p=0.7604, ns: p=0.9908). Overall, neither glial overexpression of sl or human PLCG2 variants significantly altered $A\beta_{42}$ related locomotor impairment, indicating their elevated expression in glia does not further compromise CNS function (a broad readout of locomotor behaviour). Furthermore, there was no significant difference in locomotor behaviour between transgenic overexpression of sl vs. its ortholog PLCG2 in glia (One-way ANOVA with Sidak's

multiple comparison test; n=5-12, F=6.213, ns: p=0.3020), reinforcing conserved functions between the fly *sl* and human *PLCG2* genes.

Additionally, comparing transgenic overexpression of wildtype (P522) vs. AD-protective (R522) PLCG2 variants revealed no major difference in locomotor behaviour, with the R522 variant expressing flies travelling on average 3 mm further (48 mm), (One-way ANOVA with Sidak's multiple comparison test; n=5-12, F=6.213, ns: p=0.9912). This demonstrated the hypermorphic R522 variant does not contribute to altered CNS functions under $A\beta_{42}$ pathology.

Next, changes to lifespan following glial overexpression of sl and human PLCG2 variants were analysed (Figure 5.12B). Survival of flies expressing Repo-Gal4 driver alone (w-) displayed a typical trajectory for flies aged at 30ºC, with no premature deaths observed. The median lifespan of the Repo-Gal4 driver control (w-) is 40 days, however, $A\beta_{42}$ expressing, pJFRC5 vector control flies exhibit a reduced survival of 36 days (Log rank Mantel-Cox test; n=196-260, χ^2= 81.41, df=1, ****p<0.0001), demonstrating co-expression of $A\beta_{42}$ and the empty pJFRC5 vector leads to a measurable survival deficit and thus serves as a suitable control for evaluating the effects of sl and human PLCG2 variant expression on modifying $A\beta_{42}$ induced survival deficits.

Glial overexpression of sl exacerbated $A\beta_{42}$ related survival deficits, shortening the median lifespan by 9 days compared to $A\beta_{42}$ expressing, pJFRC5 vector controls (Log-rank Mantel-Cox test; n=188-196, χ^2=29.29, df=1, ****p<0.0001). Transgenic glial overexpression of the wildtype PLCG2 variant (P522), similarly intensified $A\beta_{42}$ associated survival deficits, causing a significant reduction to median lifespan by 11 days compared with $A\beta_{42}$ expressing, pJFRC5 vector controls (Log-rank, Mantel-Cox test; n=182-196, χ^2=47.49, ****p<0.0001). Together this data, indicates glial overexpression of sl and the human PLCG2 wildtype variant (P522), are detrimental to survival in response to $A\beta_{42}$ pathology. Interestingly, survival trajectories of flies overexpressing sl and the wildtype PLCG2 variant (P522), showed a subtle difference in median lifespan of only 2 days (Log-rank Mantel-Cox test; n=182-188, χ^2: 2.398, df=1, ns: p=0.1215). This demonstrated sl and its conserved human PLCG2 ortholog exacerbated $A\beta_{42}$ related survival deficits to a similar extent, showing to be functionally analogous in modifying $A\beta_{42}$ associated phenotypes.

Comparison of survival trajectories following elevated glial expression of the wildtype (P522) vs AD protective (R522) PLCG2 variants revealed the R522 variant improved amyloid associated survival deficits caused by P522 variant expression. In this instance, the R522 variant extended median lifespan by 8 days compared with the P522 variant (Log-rank,

Mantel-Cox test; n=182-232, χ^2=13.88, df=1, ***p=0.0002), indicating greater protection of the R522 variant against $A\beta_{42}$ related pathology compared with the wildtype P522 variant. None the less, the median lifespan of R522 variant expressing flies was in fact shorter than the $A\beta_{42}$ expressing, empty pJFRC5 vector control, by 3 days (Log-Rank, Mantle-Cox test; n=196-232, χ^2=20.61, df=1, ****p<0.0001). These findings highlight that though less severe than the wildtype P522 variant, the protective R522 variant of PLCG2 did not fully rescue $A\beta_{42}$ related survival deficits back to wildtype survival.

Following assessment of both survival and locomotor phenotypes it is evident that increased glial expression of sl and the wildtype PLCG2-P522 common variant exacerbated $A\beta_{42}$ associated survival deficits but did not impact to $A\beta_{42}$ related locomotor impairment. Additionally, the protective PLCG2-R522 variant in *Drosophila* improved $A\beta_{42}$ associated survival deficits of the wildtype PLCG2-P522 variant but did not completely rescue associated deficits of $A\beta_{42}$ induced toxicity. Transgenic over-expression of the PLCG2-R522 variant in glia also did not modify $A\beta_{42}$ induced locomotor deficits.

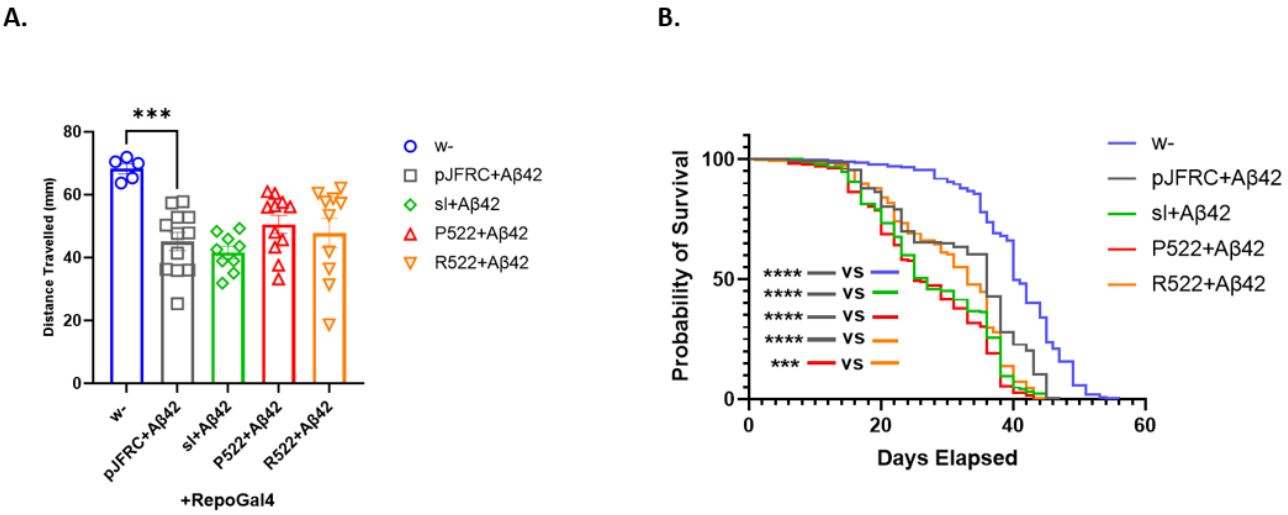

Figure 5.12: Transgenic overexpression of sl and human PLCG2 variants modify Aβ$_{42}$ associated survival but not locomotor phenotypes.

*A) Locomotor behaviour and B) survival trajectories following pan-glial targeted expression of w-, empty pJFRC5 vector, sl and human PLCG2 variants in Drosophila models of glial Aβ$_{42}$ induced toxicity. A) Average distance travelled (mm) in 10 seconds for both male and female flies combined at 3-week timepoints. Individual data points represent the average distance travelled by all flies in a single vial averaged over five consecutive RING trials (1n). A total of n=5-12 vials were analysed and statistical differences calculated from one-way ANOVA with Sidak's multiple comparison test. Statistical differences are marked with asterisks (***p=0.0006). Error bars represent ±SEM. B) Survival curves for female (24 hours mated) and male flies combined, aged at 30ºC, n=182-260. Statistical significance was calculated from Log-rank, Mantel-Cox test and are indicated by asterisks (from top to bottom: ****p<0.0001, ****p<0.0001, ****p<0.0001, ****p<0.0001, ***p=0.0002).*

5.2.8. Glial sl or Human PLCG2 Variants do not Alter Total Aβ$_{42}$ Load

Survival phenotypes suggests a detrimental role for glial sl and human PLCG2 WT variants expression on Aβ$_{42}$ associated pathology. Widespread accumulation of Aβ$_{42}$ in the fly brain is observed following glia expression of the human Aβ$_{42}$ transgene. I therefore looked at changes in Aβ$_{42}$ load of the fly brain following glial increased expression of sl and human PLCG2 variants (P522 vs R522).

At 14 d.p.e, anti-Aβ immunostaining in fly brains revealed widespread accumulation of Aβ throughout in flies expressing $Aβ_{42}$ (Figure 5.13C), with an expected difference to Repo-Gal4 driver only flies (w-) where no Aβ was detected. Visually, the distribution and abundance of Aβ deposits appeared comparable between glial expression of sl and human PLCG2 variants (P522 and R522), however, Aβ deposits appeared more concentrated in fly brains expressing the pJFRC5 vector control (Figure 5.13C).

Aβ abundance in the midbrain was calculated by setting a fluorescence threshold to distinguish Aβ deposits from background brain fluorescence. The area above this set threshold therefore provided the area of Aβ deposits in the midbrain (Figure 5.13A). This provided a semi-quantitative measure to the changes in $Aβ_{42}$ load between genotypes examined. Aβ positive area in the midbrain significantly increased between the $Aβ_{42}$ expressing, empty pJFRC5 vector control group and the Repo-Gal4 driver only control group (w-) that did not express $Aβ_{42}$ (Kruskal-Wallis test with Dunn's multiple comparison; n=7-12, ****$p<0.0001$). This demonstrated glial presence of the empty pJFRC5 vector in an $Aβ_{42}$ background provided a positive control for $Aβ_{42}$ accumulation. Although there was a large distribution in the datapoints, some trends in $Aβ_{42}$ load were observed upon comparison with the $Aβ_{42}$ expressing, pJFRC5 empty vector control.

Firstly, glial overexpression of sl decreased the area of Aβ per brain by around 36%, compared with the pJFRC5+$Aβ_{42}$ control. Although this was not statistically significant (Kruskal-Wallis test with Dunn's multiple comparison; n=7-12, ns: $p=0.1996$) it highlighted a trend towards reduced levels of Aβ in the brain at 14 d.p.e upon increased glial sl expression. Human PLCG2 (P522/R522), variants did not show major differences in the area of Aβ per brain calculated compared with the pJFRC5+ $Aβ_{42}$ control. The wildtype PLCG2-P522 variant showed an 8% decrease in Aβ positive area per brain whilst flies expressing the hypermorphic PLCG2-R522 variant exhibited a 7% increase (Kruskal-Wallis test with Dunn's multiple comparison; n=7-12, pJFRC5 vs PLCG2-P522 ns: $p=0.9983$, and pJFRC5 vs PLCG2-R522: ns: $p>0.9999$). These findings present transgenic glial overexpression of sl and human PLCG2 variants (P522/R522), do not alter total $Aβ_{42}$ load in the fly brain at 14 d.p.e.

Moreover, the overall difference to the area of Aβ deposition quantified between the wildtype and hypermorphic PLCG2 variants (P522 vs R522), was non-significant (Kruskal-Wallis test with Dunn's multiple comparison test; n=7-12, ns: $p>0.9999$), indicating that the gain of function P522R mutation did not influence total $Aβ_{42}$ load in *Drosophila* brains. Finally, there was no notable changes to the area of Aβ deposition in the midbrain upon increased glial sl expression versus its human ortholog PLCG2 (Kruskal-Wallis test with Dunn's multiple

comparison test; n=7-12, ns: p>0.9999, affirming that the two genes shared conserved roles in $A\beta_{42}$ handling.

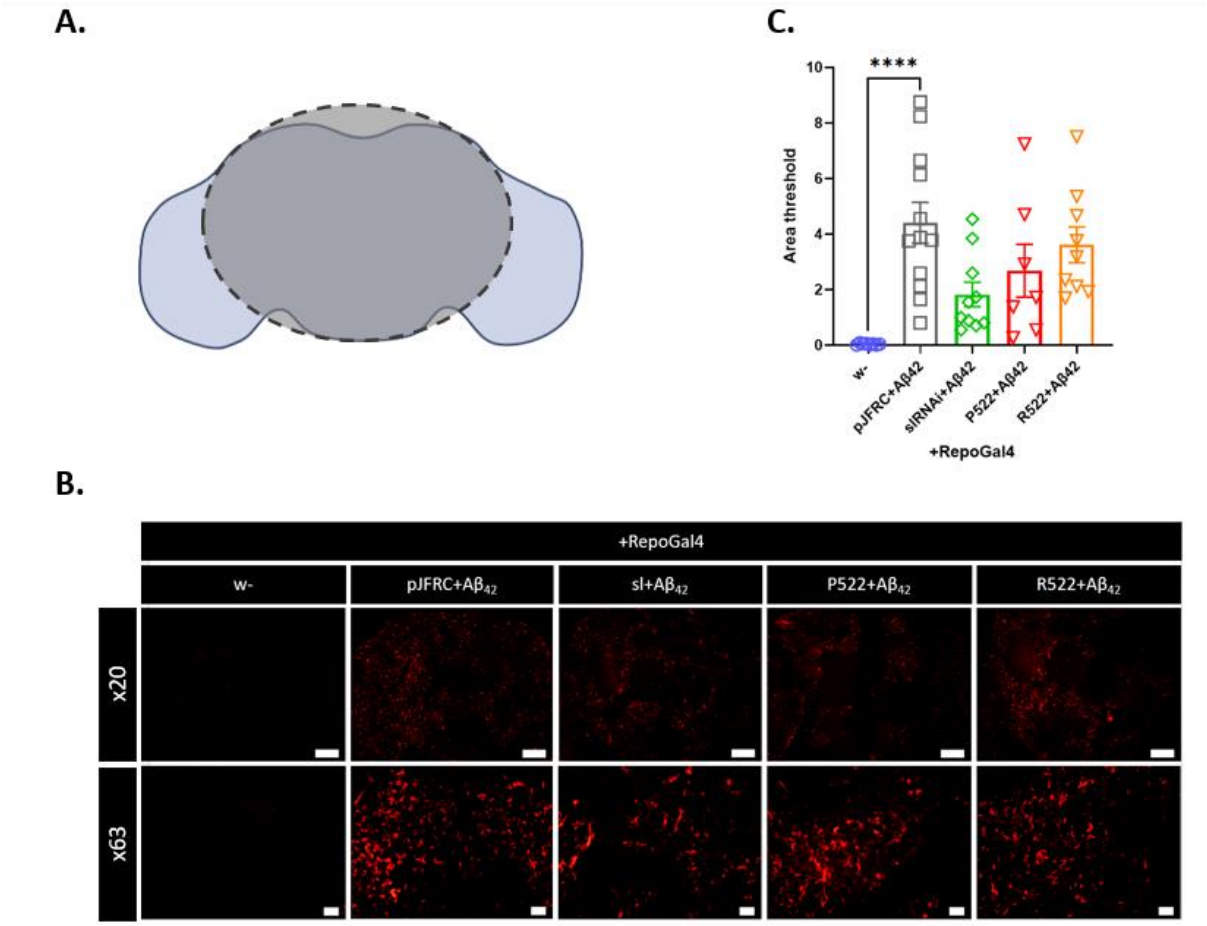

Figure 5.13: $A\beta_{42}$ pathology in brains over-expressing sl and human PLCG2 variants in glia.

*A) The grey shaded ellipse highlights the region of interest (ROI), drawn for image analysis used to quantify total $A\beta_{42}$ burden in the midbrain. B) Representative maximal orthogonal projections of fly brains immunostained for Aβ (6E10) at 14 d.p.e (Scale bars are 50 and 10 µm for x20 and x63 magnification respectively). C) Total $A\beta_{42}$ load quantified using area threshold analysis for n=7-12 fly brains. Individual values ±SEM are plotted with statistical differences marked by asterisks (****p<0.0001). Statistical differences were calculated by Kruskal-Wallis with Dunn's multiple comparison test.*

5.2.9. Glial Expression of sl and Human PLCG2 Variants do not Alter PIP2/PIP3 Dynamics in response to $A\beta_{42}$ accumulation

Literature points to the involvement of dysregulated PIP2 and PIP3 metabolism in AD pathology (Volpatti et al. 2019; Tariq and Luikart 2021). Changes to PIP2 and PIP3 in response to $A\beta_{42}$ accumulation and combined overexpression of glial sl and PLCG2 variants (P522 & R522) were therefore explored. Following glial overexpression of sl and PLCG2 variants, levels of PIP2 and PIP3 were visualised using PLCδ-PH and GRP1-PH GFP reporters respectively at 7 d.p.e in fly brains exhibiting widespread $A\beta_{42}$ accumulation.

All genotypes co-expressing $A\beta_{42}$ exhibited clear accumulation of $A\beta_{42}$, distributed mainly in the cortex and neuropil regions of the brain. Aβ deposition however, appeared more concentrated in flies co-expressing the PLCG2-R522 variant and UAS-PLCδ-PH::GFP reporter in glia compared to other genotypes examined. However, co-expression of the PLCG2-R522 variant with the GRP1-PH::GFP reporter displayed comparable $A\beta_{42}$ deposition with other $A\beta_{42}$ expressing genotypes.

In the presence of $A\beta_{42}$ accumulation, PLCδ-PH and GRP1-PH GFP reporters exhibited different responses. First, the measured area of GFP in the midbrain above the set background threshold significantly diminished by ~80% in $A\beta_{42}$ expressing pJFRC5 control flies compared to non-$A\beta_{42}$ expressing flies (w-) (Kruskal-Wallis test with Dunn's multiple comparison; n=8-34, ****p<0.0001) (Figure 5.13). In this instance, the diminished GFP fluorescence is likely owing to Gal4 titration upon addition of an extra UAS site, rather than lowered levels of PIP2 itself. On the other hand, GFP fluorescence from the GRP1-PH reporter significantly increased in $A\beta_{42}$ expressing pJFRC5 controls compared to non-$A\beta_{42}$ expressing flies (w-) (One-way ANOVA with Sidak's multiple comparison test; n=9-13, F=23.00, ****p<0.0001) (Figure 5.14). Since expression of the GRP1-PH reporter is not UAS controlled, the GFP signal is not influenced by Gal4 titration and therefore the increase in signal could be indicative of elevated PIP3 levels in response to $A\beta_{42}$ accumulation. Co-expression of $A\beta_{42}$ and the pJFRC5 vector were used as the control in determining changes to PIP2 and PIP3 in response to $A\beta_{42}$ accumulation, following overexpression of sl and human PLCG2 variants in glia.

5.2.9.1. Response of PIP2 dynamics

Increased expression of sl and human PLCG2 in glia did not alter the distribution or levels of PIP2 in response to $A\beta_{42}$ accumulation, as shown by no difference in the distribution or %

area of GFP in the midbrain compared to $A\beta_{42}$ expressing pJFRC5 empty vector controls (Figure 5.14A&B) (Kruskal-Wallis test with Dunn's multiple comparison; n=8-34, pJFRC5+$A\beta_{42}$ vs sl+$A\beta_{42}$: ns: p=0.2897; pJFRC5+$A\beta_{42}$ vs PLCG2-P522: ns: p>0.9999). The % area GFP 'positive' and the glial distribution of GFP fluorescence was also comparable between glial overexpression of sl and human PLCG2 (Kruskal-Wallis test with Dunn's multiple comparison; n=8-34, ns: p>0.9999), highlighting conservation in PIP2 metabolism between the two orthologs. Furthermore, the distribution and levels of PIP2 were comparable between the wildtype vs AD protective PLCG2 variants (P522 vs R522), when expressed in glia (Kruskal-Wallis test with Dunn's multiple comparison test; n=8-34, ns: p>0.9999). This suggests the R522 variant did alter the pool of PIP2 substrate in response to $A\beta_{42}$ pathology.

A.

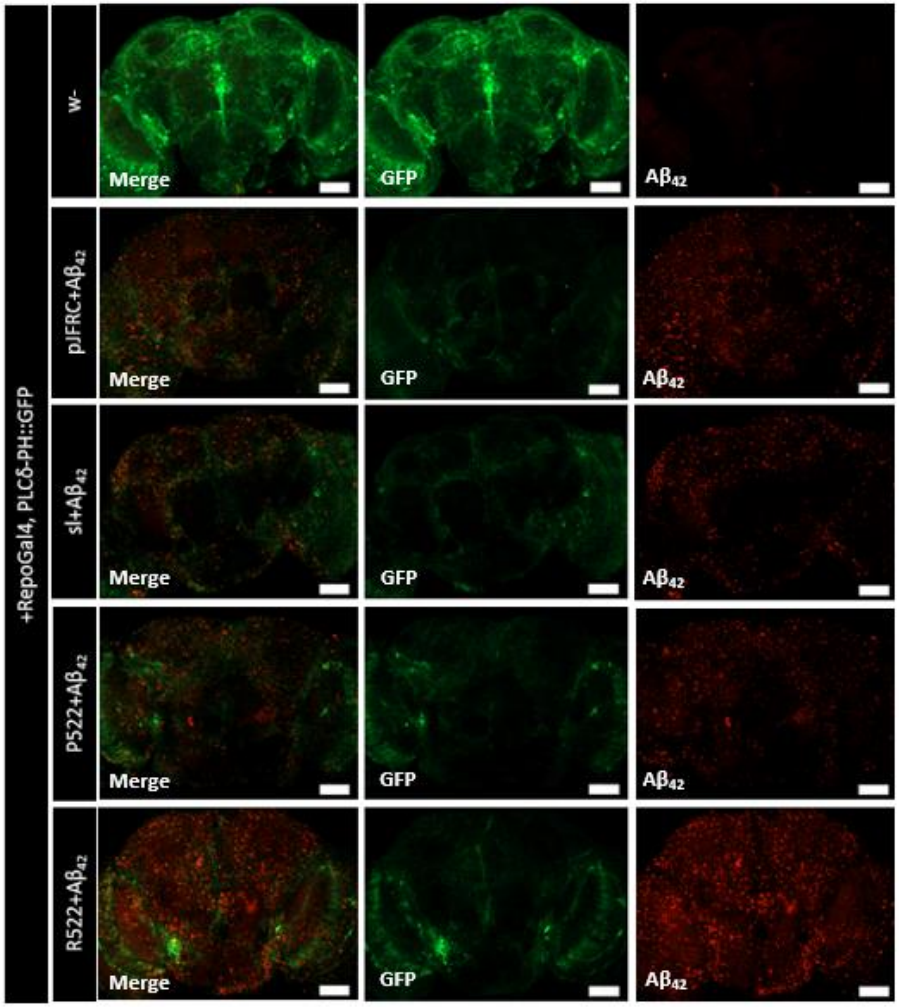

B.

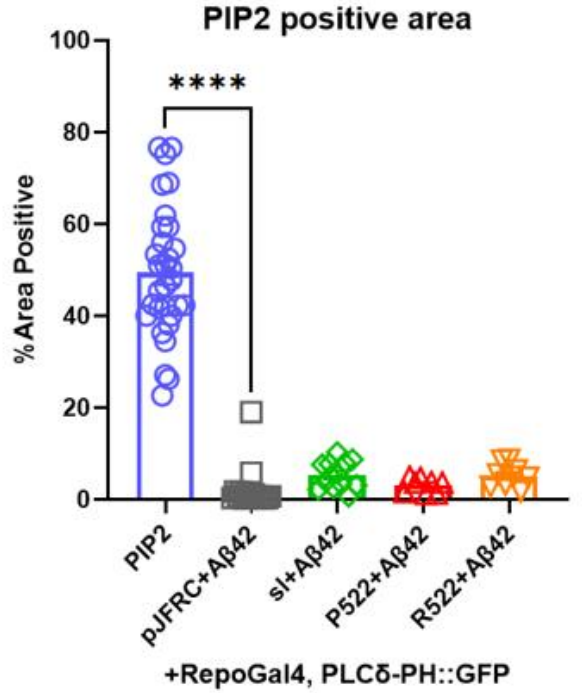

(See figure legend on the next page)

Figure 5.14: Glial overexpression of sl and human PLCG2 variants do not alter glial localisation or abundance of PIP2, in response to $A\beta_{42}$ accumulation.

*A) Representative maximum orthogonal projections of fly brains (7 d.p.e) with glial targeted expression of the PLCδ-PH::GFP reporter (GFP) and $A\beta_{42}$ (x20) (Scale Bar: 50 μm). Brains immunostained with anti-Aβ (6E10B) (red). B) Chart showing % area of GFP above set threshold in the midbrain quantified for genotypes indicated. Data represents individual mean gray values from a total of n=34 (w-), n= 25 (pJFRC5+$A\beta_{42}$), n=15 (sl+$A\beta_{42}$), n=8 (P522+$A\beta_{42}$), n=9 (R522+$A\beta_{42}$) fly brains (mixed males and females) with error bars shown as ±SEM. Statistical differences were calculated by Kruskal-Wallis test with Dunn's multiple comparison test and reported with asterisks ****p<0.0001.*

5.2.9.2. Response of PIP3 dynamics

Glial overexpression of sl and human PLCG2 did not alter PIP3 localisation or abundance in the fly brain in response to $A\beta_{42}$ accumulation (Figure 5.15A&B). The intensity and distribution of the GRP1-PH::GFP reporter remained comparable to the $A\beta_{42}$ expressing pJFRC5 controls (One-way ANOVA with Sidak's multiple comparison test; n=9-13, F=23.00, pJFRC5+$A\beta_{42}$ vs sl+$A\beta_{42}$: ns: p=0.9995; pJFRC5+$A\beta_{42}$ vs PLCG2-P522: ns: p>0.9999). Fly brains overexpressing sl and PLCG2 in glia exhibited similar distribution of the GRP1-PH reporter as well as measured GFP intensity (One-way ANOVA with Sidak's multiple comparison test; n=9-13, F=23.00, ns: p>0.9999), indicating conserved functions of sl and PLCG2 in regulating PIP3 dynamics in response to $A\beta_{42}$ accumulation. Finally, glial expression of the rare R522 variant did not alter localisation or abundance of PIP3 following accumulation of $A\beta_{42}$ in the fly brain. The distribution and GFP intensity of the GRP1-PH reporter remained comparable to that of the common PLCG2 variant (P522R), (One-way ANOVA with Sidak's multiple comparison test; n=9-13, F=23.00, ns: p=0.6495), highlighting the R522 variant did not alter PLCG2 function in PIP3 metabolism.

In summary, PIP2 and PIP3 dynamics are not altered in response to combined overexpression of glial sl/PLCG2 and $A\beta_{42}$. Furthermore, glial expression of the rare R522 variant did not alter PIP2/PIP3 metabolism.

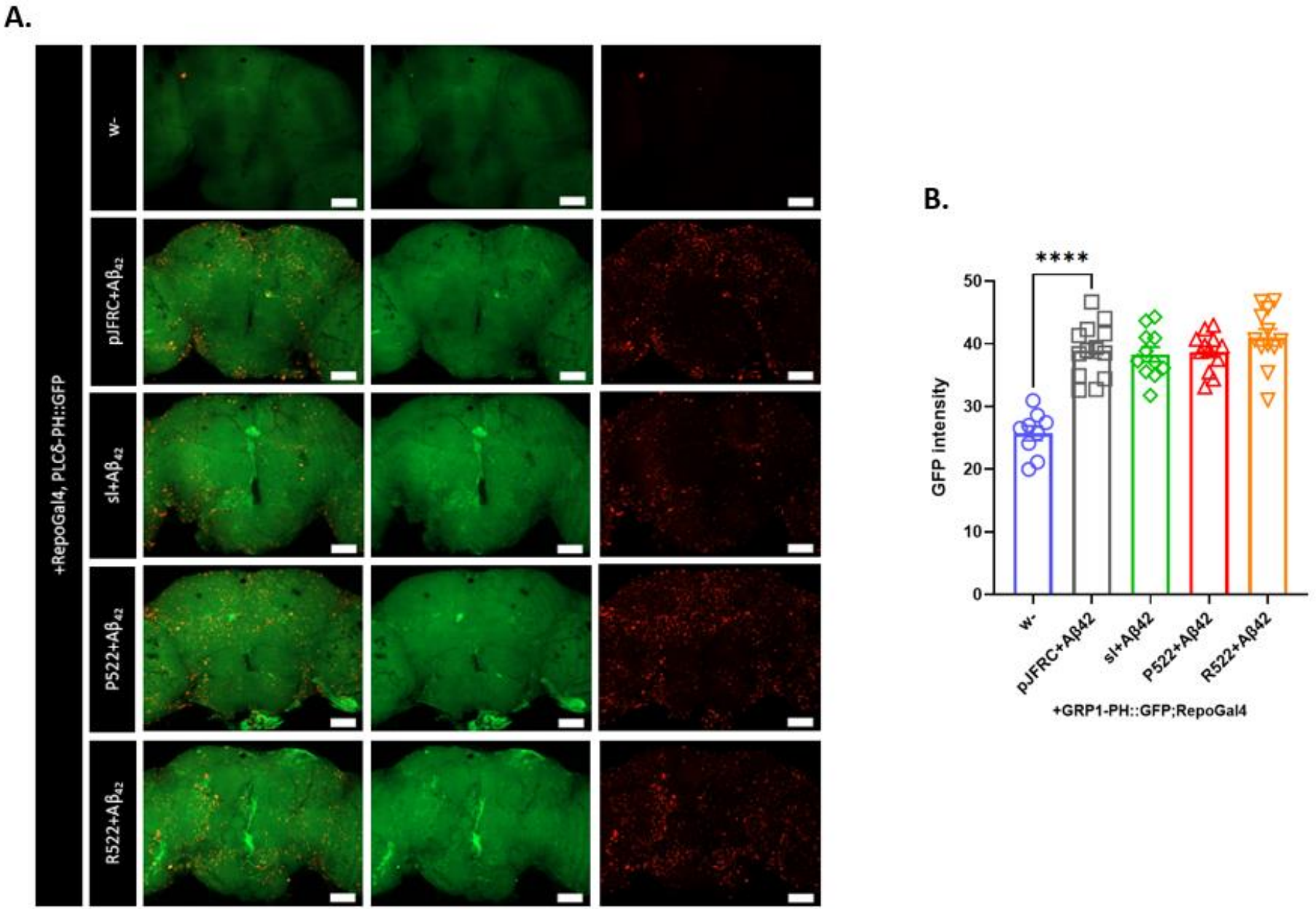

(See figure legend on next page)

Figure 5.15: Glial overexpression of sl and human PLCG2 variants do not alter localisation or abundance of PIP3 in response to $A\beta_{42}$ accumulation.

*A) Representative maximum orthogonal projections of fly brains (7 d.p.e) with ubiquitously expressed GRP1-PH::GFP reporter (GFP) and glial driven $A\beta_{42}$ expression. Brains are immunostained for anti-Aβ (6E10) (x20) (Scale bar: 50 μm) B) Chart showing GFP intensity of the GRP1-PH reporter in the midbrain quantified by mean gray analysis for genotypes indicated. GFP intensity significantly elevates in $A\beta_{42}$ expressing models. Data represents individual mean gray values from a total of n=9 (w-), n=13 (pJFRC5+$A\beta_{42}$), n=11 (sl+$A\beta_{42}$), n=12 (P522+$A\beta_{42}$), n=12 (R522+$A\beta_{42}$) fly brains (mixed males and females) with error bars shown as ±SEM. Statistical differences were calculated by One-way ANOVA with Sidak's multiple comparison test and reported with asterisks ****p<0.0001.*

5.3. Discussion

Discovery of the rare R522 coding variant in the PLCG2 gene that is protective for AD prompted initial characterisation of PLCG2 functions in microglia and further understanding of mechanisms by which the R522 variant contributes to reduced risk of LOAD. Initial functional studies in cell and mouse microglia/macrophage models characterised the R522 variant as a functional hypermorph, that subtly increases phospholipase activity of PLCG2, resulting in PIP2 depletion, IP3 accumulation, increased Ca^{2+} signalling, enhanced cell survival, inflammatory response and altered phagocytic/endocytic responses (Magno et al. 2019; Maguire et al. 2021; Takalo et al. 2020). Glial functions of the human PLCG2 wildtype (P522), and protective (R522), variants have yet to be modelled in *Drosophila* and particularly knowledge of their roles in glial responses to $A\beta_{42}$ pathology is limited.

5.3.1. Generation and Characterisation of Transgenic *sl* and Human *PLCG2* Overexpression Lines in *Drosophila*

For the purpose of this chapter, transgenic overexpression models of the fly *sl* gene and human PLCG2 variants; wildtype (P522), or AD associated (R522) were generated. Expression of human PLCG2 was confirmed in transgenic PLCG2 expressing fly models upon western blot analysis with anti-hPLCG2 antibody. Experiments outlined in this chapter highlight functional conservation between the fly *sl* and human *PLCG2* genes, where they show to play similar roles in glial biology and $A\beta_{42}$ pathology. Expression of human PLCG2 rescued the wing size of a sl CRIMIC null mutant, demonstrating PLCG2 and sl are functionally analogous. Endogenous expression of human *PLCG2* in place of the fly *sl* gene however exhibited partial lethality in males, suggesting some level of toxicity owing to expression of its human ortholog. This was further evidenced in expression of the hypermorphic PLCG2-R522 variant, where complete lethality was observed. Sl overexpression however did not pose any viability defects. Restricted glial expression of human PLCG2 variants also did not cause viability defects, indicating lethality observed was perhaps a result of disrupted PIP2 metabolism, early in development. This idea can be explored by bypassing developmental expression of human PLCG2 variants using the inducible $Gal80^{ts}$ mutant. Sl importantly regulates cell growth, regulating wing size (Murillo-Maldonado et al. 2011). Expression of the human PLCG2 ortholog slightly increased wing size above wildtype, indicating overstimulation in cell growth which may in turn have negatively impacted viability. This would further explain why the hyper-functional PLCG2-

R522 variant caused an even stronger impact on viability, where complete lethality in males was seen.

Under physiologically aged conditions, pan-glial overexpression of sl and human PLCG2 did not influence survival or locomotor behaviour in adult flies. However, glial overexpression of sl and the wildtype human PLCG2 variant exacerbated $A\beta_{42}$ associated survival deficits, highlighting a specific interaction with sl/PLCG2 and Aβ toxicity. This was independent of changes to gross neurological function and total $A\beta_{42}$ load in the brain. Together with findings in chapter 4, this data supports a role for glial sl/PLCG2 activity in modifying $A\beta_{42}$ associated survival phenotypes in *Drosophila*, which is independent of $A\beta_{42}$ pathology. As $A\beta_{42}$ load in the brain was measured through semi-quantitative image analysis, an important next step for future experiments will be to use a more quantitative method to measure $A\beta_{42}$ levels in the fly brain, such as the highly sensitive MSD assay (used in Chapter 4, section 4.2.9). The MSD assay would provide a means to assess both soluble and insoluble levels of $A\beta_{42}$ in the fly brain, allowing a more thorough investigation into the effects glial sl/PLCG2 overexpression has on $A\beta_{42}$ pathology.

Other studies have shown PLCG2 expression correlates with disease progression. For instance, LOAD patients exhibit upregulated PLCG2 expression in several brain regions and a significant positive correlation between PLCG2 expression and amyloid plaque density. Furthermore, in a 5XFAD amyloid mouse model, PLCG2 expression increased in a disease progression dependent manner and was found highly expressed in plaque-induced microglia (Tsai et al. 2022). This adds to the accruing evidence that PLCG2 plays an important role in AD pathophysiology and could be a potential target for microglia-targeted AD therapies.

Work presented in this chapter outlines glial roles of sl and human PLCG2. Whilst no other study to date has modelled glial specific functions of sl in the fly, its ortholog PLCG2 has been more extensively investigated in mouse and human iPSC derived microglial/macrophage models. In microglia, PLCG2 has been implicated as a key signalling node acting downstream of receptors TREM2 and TLR (Andreone et al. 2020). *Drosophila* do not have a conserved homologue of TREM2, indicating sl/PLCG2 must signal downstream of alternative pathways in flies. These pathways are discussed in further detail in the general discussion chapter. TLRs however, are conserved in the fly and are important for innate immunological responses. In flies, sl/PLCG2 could therefore mediate pro-inflammatory responses downstream of TLR. Overstimulation of TLR with ligands such as Aβ oligomers coupled with increased expression of sl/PLCG2 could result in chronic inflammatory response which ultimately drives neurotoxicity and cell death. This could be

one possible explanation for why overexpression of sl and PLCG2 exacerbated $A\beta_{42}$ associated survival deficits.

Alternatively, the non-receptor tyrosine kinase Syk, has been implicated in activation of PLCG2 upon binding immunoreceptor-tyrosine based activation motifs, such as that found on the transmembrane adaptor DAP12 associated with the TREM2 receptor (Gratuze et al. 2018) A conserved homolog of Syk exists in the fly called shark, which has been found to interact with the major glial engulfment receptor Draper. Shark activity is essential for Draper mediated phagocytosis of axonal debris and neuronal corpses by glia (Ziegenfuss et al. 2008). It is therefore possible sl/PLCG2 signals downstream of Draper via shark to play a role in glial engulfment, however, future experiments analysing epistatic interaction between sl and shark will be needed to confirm this.

5.3.2. Modelling Functional Changes of the AD-Associated with PLCG2-R522 variant in *Drosophila*

The R522 variant in the *PLCG2* gene represents the first classically druggable target to be identified from GWAS. Understanding how its activity in glia protects against LOAD will be important for the design of new therapeutics. As such, having a broad range of model systems, flies, mice and cells, to decipher its functions is important. Here we used *Drosophila* to model glial specific functional changes associated with the PLCG2-R522 coding variant, providing further insight into how the P522R protein change contributes to reduced risk of LOAD.

Our functional studies of the PLCG2-R522 coding variant showed glial overexpression of the R522 variant did not alter PIP2 substrate levels, nor influence survival or locomotor behaviour, under normal physiological conditions. Functional characterisation of the R522 variant in human iPSC derived microglia/macrophages however collectively show a small hypermorphic effect of this variant, which equates to mildly increased phospholipase activity, PIP2 substrate depletion and increased calcium signalling (Magno et al. 2019; Maguire et al. 2021). In BMDMs from KI mice models, the R522 variant has also been associated with enhanced cell survival after removal of macrophage colony stimulation factor. This highlights key functional differences of the R522 variant expression in fly vs cell models, whereby flies did not replicate PIP2 and survival phenotypes of PLCG2-R522 variant expression. This could be attributed to a number of reasons, such as differences in cell homology and lack of conservation in genes that regulate downstream PLCG2 signalling, for instance TREM2.

Furthermore, a slight caveat to the current expression system being used is that endogenous expression of the fly *sl* gene is still present and may have confounded effects of the R522 protective variant. Instead, replacing endogenous expression of the fly *sl* gene with human PLCG2 variants would have provided a more genetically sound approach. In theory this would have been possible to achieve using the sl CRIMIC mutant line which has a Trojan Gal4 driver integrated into its cassette, however, the lethality seen upon endogenous expression of the human PLCG2 variants (as discussed above), made this approach practically challenging. At this stage, availability of a sl null mutant would have been advantageous to exclusively study the effects of human PLCG2 variants without the confounding effects of endogenous fly sl expression.

In *Drosophila* models, the R522 variant significantly improved $A\beta_{42}$ related survival deficits compared to the wildtype P522 variant, supporting the protective nature of the R522 variant in LOAD pathology. Moreover, this supports increasing PLCG2 activity in glia could provide therapeutic benefit in AD. Maguire and colleagues have demonstrated the R522 variant reduced phagocytic activity in human iPSC derived microglia and macrophages, which was rescued upon overloading the cells with PIP2 (Maguire et al. 2021). An alternative study however, demonstrated that with lower concentrations of the phagocytic target, the R522 variant expressed in BV2 microglia-like cells increased phagocytic capacity (Takalo et al. 2020). These conflicting results indicate that phagocytic impairment is likely the result of a sustained and greater challenge on PLCG2 signalling, such as when higher concentrations of phagocytic target are used. Nonetheless, both studies demonstrate regulation of PIP2 levels is essential for microglial phagocytic response.

PIP2 modulates actin dynamics, supporting initial formation of the phagosome cup (Desale & Chinnathambi, 2021). Reduction of PIP2 at the plasma membrane has been shown to reduce phagocytic activity in mouse macrophage-like cell line – RAW 264.7. (Botelho et al. 2000). It is therefore probable that the depletion of PIP2 by the hypermorphic R522 variant contributes to the reduced microglial phagocytic activity by impeding the cell's ability to form phagosomes. The R522 variant is therefore speculated to provide protection against LOAD pathophysiology by reducing microglial phagocytic activity. This is supported by observations that increased phagocytosis can be an aggravating factor of AD pathology (Nizami et al. 2019), whereby inhibiting microglial phagocytosis can help prevent inflammatory neuronal death (Neher et al. 2011). Additionally, increased synaptic pruning (microglial phagocytosis of synapses) has been implicated in AD (Rajendran & Paolicelli, 2018). Reducing phagocytosis of damaged but viable neurons and synapses therefore seems beneficial to

LOAD pathology, preventing excessive pruning and could be achieved upon microglial expression of the hypermorphic R522 variant.

How the PLCG2-R522 variant influences microglial responses to $A\beta_{42}$ pathology has not been as extensively investigated. Maguire et al demonstrated endocytic uptake of soluble $A\beta_{42}$ oligomers in R522 expressing macrophage and microglial derived human iPSC models was increased, demonstrating increased clearance of $A\beta_{42}$ (Maguire et al. 2021). Additionally, a more recent study in chimeric AD mouse models revealed expressing the R522 variant induced microglial transcriptional changes that promoted antigen presentation and increased capacity to recruit CD8+ T-cells, indicating an important cross talk between T cells and microglia in AD (Claes et al. 2022). Our study further revealed in *Drosophila* models the R522 variant significantly improved $A\beta_{42}$ related survival deficits compared to the wildtype P522 variant, highlighting increasing PLCG2 activity in glia may provide protective benefit over wildtype PLCG2 activity. The R522 variant however does not fully rescue survival or locomotor deficits associated with $A\beta_{42}$ pathology, therefore whilst the hypermorphic R522 variant does not accelerate $A\beta_{42}$ dependent degeneration it neither contributes to protection against it. Instead, expression of the R522 variant in *Drosophila* models appears to keep $A\beta_{42}$ dependent degeneration at bay. Furthermore, despite other model systems demonstrating a role for the R522 variant in enhanced endocytic clearance of $A\beta_{42}$ we did not observe any changes to total $A\beta_{42}$ load in fly brains, highlighting in *Drosophila* the R522 variant regulates survival independent to changes in $A\beta_{42}$ pathology. As demonstrated by functional characterisation of the R522, mild gain of function variant in flies, flies can be a suitable system for modelling small functional changes of AD risk genes, so long as experiments are appropriately powered.

5.3.3. Monitoring PIP2/PIP3 in the Brain following Transgenic Glial Overexpression of sl and Human PLCG2 Variants in Aged vs AD *Drosophila* Models

Phosophinositols role in glial biology and how changes to PI metabolism contributes to the onset and progression of AD pathology is far from understood, yet an important pathological event to explore given PIP2 and PIP3 signalling plays important roles in phagocytosis and cell motility, which are critical functions of microglia.

Use of our *in vivo* glial optimised PIP2/PIP3 GFP reporter system allowed quantification of PIP2/PIP3 dynamics in response to misexpression of sl/PLCG2. In healthy *Drosophila* models increased glial sl/PLCG2 expression and sustained expression of the hypermorphic

R522 variant in glia, did not alter glial PIP2 levels. This was unexpected as we had previously demonstrated reducing glial sl expression elevated PIP2 levels (See Chapter 4, Figure 4.19), but also the hypermorphic R522 variant has been previously reported to potentiate PLCG2 hydrolysis of PIP2, resulting in PIP2 depletion. This has been demonstrated both *in vitro* after exposure to LPS or $A\beta_{42}$ and *in vivo*, where basal levels of PIP2 were decreased in mouse microglia expressing the R522 variant compared to the wildtype P522 variant (Maguire et al. 2021). We also note a significant decrease in GFP fluorescence of PLCδ-PH reporter upon expression of the pJFRC5 empty vector control. This pronounced reduction in signal may in part be explained by titration of Gal4 and chromosomal insertion site of the pJFRC5 empty vector. Due to the significant drop in GFP signal, flies carrying the pJFRC5 empty vector were thus chosen as the most appropriate baseline control for sl/PLCG2 overexpression experiments.

As discussed above, the resulting endogenous expression of sl in these models may have suppressed the effects of hypermorphic R522 variant. This could explain why we did not observe depletion of PIP2 substrate. However, this does not explain why increased glial sl expression did not reduce PIP2 levels, particularly as we have already demonstrated decreased sl expression in glia elevated PIP2. In this instance, it could be sl expression was not increased enough to see an effect on PIP2 metabolism but also that compensatory mechanisms may be working towards restoring the balance of PIP2 in the membrane. PIP2 levels can be restored upon either the conversion of PIP3 back into PIP2 via PTEN or through enhanced PIP2 synthesis from its precursor PI4P by PI4P5 kinases. As there was no compensatory change in PIP3 levels upon modulating glial sl expression this highlighted that the balance between PIP2 and PIP3 were maintained. Furthermore, the changes in PIP2/PIP3 levels were measured upon semi-quantitative image analysis of fluorescence intensity. Instead, more quantitative approaches such as mass ELISAs and high-performance liquid chromatography could have been used for a more sensitive measure of various PIP species in whole brain homogenates and may have revealed subtler changes to their metabolism.

With accumulating evidence linking dysregulated lipid metabolism and AD pathology, I therefore explored whether changes in PIP2/PIP3 metabolism influenced $A\beta_{42}$ pathology in *Drosophila*. Glial overexpression of sl or PLCG2 variants did not alter PIP2 or PIP3 levels in healthy aged models, suggesting their levels must be tightly regulated *in vivo*. Changes that do occur may be more subtle and may require more sensitive assays for detection. However, it was clear there was no correlation between the deposition of $A\beta_{42}$ and the localisation of PIP2 or PIP3, suggesting glia do not adapt membrane composition in

response to proximity of amyloid deposits. PIP3 levels were also increased in response to $A\beta_{42}$ accumulation, indicating $A\beta_{42}$ induced PIP3 signalling which is an important mediator of the PI3K-AKT pathway, which regulates a number of cellular processes including survival, autophagy, proliferation and cell growth.

5.3.4. Conclusions

This chapter aimed to elaborate on glial specific functions of the human PLCG2 gene, as well as functional changes associated with the gain of function LOAD protective P522R variant. With the generation of transgenic *Drosophila* models of human PLCG2 expression, I have demonstrated functional conservation between the fly *sl* and human *PLCG2* genes, highlighting cellular functions of PLCG2 can be effectively modelled by its *Drosophila* counterpart, sl. As hypothesised, the hypermorphic R522 variant demonstrated reduced risk against Aβ toxicity compared to the more common P522 variant, showing improvement to $A\beta_{42}$ related survival, emphasizing the idea that manipulating PLCG2 activity in glia can be a potential therapeutic target in reducing $A\beta_{42}$ dependent degeneration. Finally, in modelling functional changes associated with the R522 hypermorphic variant, functional differences between model systems have been highlighted. The current fly model does not recapitulate all changes seen with expression of the R522 variant in human iPSC and mouse microglial/macrophage models. For instance, the influence on PIP2 metabolism and survival differ between model systems. Future experiments will work on developing a system that allows for expression of human PLCG2 variants in place of endogenous sl expression to hopefully account for these differences.

Chapter 6: Discussion

6.1. Summary of Main Findings

Work from this thesis has assessed glial roles of AD risk genes orthologs in *Drosophila* models, with the aim to better understand how glial risk gene activity contributes to AD pathogenesis. Results from Chapter 3 revealed novel candidates, including orthologs of human *MEF2C*, *NME8* and *ACE* that modulate glial activity to contribute to longevity and overall maintenance of a healthy ageing nervous system. These genes should be considered promising candidates for follow up experiments (discussed below). Chapter 4 of this thesis has provided greater characterisation of a glial driven model of $A\beta_{42}$ toxicity, evidencing extracellular accumulation of insoluble $A\beta_{42}$ aggregates with age and $A\beta_{42}$ associated phenotypes (i.e. survival and locomotor deficits). Experiments outlined in this thesis suggest a conserved role for glial sl/PLCG2 in modifying $A\beta_{42}$ toxicity and highlight a protective role of the AD associated R522 variant in modifying $A\beta_{42}$ toxicity compared with the wildtype P522 variant in PLCG2 (see Chapter 4 and 5). Furthermore, this thesis reports for the first time the characterisation of novel PIP2 and PIP3 fluorescent reporter tools in the intact fly brain and their use in defining the cellular distribution of PIP2 and PIP3, as well as the contribution of these phospholipids to Aβ pathology. My findings indicate that the elevation of PIP3 may be contributing to the amelioration of $A\beta_{42}$ associated survival deficits upon reduced glial expression of sl and therefore makes a case for further exploration of phosphoinositols contribution in AD pathophysiology. Taken together, findings in this thesis support the notion that glia contribute to AD pathophysiology and by manipulating glial activity of AD risk genes such as PLCG2, we may find novel ways to therapeutically treat AD.

6.2. *Drosophila* as a Screening Tool to Study Glial Functions of AD Risk Genes

The genetic screen outlined in Chapter 3 of this thesis demonstrates files can provide a rapid and efficient means of triaging several candidate genes defined from LOAD GWAS, understanding their functional importance in glia and whether they contribute to healthy ageing of the brain. In particular, the optimised RING assay apparatus, with improvements to the design, enabled rapid and reproducible screening of fly locomotor behaviour, for a readout of glial mediated neurological dysfunction. Many of the human AD risk genes share a conserved ortholog in the fly, for which there are several genetic tools available allowing us

to manipulate their expression and study their functions in a simpler *in vivo* system compared to mammalian models. These include null alleles, over-expression or RNAi mediated KD. Disrupting gene function via RNAi KD serves a robust strategy for understanding gene functions and has been used to discover novel functions of genes involved in neurodegenerative processes (Higham et al. 2019; Clark et al. 2006). The $Gal80^{ts}$/Gal4 expression system has been of particular importance for this screen, enabling fine-tuned expression of UAS-RNAi transgenes to glial cells, exclusively at adult specific stages. This inducible cell specific regulation of gene expression is a major advantage of using the fly system and is not so easily achieved with more complex mammalian models.

The screen implicated glial activity of AD risk gene homologues *MEF2C*, *NME8* and *ACE* in regulating the survival of adult flies, as well as nervous system functioning required to coordinate locomotor behaviour. I postulate these genes could be important to homeostatic functions of glia, such as providing trophic support to neurons or effective clearance mechanisms and why their reduced expression in glia is detrimental to the overall health and longevity of the fly. Glial dysfunction has been implicated in the progression of AD and importantly communication between glia and neurons is essential for synaptic homeostasis and neuronal network function (Araque & Navarrete, 2010). Given the critical role of these genes in glia for physiological ageing, follow up studies should consider how these genes contribute to the progression of AD related pathology, such as modifying $A\beta_{42}$ and tau induced toxicity.

Whilst this was one of the first genetic screens to investigate glial phenotypes of conserved AD risk genes, it supports the use of flies as a valid screening tool for gaining insight into the pathomechanisms of AD. Other studies to date have focused on neuronal phenotypes to identify genetic modifiers of $A\beta_{42}$ and tau induced toxicity. These have identified several mechanisms underlying AD pathogenesis, including redox reaction, transcriptional regulation, cholesterol metabolism, tau phosphorylation, apoptosis and cytoskeletal rearrangement (Shulman and Feany 2003; Finelli et al. 2004; Cao et al. 2008; Rival et al. 2009; Shulman et al. 2014; Dourlen et al. 2017).

Historically, flies have been the standard model organism for conducting large genetic *in vivo* screens, owing to their practicality, short generation time and statistical power through relatively large biological replicate group size allows high throughput genetic analyses to be performed. Over the last decade advancements in genetic tools have been made that make it increasingly feasible to conduct large genetic screens in cells using CRISPR technology (Wang et al. 2014). Whilst this allows modelling of gene functions in a more physiologically relevant cell type, *in vitro* studies do not encapsulate the full complexity of an *in vivo* system

that flies can provide, such as being able to model behavioural phenotypes like changes in sleep or learning and memory etc.

6.3. Modulating PLCG2/sl Activity in Glia as a Target for AD Therapy

Findings from this thesis strongly support modulating sl/PLCG2 activity in glia as a target for modifying $A\beta_{42}$ induced toxicity. Specifically, results here have shown glial KD of the fly PLCG2 ortholog, sl rescues $A\beta_{42}$ induced survival deficits, whilst overexpression of human PLCG2 and sl in glia exacerbates the phenotype. This was independent of changes to brain Aβ pathology and $A\beta_{42}$ associated behavioural deficits. Furthermore, survival phenotypes were specific to glial induced $A\beta_{42}$ toxicity as increased or decreased glial sl/PLCG2 expression did not compromise survival under normal physiological aged conditions. This is in contrast to complete PLCG2 KO in human iPSC macrophage and microglia models, which present a deleterious effect on survival under non-pathological conditions (Andreone et al. 2020; Obst et al. 2021). Overall, these findings suggest that decreasing glial sl/PLCG2 activity (but not complete KO) could provide therapeutic benefit for AD by ameliorating $A\beta_{42}$ associated pathology, whilst overexpressing sl/PLCG2 would have the adverse effect.

On the other hand, the mild gain of function PLCG2-R522 variant, associated with reduced LOAD risk, improved $A\beta_{42}$ associated survival deficits compared to the common PLCG2-P522 variant when expressed in glia. This supports the protective nature of this variant in AD but also indicates a small window for which we can therapeutically modulate PLCG2 activity, to promote protection as opposed to disease. Whilst a subtle increase in PLCG2 enzymatic activity is protective of AD, overactivation could be detrimental as shown by overexpressing the common PLCG2-P522 variant in a glial $A\beta_{42}$ *Drosophila* model. This is further corroborated by a study showing strong hypermorphic PLCG2 variants such as the S707Y implicated in severe APLAID, dampens key microglial functions such as phagocytosis and cytokine release in a human iPSC-derived microglia model (Daniel Bull UCL; data not published). Small molecules that modulate PLCG2 activity to mimic the neuroprotective effects of the R522 variant will therefore be important to identify and develop into drugs.

PLCG2 hydrolysis of PIP2 indirectly regulates levels of PIP3, the main effector of the PI3K/AKT signalling (Rameh and Cantley 1999). Glial sl/PLCG2 could therefore be modifying $A\beta_{42}$ associated survival deficits through PI3K/AKT dependent signalling, independent of Aβ. AKT is a serine/threonine kinase involved in regulating downstream signalling events important to metabolism, cell proliferation, survival, growth, motility and autophagy (Lawlor and Alessi 2001; Brazil et al. 2004). AKT has several downstream targets

(Figure 6.1). In particular, GSK-3β, Bad, Bax, and caspase 9 have been linked to pro-survival and anti-apoptotic effects (Datta et al. 1999; Franke et al. 1997)There is also evidence that activation of PI3K/AKT signalling can be protective against Aβ neurotoxicity *in vitro* (Martín et al. 2001; Wei et al. 2002) and potentially *in vivo* (Stein & Johnson, 2002). However, the role of AKT in AD pathology is conflicting, with evidence also for the contrary (Griffin et al. 2005; Pei et al. 2003). Results from this thesis have shown that in a glial model of $A\beta_{42}$ toxicity, reduced sl expression in glia elevated PIP3 (see Chapter 4: Figure 4.26). More PIP3 is therefore available for AKT activation and subsequent regulation of downstream targets highlighted in Figure 6.1. Given the role of these targets in anti-apoptotic and pro-survival pathways, it is possible increased PI3K/AKT signalling may account for the amelioration of $A\beta_{42}$ survival deficits following glial sl KD. Flies could be used to test downstream phosphorylated targets of AKT, detected upon western blotting. Increased phosphorylation of downstream targets, such as GSK-3β or Bax, would provide indication of increased AKT dependent signalling.

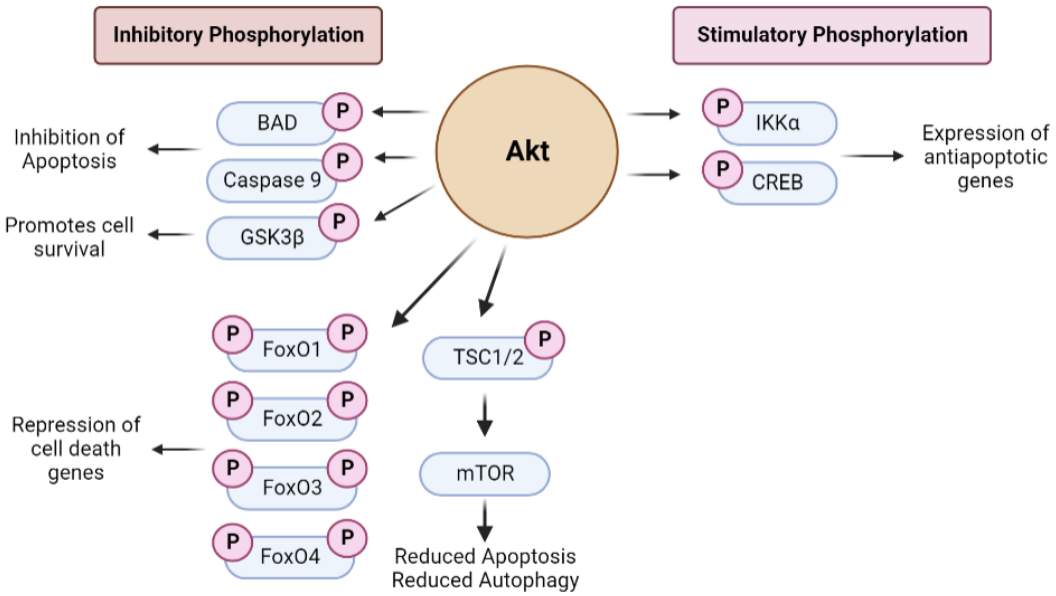

Figure 6.1. Downstream regulatory targets of AKT.

AKT phosphorylates several downstream targets to have either an inhibitory or stimulatory effect on protein function. Through downstream pathways outlined, AKT mediates pro-survival and anti-apoptotic effects.

Alternatively, glial sl/PLCG2 activity could be regulating glial mediated synaptic elimination independent of Aβ load. Aberrant elimination of synapses is an early hallmark of AD and correlates with cognitive decline (Rajendran and Paolicelli 2018; Henstridge et al. 2019) . Furthermore, inhibiting microglial phagocytosis prevents inflammatory neuronal death (Neher et al. 2011), whilst increased phagocytosis of apoptotic neurons has been observed in APOE-overexpressing cells (Muth et al. 2019). It is therefore possible through regulation of glial mediated synaptic elimination, sl/PLCG2 modifies $A\beta_{42}$ associated survival deficits. In line with this hypothesis, Maguire et al demonstrated the R522 variant reduced phagocytic uptake of *E.coli* and zymosan (a bioparticle derived from *S.cerevisiae* cell wall) in mouse macrophage, microglia and human iPSC derived microglial models (Maguire et al. 2021). Furthermore, sl has been shown to regulate glial engulfment in flies, whereby KD impaired glial engulfment of severed axons (Freya Storer, data not published). sl/PLCG2 role in PIP2 catalysis likely contributes to its ability to regulate phagocytosis, whereby the depletion of PIP2 and concomitant rise in PIP3 is required in early stages of phagophore formation and completion of phagocytosis (Hilpelä et al. 2004; Scott et al. 2005). Taken together, the reduction in phagocytic activity that would otherwise drive excessive synaptic pruning and neuronal death could contribute to the protective effect of sl KD and R522 variant expression in $A\beta_{42}$ associated survival deficits. Future research to investigate changes in glial engulfment and synaptic loss in a *Drosophila* Aβ model would help to understand this further.

In addition to reduced phagocytic activity, Maguire et al showed the AD protective R522 variant increased endocytic clearance of soluble $A\beta_{42}$ oligomers in iPSC derived microglia compared to the common P522 variant (Maguire et al. 2021). Enhanced clearance of Aβ is favourable in AD, as to prevent build-up of plaques which correlates with deleterious impact on metabolic processes and cellular function, including induced apoptosis of neuronal cells (Kechko et al. 2019). However, in our *Drosophila* $A\beta_{42}$ model, overexpression of the R522 variant in glia did not appear to alter brain Aβ load (see Chapter 5, Fig 5.13), reaffirming in flies pathways independent of Aβ clearance contribute to the protective effect of the R522 variant.

In our fly model, signalling pathways upstream of sl/PLCG2 specific to glia are unknown and thus epistatic studies to establish upstream genetic interactors of sl/PLCG2 signalling are required in future experiments. In mammalian microglia, PLCG2 has been shown to signal downstream of TREM2, mediating cell survival, lipid metabolism and phagocytosis. Independent of TREM2, PLCG2 also signals downstream of TLR to mediate inflammatory responses (Andreone et al. 2020). As flies do not have a conserved homolog of TREM2, but

do have homologs of TLRs, it is possible sl/PLCG2 signals downstream of fly Toll receptors to control immune responses (Bilak et al. 2003)

Alternatively, sl/PLCG2 could be involved in other signalling pathways in flies. For instance, the EGF receptor is a RTK implicated in activation of PLC-γ isozymes (Wahl et al. 1987; Nishibe et al. 1990) and is conserved in flies. Results described by Thackeray, 1998 suggest sl is a direct or indirect attenuator of the EGF receptor signal in pathways regulating R7 photoreceptor development. In the absence of sl activity, the EGF receptor signal is allowed to persist resulting in overactivation of the MAPK cascade and the production of extra R7 photoreceptor (Thackeray et al. 1998). Over-expression of sl/PLCG2 would therefore lead to a greater attenuation of the EGF receptor signal and subsequent downregulation of MAPK/ERK pathway that controls cell survival. This provides a possible explanation as to why overexpressing sl/PLCG2 in glia intensified $A\beta_{42}$ associated survival deficits, where the cells are more vulnerable to death. A genetic interaction between sl/PLCG2 and the EGF receptor could be assessed by knocking down the EGF receptor and seeing if there is a rescue in the $A\beta_{42}$ associated survival deficits.

Alternatively, the non-receptor tyrosine kinase Syk, has been implicated in activation of PLCG2 upon binding immunoreceptor-tyrosine based activation motifs, such as that found on the transmembrane adaptor DAP12 associated with the TREM2 receptor (Gratuze et al. 2018). A conserved homolog of Syk exists in the fly called shark, which has been found to interact with the major glial engulfment receptor Draper. Shark activity is essential for Draper mediated phagocytosis of axonal debris and neuronal corpses by glia (Ziegenfuss et al. 2008). A role for Draper in glia has also been shown to ameliorate Aβ toxicity, reducing Aβ peptide levels, rescuing locomotor deficits and extending lifespan (Ray et al. 2017). It is therefore possible sl/PLCG2 signals downstream of Draper via shark to play a role in glial engulfment and modified phenotypes of Aβ toxicity. Future experiments analysing epistatic interaction between sl and shark will be important to confirm this.

Overall, *Drosophila* have provided a suitable model for studying conserved functions of human PLCG2 *in vivo,* where work from this thesis demonstrates analogous functions of the fly sl and human *PLCG2* gene throughout physiology and $A\beta_{42}$ related pathology. Specifically, expression of human PLCG2 rescued wing size of a sl LOF mutant, affirming functional conservation between the fly and human genes (see Chapter 5: Figure 5.8). In addition to the rescue of small wing phenotype, future experiments could validate the rescue of other physiological defects, such as PIP2 metabolism, and development of extra R7 photoreceptors. In addition, knocking down sl in glia increased basal levels of PIP2 under physiological conditions, aligning with knowledge of PLCG2 as a PIP2 metabolising enzyme

(Rhee and Choi 1992). Furthermore, generation of transgenic overexpression fly models allowed further exploration into glial functions of human PLCG2 variants – common vs AD-protective *in vivo*. In this study, overexpression of human PLCG2 variants was restricted to glia using the pan glial driver Repo-Gal4, however future experiments should consider using the sl CRIMIC promotor trap tool to achieve expression of sl and human PLCG2 variants in all cells that express sl endogenously. This may need to be combined with temperature inducible Gal80 to bypass developmental lethality caused by expression of human PLCG2 variants.

6.4. Are PIPs Important in AD?

This thesis aimed to define the distribution of PIP2 and PIP3 within the fly brain and explore their contribution in the onset and progression of AD pathology. Firstly, characterisation of chimeric GFP reporters fused to PLCδ and GRP1 PH domains demonstrated the ability to visualise PI(4,5)P2 and PI(3,4,5)P3 species respectively in the intact fly brain, under confocal microscopy. These reporters provided a means to evaluate relative changes in PIP2 and PIP3 throughout the brain of an *in vivo* model system, as well as determine their distribution at a cellular level. In particular, glial targeted expression of the PLδ1-PH::GFP reporter revealed glial specific distribution and levels of PIP2. Importantly, the PIP2 specific reporter successfully detected increased levels in glial PIP2 following glial targeted KD of sl, which was anticipated (see Chapter 4, Figure 4.15). Current image analysis methods (see Chapter 2; Section: 2.7.2 & 2.7.3) used to measure PIP2 and PIP3 within the fly brain are semi quantitative and therefore future experiments may wish to consider a more quantitative approach, such as ELISAs that would measure absolute levels PIP2/PIP3 in the entire fly brain, however at the expense of cell specificity.

Work presented in this thesis supports a role of PIPs in AD pathophysiology, where we evidence a potential contribution for PIP3 in alleviating $A\beta_{42}$ survival related deficits following glial KD of sl. Glial sl KD alone did not influence levels of PIP3 in the fly brain however, in the combined presence of amyloid accumulation PIP3 was elevated. On the other hand, from experiments within this thesis, there was no evidence of a similar contributory role for PIP2. Transgenic overexpression of sl and human PLCG2 variants however saw no changes to PIP2 or PIP3 dynamics both with and without the presence of $A\beta_{42}$, which was unexpected given the enzymes role in lipid metabolism. Even more so as the R522 variant has previously been linked to reduced PIP2 levels in both human iPSC microglia and mouse

models (Maguire et al. 2021). It could be that driving glial overexpression of sl and human PLCG2 variants was not strong enough to alter overall PIP2/PIP3 levels within the fly brain, as their levels are tightly regulated by several kinases and phosphatases, primarily PI3K and PTEN. It could also be that the changes in PIP levels may be more subtle, requiring more sensitive and quantitative assays for their detection, for instance mass spectrometry or ELISAs.

Additionally, from these experiments it can be deduced that $A\beta_{42}$ may influence glial membrane PIP2 composition, such that membranes in closer proximity to $A\beta_{42}$ deposits exhibited lower levels of PIP2 (see Chapter 4, Figure 4.28). Previous work from Berman and colleges supports this finding, showing loss of membrane PIP2 in cultured neurons treated with Aβ oligomers, which was rescued upon removal of Aβ. Furthermore, reduced activity of the major PIP2 phosphatase, synaptojanin, maintained levels of PIP2 in the presence of Aβ (Berman et al. 2008). Given important roles of PIP2 in actin filament formation, a key step in phagocytosis, the depletion of PIP2 could impede the ability of glia to form phagosomes, which is an important mechanism in the effective removal of Aβ (Ries & Sastre, 2016). Aβ toxicity therefore may in part be attributed to decreased signalling through PIP2. Together these results support increasing PIP2 as a potential target in protecting against Aβ toxicity**.**

Conversely, depletion of PLCG2 enzyme substrate, PIP2, is thought to contribute to the protective effect of the PLCG2-R522 variant in AD pathology, by potentially preventing chronic enzyme activation or reducing sensitivity to further receptor mediated stimulation (Maguire et al. 2021). As PIP2 levels remained unaltered upon glial overexpression of the R522 variant in flies, it was not possible to make the same conclusion in the current fly model system used in this thesis. None the less, depletion of substrate PIP2 in R522 variant expressing cells has been found to contribute to the overall reduced phagocytic phenotype observed in these cells, as increasing PIP2 increased the rate of phagocytosis (Maguire et al. 2021). As discussed above, PIP2 is critical in steps of phagocytosis, where the careful control of PIP2 hydrolysis by PLCG2 is important in phagosome formation. The hypermorphic effect of the R522 variant leads to increased PIP2 hydrolysis and thus consequently impacting the cell's ability to form phagosomes. Whilst phagocytosis is important in preventing build-up of toxic protein aggregates such as Aβ, reduced microglial phagocytosis can however favourably prevent excessive pruning of synapses and inflammatory neuronal death, which has been implicated in AD (Neher et al. 2011; Rajendran & Paolicelli, 2018). Reduced phagocytic activity and subsequently reduced phagocytosis of damaged yet viable neurons and synapses is therefore postulated to contribute to the protective effect of the R522 variant in AD. Determining whether glial

overexpression of the R522 variant similarly reduces glial engulfment in a fly model will therefore be worth exploring in future experiments.

Beside *PLCG2*, several other AD risk genes expressed in microglia, have also been linked to phospholipid metabolism such as, *INPP5D*, *PLD3*, *CD2AP*, *PICALM* and *SLC24A4* (Tan et al. 2019; Sims et al. 2020), providing further evidence of the importance in regulating PIP levels in AD pathology. Additionally, with the increasing body of evidence pointing towards PIPs role in important homeostatic functions of microglia, targeting PIPs may therefore be a way to therapeutically modulate microglial function in AD (Phillips and Maguire 2021). Further research into how PIP imbalances impact glial functions and thus contribute the onset and progression of AD is however needed.

6.5. Therapeutically Targeting Glial Activity in AD

Recent GWAS have highlighted several microglial-enriched genes associated with risk of LOAD, suggesting targeting these cells and their functions might have important therapeutic potential in the future. Data presented in this thesis supports this by demonstrating amyloid associated phenotypes can be altered upon manipulating expression of glial genes such as *sl/PLCG2*. Furthermore, glial expression of *Drosophila* orthologs of AD risk genes, such as *Mef2/MEF2C* and *CG18130/NME8* were found to be critical to nervous system functioning and longevity in adult flies, highlighting that glial genes are also important in the maintenance of a ‘healthy’ ageing nervous system. Other microglial genes associated with AD risk have also been identified as possible therapeutic targets for manipulating microglia functions in AD (Wes et al. 2016; Bemiller et al. 2017; Krasemann et al. 2017; Zhang et al. 2021; Ennerfelt et al. 2022). One promising target is the microglial transmembrane receptor TREM2 which proves critical in the maintenance of homeostatic microglial phenotypes (Krasemann et al. 2017). Loss of function TREM2 mutations are associated with impaired microglial phagocytosis (Yeh et al. 2016), migration (Mazaheri et al. 2017), lipid metabolism (Nugent et al. 2020), survival and pro-inflammatory responses (Zhong et al. 2017), all of which represent key microglial responses to neurodegeneration. Activation of TREM2 in microglia is therefore thought to be neuroprotective by enhancing key homeostatic microglial functions.

It is clear microglia are important in AD pathogenesis but how to target these cells is another question, which is further challenged by the difficulty in therapeutics crossing the blood brain barrier. On the one hand, there is evidence to show microglia can help protect against AD by

minimising toxic accumulation of Aβ. However, unbridled microglial activation can lead to aberrant chronic inflammation and synapse elimination that drives neurotoxicity (Hansen et al. 2018). Single cell transcriptomic analysis reveals context dependent microglial subclusters, underscoring their disparate roles in the development and progression of AD pathology (Masuda et al. 2020). The heterogeneity of microglia throughout AD progression could therefore be potentially therapeutically exploited, however a more comprehensive molecular view of microglial signatures throughout ageing and AD development is required in order to fully understand how to target these cells therapeutically. Future studies using single cell transcriptomic analysis could help identify novel markers, pathways and regulatory factors that are critical to microglial functions in both health and disease.

6.6. Future Perspectives

This thesis adds to an existing body of evidence that modulating glial activity of AD risk genes could provide important therapeutic potential for AD pathology. In the immediate future, experiments validating RNAi KD of target genes will be of most importance to this work. This can be achieved through quantifying levels of target gene KD by qPCR, but also use of null mutant alleles could help affirm phenotypic observations of gene KD. Secondly, it will be of interest to elucidate mechanisms for which *sl/PLCG2* and other AD risk genes identified from the screen contribute to $A\beta_{42}$ associated pathology, as to identify novel pathways to target AD. It would also be interesting to use flies for epistatic analysis of two AD risk gene hits, as to determine communal pathways in which risk genes may be acting. Experiments outlined in this thesis used a binary UAS/GAL4 expression system to drive sl KD and $A\beta_{42}$ production simultaneously in glia. As glial sl KD may influence glial production of $A\beta_{42}$, future experiments should consider the use of a QUAS/QF2 expression system in parallel with UAS/GAL4 to allow manipulation of gene expression in two independent tissues or cell types, according to which tissue/cell specific QF2 or Gal4 driver is used. This dual expression system could be used to independently manipulate glial genes (i.e. *sl*) in tandem with neuronal production of $A\beta_{42}$ – a more physiologically relevant model. Finally, using the sl CRIMIC promoter trap tool to generate a fully humanised PLCG2 expression system in the fly will be advantageous to this current work, as to study the effects of human PLCG2 variants without the confounding expression of endogenous sl and could be used to validate rescue of $A\beta_{42}$ dependent survival phenotypes.

This study has used gene KD and transgenic overexpression approaches to explore glial functions of AD risk gene, *PLCG2*. With the advances in CRISPR technology it is possible to generate KO and KI mutants of AD risk gene loci and single risk gene variants - an approach that has been taken for similar functional studies of PLCG2 in mouse and iPSC microglial models (Andreone et al. 2020; Maguire et al. 2021; Takalo et al. 2020). Sequence alignment of the Pro522 residue in *Drosophila* sl however indicates an aa change to Alanine (Ala579). As the Pro522 residue is not conserved in flies, KI mutants of the P522R protective variant could not be made in flies. Instead transgenic overexpression of the common (P522) vs rare protective (R522) AD PLCG2 human variants were used to model functional changes associated with the AD associated R522 variant in flies.

This thesis detailed an unbiased genetic screen and direct candidate gene-based approach for studying AD risk genes contribution to AD, focused on studying the effect of single AD risk loci and variants in disease. However, AD is considered to be mediated by the cumulative effect of several genes (Sims et al. 2020). Studying the polygenic risk of AD in the fly may be challenging to achieve however, human iPSCs retain genetic background information from their donor and therefore could be used to model the complex genetic architecture of AD. iPSCs generated from humans with high and low polygenic risk could provide a means to study the combined effect of these gene, leading to insights in disease biology and pathological mechanisms involved in AD.

More broadly, research must focus efforts on identifying causal variants in LOAD pathology. Whilst GWAS has identified around 75 genetic loci associated with LOAD to date (Bellenguez et al. 2022), the search for causal AD risk genes and variants requires us to look beyond GWAS. GWAS captures the most common genetic variances through linkage disequilibrium, however a considerable proportion of genetic risk remains undetected. Additionally, many of the disease associated variants reside in non-coding regions, making it harder to interpret their contribution in disease risk, as well as determining the causal gene affected by these variants. Typically, disease associated SNPs are assigned to the gene within closest proximity however, it is not always the case that the SNP has a functional interaction or influence on that gene. Fine mapping aims to identify causal cell types, variants and genes in the region of disease association, using a set of statistical methods and integration of epigenetic, transcriptomic and proteomic data (Novikova et al. 2021). Fine mapping is therefore an essential component of post GWAS analysis that can be used to nominate candidate causal genes for further testing in *in vitro/in vivo* models (Schwartzentruber et al. 2021).

Whilst GWAS will undoubtedly identify more associations through increased sample sizes and greater power in the future, rare or low frequency variants are less likely to be detected through GWAS, which targets common variants. Next generation sequencing technologies such as whole genome and exome sequencing have been the primary method for detection of rare genetic variants (population frequency less than 1%), and have successfully identified a number of rare protein coding variants associated with AD (Guerreiro et al. 2013; Jonsson et al. 2012; Jonsson et al. 2013; Cruchaga et al. 2014; Bis et al. 2018). Despite the successes of whole genome and exome sequencing, the high costs of these technologies prohibit broad use within the field. Strategies to circumvent the expenses of sequencing include targeted sequencing, exome arrays and selection of highly informative subjects ie: members from multiply affected families, specific populations with low heterogeneity or extremes of the phenotypes. Exome-wide microarrays in particular have been a promising approach for rare variant detection, with the advantage of identifying SNPs within the protein coding portion of the genome. These coding variations are not only easier to functionally characterise but are also expected to have larger effect sizes than GWAS loci. Although limited to known variants selected from whole exome sequencing studies, this approach was successfully used by Sims and colleagues to identify novel AD coding variants in TREM2, ABI3 and PLCG2 (Sims et al. 2017) Despite their small statistical effect, these variants have shown important biological implications of disease relevance (Yeh et al. 2016; Ulland et al. 2017; Krasemann et al. 2017; Magno et al. 2019; Maguire et al. 2021).

Finally, bridging the gap between genetic association and mechanistic insight requires functional studies in appropriate *in vivo/in vitro* models. This thesis has importantly demonstrated flies are a valuable high throughput tool for characterising conserved AD risk genes, determining their roles across physiology and AD related pathology. Other functional studies of AD risk loci in flies have revealed mechanistic insight into risk genes such as *BIN1*, *PICALM* and *PTK2B*, providing further evidence of the value fly models have in validating genetic association from GWAS and uncovering underlying mechanisms of AD (Dourlen et al. 2017; Yu et al. 2020; Lambert et al. 2022). However, the fly model is not suited to studying all genetic risk in AD, as some of the risk genes such as TREM2 and CD33 are not conserved in the fly. Instead, mouse and human iPSC models have been invaluable for functional studies with these genes (Griciuc et al. 2013, 2019; Krasemann et al. 2017; Zhong et al. 2017). Overall functional genomics has revealed important pathways involved in AD such as immunity, endocytosis, lipid metabolism, Aβ and tau processing and ubiquitination (Jones et al. 2010; Hardy et al. 2014). Future studies should take an integrated multi-omics approach, using a wide range of model systems to establish and accelerate the understanding of mechanisms that underlie complex diseases such as AD.

Bibliography

Akalal, D.-B. G., Wilson, C. F., Zong, L., Tanaka, N. K., Ito, K., & Davis, R. L. (2006a). Roles for *Drosophila* mushroom body neurons in olfactory learning and memory. *Learning & Memory*, *13*(5), 659–668. https://doi.org/10.1101/lm.221206

Akalal, D.-B. G., Wilson, C. F., Zong, L., Tanaka, N. K., Ito, K., & Davis, R. L. (2006b). Roles for *Drosophila* mushroom body neurons in olfactory learning and memory. *Learning & Memory*, *13*(5), 659–668. https://doi.org/10.1101/lm.221206

Akiyama, H., Barger, S., Barnum, S., Bradt, B., Bauer, J., Cole, G. M., Cooper, N. R., Eikelenboom, P., Emmerling, M., Fiebich, B. L., Finch, C. E., Frautschy, S., Griffin, W. S. T., Hampel, H., Hull, M., Landreth, G., Lue, L. F., Mrak, R., MacKenzie, I. R., … Wyss-Coray, T. (2000). Inflammation and Alzheimer's disease. *Neurobiology of Aging*, *21*(3), 383. https://doi.org/10.1016/S0197-4580(00)00124-X

Al-Anzi, B., Armand, E., Nagamei, P., Olszewski, M., Sapin, V., Waters, C., Zinn, K., Wyman, R. J., & Benzer, S. (2010). The Leucokinin Pathway and Its Neurons Regulate Meal Size in Drosophila. *Current Biology*, *20*(11), 969–978. https://doi.org/10.1016/j.cub.2010.04.039

Ali, Y. O., Escala, W., Ruan, K., & Zhai, R. G. (2011). Assaying locomotor, learning, and memory deficits in Drosophila models of neurodegeneration. *Journal of Visualized Experiments*, *49*. https://doi.org/10.3791/2504

Allen, M., Carrasquillo, M. M., Funk, C., Heavner, B. D., Zou, F., Younkin, C. S., Burgess, J. D., Chai, H.-S., Crook, J., Eddy, J. A., Li, H., Logsdon, B., Peters, M. A., Dang, K. K., Wang, X., Serie, D., Wang, C., Nguyen, T., Lincoln, S., … Ertekin-Taner, N. (2016). Human whole genome genotype and transcriptome data for Alzheimer's and other neurodegenerative diseases. *Scientific Data*, *3*(1), 160089. https://doi.org/10.1038/sdata.2016.89

Ambegaokar, S. S., & Jackson, G. R. (2011). Functional genomic screen and network analysis reveal novel modifiers of tauopathy dissociated from tau phosphorylation. *Human Molecular Genetics*, *20*(24), 4947–4977. https://doi.org/10.1093/hmg/ddr432

An, W.-L., Cowburn, R. F., Li, L., Braak, H., Alafuzoff, I., Iqbal, K., Iqbal, I.-G., Winblad, B., & Pei, J.-J. (2003). Up-Regulation of Phosphorylated/Activated p70 S6 Kinase and Its Relationship to Neurofibrillary Pathology in Alzheimer's Disease. *The American Journal of Pathology*, *163*(2), 591–607. https://doi.org/10.1016/S0002-9440(10)63687-5

Andreone, B. J., Przybyla, L., Llapashtica, C., Rana, A., Davis, S. S., van Lengerich, B., Lin, K., Shi, J., Mei, Y., Astarita, G., Di Paolo, G., Sandmann, T., Monroe, K. M., & Lewcock, J. W. (2020). Alzheimer's-associated PLCγ2 is a signaling node required for both TREM2 function and the inflammatory response in human microglia. *Nature Neuroscience*, *23*(8), 927–938. https://doi.org/10.1038/S41593-020-0650-6

Andrews, S. J., Fulton-Howard, B., & Goate, A. (2019). Protective Variants in Alzheimer's Disease. *Current Genetic Medicine Reports*, *7*(1), 1. https://doi.org/10.1007/S40142-019-0156-2

Anstey, K. J., Peters, R., Mortby, M. E., Kiely, K. M., Eramudugolla, R., Cherbuin, N., Huque, M. H., & Dixon, R. A. (2021). Association of sex differences in dementia risk factors with sex differences

in memory decline in a population-based cohort spanning 20–76 years. *Scientific Reports*, *11*(1), 7710. https://doi.org/10.1038/s41598-021-86397-7

Arancio, O. (2008). PIP2: a new key player in Alzheimer's disease. *Cellscience*, *5*(1), 44–47.

Araque, A., & Navarrete, M. (2010). Glial cells in neuronal network function. *Philosophical Transactions of the Royal Society B: Biological Sciences*, *365*(1551), 2375–2381. https://doi.org/10.1098/rstb.2009.0313

Arregui, A., Perry, E. K., Rossor, M., & Tomlinson, B. E. (1982). Angiotensin Converting Enzyme in Alzheimer's Disease: Increased Activity in Caudate Nucleus and Cortical Areas. *Journal of Neurochemistry*, *38*(5), 1490–1492. https://doi.org/10.1111/j.1471-4159.1982.tb07930.x

Arriagada, P. V., Growdon, J. H., Hedley-Whyte, E. T., & Hyman, B. T. (1992). Neurofibrillary tangles but not senile plaques parallel duration and severity of Alzheimer's disease. *Neurology*, *42*(3), 631–631. https://doi.org/10.1212/WNL.42.3.631

Assali, A., Harrington, A. J., & Cowan, C. W. (2019). Emerging roles for MEF2 in brain development and mental disorders. *Current Opinion in Neurobiology*, *59*, 49–58. https://doi.org/10.1016/j.conb.2019.04.008

Awasaki, T., Lai, S.-L., Ito, K., & Lee, T. (2008). Organization and Postembryonic Development of Glial Cells in the Adult Central Brain of Drosophila. *Journal of Neuroscience*, *28*(51), 13742–13753. https://doi.org/10.1523/JNEUROSCI.4844-08.2008

Azman, K. F., & Zakaria, R. (2022). Recent Advances on the Role of Brain-Derived Neurotrophic Factor (BDNF) in Neurodegenerative Diseases. *International Journal of Molecular Sciences*, *23*(12), 6827. https://doi.org/10.3390/ijms23126827

Bales, K. R., Verina, T., Dodel, R. C., Du, Y., Altstiel, L., Bender, M., Hyslop, P., Johnstone, E. M., Little, S. P., Cummins, D. J., Piccardo, P., Ghetti, B., & Paul, S. M. (1997). Lack of apolipoprotein E dramatically reduces amyloid β-peptide deposition. *Nature Genetics*, *17*(3), 263–264. https://doi.org/10.1038/ng1197-263

Balla, T., & Várnai, P. (2002). Visualizing Cellular Phosphoinositide Pools with GFP-Fused Protein-Modules. *Science's STKE*, *2002*(125). https://doi.org/10.1126/stke.2002.125.pl3

Bamberger, M. E., Harris, M. E., McDonald, D. R., Husemann, J., & Landreth, G. E. (2003). A cell surface receptor complex for fibrillar beta-amyloid mediates microglial activation. *The Journal of Neuroscience : The Official Journal of the Society for Neuroscience*, *23*(7), 2665–2674. https://doi.org/10.1523/JNEUROSCI.23-07-02665.2003

Barbosa, A. C., Kim, M.-S., Ertunc, M., Adachi, M., Nelson, E. D., McAnally, J., Richardson, J. A., Kavalali, E. T., Monteggia, L. M., Bassel-Duby, R., & Olson, E. N. (2008). MEF2C, a transcription factor that facilitates learning and memory by negative regulation of synapse numbers and function. *Proceedings of the National Academy of Sciences*, *105*(27), 9391–9396. https://doi.org/10.1073/pnas.0802679105

Barroeta-Espar, I., Weinstock, L. D., Perez-Nievas, B. G., Meltzer, A. C., Siao Tick Chong, M., Amaral, A. C., Murray, M. E., Moulder, K. L., Morris, J. C., Cairns, N. J., Parisi, J. E., Lowe, V. J., Petersen, R. C., Kofler, J., Ikonomovic, M. D., López, O., Klunk, W. E., Mayeux, R. P., Frosch, M. P., … Gomez-Isla, T. (2019). Distinct cytokine profiles in human brains resilient to Alzheimer's pathology. *Neurobiology of Disease*, *121*, 327–337. https://doi.org/10.1016/j.nbd.2018.10.009

Bateman, R. J., Xiong, C., Benzinger, T. L. S., Fagan, A. M., Goate, A., Fox, N. C., Marcus, D. S., Cairns, N. J., Xie, X., Blazey, T. M., Holtzman, D. M., Santacruz, A., Buckles, V., Oliver, A., Moulder, K., Aisen, P. S., Ghetti, B., Klunk, W. E., McDade, E., … Morris, J. C. (2012). Clinical and biomarker changes in dominantly inherited Alzheimer's disease. *The New England Journal of Medicine*, *367*(9), 795–804. https://doi.org/10.1056/NEJMOA1202753

Bellenguez, C., Küçükali, F., Jansen, I. E., Kleineidam, L., Moreno-Grau, S., Amin, N., Naj, A. C., Campos-Martin, R., Grenier-Boley, B., Andrade, V., Holmans, P. A., Boland, A., Damotte, V., van der Lee, S. J., Costa, M. R., Kuulasmaa, T., Yang, Q., de Rojas, I., Bis, J. C., … Lambert, J.-C. (2022). New insights into the genetic etiology of Alzheimer's disease and related dementias. *Nature Genetics*, *54*(4), 412–436. https://doi.org/10.1038/s41588-022-01024-z

Bemiller, S. M., McCray, T. J., Allan, K., Formica, S. V., Xu, G., Wilson, G., Kokiko-Cochran, O. N., Crish, S. D., Lasagna-Reeves, C. A., Ransohoff, R. M., Landreth, G. E., & Lamb, B. T. (2017). TREM2 deficiency exacerbates tau pathology through dysregulated kinase signaling in a mouse model of tauopathy. *Molecular Neurodegeneration*, *12*(1), 74. https://doi.org/10.1186/s13024-017-0216-6

Benarroch, E. E. (2013). Microglia: Multiple roles in surveillance, circuit shaping, and response to injury. *Neurology*, *81*(12), 1079–1088. https://doi.org/10.1212/WNL.0B013E3182A4A577

Benzer, S. (1967). Behavioral Mutants of Drosophila Isolated by Countercurrent Distribution. *Proceedings of the National Academy of Sciences*, *58*(3), 1112–1119. https://doi.org/10.1073/pnas.58.3.1112

Berman, D. E., Dall'Armi, C., Voronov, S. V, McIntire, L. B. J., Zhang, H., Moore, A. Z., Staniszewski, A., Arancio, O., Kim, T.-W., & Di Paolo, G. (2008). Oligomeric amyloid-β peptide disrupts phosphatidylinositol-4,5-bisphosphate metabolism. *Nature Neuroscience*, *11*(5), 547–554. https://doi.org/10.1038/nn.2100

Bertram, L., Lange, C., Mullin, K., Parkinson, M., Hsiao, M., Hogan, M. F., Schjeide, B. M. M., Hooli, B., DiVito, J., Ionita, I., Jiang, H., Laird, N., Moscarillo, T., Ohlsen, K. L., Elliott, K., Wang, X., Hu-Lince, D., Ryder, M., Murphy, A., … Tanzi, R. E. (2008). Genome-wide Association Analysis Reveals Putative Alzheimer's Disease Susceptibility Loci in Addition to APOE. *The American Journal of Human Genetics*, *83*(5), 623–632. https://doi.org/10.1016/j.ajhg.2008.10.008

Bilak, H., Tauszig-Delamasure, S., & Imler, J.-L. (2003). Toll and Toll-like receptors in Drosophila. *Biochemical Society Transactions*, *31*(3), 648–651. https://doi.org/10.1042/bst0310648

Bis, J. C., Jian, X., Kunkle, B. W., Chen, Y., Hamilton-Nelson, K. L., Bush, W. S., Salerno, W. J., Lancour, D., Ma, Y., Renton, A. E., Marcora, E., Farrell, J. J., Zhao, Y., Qu, L., Ahmad, S., Amin, N., Amouyel, P., Beecham, G. W., Below, J. E., … Farrer, L. A. (2018). Whole exome sequencing study identifies novel rare and common Alzheimer's-Associated variants involved in immune response and transcriptional regulation. *Molecular Psychiatry 2018 25:8*, *25*(8), 1859–1875. https://doi.org/10.1038/s41380-018-0112-7

Bischof, J., Björklund, M., Furger, E., Schertel, C., Taipale, J., & Basler, K. (2013). A versatile platform for creating a comprehensive UAS-ORFeome library in *Drosophila*. *Development*, *140*(11), 2434–2442. https://doi.org/10.1242/dev.088757

Bloomquist, B. T., Shortridge, R. D., Schneuwly, S., Perdew, M., Montell, C., Steller, H., Rubin, G., & Pak, W. L. (1988). Isolation of a putative phospholipase c gene of drosophila, norpA, and its role in phototransduction. *Cell*, *54*(5), 723–733. https://doi.org/10.1016/S0092-8674(88)80017-5

Bolkan, B. J., Triphan, T., & Kretzschmar, D. (2012). -Secretase Cleavage of the Fly Amyloid Precursor Protein Is Required for Glial Survival. *Journal of Neuroscience*, *32*(46), 16181–16192. https://doi.org/10.1523/JNEUROSCI.0228-12.2012

Booth, G. E., Kinrade, E. F., & Hidalgo, A. (2000). Glia maintain follower neuron survival during Drosophila CNS development. *Development*, *127*(2), 237–244. https://doi.org/10.1242/dev.127.2.237

Borchelt, D. R., Ratovitski, T., van Lare, J., Lee, M. K., Gonzales, V., Jenkins, N. A., Copeland, N. G., Price, D. L., & Sisodia, S. S. (1997). Accelerated Amyloid Deposition in the Brains of Transgenic Mice Coexpressing Mutant Presenilin 1 and Amyloid Precursor Proteins. *Neuron*, *19*(4), 939–945. https://doi.org/10.1016/S0896-6273(00)80974-5

Botelho, R. J., Teruel, M., Dierckman, R., Anderson, R., Wells, A., York, J. D., Meyer, T., & Grinstein, S. (2000). Localized Biphasic Changes in Phosphatidylinositol-4,5-Bisphosphate at Sites of Phagocytosis. *The Journal of Cell Biology*, *151*(7), 1353–1367. http://www.jcb.org/cgi/content/full/151/7/1353

Bour, B. A., O'Brien, M. A., Lockwood, W. L., Goldstein, E. S., Bodmer, R., Taghert, P. H., Abmayr, S. M., & Nguyen, H. T. (1995). Drosophila MEF2, a transcription factor that is essential for myogenesis. *Genes & Development*, *9*(6), 730–741. https://doi.org/10.1101/gad.9.6.730

Boyarko, B., & Hook, V. (2021). Human Tau Isoforms and Proteolysis for Production of Toxic Tau Fragments in Neurodegeneration. *Frontiers in Neuroscience*, *15*. https://doi.org/10.3389/fnins.2021.702788

Braak, H., & Braak, E. (1991). Neuropathological stageing of Alzheimer-related changes. *Acta Neuropathologica*, *82*(4), 239–259. https://doi.org/10.1007/BF00308809

Braak, H., & Braak, E. (1995). Staging of alzheimer's disease-related neurofibrillary changes. *Neurobiology of Aging*, *16*(3), 271–278. https://doi.org/10.1016/0197-4580(95)00021-6

Brand, A. H., & Perrimon, N. (1993). Targeted gene expression as a means of altering cell fates and generating dominant phenotypes. *Development*, *118*(2), 401–415. https://doi.org/10.1242/dev.118.2.401

Brazil, D. P., Yang, Z.-Z., & Hemmings, B. A. (2004). Advances in protein kinase B signalling: AKTion on multiple fronts. *Trends in Biochemical Sciences*, *29*(5), 233–242. https://doi.org/10.1016/j.tibs.2004.03.006

Breijyeh, Z., Karaman, R., Muñoz-Torrero, D., & Dembinski, R. (2020). Comprehensive Review on Alzheimer's Disease: Causes and Treatment. *Molecules 2020, Vol. 25, Page 5789*, *25*(24), 5789. https://doi.org/10.3390/MOLECULES25245789

Brody, D. L., Jiang, H., Wildburger, N., & Esparza, T. J. (2017). Non-canonical soluble amyloid-beta aggregates and plaque buffering: controversies and future directions for target discovery in Alzheimer's disease. *Alzheimer's Research & Therapy*, *9*(1). https://doi.org/10.1186/S13195-017-0293-3

Brouwers, N., Sleegers, K., & Van Broeckhoven, C. (2008). Molecular genetics of Alzheimer's disease: An update. *Annals of Medicine*, *40*(8), 562–583. https://doi.org/10.1080/07853890802186905

Buerger, K., Ewers, M., Pirttila, T., Zinkowski, R., Alafuzoff, I., Teipel, S. J., DeBernardis, J., Kerkman, D., McCulloch, C., Soininen, H., & Hampel, H. (2006). CSF phosphorylated tau protein correlates with neocortical neurofibrillary pathology in Alzheimer's disease. *Brain*, *129*(11), 3035–3041. https://doi.org/10.1093/brain/awl269

Caccamo, A., Majumder, S., Richardson, A., Strong, R., & Oddo, S. (2010). Molecular Interplay between Mammalian Target of Rapamycin (mTOR), Amyloid-β, and Tau. *Journal of Biological Chemistry*, *285*(17), 13107–13120. https://doi.org/10.1074/jbc.M110.100420

Cao, W., Song, H.-J., Gangi, T., Kelkar, A., Antani, I., Garza, D., & Konsolaki, M. (2008). Identification of Novel Genes That Modify Phenotypes Induced by Alzheimer's β-Amyloid Overexpression in Drosophila. *Genetics*, *178*(3), 1457–1471. https://doi.org/10.1534/genetics.107.078394

Carmine-Simmen, K., Proctor, T., Tschäpe, J., Poeck, B., Triphan, T., Strauss, R., & Kretzschmar, D. (2009). Neurotoxic effects induced by the Drosophila amyloid-β peptide suggest a conserved toxic function. *Neurobiology of Disease*, *33*(2), 274–281. https://doi.org/10.1016/j.nbd.2008.10.014

Casas-Tinto, S., Zhang, Y., Sanchez-Garcia, J., Gomez-Velazquez, M., Rincon-Limas, D. E., & Fernandez-Funez, P. (2011). The ER stress factor XBP1s prevents amyloid-β neurotoxicity. *Human Molecular Genetics*, *20*(11), 2144–2160. https://doi.org/10.1093/HMG/DDR100

Casci, I., & Pandey, U. B. (2015). A fruitful endeavor: Modeling ALS in the fruit fly. *Brain Research*, *1607*, 47–74. https://doi.org/10.1016/j.brainres.2014.09.064

Castellano, J. M., Kim, J., Stewart, F. R., Jiang, H., DeMattos, R. B., Patterson, B. W., Fagan, A. M., Morris, J. C., Mawuenyega, K. G., Cruchaga, C., Goate, A. M., Bales, K. R., Paul, S. M., Bateman, R. J., & Holtzman, D. M. (2011). Human apoE Isoforms Differentially Regulate Brain Amyloid- Peptide Clearance. *Science Translational Medicine*, *3*(89), 89ra57–89ra57. https://doi.org/10.1126/scitranslmed.3002156

Castillo, E., Leon, J., Mazzei, G., Abolhassani, N., Haruyama, N., Saito, T., Saido, T., Hokama, M., Iwaki, T., Ohara, T., Ninomiya, T., Kiyohara, Y., Sakumi, K., LaFerla, F. M., & Nakabeppu, Y. (2017). Comparative profiling of cortical gene expression in Alzheimer's disease patients and mouse models demonstrates a link between amyloidosis and neuroinflammation. *Scientific Reports*, *7*(1), 17762. https://doi.org/10.1038/s41598-017-17999-3

Cedazo-Mínguez, A. (2007). Apolipoprotein E and Alzheimer's disease: molecular mechanisms and therapeutic opportunities. *Journal of Cellular and Molecular Medicine*, *11*(6), 1227–1238. https://doi.org/10.1111/j.1582-4934.2007.00130.x

Chatterjee, S., Sang, T. K., Lawless, G. M., & Jackson, G. R. (2009). Dissociation of tau toxicity and phosphorylation: role of GSK-3β, MARK and Cdk5 in a Drosophila model. *Human Molecular Genetics*, *18*(1), 164. https://doi.org/10.1093/HMG/DDN326

Chell, J. M., & Brand, A. H. (2010). Nutrition-Responsive Glia Control Exit of Neural Stem Cells from Quiescence. *Cell*, *143*(7), 1161–1173. https://doi.org/10.1016/j.cell.2010.12.007

Chen, G. F., Xu, T. H., Yan, Y., Zhou, Y. R., Jiang, Y., Melcher, K., & Xu, H. E. (2017). Amyloid beta: Structure, biology and structure-based therapeutic development. In *Acta Pharmacologica*

Sinica (Vol. 38, Issue 9, pp. 1205–1235). Nature Publishing Group. https://doi.org/10.1038/aps.2017.28

Chen, X., Li, Y., Huang, J., Cao, D., Yang, G., Liu, W., Lu, H., & Guo, A. (2007). Study of tauopathies by comparing Drosophila and human tau in Drosophila. *Cell and Tissue Research*, *329*(1), 169–178. https://doi.org/10.1007/s00441-007-0401-y

Chong, Z. Z., Shang, Y. C., Wang, S., & Maiese, K. (2012). A critical kinase cascade in neurological disorders: PI3K, Akt and mTOR. *Future Neurology*, *7*(6), 733–748. https://doi.org/10.2217/fnl.12.72

Chow, V. W., Mattson, M. P., Wong, P. C., & Gleichmann, M. (2010). An Overview of APP Processing Enzymes and Products. *NeuroMolecular Medicine*, *12*(1), 1–12. https://doi.org/10.1007/s12017-009-8104-z

Cifuentes, M. E., Delaney, T., & Rebecchi, M. J. (1994). D-myo-inositol 1,4,5-trisphosphate inhibits binding of phospholipase C-delta 1 to bilayer membranes. *Journal of Biological Chemistry*, *269*(3), 1945–1948. https://doi.org/10.1016/S0021-9258(17)42118-1

Citron, M., Oltersdorf, T., Haass, C., McConlogue, L., Hung, A. Y., Seubert, P., Vigo-Pelfrey, C., Lieberburg, I., & Selkoe, D. J. (1992). Mutation of the β-amyloid precursor protein in familial Alzheimer's disease increases β-protein production. *Nature*, *360*(6405), 672–674. https://doi.org/10.1038/360672a0

Claes, C., England, W. E., Danhash, E. P., Kiani Shabestari, S., Jairaman, A., Chadarevian, J. P., Hasselmann, J., Tsai, A. P., Coburn, M. A., Sanchez, J., Lim, T. E., Hidalgo, J. L. S., Tu, C., Cahalan, M. D., Lamb, B. T., Landreth, G. E., Spitale, R. C., Blurton-Jones, M., & Davtyan, H. (2022). The P522R protective variant of PLCG2 promotes the expression of antigen presentation genes by human microglia in an Alzheimer's disease mouse model. *Alzheimer's & Dementia*. https://doi.org/10.1002/ALZ.12577

Clark, I. E., Dodson, M. W., Jiang, C., Cao, J. H., Huh, J. R., Seol, J. H., Yoo, S. J., Hay, B. A., & Guo, M. (2006). Drosophila pink1 is required for mitochondrial function and interacts genetically with parkin. *Nature*, *441*(7097), 1162–1166. https://doi.org/10.1038/nature04779

Clark, R. I., Tan, S. W. S., Péan, C. B., Roostalu, U., Vivancos, V., Bronda, K., Pilátová, M., Fu, J., Walker, D. W., Berdeaux, R., Geissmann, F., & Dionne, M. S. (2013). MEF2 Is an In Vivo Immune-Metabolic Switch. *Cell*, *155*(2), 435–447. https://doi.org/10.1016/j.cell.2013.09.007

Cohen, A. D., & Klunk, W. E. (2014). Early detection of Alzheimer's disease using PiB and FDG PET. *Neurobiology of Disease*, *72*, 117–122. https://doi.org/10.1016/j.nbd.2014.05.001

Corbin, J. A., Dirkx, R. A., & Falke, J. J. (2004). GRP1 Pleckstrin Homology Domain: Activation Parameters and Novel Search Mechanism for Rare Target Lipid. *Biochemistry*, *43*(51), 16161–16173. https://doi.org/10.1021/bi049017a

Corder, E. H., Saunders, A. M., Strittmatter, W. J., Schmechel, D. E., Gaskell, P. C., Small, G. W., Roses, A. D., Haines, J. L., & Pericak-Vance, M. A. (1993). Gene dose of apolipoprotein E type 4 allele and the risk of Alzheimer's disease in late onset families. *Science (New York, N.Y.)*, *261*(5123), 921–923. http://www.ncbi.nlm.nih.gov/pubmed/8346443

Cremona, O., Di Paolo, G., Wenk, M. R., Lüthi, A., Kim, W. T., Takei, K., Daniell, L., Nemoto, Y., Shears, S. B., Flavell, R. A., McCormick, D. A., & De Camilli, P. (1999). Essential Role of Phosphoinositide

Metabolism in Synaptic Vesicle Recycling. *Cell*, *99*(2), 179–188. https://doi.org/10.1016/S0092-8674(00)81649-9

Crittenden, J. R., Skoulakis, E. M. C., Goldstein, Elliott. S., & Davis, R. L. (2018). Drosophila mef2 is essential for normal mushroom body and wing development. *Biology Open*. https://doi.org/10.1242/bio.035618

Crowther, D. C., Kinghorn, K. J., Miranda, E., Page, R., Curry, J. A., Duthie, F. A. I., Gubb, D. C., & Lomas, D. A. (2005). Intraneuronal Aβ, non-amyloid aggregates and neurodegeneration in a Drosophila model of Alzheimer's disease. *Neuroscience*, *132*(1), 123–135. https://doi.org/10.1016/j.neuroscience.2004.12.025

Cruchaga, C., Karch, C. M., Jin, S. C., Benitez, B. A., Cai, Y., Guerreiro, R., Harari, O., Norton, J., Budde, J., Bertelsen, S., Jeng, A. T., Cooper, B., Skorupa, T., Carrell, D., Levitch, D., Hsu, S., Choi, J., Ryten, M., Hardy, J., … Goate, A. M. (2014). Rare coding variants in the phospholipase D3 gene confer risk for Alzheimer's disease. *Nature*, *505*(7484), 550–554. https://doi.org/10.1038/nature12825

Cuddy, L. K., Prokopenko, D., Cunningham, E. P., Brimberry, R., Song, P., Kirchner, R., Chapman, B. A., Hofmann, O., Hide, W., Procissi, D., Hanania, T., Leiser, S. C., Tanzi, R. E., & Vassar, R. (2020). Aβ-accelerated neurodegeneration caused by Alzheimer's-associated *ACE* variant R1279Q is rescued by angiotensin system inhibition in mice. *Science Translational Medicine*, *12*(563). https://doi.org/10.1126/scitranslmed.aaz2541

Czech, M. P. (2000). PIP2 and PIP3. *Cell*, *100*(6), 603–606. https://doi.org/10.1016/S0092-8674(00)80696-0

Dagda, R. K., Cherra, S. J., Kulich, S. M., Tandon, A., Park, D., & Chu, C. T. (2009). Loss of PINK1 function promotes mitophagy through effects on oxidative stress and mitochondrial fission. *The Journal of Biological Chemistry*, *284*(20), 13843–13855. https://doi.org/10.1074/JBC.M808515200

Daigle, I., & Li, C. (1993). apl-1, a Caenorhabditis elegans gene encoding a protein related to the human beta-amyloid protein precursor. *Proceedings of the National Academy of Sciences*, *90*(24), 12045–12049. https://doi.org/10.1073/pnas.90.24.12045

Dall'Armi, C., Devereaux, K. A., & Di Paolo, G. (2013). The Role of Lipids in The Control of Autophagy. *Current Biology : CB*, *23*(1), R33. https://doi.org/10.1016/J.CUB.2012.10.041

Dan L Lindsley, & Georgianna G Zimm. (1992). *The Genome of Drosophila Melanogaster*. Academic Press. https://books.google.co.uk/books?hl=en&lr=&id=sklm5UmoGykC&oi=fnd&pg=PP1&ots=g6a50nnF1W&sig=202tLO2c7OrZfvBHKShnTUA-DW8&redir_esc=y#v=onepage&q&f=false

Datta, S. R., Brunet, A., & Greenberg, M. E. (1999). Cellular survival: a play in three Akts. *Cold Spring Harbor Laboratory Press*. www.genesdev.org

De Gregorio, E., Spellman, P. T., Tzou, P., Rubin, G. M., & Lemaitre, B. (2002). The Toll and Imd pathways are the major regulators of the immune response in Drosophila. *The EMBO Journal*, *21*(11), 2568. https://doi.org/10.1093/EMBOJ/21.11.2568

De Loof, A., & Schoofs, L. (2019). Alzheimer's Disease: Is a Dysfunctional Mevalonate Biosynthetic Pathway the Master-Inducer of Deleterious Changes in Cell Physiology? *OBM Neurobiology*, *3*(4), 1–1. https://doi.org/10.21926/obm.neurobiol.1904046

De Strooper, B., Saftig, P., Craessaerts, K., Vanderstichele, H., Guhde, G., Annaert, W., Von Figura, K., & Van Leuven, F. (1998). Deficiency of presenilin-1 inhibits the normal cleavage of amyloid precursor protein. *Nature*, *391*(6665), 387–390. https://doi.org/10.1038/34910

Deczkowska, A., Matcovitch-Natan, O., Tsitsou-Kampeli, A., Ben-Hamo, S., Dvir-Szternfeld, R., Spinrad, A., Singer, O., David, E., Winter, D. R., Smith, L. K., Kertser, A., Baruch, K., Rosenzweig, N., Terem, A., Prinz, M., Villeda, S., Citri, A., Amit, I., & Schwartz, M. (2017). Mef2C restrains microglial inflammatory response and is lost in brain ageing in an IFN-I-dependent manner. *Nature Communications*, *8*(1), 717. https://doi.org/10.1038/s41467-017-00769-0

Delestro, F., Scheunemann, L., Pedrazzani, M., Tchenio, P., Preat, T., & Genovesio, A. (2020). In vivo large-scale analysis of Drosophila neuronal calcium traces by automated tracking of single somata. *Scientific Reports*, *10*(1), 7153. https://doi.org/10.1038/s41598-020-64060-x

Desai, A. K., & Grossberg, G. T. (2005). *Diagnosis and treatment of Alzheimer's disease*. https://pdfs.semanticscholar.org/cc35/4465e6d6192a716e52eb56733dc0f45bae34.pdf

Desale, S. E., & Chinnathambi, S. (2021). Phosphoinositides signaling modulates microglial actin remodeling and phagocytosis in Alzheimer's disease. *Cell Communication and Signaling*, *19*(1), 28. https://doi.org/10.1186/s12964-021-00715-0

De Strooper, B., & Karran, E. (2016). The Cellular Phase of Alzheimer's Disease. *Cell*, *164*(4), 603–615. https://doi.org/10.1016/j.cell.2015.12.056

Deture, M. A., & Dickson, D. W. (2019). The neuropathological diagnosis of Alzheimer's disease. *Molecular Neurodegeneration 2019 14:1*, *14*(1), 1–18. https://doi.org/10.1186/S13024-019-0333-5

Diao, F., Ironfield, H., Luan, H., Diao, F., Shropshire, W. C., Ewer, J., Marr, E., Potter, C. J., Landgraf, M., & White, B. H. (2015). Plug-and-Play Genetic Access to Drosophila Cell Types using Exchangeable Exon Cassettes. *Cell Reports*, *10*(8), 1410–1421. https://doi.org/10.1016/j.celrep.2015.01.059

Dickson, E. J., & Hille, B. (2019). Understanding phosphoinositides: rare, dynamic, and essential membrane phospholipids. *Biochemical Journal*, *476*(1), 1–23. https://doi.org/10.1042/BCJ20180022

Dietzl, G., Chen, D., Schnorrer, F., Su, K.-C., Barinova, Y., Fellner, M., Gasser, B., Kinsey, K., Oppel, S., Scheiblauer, S., Couto, A., Marra, V., Keleman, K., & Dickson, B. J. (2007). A genome-wide transgenic RNAi library for conditional gene inactivation in Drosophila. *Nature*, *448*(7150), 151–156. https://doi.org/10.1038/nature05954

Dixit, R., Ross, J. L., Goldman, Y. E., & Holzbaur, E. L. F. (2008). Differential Regulation of Dynein and Kinesin Motor Proteins by Tau. *Science*, *319*(5866), 1086–1089. https://doi.org/10.1126/science.1152993

Doherty, J., Logan, M. A., Tasdemir, O. E., & Freeman, M. R. (2009). Ensheathing Glia Function as Phagocytes in the Adult Drosophila Brain. *Journal of Neuroscience*, *29*(15), 4768–4781. https://doi.org/10.1523/JNEUROSCI.5951-08.2009

Dourlen, P., Fernandez-Gomez, F. J., Dupont, C., Grenier-Boley, B., Bellenguez, C., Obriot, H., Caillierez, R., Sottejeau, Y., Chapuis, J., Bretteville, A., Abdelfettah, F., Delay, C., Malmanche, N., Soininen, H., Hiltunen, M., Galas, M.-C., Amouyel, P., Sergeant, N., Buée, L., … Dermaut, B. (2017). Functional screening of Alzheimer risk loci identifies PTK2B as an in vivo modulator and early marker of Tau pathology. *Molecular Psychiatry*, *22*(6), 874–883. https://doi.org/10.1038/mp.2016.59

Drummond, E., & Wisniewski, T. (2017). Alzheimer's Disease: Experimental Models and Reality. *Acta Neuropathologica*, *133*(2), 155. https://doi.org/10.1007/S00401-016-1662-X

Dugina, V., Alieva, I., Khromova, N., Kireev, I., Gunning, P. W., & Kopnin, P. (2016). Interaction of microtubules with the actin cytoskeleton via cross-talk of EB1-containing +TIPs and γ-actin in epithelial cells. *Oncotarget*, *7*(45), 72699–72715. https://doi.org/10.18632/oncotarget.12236

Duriez, B., Duquesnoy, P., Escudier, E., Bridoux, A. M., Escalier, D., Rayet, I., Marcos, E., Vojtek, A. M., Bercher, J. F., & Amselem, S. (2007). A common variant in combination with a nonsense mutation in a member of the thioredoxin family causes primary ciliary dyskinesia. *Proceedings of the National Academy of Sciences of the United States of America*, *104*(9), 3336–3341. https://doi.org/10.1073/pnas.0611405104

Ebens, A. J., Garren, H., Cheyette, B. N. R., & Zipursky, S. L. (1993). The Drosophila anachronism locus: A glycoprotein secreted by glia inhibits neuroblast proliferation. *Cell*, *74*(1), 15–27. https://doi.org/10.1016/0092-8674(93)90291-W

Edbauer, D., Willem, M., Lammich, S., Steiner, H., & Haass, C. (2002). Insulin-degrading Enzyme Rapidly Removes the β-Amyloid Precursor Protein Intracellular Domain (AICD). *Journal of Biological Chemistry*, *277*(16), 13389–13393. https://doi.org/10.1074/jbc.M111571200

Edison, P., Archer, H. A., Hinz, R., Hammers, A., Pavese, N., Tai, Y. F., Hotton, G., Cutler, D., Fox, N., Kennedy, A., Rossor, M., & Brooks, D. J. (2007). Amyloid, hypometabolism, and cognition in Alzheimer disease: An [11C]PIB and [18F]FDG PET study. *Neurology*, *68*(7), 501–508. https://doi.org/10.1212/01.wnl.0000244749.20056.d4

Efthymiou, A. G., & Goate, A. M. (2017). Late onset Alzheimer's disease genetics implicates microglial pathways in disease risk. *Molecular Neurodegeneration*, *12*(1). https://doi.org/10.1186/S13024-017-0184-X

El Khoury, J. B., Moore, K. J., Means, T. K., Leung, J., Terada, K., Toft, M., Freeman, M. W., & Luster, A. D. (2003). CD36 mediates the innate host response to beta-amyloid. *The Journal of Experimental Medicine*, *197*(12), 1657–1666. https://doi.org/10.1084/JEM.20021546

Elder, G. A., Gama Sosa, M. A., & De Gasperi, R. (2010). Transgenic Mouse Models of Alzheimer's Disease. *Mount Sinai Journal of Medicine: A Journal of Translational and Personalized Medicine*, *77*(1), 69–81. https://doi.org/10.1002/msj.20159

Emori, Y., Sugaya, R., Akimaru, H., Higashijima, S., Shishido, E., Saigo, K., & Homma, Y. (1994). Drosophila phospholipase C-gamma expressed predominantly in blastoderm cells at cellularization and in endodermal cells during later embryonic stages. *Journal of Biological Chemistry*, *269*(30), 19474–19479. https://doi.org/10.1016/S0021-9258(17)32193-2

Ennerfelt, H., Frost, E. L., Shapiro, D. A., Holliday, C., Zengeler, K. E., Voithofer, G., Bolte, A. C., Lammert, C. R., Kulas, J. A., Ulland, T. K., & Lukens, J. R. (2022). SYK coordinates

neuroprotective microglial responses in neurodegenerative disease. *Cell*, *185*(22), 4135-4152.e22. https://doi.org/10.1016/j.cell.2022.09.030

Eriksen, J. L., Sagi, S. A., Smith, T. E., Weggen, S., Das, P., McLendon, D. C., Ozols, V. V., Jessing, K. W., Zavitz, K. H., Koo, E. H., & Golde, T. E. (2003). NSAIDs and enantiomers of flurbiprofen target γ-secretase and lower Aβ42 in vivo. *Journal of Clinical Investigation*, *112*(3), 440–449. https://doi.org/10.1172/JCI18162

Ernest James Phillips, T., & Maguire, E. (2021). Phosphoinositides: Roles in the Development of Microglial-Mediated Neuroinflammation and Neurodegeneration. *Frontiers in Cellular Neuroscience*, *15*. https://doi.org/10.3389/fncel.2021.652593

Escott-Price, V., Sims, R., Bannister, C., Harold, D., Vronskaya, M., Majounie, E., Badarinarayan, N., Morgan, K., Passmore, P., Holmes, C., Powell, J., Brayne, C., Gill, M., Mead, S., Goate, A., Cruchaga, C., Lambert, J.-C., van Duijn, C., Maier, W., … Williams, J. (2015). Common polygenic variation enhances risk prediction for Alzheimer's disease. *Brain*, *138*(12), 3673–3684. https://doi.org/10.1093/brain/awv268

Esparza, T. J., Wildburger, N. C., Jiang, H., Gangolli, M., Cairns, N. J., Bateman, R. J., & Brody, D. L. (2016). Soluble Amyloid-beta Aggregates from Human Alzheimer's Disease Brains. *Scientific Reports*, *6*(1), 38187. https://doi.org/10.1038/srep38187

Esparza, T. J., Zhao, H., Cirrito, J. R., Cairns, N. J., Bateman, R. J., Holtzman, D. M., & Brody, D. L. (2013). Amyloid-beta oligomerization in Alzheimer dementia versus high-pathology controls. *Annals of Neurology*, *73*(1), 104–119. https://doi.org/10.1002/ana.23748

Fan, Z., Brooks, D. J., Okello, A., & Edison, P. (2017). An early and late peak in microglial activation in Alzheimer's disease trajectory. *Brain : A Journal of Neurology*, *140*(3), 792–803. https://doi.org/10.1093/BRAIN/AWW349

Farrer, L. A. (1997). Effects of Age, Sex, and Ethnicity on the Association Between Apolipoprotein E Genotype and Alzheimer Disease. *JAMA*, *278*(16), 1349. https://doi.org/10.1001/jama.1997.03550160069041

Fay, D. S., Fluet, A., Johnson, C. J., & Link, C. D. (1998). In Vivo Aggregation of β-Amyloid Peptide Variants. *Journal of Neurochemistry*, *71*(4), 1616–1625. https://doi.org/10.1046/j.1471-4159.1998.71041616.x

Feany, M. B., & Bender, W. W. (2000). A Drosophila model of Parkinson's disease. *Nature*, *404*(6776), 394–398. https://doi.org/10.1038/35006074

Fernandez-Funez, P., de Mena, L., & Rincon-Limas, D. E. (2015). Modeling the complex pathology of Alzheimer's disease in Drosophila. *Experimental Neurology*, *274*(0 0), 58. https://doi.org/10.1016/J.EXPNEUROL.2015.05.013

Ferreira-Vieira, T. H., Guimaraes, I. M., Silva, F. R., & Ribeiro, F. M. (2016). Alzheimer's disease: Targeting the Cholinergic System. *Current Neuropharmacology*, *14*(1), 101–115. https://doi.org/10.2174/1570159X13666150716165726

Ferri, C. P., Prince, M., Brayne, C., Brodaty, H., Fratiglioni, L., Ganguli, M., Hall, K., Hasegawa, K., Hendrie, H., Huang, Y., Jorm, A., Mathers, C., Menezes, P. R., Rimmer, E., & Scazufca, M. (2005). Global prevalence of dementia: a Delphi consensus study. *The Lancet*, *366*(9503), 2112–2117. https://doi.org/10.1016/S0140-6736(05)67889-0

Finelli, A., Kelkar, A., Song, H. J., Yang, H., & Konsolaki, M. (2004). A model for studying Alzheimer's Aβ42-induced toxicity in Drosophila melanogaster. *Molecular and Cellular Neuroscience*, *26*(3), 365–375. https://doi.org/10.1016/J.MCN.2004.03.001

Folwell, J., Cowan, C. M., Ubhi, K. K., Shiabh, H., Newman, T. A., Shepherd, D., & Mudher, A. (2010). Aβ exacerbates the neuronal dysfunction caused by human tau expression in a Drosophila model of Alzheimer's disease. *Experimental Neurology*, *223*(2), 401–409. https://doi.org/10.1016/j.expneurol.2009.09.014

Fossgreen, A., Brückner, B., Czech, C., Masters, C. L., Beyreuther, K., & Paro, R. (1998). Transgenic *Drosophila* expressing human amyloid precursor protein show γ-secretase activity and a blistered-wing phenotype. *Proceedings of the National Academy of Sciences*, *95*(23), 13703–13708. https://doi.org/10.1073/pnas.95.23.13703

Franke, T. F., Kaplan, D. R., & Cantley, L. C. (1997). PI3K: Downstream AKTion Blocks Apoptosis. *Cell*, *88*(4), 435–437. https://doi.org/10.1016/S0092-8674(00)81883-8

Freeman, M. R. (2015). Drosophila Central Nervous System Glia. *Cold Spring Harbor Perspectives in Biology*, *7*(11), a020552. https://doi.org/10.1101/cshperspect.a020552

Fu, G., Chen, Y., Yu, M., Podd, A., Schuman, J., He, Y., Di, L., Yassai, M., Haribhai, D., North, P. E., Gorski, J., Williams, C. B., Wang, D., & Wen, R. (2010). Phospholipase Cγ1 is essential for T cell development, activation, and tolerance. *Journal of Experimental Medicine*, *207*(2), 309–318. https://doi.org/10.1084/jem.20090880

Fuentes-Medel, Y., Ashley, J., Barria, R., Maloney, R., Freeman, M., & Budnik, V. (2012). Integration of a Retrograde Signal during Synapse Formation by Glia-Secreted TGF-β Ligand. *Current Biology*, *22*(19), 1831–1838. https://doi.org/10.1016/j.cub.2012.07.063

Games, D., Adams, D., Alessandrini, R., Barbour, R., Borthelette, P., Blackwell, C., Carr, T., Clemens, J., Donaldson, T., Gillespie, F., Guido, T., Hagopian, S., Johnson-Wood, K., Khan, K., Lee, M., Leibowitz, P., Lieberburg, I., Little, S., Masliah, E., … Zhao, J. (1995). Alzheimer-type neuropathology in transgenic mice overexpressing V717F β-amyloid precursor protein. *Nature*, *373*(6514), 523–527. https://doi.org/10.1038/373523a0

Garcia, P., Gupta, R., Shah, S., Morris, A. J., Rudge, S. A., Scarlata, S., Petrova, V., McLaughlin, S., & Rebecchi, M. J. (1995). The pleckstrin homology domain of phospholipase C-.delta.1 binds with high affinity to phosphatidylinositol 4,5-bisphosphate in bilayer membranes. *Biochemistry*, *34*(49), 16228–16234. https://doi.org/10.1021/bi00049a039

Gargano, J. W., Martin, I., Bhandari, P., & Grotewiel, M. S. (2005). Rapid iterative negative geotaxis (RING): A new method for assessing age-related locomotor decline in Drosophila. *Experimental Gerontology*, *40*(5), 386–395. https://doi.org/10.1016/j.exger.2005.02.005

Gaspar, R. C., Villarreal, S. A., Bowles, N., Hepler, R. W., Joyce, J. G., & Shughrue, P. J. (2010). Oligomers of β-amyloid are sequestered into and seed new plaques in the brains of an AD mouse model. *Experimental Neurology*, *223*(2), 394–400. https://doi.org/10.1016/J.EXPNEUROL.2009.09.001

Gatz, M., Reynolds, C. A., Fratiglioni, L., Johansson, B., Mortimer, J. A., Berg, S., Fiske, A., & Pedersen, N. L. (2006). Role of Genes and Environments for Explaining Alzheimer Disease. *Archives of General Psychiatry*, *63*(2), 168. https://doi.org/10.1001/archpsyc.63.2.168

Gaudet, P., Livstone, M. S., Lewis, S. E., & Thomas, P. D. (2011). Phylogenetic-based propagation of functional annotations within the Gene Ontology consortium. *Briefings in Bioinformatics*, *12*(5), 449–462. https://doi.org/10.1093/BIB/BBR042

Gillooly, D. J., Simonsen, A., & Stenmark, H. (2001). Phosphoinositides and phagocytosis. *The Journal of Cell Biology*, *155*(1), 15. https://doi.org/10.1083/JCB.200109001

Ginsberg, S. D., Che, S., Counts, S. E., & Mufson, E. J. (2006). Shift in the ratio of three-repeat tau and four-repeat tau mRNAs in individual cholinergic basal forebrain neurons in mild cognitive impairment and Alzheimer's disease. *Journal of Neurochemistry*, *96*(5), 1401–1408. https://doi.org/10.1111/j.1471-4159.2005.03641.x

Giong, H.-K., Subramanian, M., Yu, K., & Lee, J.-S. (2021). Non-Rodent Genetic Animal Models for Studying Tauopathy: Review of Drosophila, Zebrafish, and C. elegans Models. *International Journal of Molecular Sciences*, *22*(16), 8465. https://doi.org/10.3390/ijms22168465

Glenner, G. G., & Wong, C. W. (1984). Alzheimer's disease and Down's syndrome: Sharing of a unique cerebrovascular amyloid fibril protein. *Biochemical and Biophysical Research Communications*, *122*(3), 1131–1135. https://doi.org/10.1016/0006-291X(84)91209-9

Gloor, G. B., Nassif, N. A., Johnson-Schlitz, D. M., Preston, C. R., & Engels, W. R. (1991). Targeted Gene Replacement in Drosophila Via P Element-Induced Gap Repair. *Science*, *253*(5024), 1110–1117. https://doi.org/10.1126/science.1653452

Goate, A., Chartier-Harlin, M.-C., Mullan, M., Brown, J., Crawford, F., Fidani, L., Giuffra, L., Haynes, A., Irving, N., James, L., Mant, R., Newton, P., Rooke, K., Roques, P., Talbot, C., Pericak-Vance, M., Roses, A., Williamson, R., Rossor, M., … Hardy, J. (1991). Segregation of a missense mutation in the amyloid precursor protein gene with familial Alzheimer's disease. *Nature*, *349*(6311), 704–706. https://doi.org/10.1038/349704a0

Gómez-Isla, T., Hollister, R., West, H., Mui, S., Growdon, J. H., Petersen, R. C., Parisi, J. E., & Hyman, B. T. (1997). Neuronal loss correlates with but exceeds neurofibrillary tangles in Alzheimer's disease. *Annals of Neurology*, *41*(1), 17–24. https://doi.org/10.1002/ana.410410106

Gomez-Nicola, D., Fransen, N. L., Suzzi, S., & Perry, V. H. (2013). Regulation of Microglial Proliferation during Chronic Neurodegeneration. *Journal of Neuroscience*, *33*(6), 2481–2493. https://doi.org/10.1523/JNEUROSCI.4440-12.2013

Govind, S. (2008). Innate immunity in Drosophila: Pathogens and pathways. *Insect Science*, *15*(1), 29–43. https://doi.org/10.1111/j.1744-7917.2008.00185.x

Gratuze, M., Leyns, C. E. G., & Holtzman, D. M. (2018). New insights into the role of TREM2 in Alzheimer's disease. *Molecular Neurodegeneration*, *13*(1), 66. https://doi.org/10.1186/s13024-018-0298-9

Greeve, I., Kretzschmar, D., Tschäpe, J.-A., Beyn, A., Brellinger, C., Schweizer, M., Nitsch, R. M., & Reifegerste, R. (2004). Age-Dependent Neurodegeneration and Alzheimer-Amyloid Plaque Formation in Transgenic Drosophila. *Journal of Neuroscience*, *24*(16), 3899–3906. https://doi.org/10.1523/JNEUROSCI.0283-04.2004

Gresset, A., Sondek, J., & Harden, T. K. (2012). The Phospholipase C Isozymes and Their Regulation. *Sub-Cellular Biochemistry*, *58*, 61. https://doi.org/10.1007/978-94-007-3012-0_3

Griciuc, A., Patel, S., Federico, A. N., Choi, S. H., Innes, B. J., Oram, M. K., Cereghetti, G., McGinty, D., Anselmo, A., Sadreyev, R. I., Hickman, S. E., El Khoury, J., Colonna, M., & Tanzi, R. E. (2019). TREM2 Acts Downstream of CD33 in Modulating Microglial Pathology in Alzheimer's Disease. *Neuron*, *103*(5), 820-835.e7. https://doi.org/10.1016/j.neuron.2019.06.010

Griciuc, A., Serrano-Pozo, A., Parrado, A. R., Lesinski, A. N., Asselin, C. N., Mullin, K., Hooli, B., Choi, S. H., Hyman, B. T., & Tanzi, R. E. (2013). Alzheimer's Disease Risk Gene CD33 Inhibits Microglial Uptake of Amyloid Beta. *Neuron*, *78*(4), 631–643. https://doi.org/10.1016/j.neuron.2013.04.014

Griffin, R. J., Moloney, A., Kelliher, M., Johnston, J. A., Ravid, R., Dockery, P., O'Connor, R., & O'Neill, C. (2005). Activation of Akt/PKB, increased phosphorylation of Akt substrates and loss and altered distribution of Akt and PTEN are features of Alzheimer's disease pathology. *Journal of Neurochemistry*, *93*(1), 105–117. https://doi.org/10.1111/j.1471-4159.2004.02949.x

Grover, D., Chen, J.-Y., Xie, J., Li, J., Changeux, J.-P., & Greenspan, R. J. (2022). Publisher Correction: Differential mechanisms underlie trace and delay conditioning in Drosophila. *Nature*, *604*(7904), E9–E9. https://doi.org/10.1038/s41586-022-04651-y

Grozeva, D., Saad, S., Menzies, G. E., & Sims, R. (2019). Benefits and Challenges of Rare Genetic Variation in Alzheimer's Disease. *Current Genetic Medicine Reports*, *7*(1), 53–62. https://doi.org/10.1007/s40142-019-0161-5

Guerreiro, R. J., Baquero, M., Blesa, R., Boada, M., Brás, J. M., Bullido, M. J., Calado, A., Crook, R., Ferreira, C., Frank, A., Gómez-Isla, T., Hernández, I., Lleó, A., Machado, A., Martínez-Lage, P., Masdeu, J., Molina-Porcel, L., Molinuevo, J. L., Pastor, P., … Clarimón, J. (2010). Genetic screening of Alzheimer's disease genes in Iberian and African samples yields novel mutations in presenilins and APP. *Neurobiology of Aging*, *31*(5), 725–731. https://doi.org/10.1016/j.neurobiolaging.2008.06.012

Guerreiro, R., Wojtas, A., Bras, J., Carrasquillo, M., Rogaeva, E., Majounie, E., Cruchaga, C., Sassi, C., Kauwe, J. S. K., Younkin, S., Hazrati, L., Collinge, J., Pocock, J., Lashley, T., Williams, J., Lambert, J.-C., Amouyel, P., Goate, A., Rademakers, R., … Hardy, J. (2013). TREM2 Variants in Alzheimer's Disease. *New England Journal of Medicine*, *368*(2), 117–127. https://doi.org/10.1056/NEJMoa1211851

Guo, Y., Li, Z., & Lin, X. (2014). Hs3st-A and Hs3st-B regulate intestinal homeostasis in Drosophila adult midgut. *Cellular Signalling*, *26*(11), 2317–2325. https://doi.org/10.1016/j.cellsig.2014.07.015

Guo, Y., Pan, W., Liu, S., Shen, Z., Xu, Y., & Hu, L. (2020). ERK/MAPK signalling pathway and tumorigenesis (Review). *Experimental and Therapeutic Medicine*. https://doi.org/10.3892/etm.2020.8454

Halet, G. (2005). Imaging phosphoinositide dynamics using GFP-tagged protein domains. *Biology of the Cell*, *97*(7), 501–518. https://doi.org/10.1042/BC20040080

Hansen, D. V., Hanson, J. E., & Sheng, M. (2018a). Microglia in Alzheimer's disease. *The Journal of Cell Biology*, *217*(2), 459. https://doi.org/10.1083/JCB.201709069

Hansen, D. v., Hanson, J. E., & Sheng, M. (2018b). Microglia in Alzheimer's disease. *Journal of Cell Biology*, *217*(2), 459–472. https://doi.org/10.1083/jcb.201709069

Harden, T. K., & Sondek, J. (2006). REGULATION OF PHOSPHOLIPASE C ISOZYMES BY RAS SUPERFAMILY GTPASES. *Annual Review of Pharmacology and Toxicology*, *46*(1), 355–379. https://doi.org/10.1146/annurev.pharmtox.46.120604.141223

Hardy, J., & Allsop, D. (1991). Amyloid deposition as the central event in the aetiology of Alzheimer's disease. *Trends in Pharmacological Sciences*, *12*, 383–388. https://doi.org/10.1016/0165-6147(91)90609-V

Hardy, J., Bogdanovic, N., Winblad, B., Portelius, E., Andreasen, N., Cedazo-Minguez, A., & Zetterberg, H. (2014). Pathways to Alzheimer's disease. *Journal of Internal Medicine*, *275*(3), 296–303. https://doi.org/10.1111/joim.12192

Hardy, J., & Selkoe, D. J. (2002a). The Amyloid Hypothesis of Alzheimer's Disease: Progress and Problems on the Road to Therapeutics. *Science*, *297*(5580), 353–356. https://doi.org/10.1126/science.1072994

Hardy, J., & Selkoe, D. J. (2002b). The amyloid hypothesis of Alzheimer's disease: Progress and problems on the road to therapeutics. *Science*, *297*(5580), 353–356. https://doi.org/10.1126/SCIENCE.1072994/ASSET/C4ED1918-4F2B-4649-BA69-684D0145F32B/ASSETS/GRAPHIC/SE2820694002.JPEG

Harman, D. (2006). Alzheimer's Disease Pathogenesis: Role of Aging. *Annals of the New York Academy of Sciences*, *1067*(1), 454–460. https://doi.org/10.1196/annals.1354.065

Hashimoto, A., Takeda, K., Inaba, M., Sekimata, M., Kaisho, T., Ikehara, S., Homma, Y., Akira, S., & Kurosaki, T. (2000). Cutting edge: essential role of phospholipase C-gamma 2 in B cell development and function. *Journal of Immunology (Baltimore, Md. : 1950)*, *165*(4), 1738–1742. https://doi.org/10.4049/JIMMUNOL.165.4.1738

Heidary, G., & Fortini, M. E. (2001). Identification and characterization of the Drosophila tau homolog. *Mechanisms of Development*, *108*(1–2), 171–178. https://doi.org/10.1016/S0925-4773(01)00487-7

Hemming, M. L., & Selkoe, D. J. (2005). Amyloid β-protein is degraded by cellular angiotensin-converting enzyme (ACE) and elevated by an ACE inhibitor. *Journal of Biological Chemistry*, *280*(45), 37644–37650. https://doi.org/10.1074/jbc.M508460200

Heneka, M. T., Carson, M. J., Khoury, J. El, Landreth, G. E., Brosseron, F., Feinstein, D. L., Jacobs, A. H., Wyss-Coray, T., Vitorica, J., Ransohoff, R. M., Herrup, K., Frautschy, S. A., Finsen, B., Brown, G. C., Verkhratsky, A., Yamanaka, K., Koistinaho, J., Latz, E., Halle, A., … Kummer, M. P. (2015). Neuroinflammation in Alzheimer's disease. *The Lancet Neurology*, *14*(4), 388–405. https://doi.org/10.1016/S1474-4422(15)70016-5

Henstridge, C. M., Tzioras, M., & Paolicelli, R. C. (2019). Glial Contribution to Excitatory and Inhibitory Synapse Loss in Neurodegeneration. *Frontiers in Cellular Neuroscience*, *13*. https://doi.org/10.3389/fncel.2019.00063

Hermida, M. A., Dinesh Kumar, J., & Leslie, N. R. (2017). GSK3 and its interactions with the PI3K/AKT/mTOR signalling network. *Advances in Biological Regulation*, *65*, 5–15. https://doi.org/10.1016/J.JBIOR.2017.06.003

Hickman, S. E., Allison, E. K., & el Khoury, J. (2008). Microglial Dysfunction and Defective -Amyloid Clearance Pathways in Aging Alzheimer's Disease Mice. *Journal of Neuroscience*, *28*(33), 8354–8360. https://doi.org/10.1523/JNEUROSCI.0616-08.2008

Higham, J. P., Malik, B. R., Buhl, E., Dawson, J. M., Ogier, A. S., Lunnon, K., & Hodge, J. J. L. (2019). Alzheimer's Disease Associated Genes Ankyrin and Tau Cause Shortened Lifespan and Memory Loss in Drosophila. *Frontiers in Cellular Neuroscience*, *13*. https://doi.org/10.3389/fncel.2019.00260

Hilpelä, P., Vartiainen, M. K., & Lappalainen, P. (2004a). *Regulation of the Actin Cytoskeleton by PI(4,5)P2 and PI(3,4,5)P3* (pp. 117–163). https://doi.org/10.1007/978-3-642-18805-3_5

Hilpelä, P., Vartiainen, M. K., & Lappalainen, P. (2004b). *Regulation of the Actin Cytoskeleton by PI(4,5)P2 and PI(3,4,5)P3* (pp. 117–163). https://doi.org/10.1007/978-3-642-18805-3_5

Hodges, A. K., Piers, T. M., Collier, D., Cousins, O., & Pocock, J. M. (2021). Pathways linking Alzheimer's disease risk genes expressed highly in microglia. *Neuroimmunology and Neuroinflammation*, *2020*. https://doi.org/10.20517/2347-8659.2020.60

Hollingworth, P., Harold, D., Sims, R., Gerrish, A., Lambert, J.-C., Carrasquillo, M. M., Abraham, R., Hamshere, M. L., Pahwa, J. S., Moskvina, V., Dowzell, K., Jones, N., Stretton, A., Thomas, C., Richards, A., Ivanov, D., Widdowson, C., Chapman, J., Lovestone, S., … Williams, J. (2011). Common variants at ABCA7, MS4A6A/MS4A4E, EPHA1, CD33 and CD2AP are associated with Alzheimer's disease. *Nature Genetics*, *43*(5), 429–435. https://doi.org/10.1038/ng.803

Homma, Y., Takenawa, T., Emori, Y., Sorimachi, H., & Suzuki, K. (1989). Tissue- and cell type-specific expression of mRNAS for four types of inositol phospholipid-specific phospholipase C. *Biochemical and Biophysical Research Communications*, *164*(1), 406–412. https://doi.org/10.1016/0006-291X(89)91734-8

Hong, S., Dissing-Olesen, L., & Stevens, B. (2016). New insights on the role of microglia in synaptic pruning in health and disease. *Current Opinion in Neurobiology*, *36*, 128. https://doi.org/10.1016/J.CONB.2015.12.004

Hu, Y., Flockhart, I., Vinayagam, A., Bergwitz, C., Berger, B., Perrimon, N., & Mohr, S. E. (2011). An integrative approach to ortholog prediction for disease-focused and other functional studies. *BMC Bioinformatics*, *12*(1), 357. https://doi.org/10.1186/1471-2105-12-357

Huang, Y., & Mahley, R. W. (2014). Apolipoprotein E: Structure and function in lipid metabolism, neurobiology, and Alzheimer's diseases. In *Neurobiology of Disease* (Vol. 72, Issue Part A, pp. 3–12). NIH Public Access. https://doi.org/10.1016/j.nbd.2014.08.025

Hurst, D., Rylett, C. M., Isaac, R. E., & Shirras, A. D. (2003). The drosophila angiotensin-converting enzyme homologue Ance is required for spermiogenesis. *Developmental Biology*, *254*(2), 238–247. https://doi.org/10.1016/S0012-1606(02)00082-9

Hutton, M., Lendon, C. L., Rizzu, P., Baker, M., Froelich, S., Houlden, H., Pickering-Brown, S., Chakraverty, S., Isaacs, A., Grover, A., Hackett, J., Adamson, J., Lincoln, S., Dickson, D., Davies, P., Petersen, R. C., Stevens, M., de Graaff, E., Wauters, E., … Heutink, P. (1998). Association of missense and 5'-splice-site mutations in tau with the inherited dementia FTDP-17. *Nature*, *393*(6686), 702–705. https://doi.org/10.1038/31508

Iijima, K., Liu, H.-P., Chiang, A.-S., Hearn, S. A., Konsolaki, M., & Zhong, Y. (2004). Dissecting the pathological effects of human Aβ40 and Aβ42 in *Drosophila* : A potential model for Alzheimer's disease. *Proceedings of the National Academy of Sciences*, *101*(17), 6623–6628. https://doi.org/10.1073/pnas.0400895101

Ishiura, S., Asai, M., Hattori, C., Hotoda, N., Szabo, B., Sasagawa, N., & Tanuma, S. (2013). *APP α-Secretase, a Novel Target for Alzheimer Drug Therapy*. https://www.ncbi.nlm.nih.gov/books/NBK6595/

Jack, C. R., Petersen, R. C., Xu, Y. C., O'Brien, P. C., Smith, G. E., Ivnik, R. J., Boeve, B. F., Waring, S. C., Tangalos, E. G., & Kokmen, E. (1999). Prediction of AD with MRI-based hippocampal volume in mild cognitive impairment. *Neurology*, *52*(7), 1397–1403. https://doi.org/10.1212/WNL.52.7.1397

Jackson, G. R., Wiedau-Pazos, M., Sang, T. K., Wagle, N., Brown, C. A., Massachi, S., & Geschwind, D. H. (2002). Human wild-type tau interacts with wingless pathway components and produces neurofibrillary pathology in Drosophila. *Neuron*, *34*(4), 509–519. https://doi.org/10.1016/S0896-6273(02)00706-7

Jackson, J. T., Mulazzani, E., Nutt, S. L., & Masters, S. L. (2021). The role of PLCγ2 in immunological disorders, cancer, and neurodegeneration. *Journal of Biological Chemistry*, *297*(2), 100905. https://doi.org/10.1016/j.jbc.2021.100905

Jansen, I. E., Savage, J. E., Watanabe, K., Bryois, J., Williams, D. M., Steinberg, S., Sealock, J., Karlsson, I. K., Hägg, S., Athanasiu, L., Voyle, N., Proitsi, P., Witoelar, A., Stringer, S., Aarsland, D., Almdahl, I. S., Andersen, F., Bergh, S., Bettella, F., … Posthuma, D. (2019). Genome-wide meta-analysis identifies new loci and functional pathways influencing Alzheimer's disease risk. *Nature Genetics*, *51*(3), 404–413. https://doi.org/10.1038/s41588-018-0311-9

Jeon, Y., Lee, J. H., Choi, B., Won, S. Y., & Cho, K. S. (2020). Genetic Dissection of Alzheimer's Disease Using Drosophila Models. *International Journal of Molecular Sciences 2020, Vol. 21, Page 884*, *21*(3), 884. https://doi.org/10.3390/IJMS21030884

Ji, K., Akgul, G., Wollmuth, L. P., & Tsirka, S. E. (2013). Microglia Actively Regulate the Number of Functional Synapses. *PLoS ONE*, *8*(2), e56293. https://doi.org/10.1371/journal.pone.0056293

Ji, Q., Winnier, G. E., Niswender, K. D., Horstman, D., Wisdom, R., Magnuson, M. A., & Carpenter, G. (1997). Essential role of the tyrosine kinase substrate phospholipase C-γ1 in mammalian growth and development. *Proceedings of the National Academy of Sciences*, *94*(7), 2999–3003. https://doi.org/10.1073/pnas.94.7.2999

Jiang, Q., Lee, C. Y. D., Mandrekar, S., Wilkinson, B., Cramer, P., Zelcer, N., Mann, K., Lamb, B., Willson, T. M., Collins, J. L., Richardson, J. C., Smith, J. D., Comery, T. A., Riddell, D., Holtzman, D. M., Tontonoz, P., & Landreth, G. E. (2008). ApoE promotes the proteolytic degradation of Abeta. *Neuron*, *58*(5), 681–693. https://doi.org/10.1016/j.neuron.2008.04.010

Jiao, S.-S., Shen, L.-L., Zhu, C., Bu, X.-L., Liu, Y.-H., Liu, C.-H., Yao, X.-Q., Zhang, L.-L., Zhou, H.-D., Walker, D. G., Tan, J., Götz, J., Zhou, X.-F., & Wang, Y.-J. (2016). Brain-derived neurotrophic factor protects against tau-related neurodegeneration of Alzheimer's disease. *Translational Psychiatry*, *6*(10), e907–e907. https://doi.org/10.1038/tp.2016.186

Johnson, K. A., Fox, N. C., Sperling, R. A., & Klunk, W. E. (2012). Brain Imaging in Alzheimer Disease. *Cold Spring Harbor Perspectives in Medicine*, *2*(4), a006213–a006213. https://doi.org/10.1101/cshperspect.a006213

Jones, L., Holmans, P. A., Hamshere, M. L., Harold, D., Moskvina, V., Ivanov, D., Pocklington, A., Abraham, R., Hollingworth, P., Sims, R., Gerrish, A., Pahwa, J. S., Jones, N., Stretton, A., Morgan, A. R., Lovestone, S., Powell, J., Proitsi, P., Lupton, M. K., … Williams, J. (2010). Genetic Evidence Implicates the Immune System and Cholesterol Metabolism in the Aetiology of Alzheimer's Disease. *PLOS ONE*, *5*(11), e13950. https://doi.org/10.1371/JOURNAL.PONE.0013950

Jonsson, T., Atwal, J. K., Steinberg, S., Snaedal, J., Jonsson, P. V., Bjornsson, S., Stefansson, H., Sulem, P., Gudbjartsson, D., Maloney, J., Hoyte, K., Gustafson, A., Liu, Y., Lu, Y., Bhangale, T., Graham, R. R., Huttenlocher, J., Bjornsdottir, G., Andreassen, O. A., … Stefansson, K. (2012). A mutation in APP protects against Alzheimer's disease and age-related cognitive decline. *Nature*, *488*(7409), 96–99. https://doi.org/10.1038/nature11283

Jonsson, T., Stefansson, H., Steinberg, S., Jonsdottir, I., Jonsson, P. V., Snaedal, J., Bjornsson, S., Huttenlocher, J., Levey, A. I., Lah, J. J., Rujescu, D., Hampel, H., Giegling, I., Andreassen, O. A., Engedal, K., Ulstein, I., Djurovic, S., Ibrahim-Verbaas, C., Hofman, A., … Stefansson, K. (2013). Variant of *TREM2* Associated with the Risk of Alzheimer's Disease. *New England Journal of Medicine*, *368*(2), 107–116. https://doi.org/10.1056/NEJMoa1211103

Karahan, H., Smith, D. C., Kim, B., Dabin, L. C., Al-Amin, M. M., Wijeratne, H. R. S., Pennington, T., Viana di Prisco, G., McCord, B., Lin, P. B., Li, Y., Peng, J., Oblak, A. L., Chu, S., Atwood, B. K., & Kim, J. (2021). Deletion of Abi3 gene locus exacerbates neuropathological features of Alzheimer's disease in a mouse model of Aβ amyloidosis. *Science Advances*, *7*(45). https://doi.org/10.1126/sciadv.abe3954

Karch, C. M., & Goate, A. M. (2015). Alzheimer's disease risk genes and mechanisms of disease pathogenesis. *Biological Psychiatry*, *77*(1), 43. https://doi.org/10.1016/J.BIOPSYCH.2014.05.006

Kavran, J. M., Klein, D. E., Lee, A., Falasca, M., Isakoff, S. J., Skolnik, E. Y., & Lemmon, M. A. (1998). Specificity and Promiscuity in Phosphoinositide Binding by Pleckstrin Homology Domains. *Journal of Biological Chemistry*, *273*(46), 30497–30508. https://doi.org/10.1074/jbc.273.46.30497

Kechko, O. I., Petrushanko, I. Yu., Brower, C. S., Adzhubei, A. A., Moskalev, A. A., Piatkov, K. I., Mitkevich, V. A., & Makarov, A. A. (2019). Beta-amyloid induces apoptosis of neuronal cells by inhibition of the Arg/N-end rule pathway proteolytic activity. *Aging*, *11*(16), 6134–6152. https://doi.org/10.18632/aging.102177

Kehoe, P. G. (2018). The coming of age of the angiotensin hypothesis in Alzheimer's disease: Progress toward disease prevention and treatment? In *Journal of Alzheimer's Disease* (Vol. 62, Issue 3, pp. 1443–1466). IOS Press. https://doi.org/10.3233/JAD-171119

Keller, L. C., Cheng, L., Locke, C. J., Müller, M., Fetter, R. D., & Davis, G. W. (2011). Glial-Derived Prodegenerative Signaling in the Drosophila Neuromuscular System. *Neuron*, *72*(5), 760–775. https://doi.org/10.1016/j.neuron.2011.09.031

Kerr, K. S., Fuentes-Medel, Y., Brewer, C., Barria, R., Ashley, J., Abruzzi, K. C., Sheehan, A., Tasdemir-Yilmaz, O. E., Freeman, M. R., & Budnik, V. (2014). Glial Wingless/Wnt Regulates Glutamate

Receptor Clustering and Synaptic Physiology at the Drosophila Neuromuscular Junction. *Journal of Neuroscience*, *34*(8), 2910–2920. https://doi.org/10.1523/JNEUROSCI.3714-13.2014

Khwaja, A. (1999). Akt is more than just a Bad kinase. *Nature*, *401*(6748), 33–34. https://doi.org/10.1038/43354

Kim, S., Fountoulakis, M., Cairns, N. J., & Lubec, G. (2002). Human brain nucleoside diphosphate kinase activity is decreased in Alzheimer's disease and Down syndrome. *Biochemical and Biophysical Research Communications*, *296*(4), 970–975. https://doi.org/10.1016/S0006-291X(02)02035-1

Kim, Y. C., & Guan, K. L. (2015). mTOR: a pharmacologic target for autophagy regulation. *The Journal of Clinical Investigation*, *125*(1), 25. https://doi.org/10.1172/JCI73939

Kisseleva, M. V., Wilson, M. P., & Majerus, P. W. (2000). The isolation and characterization of a cDNA encoding phospholipid-specific inositol polyphosphate 5-phosphatase. *The Journal of Biological Chemistry*, *275*(26), 20110–20116. https://doi.org/10.1074/JBC.M910119199

Klarlund, J. K., Guilherme, A., Holik, J. J., Virbasius, J. V., Chawla, A., & Czech, M. P. (1997). Signaling by Phosphoinositide-3,4,5-Trisphosphate Through Proteins Containing Pleckstrin and Sec7 Homology Domains. *Science*, *275*(5308), 1927–1930. https://doi.org/10.1126/science.275.5308.1927

Koch, I., Schwarz, H., Beuchle, D., Goellner, B., Langegger, M., & Aberle, H. (2008). Drosophila Ankyrin 2 Is Required for Synaptic Stability. *Neuron*, *58*(2), 210–222. https://doi.org/10.1016/j.neuron.2008.03.019

Koffie, R. M., Meyer-Luehmann, M., Hashimoto, T., Adams, K. W., Mielke, M. L., Garcia-Alloza, M., Micheva, K. D., Smith, S. J., Kim, M. L., Lee, V. M., Hyman, B. T., & Spires-Jones, T. L. (2009). Oligomeric amyloid β associates with postsynaptic densities and correlates with excitatory synapse loss near senile plaques. *Proceedings of the National Academy of Sciences*, *106*(10), 4012–4017. https://doi.org/10.1073/pnas.0811698106

Konopka, R. J., & Benzer, S. (1971). Clock mutants of Drosophila melanogaster. *Proceedings of the National Academy of Sciences of the United States of America*, *68*(9), 2112–2116. https://doi.org/10.1073/pnas.68.9.2112

Krasemann, S., Madore, C., Cialic, R., Baufeld, C., Calcagno, N., El Fatimy, R., Beckers, L., O'Loughlin, E., Xu, Y., Fanek, Z., Greco, D. J., Smith, S. T., Tweet, G., Humulock, Z., Zrzavy, T., Conde-Sanroman, P., Gacias, M., Weng, Z., Chen, H., … Butovsky, O. (2017). The TREM2-APOE Pathway Drives the Transcriptional Phenotype of Dysfunctional Microglia in Neurodegenerative Diseases. *Immunity*, *47*(3), 566-581.e9. https://doi.org/10.1016/J.IMMUNI.2017.08.008

Kuchibhotla, K. V., Goldman, S. T., Lattarulo, C. R., Wu, H.-Y., Hyman, B. T., & Bacskai, B. J. (2008). Aβ Plaques Lead to Aberrant Regulation of Calcium Homeostasis In Vivo Resulting in Structural and Functional Disruption of Neuronal Networks. *Neuron*, *59*(2), 214–225. https://doi.org/10.1016/j.neuron.2008.06.008

Kumar, A., Singh, A., & Ekavali. (2015). A review on Alzheimer's disease pathophysiology and its management: an update. *Pharmacological Reports*, *67*(2), 195–203. https://doi.org/10.1016/j.pharep.2014.09.004

Kunkle, B. W., Grenier-Boley, B., Sims, R., Bis, J. C., Damotte, V., Naj, A. C., Boland, A., Vronskaya, M., van der Lee, S. J., Amlie-Wolf, A., Bellenguez, C., Frizatti, A., Chouraki, V., Martin, E. R., Sleegers, K., Badarinarayan, N., Jakobsdottir, J., Hamilton-Nelson, K. L., Moreno-Grau, S., … Pericak-Vance, M. A. (2019). Genetic meta-analysis of diagnosed Alzheimer's disease identifies new risk loci and implicates Aβ, tau, immunity and lipid processing. *Nature Genetics*, *51*(3), 414–430. https://doi.org/10.1038/s41588-019-0358-2

Lago-Baldaia, I., Fernandes, V. M., & Ackerman, S. D. (2020). More Than Mortar: Glia as Architects of Nervous System Development and Disease. *Frontiers in Cell and Developmental Biology*, *8*. https://doi.org/10.3389/fcell.2020.611269

Lahiri, D. K., Maloney, B., Rogers, J. T., & Ge, Y. W. (2013). PuF, an antimetastatic and developmental signaling protein, interacts with the Alzheimer's amyloid-β precursor protein via a tissue-specific proximal regulatory element (PRE). *BMC Genomics*, *14*(1). https://doi.org/10.1186/1471-2164-14-68

Lambert, E., Saha, O., Soares Landeira, B., Melo de Farias, A. R., Hermant, X., Carrier, A., Pelletier, A., Gadaut, J., Davoine, L., Dupont, C., Amouyel, P., Bonnefond, A., Lafont, F., Abdelfettah, F., Verstreken, P., Chapuis, J., Barois, N., Delahaye, F., Dermaut, B., … Dourlen, P. (2022). The Alzheimer susceptibility gene BIN1 induces isoform-dependent neurotoxicity through early endosome defects. *Acta Neuropathologica Communications*, *10*(1), 1–23. https://doi.org/10.1186/S40478-021-01285-5/FIGURES/8

Lambert, J. C., Ibrahim-Verbaas, C. A., Harold, D., Naj, A. C., Sims, R., Bellenguez, C., Jun, G., DeStefano, A. L., Bis, J. C., Beecham, G. W., Grenier-Boley, B., Russo, G., Thornton-Wells, T. A., Jones, N., Smith, A. v, Chouraki, V., Thomas, C., Ikram, M. A., Zelenika, D., … Seshadri, S. (2013). Meta-analysis of 74,046 individuals identifies 11 new susceptibility loci for Alzheimer's disease. *Nature Genetics*, *45*(12), 1452–1458. https://doi.org/10.1038/ng.2802

Lambert, J.-C., Araria-Goumidi, L., Myllykangas, L., Ellis, C., Wang, J. C., Bullido, M. J., Harris, J. M., Artiga, M. J., Hernandez, D., Kwon, J. M., Frigard, B., Petersen, R. C., Cumming, A. M., Pasquier, F., Sastre, I., Tienari, P. J., Frank, A., Sulkava, R., Morris, J. C., … Chartier-Harlin, M.-C. (2002). Contribution of APOE promoter polymorphisms to Alzheimer's disease risk. *Neurology*, *59*(1), 59–66. http://www.ncbi.nlm.nih.gov/pubmed/12105308

Lambert, J.-C., Heath, S., Even, G., Campion, D., Sleegers, K., Hiltunen, M., Combarros, O., Zelenika, D., Bullido, M. J., Tavernier, B., Letenneur, L., Bettens, K., Berr, C., Pasquier, F., Fiévet, N., Barberger-Gateau, P., Engelborghs, S., de Deyn, P., Mateo, I., … Amouyel, P. (2009). Genome-wide association study identifies variants at CLU and CR1 associated with Alzheimer's disease. *Nature Genetics*, *41*(10), 1094–1099. https://doi.org/10.1038/ng.439

Landman, N., Jeong, S. Y., Shin, S. Y., Voronov, S. V., Serban, G., Kang, M. S., Park, M. K., Di Paolo, G., Chung, S., & Kim, T.-W. (2006). Presenilin mutations linked to familial Alzheimer's disease cause an imbalance in phosphatidylinositol 4,5-bisphosphate metabolism. *Proceedings of the National Academy of Sciences*, *103*(51), 19524–19529. https://doi.org/10.1073/pnas.0604954103

Lanoiselée, H.-M., Nicolas, G., Wallon, D., Rovelet-Lecrux, A., Lacour, M., Rousseau, S., Richard, A.-C., Pasquier, F., Rollin-Sillaire, A., Martinaud, O., Quillard-Muraine, M., de la Sayette, V., Boutoleau-Bretonniere, C., Etcharry-Bouyx, F., Chauviré, V., Sarazin, M., le Ber, I., Epelbaum, S., Jonveaux, T., … collaborators of the CNR-MAJ project, collaborators of the C.-M. (2017). APP,

PSEN1, and PSEN2 mutations in early-onset Alzheimer disease: A genetic screening study of familial and sporadic cases. *PLoS Medicine*, *14*(3), e1002270. https://doi.org/10.1371/journal.pmed.1002270

Laplante, M., & Sabatini, D. M. (2009). mTOR signaling at a glance. *Journal of Cell Science*, *122*(20), 3589. https://doi.org/10.1242/JCS.051011

Lawlor, M. A., & Alessi, D. R. (2001). PKB/Akt: a key mediator of cell proliferation, survival and insulin responses? *Journal of Cell Science*, *114*(16), 2903–2910. https://doi.org/10.1242/jcs.114.16.2903

LeBlanc, A. C., Papadopoulos, M., Bélair, C., Chu, W., Crosato, M., Powell, J., & Goodyer, C. G. (2002). Processing of Amyloid Precursor Protein in Human Primary Neuron and Astrocyte Cultures. *Journal of Neurochemistry*, *68*(3), 1183–1190. https://doi.org/10.1046/j.1471-4159.1997.68031183.x

Lee, E. B., Kinch, K., Johnson, V. E., Trojanowski, J. Q., Smith, D. H., & Stewart, W. (2019). A nonsynonymous mutation in PLCG2 reduces the risk of Alzheimer's disease, dementia with Lewy bodies and frontotemporal dementia, and increases the likelihood of longevity. *Acta Neuropathol*, *138*(3), 237–250. https://doi.org/10.1007/s00401-019-02030-y

Lee, J.-H., Yang, D.-S., Goulbourne, C. N., Im, E., Stavrides, P., Pensalfini, A., Chan, H., Bouchet-Marquis, C., Bleiwas, C., Berg, M. J., Huo, C., Peddy, J., Pawlik, M., Levy, E., Rao, M., Staufenbiel, M., & Nixon, R. A. (2022). Faulty autolysosome acidification in Alzheimer's disease mouse models induces autophagic build-up of Aβ in neurons, yielding senile plaques. *Nature Neuroscience*, *25*(6), 688–701. https://doi.org/10.1038/s41593-022-01084-8

Lee, P.-T., Zirin, J., Kanca, O., Lin, W.-W., Schulze, K. L., Li-Kroeger, D., Tao, R., Devereaux, C., Hu, Y., Chung, V., Fang, Y., He, Y., Pan, H., Ge, M., Zuo, Z., Housden, B. E., Mohr, S. E., Yamamoto, S., Levis, R. W., … Bellen, H. J. (2018). A gene-specific T2A-GAL4 library for Drosophila. *ELife*, *7*. https://doi.org/10.7554/eLife.35574

Lee, T., & Luo, L. (1999). Mosaic analysis with a repressible neurotechnique cell marker for studies of gene function in neuronal morphogenesis. *Neuron*, *22*(3), 451–461. https://doi.org/10.1016/S0896-6273(00)80701-1

Lehmann, D. J., Cortina-Borja, M., Warden, D. R., Smith, A. D., Sleegers, K., Prince, J. A., van Duijn, C. M., & Kehoe, P. G. (2005). Large meta-analysis establishes the ACE insertion-deletion polymorphism as a marker of Alzheimer's disease. *American Journal of Epidemiology*, *162*(4), 305–317. https://doi.org/10.1093/aje/kwi202

Lemmon, M. A., & Ferguson, K. M. (2000). Signal-dependent membrane targeting by pleckstrin homology (PH) domains. *Biochemical Journal*, *350*(Pt 1), 1. https://doi.org/10.1042/0264-6021:3500001

Lewis, J., Dickson, D. W., Lin, W.-L., Chisholm, L., Corral, A., Jones, G., Yen, S.-H., Sahara, N., Skipper, L., Yager, D., Eckman, C., Hardy, J., Hutton, M., & McGowan, E. (2001). Enhanced Neurofibrillary Degeneration in Transgenic Mice Expressing Mutant Tau and APP. *Science*, *293*(5534), 1487–1491. https://doi.org/10.1126/science.1058189

Li, H., Janssens, J., De Waegeneer, M., Kolluru, S. S., Davie, K., Gardeux, V., Saelens, W., David, F. P. A., Brbić, M., Spanier, K., Leskovec, J., McLaughlin, C. N., Xie, Q., Jones, R. C., Brueckner, K., Shim, J., Tattikota, S. G., Schnorrer, F., Rust, K., … Zinzen, R. P. (2022). Fly Cell Atlas: A single-

nucleus transcriptomic atlas of the adult fruit fly. *Science*, *375*(6584). https://doi.org/10.1126/science.abk2432

Li, X., Alafuzoff, I., Soininen, H., Winblad, B., & Pei, J.-J. (2005). Levels of mTOR and its downstream targets 4E-BP1, eEF2, and eEF2 kinase in relationships with tau in Alzheimer's disease brain. *FEBS Journal*, *272*(16), 4211–4220. https://doi.org/10.1111/j.1742-4658.2005.04833.x

Li, Y., Rinne, J. O., Mosconi, L., Pirraglia, E., Rusinek, H., DeSanti, S., Kemppainen, N., Någren, K., Kim, B.-C., Tsui, W., & de Leon, M. J. (2008). Regional analysis of FDG and PIB-PET images in normal aging, mild cognitive impairment, and Alzheimer's disease. *European Journal of Nuclear Medicine and Molecular Imaging*, *35*(12), 2169–2181. https://doi.org/10.1007/s00259-008-0833-y

Li, Z., Cheng, S., Lin, Q., Cao, W., Yang, J., Zhang, M., Shen, A., Zhang, W., Xia, Y., Ma, X., & Ouyang, Z. (2021). Single-cell lipidomics with high structural specificity by mass spectrometry. *Nature Communications 2021 12:1*, *12*(1), 1–10. https://doi.org/10.1038/s41467-021-23161-5

Lilly, B., Zhao, B., Ranganayakulu, G., Paterson, B. M., Schulz, R. A., & Olson, E. N. (1995). Requirement of MADS Domain Transcription Factor D-MEF2 for Muscle Formation in *Drosophila*. *Science*, *267*(5198), 688–693. https://doi.org/10.1126/science.7839146

Lin, C.-Y., Chuang, C.-C., Hua, T.-E., Chen, C.-C., Dickson, B. J., Greenspan, R. J., & Chiang, A.-S. (2013). A Comprehensive Wiring Diagram of the Protocerebral Bridge for Visual Information Processing in the Drosophila Brain. *Cell Reports*, *3*(5), 1739–1753. https://doi.org/10.1016/j.celrep.2013.04.022

Lin, Q., Schwarz, J., Bucana, C., & N. Olson, E. (1997). Control of Mouse Cardiac Morphogenesis and Myogenesis by Transcription Factor MEF2C. *Science*, *276*(5317), 1404–1407. https://doi.org/10.1126/science.276.5317.1404

Liu, F., Liang, Z., Wegiel, J., Hwang, Y., Iqbal, K., Grundke-Iqbal, I., Ramakrishna, N., & Gong, C. (2008). Overexpression of Dyrk1A contributes to neurofibrillary degeneration in Down syndrome. *The FASEB Journal*, *22*(9), 3224–3233. https://doi.org/10.1096/fj.07-104539

Liu, Y., Yu, J. T., Wang, H. F., Hao, X. K., Yang, Y. F., Jiang, T., Zhu, X. C., Cao, L., Zhang, D. Q., & Tan, L. (2014). Association between NME8 Locus Polymorphism and Cognitive Decline, Cerebrospinal Fluid and Neuroimaging Biomarkers in Alzheimer's Disease. *PLoS ONE*, *9*(12). https://doi.org/10.1371/JOURNAL.PONE.0114777

Lleó, A., Berezovska, O., Herl, L., Raju, S., Deng, A., Bacskai, B. J., Frosch, M. P., Irizarry, M., & Hyman, B. T. (2004). Nonsteroidal anti-inflammatory drugs lower Aβ42 and change presenilin 1 conformation. *Nature Medicine*, *10*(10), 1065–1066. https://doi.org/10.1038/nm1112

Lo Vasco, V. R. (2018). The Phosphoinositide Signal Transduction Pathway in the Pathogenesis of Alzheimer's Disease. *Current Alzheimer Research*, *15*(4), 355–362. https://doi.org/10.2174/1567205014666170829100230

Lord, J., Lu, A. J., & Cruchaga, C. (2014). Identification of rare variants in Alzheimer's disease. *Frontiers in Genetics*, *5*(OCT), 369. https://doi.org/10.3389/FGENE.2014.00369/BIBTEX

Luo, L., Martin-Morris, L., & White, K. (1990). Identification, secretion, and neural expression of APPL, a Drosophila protein similar to human amyloid protein precursor. *The Journal of Neuroscience*, *10*(12), 3849–3861. https://doi.org/10.1523/JNEUROSCI.10-12-03849.1990

Luo, L., Tully, T., & White, K. (1992). Human amyloid precursor protein ameliorates behavioral deficit of flies deleted for appl gene. *Neuron*, *9*(4), 595–605. https://doi.org/10.1016/0896-6273(92)90024-8

Lyons, M. R., Schwarz, C. M., & West, A. E. (2012). Members of the Myocyte Enhancer Factor 2 Transcription Factor Family Differentially Regulate Bdnf Transcription in Response to Neuronal Depolarization. *Journal of Neuroscience*, *32*(37), 12780–12785. https://doi.org/10.1523/JNEUROSCI.0534-12.2012

Ma, J., & Ptashne, M. (1987). The carboxy-terminal 30 amino acids of GAL4 are recognized by GAL80. *Cell*, *50*(1), 137–142. https://doi.org/10.1016/0092-8674(87)90670-2

MacDonald, J. M., Beach, M. G., Porpiglia, E., Sheehan, A. E., Watts, R. J., & Freeman, M. R. (2006). The Drosophila Cell Corpse Engulfment Receptor Draper Mediates Glial Clearance of Severed Axons. *Neuron*, *50*(6), 869–881. https://doi.org/10.1016/j.neuron.2006.04.028

Magno, L., Lessard, C. B., Martins, M., Lang, V., Cruz, P., Asi, Y., Katan, M., Bilsland, J., Lashley, T., Chakrabarty, P., Golde, T. E., & Whiting, P. J. (2019). Alzheimer's disease phospholipase C-gamma-2 (PLCG2) protective variant is a functional hypermorph. *Alzheimer's Research & Therapy*, *11*(1), 16. https://doi.org/10.1186/s13195-019-0469-0

Maguire, E., Menzies, G. E., Phillips, T., Sasner, M., Williams, H. M., Czubala, M. A., Evans, N., Cope, E. L., Sims, R., Howell, G. R., Lloyd-Evans, E., Williams, J., Allen, N. D., & Taylor, P. R. (2021). PIP2 depletion and altered endocytosis caused by expression of Alzheimer's disease-protective variant PLCγ2 R522. *The EMBO Journal*, *40*(17). https://doi.org/10.15252/embj.2020105603

Malik, M., Parikh, I., Vasquez, J. B., Smith, C., Tai, L., Bu, G., LaDu, M. J., Fardo, D. W., Rebeck, G. W., & Estus, S. (2015). Genetics ignite focus on microglial inflammation in Alzheimer's disease. *Molecular Neurodegeneration*, *10*(1), 52. https://doi.org/10.1186/s13024-015-0048-1

Maloney, J. A., Bainbridge, T., Gustafson, A., Zhang, S., Kyauk, R., Steiner, P., Van Der Brug, M., Liu, Y., Ernst, J. A., Watts, R. J., & Atwal, J. K. (2014). Molecular mechanisms of Alzheimer disease protection by the A673T allele of amyloid precursor protein. *The Journal of Biological Chemistry*, *289*(45), 30990–31000. https://doi.org/10.1074/JBC.M114.589069

Mancuso, R., Fryatt, G., Cleal, M., Obst, J., Pipi, E., Monzón-Sandoval, J., Ribe, E., Winchester, L., Webber, C., Nevado, A., Jacobs, T., Austin, N., Theunis, C., Grauwen, K., Daniela Ruiz, E., Mudher, A., Vicente-Rodriguez, M., Parker, C. A., Simmons, C., … Perry, V. H. (2019). CSF1R inhibitor JNJ-40346527 attenuates microglial proliferation and neurodegeneration in P301S mice. *Brain*, *142*(10), 3243–3264. https://doi.org/10.1093/brain/awz241

Mankidy, R., Hastings, J., & Thackeray, J. R. (2003). *Distinct Phospholipase C-Dependent Signaling Pathways in the Drosophila Eye and Wing Are Revealed by a New small wing Allele*.

Manning, C. M., Mathews, W. R., Fico, L. P., & Thackeray, J. R. (2003). Phospholipase C-gamma contains introns shared by src homology 2 domains in many unrelated proteins. *Genetics*, *164*(2), 433–442. https://doi.org/10.1093/GENETICS/164.2.433

Marchini, J., & Howie, B. (2010). Genotype imputation for genome-wide association studies. *Nature Reviews Genetics*, *11*(7), 499–511. https://doi.org/10.1038/nrg2796

Martin, B. L., Schrader-Fischer, G., Busciglio, J., Duke, M., Paganetti, P., & Yankner, B. A. (1995). Intracellular Accumulation of β-Amyloid in Cells Expressing the Swedish Mutant Amyloid

Precursor Protein. *Journal of Biological Chemistry*, *270*(45), 26727–26730. https://doi.org/10.1074/jbc.270.45.26727

Martín, D., Salinas, M., López-Valdaliso, R., Serrano, E., Recuero, M., & Cuadrado, A. (2001). Effect of the Alzheimer amyloid fragment Aβ(25-35) on Akt/PKB kinase and survival of PC12 cells. *Journal of Neurochemistry*, *78*(5), 1000–1008. https://doi.org/10.1046/j.1471-4159.2001.00472.x

Martínez-Muriana, A., Mancuso, R., Francos-Quijorna, I., Olmos-Alonso, A., Osta, R., Perry, V. H., Navarro, X., Gomez-Nicola, D., & López-Vales, R. (2016). CSF1R blockade slows the progression of amyotrophic lateral sclerosis by reducing microgliosis and invasion of macrophages into peripheral nerves. *Scientific Reports*, *6*(1), 25663. https://doi.org/10.1038/srep25663

Masters, C. L., Simms, G., Weinman, N. A., Multhaup, G., McDonald, B. L., & Beyreuther, K. (1985). Amyloid plaque core protein in Alzheimer disease and Down syndrome. *Proceedings of the National Academy of Sciences*, *82*(12), 4245–4249. https://doi.org/10.1073/pnas.82.12.4245

Masuda, T., Sankowski, R., Staszewski, O., & Prinz, M. (2020). Microglia Heterogeneity in the Single-Cell Era. *Cell Reports*, *30*(5), 1271–1281. https://doi.org/10.1016/j.celrep.2020.01.010

Matarin, M., Salih, D. A., Yasvoina, M., Cummings, D. M., Guelfi, S., Liu, W., Nahaboo Solim, M. A., Moens, T. G., Paublete, R. M., Ali, S. S., Perona, M., Desai, R., Smith, K. J., Latcham, J., Fulleylove, M., Richardson, J. C., Hardy, J., & Edwards, F. A. (2015). A Genome-wide Gene-Expression Analysis and Database in Transgenic Mice during Development of Amyloid or Tau Pathology. *Cell Reports*, *10*(4), 633–644. https://doi.org/10.1016/j.celrep.2014.12.041

Matsunaga, S., Fujishiro, H., & Takechi, H. (2019). Efficacy and Safety of Glycogen Synthase Kinase 3 Inhibitors for Alzheimer's Disease: A Systematic Review and Meta-Analysis. *Journal of Alzheimer's Disease*, *69*(4), 1031–1039. https://doi.org/10.3233/JAD-190256

Mazaheri, F., Snaidero, N., Kleinberger, G., Madore, C., Daria, A., Werner, G., Krasemann, S., Capell, A., Trümbach, D., Wurst, W., Brunner, B., Bultmann, S., Tahirovic, S., Kerschensteiner, M., Misgeld, T., Butovsky, O., & Haass, C. (2017). TREM2 deficiency impairs chemotaxis and microglial responses to neuronal injury. *EMBO Reports*, *18*(7), 1186. https://doi.org/10.15252/EMBR.201743922

Mc Donald, J. M., Savva, G. M., Brayne, C., Welzel, A. T., Forster, G., Shankar, G. M., Selkoe, D. J., Ince, P. G., & Walsh, D. M. (2010). The presence of sodium dodecyl sulphate-stable Abeta dimers is strongly associated with Alzheimer-type dementia. *Brain : A Journal of Neurology*, *133*(Pt 5), 1328–1341. https://doi.org/10.1093/BRAIN/AWQ065

McGeer, P. L., Itagaki, S., Tago, H., & McGeer, E. G. (1987). Reactive microglia in patients with senile dementia of the Alzheimer type are positive for the histocompatibility glycoprotein HLA-DR. *Neuroscience Letters*, *79*(1–2), 195–200. https://doi.org/10.1016/0304-3940(87)90696-3

McGowan, E., Pickford, F., Kim, J., Onstead, L., Eriksen, J., Yu, C., Skipper, L., Murphy, M. P., Beard, J., Das, P., Jansen, K., DeLucia, M., Lin, W.-L., Dolios, G., Wang, R., Eckman, C. B., Dickson, D. W., Hutton, M., Hardy, J., & Golde, T. (2005). Aβ42 Is Essential for Parenchymal and Vascular Amyloid Deposition in Mice. *Neuron*, *47*(2), 191–199. https://doi.org/10.1016/j.neuron.2005.06.030

McGuire, S. E., Deshazer, M., & Davis, R. L. (2005). Thirty years of olfactory learning and memory research in Drosophila melanogaster. *Progress in Neurobiology*, *76*(5), 328–347. https://doi.org/10.1016/j.pneurobio.2005.09.003

McGuire, S. E., Mao, Z., & Davis, R. L. (2004). Spatiotemporal Gene Expression Targeting with the TARGET and Gene-Switch Systems in *Drosophila*. *Science's STKE*, *2004*(220). https://doi.org/10.1126/stke.2202004pl6

McLean, C. A., Cherny, R. A., Fraser, F. W., Fuller, S. J., Smith, M. J., Konrad Vbeyreuther, Bush, A. I., & Masters, C. L. (1999). Soluble pool of Abeta amyloid as a determinant of severity of neurodegeneration in Alzheimer's disease. *Annals of Neurology*, *46*(6), 860–866. https://doi.org/10.1002/1531-8249(199912)46:6<860::AID-ANA8>3.0.CO;2-M

McNamara, C. R., & Degterev, A. (2011). Small-molecule inhibitors of the PI3K signaling network. *Future Medicinal Chemistry*, *3*(5), 549–565. https://doi.org/10.4155/fmc.11.12

Medway, C. W., Abdul-Hay, S., Mims, T., Ma, L., Bisceglio, G., Zou, F., Pankratz, S., Sando, S. B., Aasly, J. O., Barcikowska, M., Siuda, J., Wszolek, Z. K., Ross, O. A., Carrasquillo, M., Dickson, D. W., Graff-Radford, N., Petersen, R. C., Ertekin-Taner, N., Morgan, K., … Younkin, S. G. (2014). ApoE variant p.V236E is associated with markedly reduced risk of Alzheimer's disease. *Molecular Neurodegeneration*, *9*(1), 11. https://doi.org/10.1186/1750-1326-9-11

Melom, J. E., & Littleton, J. T. (2013). Mutation of a NCKX eliminates glial microdomain calcium oscillations and enhances seizure susceptibility. *Journal of Neuroscience*, *33*(3), 1169–1178. https://doi.org/10.1523/JNEUROSCI.3920-12.2013

Mendez, M. F. (2017). Early-Onset Alzheimer Disease. *Neurologic Clinics*, *35*(2), 263–281. https://doi.org/10.1016/j.ncl.2017.01.005

Menzies, G. E., Sims, R., & Williams, J. (2017). MOLECULAR DYNAMIC MODELLING OF A NOVEL PLCG2 VARIANT REVEALS KEY PROTEIN STRUCTURAL DIFFERENCES. *Alzheimer's & Dementia*, *13*(7), P1489–P1490. https://doi.org/10.1016/j.jalz.2017.07.573

Meraz-Ríos, M. A., Toral-Rios, D., Franco-Bocanegra, D., Villeda-Hernández, J., & Campos-Peña, V. (2013). Inflammatory process in Alzheimer's Disease. *Frontiers in Integrative Neuroscience*, *7*(JUL). https://doi.org/10.3389/FNINT.2013.00059

Miners, S., Ashby, E., Baig, S., Harrison, R., Tayler, H., Speedy, E., Prince, J. A., Love, S., & Kehoe, P. G. (2009). Angiotensin-converting enzyme levels and activity in Alzheimer's disease: differences in brain and CSF ACE and association with ACE1 genotypes. *American Journal of Translational Research*, *1*(2), 163–177.

Molkentin, J. D., & Olson, E. N. (1996). Combinatorial control of muscle development by basic helix-loop-helix and MADS-box transcription factors. *Proceedings of the National Academy of Sciences*, *93*(18), 9366–9373. https://doi.org/10.1073/pnas.93.18.9366

Moloney, A., Sattelle, D. B., Lomas, D. A., & Crowther, D. C. (2010). Alzheimer's disease: insights from Drosophila melanogaster models. *Trends in Biochemical Sciences*, *35*(4), 228. https://doi.org/10.1016/J.TIBS.2009.11.004

Moran, M. F., Koch, C. A., Anderson, D., Ellis, C., England, L., Martin, G. S., & Pawson, T. (1990). Src homology region 2 domains direct protein-protein interactions in signal transduction.

Proceedings of the National Academy of Sciences of the United States of America, *87*(21), 8622. https://doi.org/10.1073/PNAS.87.21.8622

Mueller, H., Stadtmann, A., Van Aken, H., Hirsch, E., Wang, D., Ley, K., & Zarbock, A. (2010). Tyrosine kinase Btk regulates E-selectin–mediated integrin activation and neutrophil recruitment by controlling phospholipase C (PLC) γ2 and PI3Kγ pathways. *Blood*, *115*(15), 3118–3127. https://doi.org/10.1182/blood-2009-11-254185

Mullan, M., Crawford, F., Axelman, K., Houlden, H., Lilius, L., Winblad, B., & Lannfelt, L. (1992). A pathogenic mutation for probable Alzheimer's disease in the APP gene at the N–terminus of β–amyloid. *Nature Genetics*, *1*(5), 345–347. https://doi.org/10.1038/ng0892-345

Murakami, K., Irie, K., Morimoto, A., Ohigashi, H., Shindo, M., Nagao, M., Shimizu, T., & Shirasawa, T. (2002). Synthesis, aggregation, neurotoxicity, and secondary structure of various Aβ1–42 mutants of familial Alzheimer's disease at positions 21–23. *Biochemical and Biophysical Research Communications*, *294*(1), 5–10. https://doi.org/10.1016/S0006-291X(02)00430-8

Murillo-Maldonado, J. M., Bou Zeineddine, F., Stock, R., Thackeray, J., & Riesgo-Escovar, J. R. (2011). Insulin Receptor-Mediated Signaling via Phospholipase C-γ Regulates Growth and Differentiation in Drosophila. *PLOS ONE*, *6*(11), e28067. https://doi.org/10.1371/JOURNAL.PONE.0028067

Musiek, E. S., & Holtzman, D. M. (2015). Three dimensions of the amyloid hypothesis: time, space and "wingmen." *Nature Neuroscience*, *18*(6), 800–806. https://doi.org/10.1038/nn.4018

Muth, C., Hartmann, A., Sepulveda-Falla, D., Glatzel, M., & Krasemann, S. (2019). Phagocytosis of Apoptotic Cells Is Specifically Upregulated in ApoE4 Expressing Microglia in vitro. *Frontiers in Cellular Neuroscience*, *13*. https://doi.org/10.3389/fncel.2019.00181

Nakamura, Y., & Fukami, K. (2017). Regulation and physiological functions of mammalian phospholipase C. *Journal of Biochemistry*, mvw094. https://doi.org/10.1093/jb/mvw094

Nalivaeva, N. N., & Turner, A. J. (2013). The amyloid precursor protein: A biochemical enigma in brain development, function and disease. *FEBS Letters*, *587*(13), 2046–2054. https://doi.org/10.1016/j.febslet.2013.05.010

Naseri, N. N., Wang, H., Guo, J., Sharma, M., & Luo, W. (2019). The complexity of tau in Alzheimer's disease. *Neuroscience Letters*, *705*, 183–194. https://doi.org/10.1016/j.neulet.2019.04.022

Neher, J. J., Neniskyte, U., Zhao, J.-W., Bal-Price, A., Tolkovsky, A. M., & Brown, G. C. (2011). Inhibition of Microglial Phagocytosis Is Sufficient To Prevent Inflammatory Neuronal Death. *The Journal of Immunology*, *186*(8), 4973–4983. https://doi.org/10.4049/jimmunol.1003600

Nguyen, V. T. T., Sallbach, J., dos Santos Guilherme, M., & Endres, K. (2021). Influence of Acetylcholine Esterase Inhibitors and Memantine, Clinically Approved for Alzheimer's Dementia Treatment, on Intestinal Properties of the Mouse. *International Journal of Molecular Sciences*, *22*(3), 1015. https://doi.org/10.3390/ijms22031015

Nilsberth, C., Westlind-Danielsson, A., Eckman, C. B., Condron, M. M., Axelman, K., Forsell, C., Stenh, C., Luthman, J., Teplow, D. B., Younkin, S. G., Näslund, J., & Lannfelt, L. (2001). The "Arctic" APP mutation (E693G) causes Alzheimer's disease by enhanced Aβ protofibril formation. *Nature Neuroscience*, *4*(9), 887–893. https://doi.org/10.1038/nn0901-887

Nilsson, P., Saito, T., & Saido, T. C. (2014). New mouse model of Alzheimer's. *ACS Chemical Neuroscience*, *5*(7), 499–502. https://doi.org/10.1021/CN500105P/ASSET/IMAGES/LARGE/CN-2014-00105P_0002.JPEG

Nishibe, S., Wahl, M. I., Hernandez-Sotomayor, S. M., Tonks, N. K., Rhee, S. G., & Carpenter, G. (1990). Increase of the Catalytic Activity of Phospholipase C-γ1 by Tyrosine Phosphorylation. *Science*, *250*(4985), 1253–1256. https://doi.org/10.1126/science.1700866

Nishimura, I., Yang, Y., & Lu, B. (2004). PAR-1 Kinase Plays an Initiator Role in a Temporally Ordered Phosphorylation Process that Confers Tau Toxicity in Drosophila. *Cell*, *116*(5), 671–682. https://doi.org/10.1016/S0092-8674(04)00170-9

Nixon, R. A. (2013). The role of autophagy in neurodegenerative disease. *Nature Medicine*, *19*(8), 983–997. https://doi.org/10.1038/NM.3232

Nizami, S., Hall-Roberts, H., Warrier, S., Cowley, S. A., & Di Daniel, E. (2019). Microglial inflammation and phagocytosis in Alzheimer's disease: Potential therapeutic targets. *British Journal of Pharmacology*, *176*(18), 3515–3532. https://doi.org/10.1111/bph.14618

Novak, P., Schmidt, R., Kontsekova, E., Kovacech, B., Smolek, T., Katina, S., Fialova, L., Prcina, M., Parrak, V., Dal-Bianco, P., Brunner, M., Staffen, W., Rainer, M., Ondrus, M., Ropele, S., Smisek, M., Sivak, R., Zilka, N., Winblad, B., & Novak, M. (2018). FUNDAMANT: an interventional 72-week phase 1 follow-up study of AADvac1, an active immunotherapy against tau protein pathology in Alzheimer's disease. *Alzheimer's Research & Therapy*, *10*(1), 108. https://doi.org/10.1186/s13195-018-0436-1

Novikova, G., Andrews, S. J., Renton, A. E., & Marcora, E. (2021). Beyond association: successes and challenges in linking non-coding genetic variation to functional consequences that modulate Alzheimer's disease risk. *Molecular Neurodegeneration*, *16*(1), 1–13. https://doi.org/10.1186/S13024-021-00449-0/FIGURES/1

Nugent, A. A., Lin, K., van Lengerich, B., Lianoglou, S., Przybyla, L., Davis, S. S., Llapashtica, C., Wang, J., Kim, D. J., Xia, D., Lucas, A., Baskaran, S., Haddick, P. C. G., Lenser, M., Earr, T. K., Shi, J., Dugas, J. C., Andreone, B. J., Logan, T., … Di Paolo, G. (2020). TREM2 Regulates Microglial Cholesterol Metabolism upon Chronic Phagocytic Challenge. *Neuron*, *105*(5), 837-854.e9. https://doi.org/10.1016/j.neuron.2019.12.007

Obst, J., Hall-Roberts, H. L., Smith, T. B., Kreuzer, M., Magno, L., Di Daniel, E., Davis, J. B., & Mead, E. (2021). PLCγ2 regulates TREM2 signalling and integrin-mediated adhesion and migration of human iPSC-derived macrophages. *Scientific Reports*, *11*(1), 19842. https://doi.org/10.1038/S41598-021-96144-7

Oddo, S. (2012). The role of mTOR signaling in Alzheimer disease. *Frontiers in Bioscience*, *S4*(3), 310. https://doi.org/10.2741/s310

Oddo, S., Caccamo, A., Shepherd, J. D., Murphy, M. P., Golde, T. E., Kayed, R., Metherate, R., Mattson, M. P., Akbari, Y., & LaFerla, F. M. (2003). Triple-Transgenic Model of Alzheimer's Disease with Plaques and Tangles. *Neuron*, *39*(3), 409–421. https://doi.org/10.1016/S0896-6273(03)00434-3

Olmos-Alonso, A., Schetters, S. T. T., Sri, S., Askew, K., Mancuso, R., Vargas-Caballero, M., Holscher, C., Perry, V. H., & Gomez-Nicola, D. (2016). Pharmacological targeting of CSF1R inhibits

microglial proliferation and prevents the progression of Alzheimer's-like pathology. *Brain*, *139*(3), 891–907. https://doi.org/10.1093/brain/awv379

Olsson, F., Schmidt, S., Althoff, V., Munter, L. M., Jin, S., Rosqvist, S., Lendahl, U., Multhaup, G., & Lundkvist, J. (2014). Characterization of intermediate steps in amyloid beta (Aβ) production under near-native conditions. *Journal of Biological Chemistry*, *289*(3), 1540–1550. https://doi.org/10.1074/jbc.M113.498246

Ou, J., He, Y., Xiao, X., Yu, T.-M., Chen, C., Gao, Z., & Ho, M. S. (2014). Glial cells in neuronal development: recent advances and insights from Drosophila melanogaster. *Neuroscience Bulletin*, *30*(4), 584–594. https://doi.org/10.1007/s12264-014-1448-2

Panda, D., Samuel, J. C., Massie, M., Feinstein, S. C., & Wilson, L. (2003). Differential regulation of microtubule dynamics by three- and four-repeat tau: Implications for the onset of neurodegenerative disease. *Proceedings of the National Academy of Sciences*, *100*(16), 9548–9553. https://doi.org/10.1073/pnas.1633508100

Pandey, U. B., & Nichols, C. D. (2011). Human disease models in drosophila melanogaster and the role of the fly in therapeutic drug discovery. *Pharmacological Reviews*, *63*(2), 411–436. https://doi.org/10.1124/pr.110.003293

Pant, S., & Tajkhorshid, E. (2020). Microscopic Characterization of GRP1 PH Domain Interaction with Anionic Membranes. *Journal of Computational Chemistry*, *41*(6), 489–499. https://doi.org/10.1002/jcc.26109

Paresce, D. M., Ghosh, R. N., & Maxfield, F. R. (1996). Microglial cells internalize aggregates of the Alzheimer's disease amyloid beta-protein via a scavenger receptor. *Neuron*, *17*(3), 553–565. https://doi.org/10.1016/S0896-6273(00)80187-7

Park, S. A., Ahn, S. il, & Gallo, J.-M. (2016). Tau mis-splicing in the pathogenesis of neurodegenerative disorders. *BMB Reports*, *49*(8), 405–413. https://doi.org/10.5483/BMBRep.2016.49.8.084

Pauls, S. D., & Marshall, A. J. (2017). Regulation of immune cell signaling by SHIP1: A phosphatase, scaffold protein, and potential therapeutic target. *European Journal of Immunology*, *47*(6), 932–945. https://doi.org/10.1002/eji.201646795

Pei, J.-J., An, W.-L., Zhou, X.-W., Nishimura, T., Norberg, J., Benedikz, E., Götz, J., & Winblad, B. (2006). P70 S6 kinase mediates tau phosphorylation and synthesis. *FEBS Letters*, *580*(1), 107–114. https://doi.org/10.1016/j.febslet.2005.11.059

Pei, J.-J., Khatoon, S., An, W.-L., Nordlinder, M., Tanaka, T., Braak, H., Tsujio, I., Takeda, M., Alafuzoff, I., Winblad, B., Cowburn, R. F., Grundke-Iqbal, I., & Iqbal, K. (2003). Role of protein kinase B in Alzheimer's neurofibrillary pathology. *Acta Neuropathologica*, *105*(4), 381–392. https://doi.org/10.1007/s00401-002-0657-y

Peng, Q., Malhotra, S., Torchia, J. A., Kerr, W. G., Coggeshall, K. M., & Humphrey, M. B. (2010). TREM2- and DAP12-Dependent Activation of PI3K Requires DAP10 and Is Inhibited by SHIP1. *Science Signaling*, *3*(122). https://doi.org/10.1126/scisignal.2000500

Periz, G., & Fortini, M. E. (2004). Functional reconstitution of ?-secretase through coordinated expression of presenilin, nicastrin, Aph-1, and Pen-2. *Journal of Neuroscience Research*, *77*(3), 309–322. https://doi.org/10.1002/jnr.20203

Perkins, L. A., Holderbaum, L., Tao, R., Hu, Y., Sopko, R., McCall, K., Yang-Zhou, D., Flockhart, I., Binari, R., Shim, H.-S., Miller, A., Housden, A., Foos, M., Randkelv, S., Kelley, C., Namgyal, P., Villalta, C., Liu, L.-P., Jiang, X., … Perrimon, N. (2015). The Transgenic RNAi Project at Harvard Medical School: Resources and Validation. *Genetics*, *201*, 843–852. https://doi.org/10.1534/genetics.115.180208

Perl, D. P. (2010). Neuropathology of Alzheimer's disease. In *Mount Sinai Journal of Medicine* (Vol. 77, Issue 1, pp. 32–42). https://doi.org/10.1002/msj.20157

Pfeiffer, B. D., Ngo, T. T. B., Hibbard, K. L., Murphy, C., Jenett, A., Truman, J. W., & Rubin, G. M. (2010). Refinement of tools for targeted gene expression in Drosophila. *Genetics*, *186*(2), 735–755. https://doi.org/10.1534/GENETICS.110.119917

Phan, T. K., Williams, S. A., Bindra, G. K., Lay, F. T., Poon, I. K. H., & Hulett, M. D. (2019). Phosphoinositides: multipurpose cellular lipids with emerging roles in cell death. *Cell Death & Differentiation*, *26*(5), 781–793. https://doi.org/10.1038/s41418-018-0269-2

Poorkaj, P., Bird, T. D., Wijsman, E., Nemens, E., Garruto, R. M., Anderson, L., Andreadis, A., Wiederholt, W. C., Raskind, M., & Schellenberg, G. D. (1998). Tau is a candidate gene for chromosome 17 frontotemporal dementia. *Annals of Neurology*, *43*(6), 815–825. https://doi.org/10.1002/ana.410430617

Porta, C., Paglino, C., & Mosca, A. (2014). Targeting PI3K/Akt/mTOR signaling in cancer. *Frontiers in Oncology*, *4 APR*, 64. https://doi.org/10.3389/FONC.2014.00064/BIBTEX

Potthoff, M. J., & Olson, E. N. (2007). MEF2: a central regulator of diverse developmental programs. *Development*, *134*(23), 4131–4140. https://doi.org/10.1242/dev.008367

Pottier, C., Ravenscroft, T. A., Brown, P. H., Finch, N. A., Baker, M., Parsons, M., Asmann, Y. W., Ren, Y., Christopher, E., Levitch, D., Van Blitterswijk, M., Cruchaga, C., Campion, D., Nicolas, G., Richard, A.-C., Guerreiro, R., Bras, J. T., Zuchner, S., Gonzalez, M. A., … Macdonald, J. T. (2016). TYROBP genetic variants in early-onset Alzheimer's disease. *Neurobiol Aging*, *48*, 222–231. https://doi.org/10.1016/j.neurobiolaging.2016.07.028

Qiu, S. (2005). A computational study of off-target effects of RNA interference. *Nucleic Acids Research*, *33*(6), 1834–1847. https://doi.org/10.1093/nar/gki324

Rajendran, L., & Paolicelli, R. C. (2018). Microglia-Mediated Synapse Loss in Alzheimer's Disease. *The Journal of Neuroscience*, *38*(12), 2911–2919. https://doi.org/10.1523/JNEUROSCI.1136-17.2017

Ramesh, M., Gopinath, P., & Govindaraju, T. (2020). Role of Post-translational Modifications in Alzheimer's Disease. *ChemBioChem*, *21*(8), 1052–1079. https://doi.org/10.1002/cbic.201900573

Rapoport, M., Dawson, H. N., Binder, L. I., Vitek, M. P., & Ferreira, A. (2002). Tau is essential to β-amyloid-induced neurotoxicity. *Proceedings of the National Academy of Sciences*, *99*(9), 6364–6369. https://doi.org/10.1073/pnas.092136199

Ray, A., Speese, S. D., & Logan, M. A. (2017). Glial draper rescues Aβ toxicity in a Drosophila model of Alzheimer's disease. *Journal of Neuroscience*, *37*(49), 11881–11893. https://doi.org/10.1523/JNEUROSCI.0862-17.2017

Rebecchi, M. J., & Pentyala, S. N. (2000). Structure, Function, and Control of Phosphoinositide-Specific Phospholipase C. *Physiological Reviews*, *80*(4), 1291–1335. https://doi.org/10.1152/physrev.2000.80.4.1291

Rebecchi, M., Peterson, A., & McLaughlin, S. (1992). Phosphoinositide-specific phospholipase C-.delta.1 binds with high affinity to phospholipid vesicles containing phosphatidylinositol 4,5-bisphosphate. *Biochemistry*, *31*(51), 12742–12747. https://doi.org/10.1021/bi00166a005

Reiter, L. T., Potocki, L., Chien, S., Gribskov, M., & Bier, E. (2001). A systematic analysis of human disease-associated gene sequences in Drosophila melanogaster. *Genome Research*, *11*(6), 1114–1125. https://doi.org/10.1101/GR.169101

Rhee, S. G., & Bae, Y. S. (1997). Regulation of Phosphoinositide-specific Phospholipase C Isozymes. *Journal of Biological Chemistry*, *272*(24), 15045–15048. https://doi.org/10.1074/jbc.272.24.15045

Rhee, S. G., & Choi, K. D. (1992). Regulation of inositol phospholipid-specific phospholipase C isozymes. *Journal of Biological Chemistry*, *267*(18), 12393–12396. https://doi.org/10.1016/S0021-9258(18)42284-3

Riedel, G., Platt, B., & Micheau, J. (2003). Glutamate receptor function in learning and memory. *Behavioural Brain Research*, *140*(1–2), 1–47. http://www.ncbi.nlm.nih.gov/pubmed/12644276

Ries, M., & Sastre, M. (2016). Mechanisms of Aβ Clearance and Degradation by Glial Cells. *Frontiers in Aging Neuroscience*, *8*. https://doi.org/10.3389/fnagi.2016.00160

Rival, T., Page, R. M., Chandraratna, D. S., Sendall, T. J., Ryder, E., Liu, B., Lewis, H., Rosahl, T., Hider, R., Camargo, L. M., Shearman, M. S., Crowther, D. C., & Lomas, D. A. (2009). Fenton chemistry and oxidative stress mediate the toxicity of the β-amyloid peptide in a *Drosophila* model of Alzheimer's disease. *European Journal of Neuroscience*, *29*(7), 1335–1347. https://doi.org/10.1111/j.1460-9568.2009.06701.x

Rival, T., Soustelle, L., Strambi, C., Besson, M.-T., Iché, M., & Birman, S. (2004). Decreasing Glutamate Buffering Capacity Triggers Oxidative Stress and Neuropil Degeneration in the Drosophila Brain. *Current Biology*, *14*(7), 599–605. https://doi.org/10.1016/j.cub.2004.03.039

Roberson, E. D., & Mucke, L. (2006). 100 Years and Counting: Prospects for Defeating Alzheimer's Disease. *Science*, *314*(5800), 781–784. https://doi.org/10.1126/science.1132813

Rodrigue, K. M., Kennedy, K. M., & Park, D. C. (2009). Beta-Amyloid Deposition and the Aging Brain. *Neuropsychology Review*, *19*(4), 436. https://doi.org/10.1007/S11065-009-9118-X

Roman, G., & Davis, R. L. (2001). Molecular biology and anatomy ofDrosophila olfactory associative learning. *BioEssays*, *23*(7), 571–581. https://doi.org/10.1002/bies.1083

Romero, E., Cha, G.-H., Verstreken, P., Ly, C. V., Hughes, R. E., Bellen, H. J., & Botas, J. (2008). Suppression of Neurodegeneration and Increased Neurotransmission Caused by Expanded Full-Length Huntingtin Accumulating in the Cytoplasm. *Neuron*, *57*(1), 27–40. https://doi.org/10.1016/j.neuron.2007.11.025

Rooke, J., Pan, D., Xu, T., & Rubin, G. M. (1996). KUZ, a Conserved Metalloprotease-Disintegrin Protein with Two Roles in ***Drosophila*** Neurogenesis. *Science*, *273*(5279), 1227–1231. https://doi.org/10.1126/science.273.5279.1227

Roote, J., & Prokop, A. (2013). How to Design a Genetic Mating Scheme: A Basic Training Package for *Drosophila* Genetics. *G3 Genes|Genomes|Genetics*, *3*(2), 353–358. https://doi.org/10.1534/g3.112.004820

Rosen, D. R., Martin-Morris, L., Luo, L. Q., & White, K. (1989). A Drosophila gene encoding a protein resembling the human beta-amyloid protein precursor. *Proceedings of the National Academy of Sciences*, *86*(7), 2478–2482. https://doi.org/10.1073/pnas.86.7.2478

Saunders, A. M., Roses, A. D., Pericak-Vance, M. A., Dole, K. C., Strittmatter, W. J., Schmechel, D. E., Szymanski, M. H., McCown, N., Manwaring, M. G., Schmader, K., Breitner, J. C. S., Goldgaber, D., Benson, M. D., Goldfarb, L., & Brown, W. T. (1993). Apolipoprotein E ∈4 allele distributions in late-onset Alzheimer's disease and in other amyloid-forming diseases. *The Lancet*, *342*(8873), 710–711. https://doi.org/10.1016/0140-6736(93)91709-U

Schafer, D. P., & Stillman, J. M. (2022). Microglia are SYK of Aβ and cell debris. *Cell*, *185*(22), 4043–4045. https://doi.org/10.1016/j.cell.2022.09.043

Schott, J. M., Fox, N. C., & Rossor, M. N. (2002). Genetics of the dementias. *Journal of Neurology, Neurosurgery & Psychiatry*, *73*(suppl 2), ii27–ii31. https://doi.org/10.1136/JNNP.73.SUPPL_2.II27

Schwartzentruber, J., Cooper, S., Liu, J. Z., Barrio-Hernandez, I., Bello, E., Kumasaka, N., Young, A. M. H., Franklin, R. J. M., Johnson, T., Estrada, K., Gaffney, D. J., Beltrao, P., & Bassett, A. (2021). Genome-wide meta-analysis, fine-mapping and integrative prioritization implicate new Alzheimer's disease risk genes. *Nature Genetics*, *53*(3), 392–402. https://doi.org/10.1038/s41588-020-00776-w

Scott, C. C., Dobson, W., Botelho, R. J., Coady-Osberg, N., Chavrier, P., Knecht, D. A., Heath, C., Stahl, P., & Grinstein, S. (2005). Phosphatidylinositol-4,5-bisphosphate hydrolysis directs actin remodeling during phagocytosis. *Journal of Cell Biology*, *169*(1), 139–149. https://doi.org/10.1083/jcb.200412162

Scott, J. L., Musselman, C. A., Adu-Gyamfi, E., Kutateladze, T. G., & Stahelin, R. V. (2012). Emerging methodologies to investigate lipid–protein interactions. *Integrative Biology*, *4*(3), 247. https://doi.org/10.1039/c2ib00143h

SELKOE, D. J. (2006). Toward a Comprehensive Theory for Alzheimer's Disease. Hypothesis: Alzheimer's Disease Is Caused by the Cerebral Accumulation and Cytotoxicity of Amyloid β-Protein. *Annals of the New York Academy of Sciences*, *924*(1), 17–25. https://doi.org/10.1111/j.1749-6632.2000.tb05554.x

Selkoe, D. J., & Hardy, J. (2016). The amyloid hypothesis of Alzheimer's disease at 25 years. *EMBO Molecular Medicine*, *8*(6), 595–608. https://doi.org/10.15252/emmm.201606210

Seo, J., Byun, M. S., Yi, D., Lee, J. H., Jeon, S. Y., Shin, S. A., Kim, Y. K., Kang, K. M., Sohn, C.-H., Jung, G., Park, J.-C., Han, S.-H., Byun, J., Mook-Jung, I., Lee, D. Y., & Choi, M. (2020). Genetic associations of in vivo pathology influence Alzheimer's disease susceptibility. *Alzheimer's Research & Therapy*, *12*(1), 156. https://doi.org/10.1186/s13195-020-00722-2

Serge Gauthier, Claire Webster, Stijn Servaes, Jose A. Morias, & Pedro Rosa-Neto. (2022). World Alzheimer Report 2022 – Life after diagnosis: Navigating treatment, care and support. *Alzheimer's Disease International*.

Sevigny, J., Chiao, P., Bussière, T., Weinreb, P. H., Williams, L., Maier, M., Dunstan, R., Salloway, S., Chen, T., Ling, Y., O'Gorman, J., Qian, F., Arastu, M., Li, M., Chollate, S., Brennan, M. S., Quintero-Monzon, O., Scannevin, R. H., Arnold, H. M., … Sandrock, A. (2016). The antibody aducanumab reduces Aβ plaques in Alzheimer's disease. *Nature*, *537*(7618), 50–56. https://doi.org/10.1038/nature19323

Shankar, G. M., Li, S., Mehta, T. H., Garcia-Munoz, A., Shepardson, N. E., Smith, I., Brett, F. M., Farrell, M. A., Rowan, M. J., Lemere, C. A., Regan, C. M., Walsh, D. M., Sabatini, B. L., & Selkoe, D. J. (2008). Amyloid-β protein dimers isolated directly from Alzheimer's brains impair synaptic plasticity and memory. *Nature Medicine*, *14*(8), 837–842. https://doi.org/10.1038/nm1782

Shaw, P. J., Cirelli, C., Greenspan, R. J., & Tononi, G. (2000). Correlates of Sleep and Waking in *Drosophila melanogaster*. *Science*, *287*(5459), 1834–1837. https://doi.org/10.1126/science.287.5459.1834

Shortridge, R. D., Yoon, J., Lending, C. R., Bloomquist, B. T., Perdew, M. H., & Pak, W. L. (1991). A Drosophila phospholipase C gene that is expressed in the central nervous system. *The Journal of Biological Chemistry*, *266*(19), 12474–12480.

Shulman, J. M., & Feany, M. B. (2003). Genetic Modifiers of Tauopathy in Drosophila. *Genetics*, *165*(3), 1233–1242. https://doi.org/10.1093/genetics/165.3.1233

Shulman, J. M., Imboywa, S., Giagtzoglou, N., Powers, M. P., Hu, Y., Devenport, D., Chipendo, P., Chibnik, L. B., Diamond, A., Perrimon, N., Brown, N. H., de Jager, P. L., & Feany, M. B. (2014). Functional screening in Drosophila identifies Alzheimer's disease susceptibility genes and implicates Tau-mediated mechanisms. *Human Molecular Genetics*, *23*(4), 870–877. https://doi.org/10.1093/hmg/ddt478

Sims, R., Hill, M., & Williams, J. (2020). The multiplex model of the genetics of Alzheimer's disease. *Nature Neuroscience*, *23*(3), 311–322. https://doi.org/10.1038/s41593-020-0599-5

Sims, R., van der Lee, S. J., Naj, A. C., Bellenguez, C., Badarinarayan, N., Jakobsdottir, J., Kunkle, B. W., Boland, A., Raybould, R., Bis, J. C., Martin, E. R., Grenier-Boley, B., Heilmann-Heimbach, S., Chouraki, V., Kuzma, A. B., Sleegers, K., Vronskaya, M., Ruiz, A., Graham, R. R., … Schellenberg, G. D. (2017). Rare coding variants in PLCG2, ABI3, and TREM2 implicate microglial-mediated innate immunity in Alzheimer's disease. *Nature Genetics*, *49*(9), 1373–1384. https://doi.org/10.1038/ng.3916

Siviter, R. J., Taylor, C. A. M., Cottam, D. M., Denton, A., Dani, M. P., Milner, M. J., Shirras, A. D., & Isaac, R. E. (2002). Ance, a Drosophila angiotensin-converting enzyme homologue, is expressed in imaginal cells during metamorphosis and is regulated by the steroid, 20-hydroxyecdysone. *Biochemical Journal*, *367*(1), 187–193. https://doi.org/10.1042/BJ20020567

Small, J. V., & Kaverina, I. (2003). Microtubules meet substrate adhesions to arrange cell polarity. *Current Opinion in Cell Biology*, *15*(1), 40–47. https://doi.org/10.1016/S0955-0674(02)00008-X

Small, Rabins, P. V, Barry, P. P., Buckholtz, N. S., DeKosky, S. T., Ferris, S. H., Finkel, S. I., Gwyther, L. P., Khachaturian, Z. S., Lebowitz, B. D., McRae, T. D., Morris, J. C., Oakley, F., Schneider, L. S., Streim, J. E., Sunderland, T., Teri, L. A., & Tune, L. E. (1997). Diagnosis and treatment of Alzheimer disease and related disorders. Consensus statement of the American Association for Geriatric Psychiatry, the Alzheimer's Association, and the American Geriatrics Society. *JAMA*, *278*(16), 1363–1371. http://www.ncbi.nlm.nih.gov/pubmed/9343469

Soto-Avellaneda, A., & Morrison, B. E. (2020). Signaling and other functions of lipids in autophagy: a review. *Lipids in Health and Disease*, *19*(1), 214. https://doi.org/10.1186/s12944-020-01389-2

Spillantini, M. G., Bird, T. D., & Ghetti, B. (2006). Frontotemporal Dementia and Parkinsonism Linked to Chromosome 17: A New Group of Tauopathies. *Brain Pathology*, *8*(2), 387–402. https://doi.org/10.1111/j.1750-3639.1998.tb00162.x

Spires, T. L., & Hyman, B. T. (2005). Transgenic models of Alzheimer's disease: Learning from animals. *NeuroRX*, *2*(3), 423–437. https://doi.org/10.1602/neurorx.2.3.423

St Johnston, D. (2002). The art and design of genetic screens: Drosophila melanogaster. In *Nature Reviews Genetics* (Vol. 3, Issue 3, pp. 176–188). Nature Publishing Group. https://doi.org/10.1038/nrg751

Stapleton, M., Liao, G., Brokstein, P., Hong, L., Carninci, P., Shiraki, T., Hayashizaki, Y., Champe, M., Pacleb, J., Wan, K., Yu, C., Carlson, J., George, R., Celniker, S., & Rubin, G. M. (2002). The Drosophila Gene Collection: Identification of Putative Full-Length cDNAs for 70% of *D. melanogaster* Genes. *Genome Research*, *12*(8), 1294–1300. https://doi.org/10.1101/gr.269102

Stein, T. D., & Johnson, J. A. (2002). Lack of Neurodegeneration in Transgenic Mice Overexpressing Mutant Amyloid Precursor Protein Is Associated with Increased Levels of Transthyretin and the Activation of Cell Survival Pathways. *The Journal of Neuroscience*, *22*(17), 7380–7388. https://doi.org/10.1523/JNEUROSCI.22-17-07380.2002

Stelzmann, R. A., Norman Schnitzlein, H., & Murllagh, F. R. (1995). An English I'ranslation of Alzheimer's 1907 Paper, "ijber eine eigenartige Erlranliung der Hirnrinde." In *Clinical Anatomy* (Vol. 8). http://info-centre.jenage.de/assets/pdfs/library/stelzmann_et_al_alzheimer_CLIN_ANAT_1995.pdf

Stewart, C. R., Stuart, L. M., Wilkinson, K., Van Gils, J. M., Deng, J., Halle, A., Rayner, K. J., Boyer, L., Zhong, R., Frazier, W. A., Lacy-Hulbert, A., Khoury, J. El, Golenbock, D. T., & Moore, K. J. (2010). CD36 ligands promote sterile inflammation through assembly of a Toll-like receptor 4 and 6 heterodimer. *Nature Immunology*, *11*(2), 155–161. https://doi.org/10.1038/NI.1836

Stokes, C. E., & Hawthorne, J. N. (1987). Reduced phosphoinositide concentrations in anterior temporal cortex of Alzheimer-diseased brains. *Journal of Neurochemistry*, *48*(4), 1018–1021. https://doi.org/10.1111/J.1471-4159.1987.TB05619.X

Stork, T., Bernardos, R., & Freeman, M. R. (2012). Analysis of Glial Cell Development and Function in Drosophila. *Cold Spring Harbor Protocols*, *2012*(1), pdb.top067587. https://doi.org/10.1101/PDB.TOP067587

Stork, T., Sheehan, A., Tasdemir-Yilmaz, O. E., & Freeman, M. R. (2014). Neuron-Glia Interactions through the Heartless FGF Receptor Signaling Pathway Mediate Morphogenesis of Drosophila Astrocytes. *Neuron*, *83*(2), 388–403. https://doi.org/10.1016/j.neuron.2014.06.026

Suh, P. G., Park, J. il, Manzoli, L., Cocco, L., Peak, J. C., Katan, M., Fukami, K., Kataoka, T., Yun, S., & Sung, H. R. (2008). Multiple roles of phosphoinositide-specific phospholipase C isozymes. *BMB Reports*, *41*(6), 415–434. https://doi.org/10.5483/BMBREP.2008.41.6.415

Suzuki, N., Cheung, T. T., Cai, X. D., Odaka, A., Otvos, L., Eckman, C., Golde, T. E., & Younkin, S. G. (1994a). An Increased Percentage of Long Amyloid β Protein Secreted by Familial Amyloid β

Protein Precursor (βApp717) Mutants. *Science*, *264*(5163), 1336–1340. https://doi.org/10.1126/SCIENCE.8191290

Suzuki, N., Cheung, T. T., Cai, X.-D., Odaka, A., Otvos, L., Eckman, C., Golde, T. E., & Younkin, S. G. (1994b). An Increased Percentage of Long Amyloid β Protein Secreted by Familial Amyloid β Protein Precursor (βApp717) Mutants. *Science*, *264*(5163), 1336–1340. https://doi.org/10.1126/science.8191290

Szepesi, Z., Manouchehrian, O., Bachiller, S., & Deierborg, T. (2018). Bidirectional Microglia–Neuron Communication in Health and Disease. *Frontiers in Cellular Neuroscience*, *12*, 323. https://doi.org/10.3389/FNCEL.2018.00323/BIBTEX

Takalo, M., Wittrahm, R., Wefers, B., Parhizkar, S., Jokivarsi, K., Kuulasmaa, T., Mäkinen, P., Martiskainen, H., Wurst, W., Xiang, X., Marttinen, M., Poutiainen, P., Haapasalo, A., Hiltunen, M., & Haass, C. (2020). The Alzheimer's disease-associated protective Plcγ2-P522R variant promotes immune functions. *Molecular Neurodegeneration*, *15*(1), 52. https://doi.org/10.1186/s13024-020-00402-7

Tan, F. H. P., & Azzam, G. (2017). Drosophila melanogaster: Deciphering Alzheimer's Disease. *The Malaysian Journal of Medical Sciences : MJMS*, *24*(2), 6–20. https://doi.org/10.21315/mjms2017.24.2.2

Tan, M., Li, J., Ma, F., Zhang, X., Zhao, Q., & Cao, X. (2019). PLD3 Rare Variants Identified in Late-Onset Alzheimer's Disease Affect Amyloid-β Levels in Cellular Model. *Frontiers in Neuroscience*, *13*. https://doi.org/10.3389/fnins.2019.00116

Tapia-Arancibia, L., Aliaga, E., Silhol, M., & Arancibia, S. (2008). New insights into brain BDNF function in normal aging and Alzheimer disease. *Brain Research Reviews*, *59*(1), 201–220. https://doi.org/10.1016/j.brainresrev.2008.07.007

Tarawneh, R., & Holtzman, D. M. (2012). The clinical problem of symptomatic Alzheimer disease and mild cognitive impairment. *Cold Spring Harbor Perspectives in Medicine*, *2*(5), a006148. https://doi.org/10.1101/cshperspect.a006148

Tariq, K., & Luikart, B. W. (2021). Striking a balance: PIP2 and PIP3 signaling in neuronal health and disease. *Exploration of Neuroprotective Therapy*, *1*(2), 86. https://doi.org/10.37349/ENT.2021.00008

Tasdemir-Yilmaz, O. E., & Freeman, M. R. (2014). Astrocytes engage unique molecular programs to engulf pruned neuronal debris from distinct subsets of neurons. *Genes & Development*, *28*(1), 20–33. https://doi.org/10.1101/gad.229518.113

Thackeray, J. R., Gaines, P. C., Ebert, P., & Carlson, J. R. (1998). small wing encodes a phospholipase C-(gamma) that acts as a negative regulator of R7 development in Drosophila. *Development (Cambridge, England)*, *125*(24), 5033–5042. http://www.ncbi.nlm.nih.gov/pubmed/9811587

Tokuda, T., Fukushima, T., Ikeda, S.-I., Sekijima, Y., Shoji, S., Yanagisawa, N., & Tamaoka, A. (1997). Plasma Levels of amyloid beta proteins Abeta1-40 and Abeta1-42(43) are elevated in Down's syndrome. *Annals of Neurology*, *41*(2), 271–273. https://doi.org/10.1002/ana.410410220

Tolar, M., Hey, J., Power, A., & Abushakra, S. (2021). Neurotoxic Soluble Amyloid Oligomers Drive Alzheimer's Pathogenesis and Represent a Clinically Validated Target for Slowing Disease

Progression. *International Journal of Molecular Sciences*, *22*(12), 6355. https://doi.org/10.3390/ijms22126355

Tomita, J., Ban, G., Kato, Y. S., & Kume, K. (2021). Protocerebral Bridge Neurons That Regulate Sleep in Drosophila melanogaster. *Frontiers in Neuroscience*, *15*. https://doi.org/10.3389/fnins.2021.647117

Tsai, A. P., Dong, C., Lin, P. B.-C., Messenger, E. J., Casali, B. T., Moutinho, M., Liu, Y., Oblak, A. L., Lamb, B. T., Landreth, G. E., Bissel, S. J., & Nho, K. (2022). PLCG2 is associated with the inflammatory response and is induced by amyloid plaques in Alzheimer's disease. *Genome Medicine*, *14*(1), 17. https://doi.org/10.1186/s13073-022-01022-0

Turner, P. R., O'Connor, K., Tate, W. P., & Abraham, W. C. (2003). Roles of amyloid precursor protein and its fragments in regulating neural activity, plasticity and memory. *Progress in Neurobiology*, *70*(1), 1–32. https://doi.org/10.1016/S0301-0082(03)00089-3

Ulland, T. K., Song, W. M., Huang, S. C.-C., Ulrich, J. D., Sergushichev, A., Beatty, W. L., Loboda, A. A., Zhou, Y., Cairns, N. J., Kambal, A., Loginicheva, E., Gilfillan, S., Cella, M., Virgin, H. W., Unanue, E. R., Wang, Y., Artyomov, M. N., Holtzman, D. M., & Colonna, M. (2017). TREM2 Maintains Microglial Metabolic Fitness in Alzheimer's Disease. *Cell*, *170*(4), 649-663.e13. https://doi.org/10.1016/j.cell.2017.07.023

van der Lee, S. J., Conway, O. J., Jansen, I., Carrasquillo, M. M., Kleineidam, L., van den Akker, E., Hernández, I., van Eijk, K. R., Stringa, N., Chen, J. A., Zettergren, A., Andlauer, T. F. M., Diez-Fairen, M., Simon-Sanchez, J., Lleó, A., Zetterberg, H., Nygaard, M., Blauwendraat, C., Savage, J. E., … Holstege, H. (2019). A nonsynonymous mutation in PLCG2 reduces the risk of Alzheimer's disease, dementia with Lewy bodies and frontotemporal dementia, and increases the likelihood of longevity. *Acta Neuropathologica*, *138*(2), 237–250. https://doi.org/10.1007/s00401-019-02026-8

van Dyck, C. H., Swanson, C. J., Aisen, P., Bateman, R. J., Chen, C., Gee, M., Kanekiyo, M., Li, D., Reyderman, L., Cohen, S., Froelich, L., Katayama, S., Sabbagh, M., Vellas, B., Watson, D., Dhadda, S., Irizarry, M., Kramer, L. D., & Iwatsubo, T. (2022). Lecanemab in Early Alzheimer's Disease. *New England Journal of Medicine*. https://doi.org/10.1056/NEJMoa2212948

Varnai, P., & Balla, T. (2006). Live cell imaging of phosphoinositide dynamics with fluorescent protein domains. *Biochimica et Biophysica Acta (BBA) - Molecular and Cell Biology of Lipids*, *1761*(8), 957–967. https://doi.org/10.1016/j.bbalip.2006.03.019

Vaz, M., & Silvestre, S. (2020). Alzheimer's disease: Recent treatment strategies. *European Journal of Pharmacology*, *887*, 173554. https://doi.org/10.1016/j.ejphar.2020.173554

VENKATESWARLU, K., GUNN-MOORE, F., OATEY, P. B., TAVARÉ, J. M., & CULLEN, P. J. (1998). Nerve growth factor- and epidermal growth factor-stimulated translocation of the ADP-ribosylation factor-exchange factor GRP1 to the plasma membrane of PC12 cells requires activation of phosphatidylinositol 3-kinase and the GRP1 pleckstrin homology domain. *Biochemical Journal*, *335*(1), 139–146. https://doi.org/10.1042/bj3350139

Verghese, P. B., Castellano, J. M., Garai, K., Wang, Y., Jiang, H., Shah, A., Bu, G., Frieden, C., & Holtzman, D. M. (2013). ApoE influences amyloid-β (Aβ) clearance despite minimal apoE/Aβ association in physiological conditions. *Proceedings of the National Academy of Sciences*, *110*(19). https://doi.org/10.1073/pnas.1220484110

Vilchez, D., Saez, I., & Dillin, A. (2014). The role of protein clearance mechanisms in organismal ageing and age-related diseases. *Nature Communications*, *5*(1), 5659. https://doi.org/10.1038/ncomms6659

Vissers, J. H. A., Manning, S. A., Kulkarni, A., & Harvey, K. F. (2016). A Drosophila RNAi library modulates Hippo pathway-dependent tissue growth. *Nature Communications*, *7*(1), 10368. https://doi.org/10.1038/ncomms10368

Vlahos, C. J., Matter, W. F., Hui, K. Y., & Brown, R. F. (1994). A specific inhibitor of phosphatidylinositol 3-kinase, 2-(4-morpholinyl)-8-phenyl-4H-1-benzopyran-4-one (LY294002). *The Journal of Biological Chemistry*, *269*(7), 5241–5248.

Volpatti, J. R., Al-Maawali, A., Smith, L., Al-Hashim, A., Brill, J. A., & Dowling, J. J. (2019). The expanding spectrum of neurological disorders of phosphoinositide metabolism. *Disease Models & Mechanisms*, *12*(8). https://doi.org/10.1242/DMM.038174

Wahl, M. I., Sweatt, J. D., & Carpenter, G. (1987). Epidermal growth factor (EGF) stimulates inositol trisphosphate formation in cells which overexpress the EGF receptor. *Biochemical and Biophysical Research Communications*, *142*(3), 688–695. https://doi.org/10.1016/0006-291X(87)91469-0

Wang, D., Feng, J., Wen, R., Marine, J.-C., Sangster, M. Y., Parganas, E., Hoffmeyer, A., Jackson, C. W., Cleveland, J. L., Murray, P. J., & Ihle, J. N. (2000). Phospholipase Cγ2 Is Essential in the Functions of B Cell and Several Fc Receptors. *Immunity*, *13*(1), 25–35. https://doi.org/10.1016/S1074-7613(00)00005-4

Wang, L., Yin, Y. L., Liu, X. Z., Shen, P., Zheng, Y. G., Lan, X. R., Lu, C. B., & Wang, J. Z. (2020). Current understanding of metal ions in the pathogenesis of Alzheimer's disease. *Translational Neurodegeneration 2020 9:1*, *9*(1), 1–13. https://doi.org/10.1186/S40035-020-00189-Z

Wang, T., Wei, J. J., Sabatini, D. M., & Lander, E. S. (2014). Genetic Screens in Human Cells Using the CRISPR-Cas9 System. *Science*, *343*(6166), 80–84. https://doi.org/10.1126/science.1246981

Weggen, S., & Beher, D. (2012). Molecular consequences of amyloid precursor protein and presenilin mutations causing autosomal-dominant Alzheimer's disease. *Alzheimer's Research & Therapy*, *4*(2), 9. https://doi.org/10.1186/alzrt107

Wei, W., Wang, X., & Kusiak, J. W. (2002). Signaling Events in Amyloid β-Peptide-induced Neuronal Death and Insulin-like Growth Factor I Protection. *Journal of Biological Chemistry*, *277*(20), 17649–17656. https://doi.org/10.1074/jbc.M111704200

Weingarten, M. D., Lockwood, A. H., Hwo, S. Y., & Kirschner, M. W. (1975). A protein factor essential for microtubule assembly. *Proceedings of the National Academy of Sciences*, *72*(5), 1858–1862. https://doi.org/10.1073/pnas.72.5.1858

Wenk, M. R., Lucast, L., Di Paolo, G., Romanelli, A. J., Suchy, S. F., Nussbaum, R. L., Cline, G. W., Shulman, G. I., McMurray, W., & De Camilli, P. (2003). Phosphoinositide profiling in complex lipid mixtures using electrospray ionization mass spectrometry. *Nature Biotechnology*, *21*(7), 813–817. https://doi.org/10.1038/nbt837

Wentzell, J. S., Bolkan, B. J., Carmine-Simmen, K., Swanson, T. L., Musashe, D. T., & Kretzschmar, D. (2012). Amyloid precursor proteins are protective in Drosophila models of progressive

neurodegeneration. *Neurobiology of Disease*, *46*(1), 78–87. https://doi.org/10.1016/j.nbd.2011.12.047

Wes, P. D., Sayed, F. A., Bard, F., & Gan, L. (2016). Targeting microglia for the treatment of Alzheimer's Disease. *Glia*, *64*(10), 1710–1732. https://doi.org/10.1002/GLIA.22988

Wißfeld, J., Mathews, M., Mossad, O., Picardi, P., Cinti, A., Redaelli, L., Pradier, L., Brüstle, O., & Neumann, H. (2021). Reporter cell assay for human CD33 validated by specific antibodies and human iPSC-derived microglia. *Scientific Reports*, *11*(1), 13462. https://doi.org/10.1038/s41598-021-92434-2

Witoelar, A., Rongve, A., Almdahl, I. S., Ulstein, I. D., Engvig, A., White, L. R., Selbæk, G., Stordal, E., Andersen, F., Brækhus, A., Saltvedt, I., Engedal, K., Hughes, T., Bergh, S., Bråthen, G., Bogdanovic, N., Bettella, F., Wang, Y., Athanasiu, L., … Andreassen, O. A. (2018). Meta-analysis of Alzheimer's disease on 9,751 samples from Norway and IGAP study identifies four risk loci. *Scientific Reports*, *8*(1), 1–8. https://doi.org/10.1038/s41598-018-36429-6

Wittmann, C. W., Wszolek, M. F., Shulman, J. M., Salvaterra, P. M., Lewis, J., Hutton, M., & Feany, M. B. (2001). Tauopathy in Drosophila: Neurodegeneration without neurofibrillary tangles. *Science*, *293*(5530), 711–714. https://doi.org/10.1126/SCIENCE.1062382/SUPPL_FILE/1062382S2_THUMB.GIF

Wolfe, M. S. (2006). The γ-Secretase Complex: Membrane-Embedded Proteolytic Ensemble. *Biochemistry*, *45*(26), 7931–7939. https://doi.org/10.1021/bi060799c

Wyss-Coray, T., & Mucke, L. (2002). Inflammation in Neurodegenerative Disease—A Double-Edged Sword. *Neuron*, *35*(3), 419–432. https://doi.org/10.1016/S0896-6273(02)00794-8

Xiang, X., Piers, T. M., Wefers, B., Zhu, K., Mallach, A., Brunner, B., Kleinberger, G., Song, W., Colonna, M., Herms, J., Wurst, W., Pocock, J. M., & Haass, C. (2018). The Trem2 R47H Alzheimer's risk variant impairs splicing and reduces Trem2 mRNA and protein in mice but not in humans. *Molecular Neurodegeneration*, *13*(1), 49. https://doi.org/10.1186/s13024-018-0280-6

Yagi, Y., Tomita, S., Nakamura, M., & Suzuki, T. (2000). Overexpression of Human Amyloid Precursor Protein in Drosophila. *Molecular Cell Biology Research Communications*, *4*(1), 43–49. https://doi.org/10.1006/mcbr.2000.0248

Yang, T., Li, S., Xu, H., Walsh, D. M., & Selkoe, D. J. (2017). Large Soluble Oligomers of Amyloid β-Protein from Alzheimer Brain Are Far Less Neuroactive Than the Smaller Oligomers to Which They Dissociate. *The Journal of Neuroscience*, *37*(1), 152–163. https://doi.org/10.1523/JNEUROSCI.1698-16.2016

Ye, K., Aghdasi, B., Luo, H. R., Moriarity, J. L., Wu, F. Y., Hong, J. J., Hurt, K. J., Bae, S. S., Suh, P.-G., & Snyder, S. H. (2002). Phospholipase Cγ1 is a physiological guanine nucleotide exchange factor for the nuclear GTPase PIKE. *Nature*, *415*(6871), 541–544. https://doi.org/10.1038/415541a

Yeh, F. L., Wang, Y., Tom, I., Gonzalez, L. C., & Sheng, M. (2016a). TREM2 Binds to Apolipoproteins, Including APOE and CLU/APOJ, and Thereby Facilitates Uptake of Amyloid-Beta by Microglia. *Neuron*, *91*(2), 328–340. https://doi.org/10.1016/j.neuron.2016.06.015

Yeh, F. L., Wang, Y., Tom, I., Gonzalez, L. C., & Sheng, M. (2016b). TREM2 Binds to Apolipoproteins, Including APOE and CLU/APOJ, and Thereby Facilitates Uptake of Amyloid-Beta by Microglia. *Neuron*, *91*(2), 328–340. https://doi.org/10.1016/J.NEURON.2016.06.015

Yu, P., Constien, R., Dear, N., Katan, M., Hanke, P., Bunney, T. D., Kunder, S., Quintanilla-Martinez, L., Huffstadt, U., Schröder, A., Jones, N. P., Peters, T., Fuchs, H., Hrabe de Angelis, M., Nehls, M., Grosse, J., Wabnitz, P., Meyer, T. P. H., Yasuda, K., … Mudde, G. C. (2005). Autoimmunity and Inflammation Due to a Gain-of-Function Mutation in Phospholipase Cγ2 that Specifically Increases External Ca2+ Entry. *Immunity*, *22*(4), 451–465. https://doi.org/10.1016/j.immuni.2005.01.018

Yu, Y., Niccoli, T., Ren, Z., Woodling, N. S., Aleyakpo, B., Szabadkai, G., & Partridge, L. (2020). PICALM rescues glutamatergic neurotransmission, behavioural function and survival in a Drosophila model of Aβ42 toxicity. *Human Molecular Genetics*, *29*(14), 2420–2434. https://doi.org/10.1093/hmg/ddaa125

Zhang, G., Wang, Z., Hu, H., Zhao, M., & Sun, L. (2021). Microglia in Alzheimer's Disease: A Target for Therapeutic Intervention. *Frontiers in Cellular Neuroscience*, *15*, 479. https://doi.org/10.3389/FNCEL.2021.749587/BIBTEX

Zhang, Y., Thompson, R., Zhang, H., & Xu, H. (2011). APP processing in Alzheimer's disease. *Molecular Brain*, *4*(1), 3. https://doi.org/10.1186/1756-6606-4-3

Zhao, J., Zhu, Y., Song, X., Xiao, Y., Su, G., Liu, X., Wang, Z., Xu, Y., Liu, J., Eliezer, D., Ramlall, T. F., Lippens, G., Gibson, J., Zhang, F., Linhardt, R. J., Wang, L., & Wang, C. (2019). 3-O-Sulfation of Heparan Sulfate Enhances Tau Interaction and Cellular Uptake. *Angewandte Chemie International Edition*, *59*(5), 1818–1827. https://doi.org/10.1002/anie.201913029

Zhao, Y., Wu, X., Li, X., Jiang, L. L., Gui, X., Liu, Y., Sun, Y., Zhu, B., Piña-Crespo, J. C., Zhang, M., Zhang, N., Chen, X., Bu, G., An, Z., Huang, T. Y., & Xu, H. (2018). TREM2 Is a Receptor for β-Amyloid that Mediates Microglial Function. *Neuron*, *97*(5), 1023-1031.e7. https://doi.org/10.1016/J.NEURON.2018.01.031

Zhao, Z., Sagare, A. P., Ma, Q., Halliday, M. R., Kong, P., Kisler, K., Winkler, E. A., Ramanathan, A., Kanekiyo, T., Bu, G., Owens, N. C., Rege, S. V, Si, G., Ahuja, A., Zhu, D., Miller, C. A., Schneider, J. A., Maeda, M., Maeda, T., … Zlokovic, B. V. (2015). Central role for PICALM in amyloid-β blood-brain barrier transcytosis and clearance. *Nature Neuroscience*, *18*(7), 978–987. https://doi.org/10.1038/nn.4025

Zhong, L., Chen, X. F., Wang, T., Wang, Z., Liao, C., Wang, Z., Huang, R., Wang, D., Li, X., Wu, L., Jia, L., Zheng, H., Painter, M., Atagi, Y., Liu, C. C., Zhang, Y. W., Fryer, J. D., Xu, H., & Bu, G. (2017). Soluble TREM2 induces inflammatory responses and enhances microglial survival. *The Journal of Experimental Medicine*, *214*(3), 597. https://doi.org/10.1084/JEM.20160844

Zhou, X.-W., Gustafsson, J.-Å., Tanila, H., Bjorkdahl, C., Liu, R., Winblad, B., & Pei, J.-J. (2008). Tau hyperphosphorylation correlates with reduced methylation of protein phosphatase 2A. *Neurobiology of Disease*, *31*(3), 386–394. https://doi.org/10.1016/j.nbd.2008.05.013

Zhu, L., Zhong, M., Elder, G. A., Sano, M., Holtzman, D. M., Gandy, S., Cardozo, C., Haroutunian, V., Robakis, N. K., & Cai, D. (2015). Phospholipid dysregulation contributes to ApoE4-associated cognitive deficits in Alzheimer's disease pathogenesis. *Proceedings of the National Academy of Sciences*, *112*(38), 11965–11970. https://doi.org/10.1073/pnas.1510011112

Zhu, L., Zhong, M., Zhao, J., Rhee, H., Caesar, I., Knight, E. M., Volpicelli-Daley, L., Bustos, V., Netzer, W., Liu, L., Lucast, L., Ehrlich, M. E., Robakis, N. K., Gandy, S. E., & Cai, D. (2013). Reduction of Synaptojanin 1 Accelerates Aβ Clearance and Attenuates Cognitive Deterioration in an Alzheimer Mouse Model. *Journal of Biological Chemistry*, *288*(44), 32050–32063. https://doi.org/10.1074/jbc.M113.504365

Zhu, Y., Nwabuisi-Heath, E., Dumanis, S. B., Tai, L. M., Yu, C., Rebeck, G. W., & Ladu, M. J. (2012). APOE genotype alters glial activation and loss of synaptic markers in mice. *Glia*, *60*(4), 559–569. https://doi.org/10.1002/glia.22289

Ziegenfuss, J. S., Biswas, R., Avery, M. A., Hong, K., Sheehan, A. E., Yeung, Y.-G., Stanley, E. R., & Freeman, M. R. (2008). Draper-dependent glial phagocytic activity is mediated by Src and Syk family kinase signalling. *Nature*, *453*(7197), 935–939. https://doi.org/10.1038/nature06901

Ziviani, E., Tao, R. N., & Whitworth, A. J. (2010). Drosophila Parkin requires PINK1 for mitochondrial translocation and ubiquitinates Mitofusin. *Proceedings of the National Academy of Sciences of the United States of America*, *107*(11), 5018–5023. https://doi.org/10.1073/PNAS.0913485107/SUPPL_FILE/PNAS.200913485SI.PDF

Zotova, E., Holmes, C., Johnston, D., Neal, J. W., Nicoll, J. A. R., & Boche, D. (2011). Microglial alterations in human Alzheimer's disease following Aβ42 immunization. *Neuropathology and Applied Neurobiology*, *37*(5), 513–524. https://doi.org/10.1111/J.1365-2990.2010.01156.X

zur Lage, P., Newton, F. G., & Jarman, A. P. (2019). Survey of the Ciliary Motility Machinery of Drosophila Sperm and Ciliated Mechanosensory Neurons Reveals Unexpected Cell-Type Specific Variations: A Model for Motile Ciliopathies. *Frontiers in Genetics*, *10*. https://doi.org/10.3389/fgene.2019.00024

Appendix

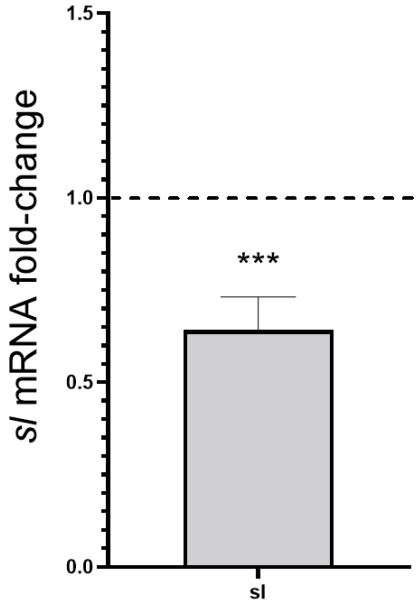

Figure 8.1 Relative expression of sl mRNA upon ubiquitous sl knockdown

sl RNAi II (32906) significantly reduces levels of sl mRNA relative to control (LacZ). Flies were reared at 29°C and aged for 7 days prior to RNA extraction. sl RNAi was expressed ubiquitously under the Tubulin-Gal4 promoter.